THE ROLE OF ALTERNATIVE OXIDASE (AOX) IN PLANT STRESS: DO PLANTS INCREASE THE ACTIVITY OF AOX IN RESPONSE TO NUTRIENT STRESS UNDER FIELD CONDITIONS?

A thesis submitted in partial fulfilment

of the requirements for the Degree of

Doctor of Philosophy in Plant Biology

in the University of Canterbury

by Ari Kornfeld

University of Canterbury

2012

Statement of originality

The work presented in this thesis is, to the best of my knowledge and belief, original. The material has not been submitted, either in whole or in part, for a degree at this or any other university.

Ari Kornfeld
April 26, 2012

Acknowledgments

Many people contributed to the success of this project. Foremost among them is Matthew Turnbull, who secured the initial funding and guided me through the entire research process. But he did much more than that: he arranged and coordinated my research trips to Franz Josef (New Zealand), England, Sweden, Australia, and Alaska; he kept me diligent in my writing, and even helped me with the often-voluminous field work. Next behind him in prominence is co-supervisor Travis Horton who guided me through the vagaries of stable isotopes and mass spectrometry and whose enthusiasm for my accomplishments kept me going through some of the hard times. Owen Atkin (The Australian National University), the overseas member of my committee, was nevertheless always available to provide feedback, advice, and insights as well as graciously providing chemical analysis for some of my plant tissue samples (and hosting me in York, England). Juliet Gerrard completes the supervisory committee; she provided advice on laboratory assays, not to mention access to equipment and facilities. I am indebted and grateful to each of them for the time and effort they devoted to my academic development.

Kevin Griffin (Columbia University, USA) provided support, advice, insights, and assistance throughout the project, but most significantly, he hosted my research at Toolik, Alaska – the subject of Chapter 6. Dan Yakir (Weizmann Institute, Israel) also provided invaluable advice on all aspects of this project, especially regarding the methods, and particularly, his insight that “it’s not a bug it’s a feature” (Section 7.2.3). Vaughan Hurry (Umeå University, Sweden) and his post-doctoral student Catherine Campbell introduced me to Western blot methods. Harvey Millar (University of Western Australia) graciously provided the AOX antibodies and advice on using them. Phil Ineson (University of York, England) loaned us a portable mass spectrometer and imbued me with the conscience of science. David Tissue hosted me at the University of Western Sydney. Jason Tylianakis provided advice on statistics. I owe special thanks to Jens Arne-Subke (University of Stirling, Scotland) for training me in mass spectrometry, stoically tolerating my blunders in the same, assisting with fieldwork, having faith in me, and for his incisive questions.

I am further indebted to David Conder for providing access to and support in the glasshouse facilities, and to Jenny Ladley, Jackie Healy and Nicole Lauren-Manuera for their technical support with laboratory space, equipment and supplies. My peers

Stephanie Searle, Carolina Sanhueza Inalaf (Universidad de Concepción, Chile), and Mary Heskel (Columbia University, USA) provided important advice, assistance, and feedback. This has truly been an international effort! Numerous people also helped with laboratory and/or field work including Darren Smalley, Claudia Godoy Lira, Ian Reeves, Meenu Joseph, and Kyle Turnbull. I owe them all a debt of gratitude.

My wife, Susan, has been tremendously supportive throughout this endeavour – I don't know how I could have done it without her!

Finally, I would like Miquel Ribas-Carbo (Universitat de les Illes Balears, Mallorca, Spain) and Margaret Barbour (University of Sydney, Australia) for agreeing to be my external examiners. (My apologies for the heft!)

This work was supported in part by grants from the Marsden Fund of the Royal Society of New Zealand (#06-UOC-028) and the US National Science Foundation International Polar Year 2007 (IPY #07-32664). I was also supported by two scholarships: a University of Canterbury Roper Scholarship and a New Zealand International Doctoral Research Scholarship. I am also grateful to the New Zealand Department of Conservation for providing access to and allowing us to harvest material from the field sites near Franz Josef.

Contents

Statement of originality ..... **iii**

Acknowledgments ..... **v**

Contents ..... **vii**

List of Tables ..... **xiii**

List of Figures ..... **xiv**

List of Abbreviations ..... **xvii**

Abstract **1**

1. Introduction and overview **3**

1.1. The ecophysiology of alternative oxidase (AOX) and cytochrome *c* oxidase (COX) 4

1.1.1. Mitochondrial function 5

1.1.2. Mitochondrial regulation 7

1.1.3. Ecophysiological perspective 9

1.2. Stable isotopes in ecophysiology and plant respiration 9

1.3. A brief history of respiratory electron partioning measurement 11

1.4. The difficulty in measuring contamination 12

1.5. Motivation for the present study 13

2. Correcting for nonlinearity effects of CF-IRMS across a wide dynamic range **15**

2.1. Introduction 16

2.2. Mathematical development 17

2.3. Experimental 22

2.3.1. Sample preparation 22

2.3.2. Isotopic analysis 24

2.3.3. Statistical analysis 27

2.4. Results and discussion 27

2.4.1. Correcting nonlinearities in $\delta^{18}O$ and $\delta^{15}N$ values 28

2.4.2. Correcting nonlinearities in $\delta O_2/N_2$ values 32

2.5. Summary 35

3. A field-compatible method for measuring alternative respiratory pathway activities *in vivo* using stable O_2 isotopes 37

3.1. Introduction 38
3.2. Materials and methods 39
3.2.1. Evacuation 40
3.2.2. Incubation 40
3.2.3. Gas transfer and storage 41
3.2.4. Isotopic analysis 41
3.2.5. Discrimination computations with contamination correction 42
3.2.6. Curvature analysis 44
3.2.7. Simulation 45
3.2.8. Statistical analysis 45
3.2.9. Experimental application of the methods 46
3.3. Results and discussion 49
3.3.1. Nonlinearity due to intrinsic variability in *D* 50
3.3.2. Contamination 52
3.3.3. Does tissue volume affect measured *D*? 58
3.3.4. Metabolic endpoints and range of measurable discrimination 60
3.4. Summary 61

4. Leaf total respiration and respiratory electron partitioning respond to different factors across nutrient gradients in the Franz Josef soil chronosequence 63

4.1. Introduction 64
4.2. Materials & methods 66
4.2.1. Field site description and harvest 66
4.2.2. Respiratory incubations 68
4.2.3. Discrimination, electron partitioning and respiration computations 69
4.2.4. Leaf tissue analysis 71
4.2.5. Statistical analysis 72
4.3. Results 74
4.3.1. Leaf traits 74
4.3.2. Respiratory measurements 79
4.3.3. AOX/COX protein concentration 83
4.4. Discussion 83

4.4.1. *R* scales with foliar N, τ_a scales with N/P 84
4.4.2. Cu and TNC (or Starch) also contribute to *R* 85
4.4.3. The influence of Cu may be mediated by AP activity 86
4.5. Summary 87

5. Nutrient deficiency reduces cytochrome *c* oxidase but not alternative oxidase activity in greenhouse-grown *Griselinia littoralis* 89

5.1. Introduction 90
5.2. Materials & methods 91
5.2.1. Plant material and growth conditions 91
5.2.2. Gas exchange measurements 91
5.2.3. Respiratory incubations 92
5.2.4. Discrimination, electron partitioning and respiration computations 93
5.2.5. Leaf tissue analysis 95
5.2.6. Statistical analysis 95
5.3. Results 97
5.3.1. Leaf traits 97
5.3.2. Photosynthesis and respiration 101
5.4. Discussion 105
5.4.1. Plant phenotype corresponded with anticipated treatment effects 105
5.4.2. Deficiency affected uptake and translocation of other minerals 106
5.4.3. Nutrient deficiency suppressed photosynthesis more strongly than respiration 106
5.4.4. Leaf AOX/COX but not electron partitioning responded to low N/P 107
5.4.5. Root CP but not AP activity declined in response to nutrient deficiency 108
5.4.6. How leaf response could be seen as similar to the root response 109
5.5. Summary 110

6. Respiratory flexibility and efficiency are affected by simulated global change in Arctic plants 111

6.1. Introduction 112
6.2. Materials & methods 114
6.2.1. Site description 114
6.2.2. Sampling procedure for respiratory incubations 115

6.2.3. Discrimination, electron partitioning and respiration computations 116
6.2.4. Leaf tissue analysis 117
6.2.5. Statistical analysis 118
6.3. Results 119
6.3.1. Community composition 119
6.3.2. Leaf traits 121
6.3.3. Respiration 127
6.3.4. Electron partitioning 127
6.3.5. Protein analysis 130
6.4. Discussion 131
6.4.1. Community composition was strongly affected by nutrient addition 131
6.4.2. Leaf physical and chemical traits responded similarly in all species 131
6.4.3. *Betula* increased electron partitioning to the cytochrome pathway in response to nutrient addition 133
6.4.4. Energy balance may explain the lack of partitioning response in *Rubus* ...133
6.4.5. Circumstantial evidence for respiratory acclimation 134
6.4.6. Plants grown in the light had higher AOX/COX concentrations 134
6.5. Summary 135

7. Thesis… synthesis 137

7.1. Overview 138
7.2. Novel methods, times three 138
7.2.1. Improving the dynamic range of CF-IRMS 138
7.2.2. The field-compatible method for measuring respiratory electron partitioning 139
7.2.3. Correcting for contamination and for nonlinearity in discrimination 141
7.3. Physiological insights 142
7.3.1. Benefits and drawbacks of ground-breaking field studies 142
7.3.2. Did plant nutrient stress lead to higher AOX activity or concentrations? .143
7.3.3. Does N/P drive respiratory electron partitioning? 143
7.3.4. Possible role for copper in respiration and AP activity. 145
7.3.5. The role of leaf carbohydrate status in regulating *R* and AP activity 146
7.3.6. The importance of energy balance in respiratory electron partitioning 146
7.3.7. Growth and maintenance respiration 147

7.4. Synthesis and conclusions 148
7.4.1. Is electron partitioning (τ_a) an appropriate physiological parameter? 148
7.4.2. Ecological advantages of respiratory flexibility? 149
7.4.3. My lasting contribution? 150

Literature cited 151

Appendices 163

Appendix 1. The cutting room floor 165

A1.1. The mobile mass spectrometer 165
A1.2. Hawkesbury experimental forest 165
A1.3. Gas leakage and/or oxidation of septa 165
A1.4. Proof of concept for my in-vial respiration measurements 166
A1.5. CN increases respiration rates despite being effective 166
A1.6. Temperature may affect measured *D* 166

Appendix 2. Supporting Information for Chapter 2 167

A2.1. Can isotope ratios be corrected using A_{28} and A_{32} directly? 167
A2.2. How Gasbench II responds to vial over- and under-pressure 168
A2.3. Variability introduced by the correction equations 169
A2.4. The need for two calibration standards 171
A2.5. Comparing Equation 8 with known equations 173
A2.6. A nonlinear regression/correction in δ values 175
A2.7. Area values for the minor isotope in ISODAT NT 175

Appendix 3. Supporting information for Chapter 3 176

A3.1. Table S3.1 Results of simulated respiration experiments. 176
A3.2. Supporting figures 177
A3.3. Miscellaneous technical notes 184
A3.3.1. Variable time *vs.* variable mass. 184
A3.3.2. Alternative CO_2 trap. 184
A3.3.3. Sample size, incubation time, and estimating O_2 consumption. 184
A3.3.4. Transfer solution. 184
A3.3.5. Determining in-vial respiration. 184
A3.3.6. Transfer contamination. 185

A3.3.7. Correcting both initial and leakage contamination in the long-term storage experiment....185
A3.3.8. Errors in variables....186
A3.4. Details and derivations of the discrimination calculations....187
A3.4.1. Derivation of the Rayleigh distillation equation....187
A3.4.2. Why we need O_2/N_2 rather than O_2 in calculating f....189
A3.4.3. Correcting $\delta^{18}O$ for initial contamination....190
A3.4.4. Correcting O^* for initial contamination....190
A3.4.5. Correcting $\delta^{18}O$ and O_2/N_2 when contamination is proportional to a gradient 191

Appendix 4. Supporting information for Chapter 4....193

A4.1. Supporting figures....193
A4.2. Supporting tables....195

Appendix 5. Supporting information for Chapter 5....197

A5.1. Supporting figures....197

Appendix 6. Supporting Information for Chapter 6....200

A6.1. Supporting table....200
A6.2. Supporting figures....201

Appendix 7. & 8. Published versions of Chapters 2 and 3....203

List of Tables

Table 2.1. Ratio of measurements with open split in "concentrating" mode (*in*) *vs* "diluting" mode (*out*) during two different sessions. 28
Table 3.1. Illustrated key to symbols and their relationships. 39
Table 3.2. Storage effects on "blank" vials stored for 10 months. 53
Table 3.3. Effects of tissue volume on computed *D*. 58
Table 3.4. Comparison of computed discrimination values, *D*, based on my method *vs.* previously published data. 59
Table 4.1. Franz Josef chronosequence site description and species sampled. 67
Table 4.2. Explanatory variables for respiration, R, electron partitioning, τa, and the activities of AP and CP, valt and vcyt, respectively. 81
Table 4.3. Activities of the AP, v_{alt}, and CP, v_{cyt} (nmol O_2 g DM^{-1} s^{-1}), for each species within each site. 82
Table 5.1. *D*, *R*, τ_a, v_{cyt}, and v_{alt} after 14 and 22 weeks of nutrient-deficiency treatments. 103
Table 6.1. AIC_c comparison of all valid combinations of species (S), nutrient addition (N) and Environment (E) effects. 122
Table 6.2. Leaf nitrogen and phosphorus content (mg g DM^{-1}) and N/P ratio (g N g P^{-1}). 124
Table 6.3. Two scenarios for calculating electron partitioning in *Betula nana* leaves. .. 129

Appendix Tables

Table S2.3. Overall variability in the corrected calibrations *vs.* instrument variability. p.169
Table S3.1. Results of simulated respiration experiments. ..... p. 176
Table S4.1. Measured discrimination values in respiratory inhibition experiments. p. 195
Table S4.2. Correlations between the variables measured at Franz Josef ..... p. 196
Table S6.1. Respiratory endpoint measurements in *Betula*, *Eriophorum*, and *Rubus*. p. 200

List of Figures

Fig 1.1. Schematic of the mitochondrial electron transport chain. 5
Fig 2.1. Sample mass spectrometer trace. 25
Fig 2.2. Nonlinearity in $\delta^{18}O$ values *vs* either (a) the measured peak area, A_{32}, or (b) the relative concentration of gas in the vial, F_{32}, which is adjusted for dilution effects of the open split. F_{32} is defined so that $F_{32,CCA} = 1$. 29
Fig 2.3. The regression curves for correcting nonlinearity in $\delta^{18}O_{meas}$ values (a), and the resulting correction (b). 30
Fig 2.4. The effects of dilution on measured F_{32}, F_{28} and $\delta O_2/N_2$ values. Calibration samples were diluted in either N_2 or He. 33
Fig 2.5. The corrected data, $\delta_{corr}O_2/N_2$, *vs*: (a) actual $\delta O_2/N_2$ values (He dilutions shown in grey), and (b) F_{28} (He dilutions only). 34
Fig 3.1. Simulated effects of D changing from 31 to 25‰. 49
Fig 3.2. Example of curvature in real data: KCN-treated soybean cotyledons. 51
Fig 3.3. Effects of initial contamination: (a, b) uncorrected data; (c, d) after correction. .54
Fig 3.4. Long-term storage effects on respiration samples: (a) uncorrected data (b) corrected data. 56
Fig 3.5. Tissue volume effects. 57
Fig 4.1. Structural leaf traits across the chronosequence sites. 74
Fig 4.2. Leaf N (a, b), P (c, d) and N/P (e, f) across sites and by species within sites (for species collected at more than one site). 76
Fig 4.3. Leaf Fe (a, b), Cu (c, d) and Fe/Cu (e, f) across sites and by species within sites (for species collected at more than one site). 77
Fig 4.4. Total nonstructural carbohydrates (TNC) and total soluble sugars by site (a) and by species collected at more than one site (b). 78
Fig 4.5. Respiration (a, b) and electron partitioning through the alternative pathway, τ_a (c, d), across sites. 79
Fig 4.6. (a) Foliar N *vs.* R and (b) foliar N/P *vs.* τ_a. 80
Fig 4.7. Western blot analysis. 83
Fig 5.1. (a) Dry mass, (b) dry matter content (DMC), and (c) specific leaf area (SLA) for new leaves, old leaves. 98
Fig 5.2. Leaf N (a), P (b) and N/P (c) for new leaves, old leaves, and roots. 99

Fig 5.3. Total nonstructural carbohydrates and sugars for new leaves, old leaves, and roots. 100
Fig 5.4. Photosynthetic capacity, A_{sat}, (a); respiration on a fresh mass basis, R_{FM}, (b); and electron partitioning through the alternative pathway, τ_a, (c), for new leaves, old leaves, and roots..... 101
Fig 5.5. Western blot response: (a) AOX/COX, (b) Porin, (c) sample blot for leaf tissue. 104
Fig 6.1. Effects of fertilization, light, and temperature modification on Alaskan tundra plant communities after 10 and 20 years. 120
Fig 6.2. Leaf dry matter content (a–c) and specific leaf area (d–f) for the three species examined: (a, d) *Betula*, (b, e) *Eriophorum*, (c, f) *Rubus*. 123
Fig 6.3. Starch, sugars, and total nonstructural carbohydrates (TNC = starch + sugars) for the three species examined: (a) *Betula* , (b) *Eriophorum*, (c) *Rubus*. 125
Fig 6.4. Respiration at 20 ºC on a leaf-mass basis, R_{20}, (a –c), and respiratory discrimination against ^{18}O in three species (d–f). 126
Fig 6.5. Respiration (a) and respiratory discrimination against ^{18}O (b) in *Betula* leaves and stems incubated separately..... 128
Fig 6.6. Western blot analysis of (a, c) *Betula* leaves and (b, d) *Eriophorum* leaves. 130

Appendix Figures

Fig S1.1. Proof of concept for my in-vial respiration measurements ..... p. 166
Fig S2.1. How Gasbench II responds to vial over- and under-pressure ..... p. 167
Figure S2.2. Can isotope ratios be corrected using A28 and A32 directly? ..... p. 168
Figure S3.1. Estimating vacuum quality based on transfer-syringe displacement. . p. 177
Figure S3.2. Estimating O_2 consumption by syringe displacement. ..... p. 177
Figure S3.3. Images of tissue volume effects treatments. ..... p. 178
Figure S3.4. Curvature may be difficult to see. ..... p. 179
Figure S3.5. Statistical power to detect curvature..... p. 180
Figure S3.6. Computed *D* as a function of maximum O_2 consumption ..... p. 181
Figure S3.7. Standard error of the regression versus total O_2 consumption..... p. 181

Figure S3.8. Error in computed *D* versus actual *D* due to various degrees of uncorrected contamination ..... p. 182

Figure S3.9. Changes in total pressure and partial pressures of N_2 and O_2 during a respiration experiment and subsequent storage. ..... p. 182

Figure S3.10. Measured changes in partial pressures of N_2 and O_2 during respiratory incubations (uncorrected for contamination). ..... p. 183

Fig S4.1. Histograms of (a) the AIC_c best-model *P* values, (b) uncorrected model-averaged *P* values and (c) model-averaged corrected *P* values. ..... p. 193

Fig S4.2. Changes in measured O_2 discrimination, *D* at Franz Josef. p. 194

Fig S5.1. Stomatal conductance (g_s) was strongly correlated with net photosynthesis (A). ..... p. 197

Fig S5.2. Respiration on a dry mass in the *Griselinia* nutrient manipulation. ..... p. 197

Fig S5.3. (a) "raw" discrimination, *D*, in *Griselinia* leaves and roots. (b) Osmocote *vs.* water ..... p. 198

Fig S5.4. Respiration *vs.* leaf N concentration in (a) new leaves, (b) old leaves, and (c) roots. ..... p. 199

Fig S6.1. Discrimination (D) *vs.* respiration (R_{20}), showing lack of correlation ..... p. 201

Fig S6.2. Relative cover of treatment plots at the Arctic LTER in 2007. ..... p. 201

List of Abbreviations

A	assimilation (net photosynthesis)
ADP	adenosine diphosphate
AOX	alternative oxidase
AP	alternative (respiratory) pathway
ATP	adenosine triphosphate
CCA	Christchurch clean air (the reference standard for $\delta^{15}N$, $\delta^{18}O$, and $\delta O_2/N_2$ values)
CF-IRMS	continuous flow isotope ratio mass spectrometry
CHO	carbohydrate
COX	cytochrome c oxidase
CP	cytochrome (respiratory) pathway
Cu	copper
D	discrimination
DM	dry mass
DMC	dry matter content (DM/FM)
EDTA	ethylenediaminetetraacetic acid
ETC	electron transport chain
δ	(Greek "delta") relative difference of isotope ratios
$\delta^{15}N$	relative difference of $^{15}N/^{14}N$ compared to the corresponding atmospheric isotope ratio.
$\delta^{18}O$	relative difference of $^{18}O/^{16}O$ compared to the corresponding atmospheric isotope ratio.
$\delta O_2/N_2$	relative difference of $^{32}O_2/^{28}N_2$ compared to the corresponding atmospheric isotope ratio.
Fe	iron

FM	fresh mass
HCN	cyanide
He	helium
HEPES	4-(2-hydroxyethyl)-1-piperazineethanesulfonic acid
HSD	honestly significant difference (Tukey's HSD statistical test)
IRMS	isotope ratio mass spectrometry
KCN	potassium cyanide
LTER	long-term ecological research
N	(mineral) nitrogen
N_2	molecular nitrogen
NAD^+	nicotinamide adenine dinucleotide (oxidized)
NADH	nicotinamide adenine dinucleotide (reduced)
ND_x	external NADH dehydrogenase
^{x}O	(x = 16, 17, 18) oxygen isotopes
O_2	dioxygen (molecular oxygen)
$^{32}O_2$	dioxygen composed of $^{16}O^{16}O$
$^{34}O_2$	dioxygen composed of $^{18}O^{16}O$
P	phosphorus
PAR	photosynthetically active radiation
Q	ubiquinone pool
Q_{10}	quotient of respiration at temperatures 10 ºC apart
R	respiration
^{x}R	isotope ratio of the amount of isotope with molecular mass x divided by the amount of the major isotope
r^2	Pearson's product-moment correlation coefficient
SD	standard deviation

SDS	sodium dodecyl sulfate
SE	standard error of the mean
SHAM	salicylhydroxamic acid
SLA	specific leaf area (area/mass)
TCEP	*tris*(2-carboxyethyl)phosphine
Tris	*tris*(hydroxymethyl)aminomethane
UC	University of Canterbury
UCP	uncoupling protein

Abstract

RATIONALE: Recent studies indicate that plants can partition electron transport through alternative oxidase (AOX) and cytochrome *c* oxidase (COX) in response to environmental cues, thus modulating respiratory efficiency. The ^{18}O discrimination method necessary for measuring electron partitioning *in vivo*, however, has been restricted to laboratory settings due to equipment constraints. Since plants grown in more natural and variable environments may not respond as predicted by laboratory experiments, I developed a new field-compatible analytical method and then applied it to three ecophysiological studies.

METHODS: To address these needs, I developed a field-compatible method in which plant tissue was incubated in 12 mL septum-capped vials for 0.5 – 3 h, after which the incubation air was transferred to 3.7 mL storage vials for subsequent measurement by mass spectrometry. I also developed mathematical tools to correct for unavoidable contamination, and to detect and address curvature in the data – whether intrinsic to the respiration or due to contamination, – and to extend the usable dynamic range of the mass spectrometer. These methods were used to investigate respiratory responses (1) in canopy trees growing across a soil nutrient gradient at the Franz Josef chronosequence, New Zealand; (2) in a nutrient manipulation experiment of *Griselinea littoralis*; and (3) in a long-term nutrient-, temperature-, and light manipulation at Toolik, Alaska, USA. Leaf dry matter content, specific leaf area, nitrogen (N), phosphorus (P), sugars, starch, and AOX/COX protein concentrations were also measured as explanatory variables. (Leaf Cu and Fe were measured at the Franz Josef chronosequence.)

RESULTS: Discrimination values computed using my methods replicated previously reported results over a range of 10 – 31‰, with precision generally better than ±0.5‰, thus demonstrating its validity as tool for measuring respiratory electron partitioning. Foliar respiration declined with site age across the soil chronosequence, increasing with leaf N levels, r^2 = 0.8, but electron partitioning declined with increasing N/P, $r^2 = 0.23$. AP activity was positively correlated with leaf P, Cu, and starch, $r^2 = 0.71$. In younger

soils, however, declines in respiration were attributed to declines in cytochrome pathway (CP) activity, whereas across the older sites respiration declined due to a reduction in AOX pathway (AP) activity. The *Griselinia* nutrient-manipulation experiment partially confirmed these results: AOX protein levels were highest in N-deficient plants rather than in plants deficient in both N and P. AP activity was very low in all leaves, however, possibly due to low illumination. In support of this claim, leaves that had developed in the sun had higher AOX/COX protein ratios than those that had developed in the greenhouse. In *Griselinia* roots, CP activity declined by more than half in response to nutrient deficiency, whereas AP activity was unchanged. At the Arctic site, only one species changed electron partitioning in response to nutrient addition. *Betula nana*, the most successful adapter to improved mineral nutrition, doubled leaf CP activity without changing AP activity. Species grown in full sun at that site also had higher AOX/COX protein ratios than those that grew in enclosures.

CONCLUSIONS: This is the first study of how engagement of terminal respiratory oxidases in plants responds to multiple nutrient deficiencies, both in nature and in a controlled environment. I have uncovered some intriguing relationships, including the possible importance of N/P to electron partitioning, as well as a role for Cu. The results also suggest that electron partitioning is sensitive to plant energy balance, as suggested by the low AP activities and low AOX/COX protein ratios in shaded plants. Perhaps most significantly, the AP and CP appeared to act independently of each other, rather than through a concerted "partitioning" process. In addition to their own scientific merit, these results illustrate the value of using the new field-compatible method to conduct ecophysiological investigations of plant respiratory electron partitioning on a much large scale, and under more realistic conditions, than has been previously possible.

1. Introduction and overview

The primary goal of this project has been to help elucidate how plant respiratory metabolism responds to environmental stress under field conditions. At the outset, however, no method was available for performing the necessary measurements in the field, so a substantial part of my effort went into developing and validating a new field-portable measurement method (the subject of Chapter 3). This method, in turn, tested the limits of our new mass spectrometry facility and I therefore had to develop new methods for extending the equipment's usable range to accommodate my needs (Chapter 2). In order to motivate this research project, the topics are presented here in reverse of the subsequent chapter odrer: I start with the ecophysiological underpinnings of this project, which then motivates the need for justifying the new field-compatible isotopic methods and issues of mass spectrometry. The introduction concludes with a brief summary of the motivations behind this project and an overview of the rest of this manuscript.

1.1. THE ECOPHYSIOLOGY OF ALTERNATIVE OXIDASE (AOX) AND CYTOCHROME *C* OXIDASE (COX)

Plant respiration releases 50-60 gigatons of carbon into the atmosphere – 10 times as much carbon as from anthropogenic sources (Gifford, 2003). Although photosynthesis may absorb around as much carbon as is released, small shifts in the relationship between the two processes could result in dramatic shifts in the amount of carbon released into the atmosphere, with possible consequences for global climate change. In particular, Valentini et. al. (2000) found that differences in respiration, rather than in photosynthesis, accounted for differences in carbon balance in forest ecosystems across Europe. The amount of CO_2 released by plants relative to photosynthetic assimilation can vary substantially depending on species and growth conditions (Atkin, Scheurwater & Pons, 2007, Millenaar & Lambers, 2003). A better understanding of the physiology of plant respiration and how it responds to environmental change, whether due to nutrition, temperature, drought, or otherwise, may therefore help us to better predict and manage future climate change. The focus of this manuscript is on nutrient stress, which affects plants globally both agriculturally and in the wild (Aerts & Chapin, 2000, Vance, Uhde-Stone & Allan, 2003) but to introduce the topic I must start with a general discussion of the function and regulation of mitochondrial respiration.

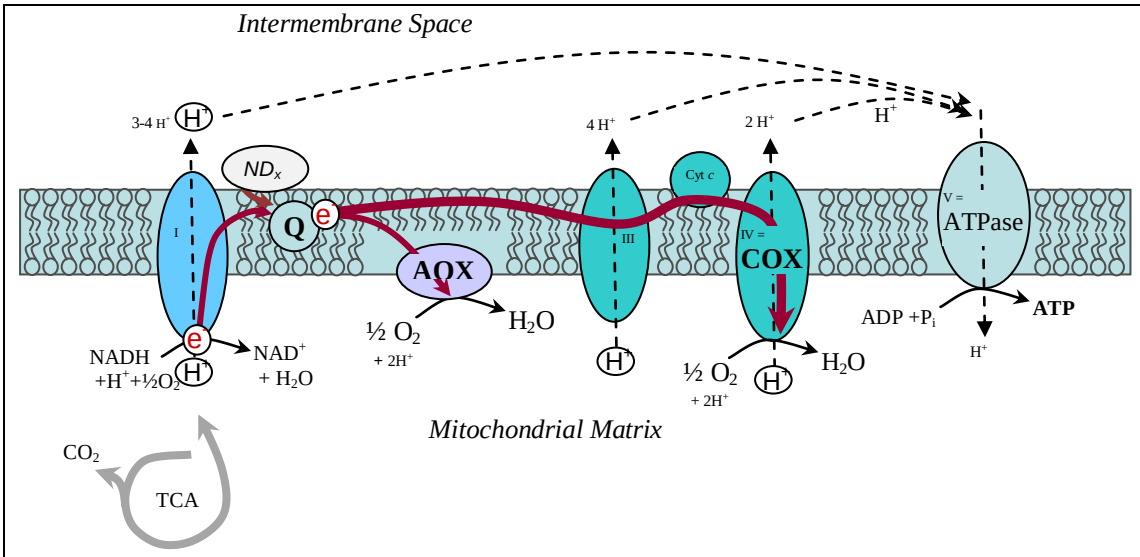

Fig 1.1. Schematic of the mitochondrial electron transport chain.

AOX: alternative oxidase; ATPase: ATP synthase; TCA: tricarboxylic acid cycle; COX: cytochrome *c* oxidase; ND_x: external NAD(P)H dehydrogenase; Q: ubiquinone pool. Thick (red) arrows indicate the flow of electrons through the electron transport pathway; dashed arrows indicate the flow of protons.

1.1.1. Mitochondrial function

Respiration is the powerhouse of life, providing both energy and metabolic substrates necessary for growth and maintenance of living tissue. The general process of respiration is well-known, but its particulars are still subjects of a very active field of research (Lambers, Robinson & Ribas-Carbo, 2005, Millar *et al.*, 2011, Millenaar & Lambers, 2003, Plaxton & Podesta, 2006, Rhoads & Subbaiah, 2007). Plant respiration oxidizes carbohydrates produced by photosynthesis into CO_2 and water, capturing metabolically-availably energy in the forms of adenosine triphosphate (ATP) and of reducing equivalents such as NADH. The first step of the process, glycolysis, partially oxidizes sugars to produce organic acids – particularly pyruvate and malate – in the cytosol or in plastids, resulting some ATP and NADH production (Plaxton, 1996). The bulk of oxidation and ATP production, however, is completed aerobically in the mitochodria through the tricarboxylic acid (TCA) cycle and electron transport chain (ETC; Fig 1.1). In this process the organic acids are fully oxidized to CO_2 by the TCA cycle, producing reductants such as NADH as part of the process. Electrons from these reducing equivalents are passed through the ETC, a series of membrane-bound proteins, which pumps protons (H^+) out of the mitochondrial matrix before ultimately completing the redox reaction by reducing O_2 to to H_2O. The energy in the proton gradient produced

by the ETC drives the synthesis of ATP from ADP. In this 'conventional' ETC flow, shared by plants and animals, O_2 is reduced by cytochrome *c* oxidase (COX). Plants, however, have an alternative pathway (AP) through the ETC, terminated by alternative oxidase (AOX), which bypasses several or all of the ETC proton pumps, thus reducing O_2 to water without much ATP production. The excess energy not stored in ATP is lost as heat, thus reducing respiratory energy efficiency. Some thermogenic plants use this side-effect to increase their temperature and volatilize chemicals that attract pollinators, a function that was recognized as early as the 1930s (Meeuse, 1975). Nevertheless, all plants examined to-date contain AOX, whether or not they are thermogenic. A broader view of respiration is therefore needed in order to understand the potential benefits of the apparently wasteful AP.

The primary role of respiration may well be energy production, considering that 30 – 70% of CO_2 assimilated by plants is respired back as CO_2 on a daily basis (Millenaar & Lambers, 2003). Nevertheless, respiration, particularly in the mitochondria, serves a multitude of functions. Intermediates of the TCA cycle are used as carbon skeletons for building molecules essential to growth as well as for the production of secondary metabolites. For example, citrate is a critical component of ammonium assimilation metabolism, requiring as much as 50% of net plant carbon (Huppe & Turpin, 1994). Citrate is produced early in the TCA cycle, but not before some reducing equivalents (and CO_2) have been produced. Root exudates also consume TCA cycle intermediates. Nutrient-deficient roots can exude as much as 25% of plant dry mass in the form of citrate and malate, in order to free essential nutrients from the soil matrix (Vance *et al.*, 2003). In such cases, the plant may need to oxidize NADH irrespective of metabolic energy needs simply to regenerate the NAD^+ needed to produce these TCA intermediates.

Mitochondria also play an essential role in maintaining plant energy balance, through direct and indirect interaction with chloroplast processes. Byproducts of photorespiration are oxidized in the mitochondria, producing NADH that can feed into the ETC. Under high light stress, reducing equivalents produced in the choloroplast may also be directly exported to the mitochondrial ETC via an external NADH dehydrogenase (ND_x, Fig 1.1), thus serving to protect the chloroplast from damage by reactive oxygen species (Yoshida, Terashima & Noguchi, 2007, Yoshida *et al.*, 2011). The mitochondrial ETC is, itself, a substantial source of membrane-damaging reactive oxygen species (ROS). When substrate supply levels are high (too much photosynthesis) or the

cytochrome pathway is restrained, the plant may need to safely consume excess reducing power as a protective measure to reduce ROS production, irrespective of metabolic energy needs (Millenaar & Lambers, 2003).

This multitude of needs implies the need for a carefully regulated system, which remains an active field of research. Here I describe some aspects of regulation related to the activation of the AP relative to the CP.

1.1.2. Mitochondrial regulation

Metabolically, AOX and COX compete for electrons in the ubiquinone pool (Fig 1.1). Several factors help determine the relative success of each pathway: enzyme concentrations may be regulated through gene expression, the enzymatic activities may be altered by the presence or absence of metabolic co-factors, or due to downstream inhibition of either pathway.

Numerous factors have been shown to regulate AOX gene expression in response to biotic and abiotic stress, especially oxidative stress (Ederli *et al.*, 2006, Feng *et al.*, 2010, Hachiya & Noguchi, 2011). Nutrient deficiency has also been associated with increased AOX levels and transcripts (Gonzalez-Meler *et al.*, 2001, Noguchi & Terashima, 2006, Watanabe *et al.*, 2010). In the case of nitrogen deficiency, allocating more resources to the smaller AOX pathway instead of the much larger COX pathway (CP) may conserve scarce nitrogen resources (Noguchi & Terashima, 2006). Total AOX concentrations, however, do not necessarily imply increased AOX activity (Florez-Sarasa *et al.*, 2009, Millenaar *et al.*, 2001).

Instead, metabolic factors may be the primary regulators of AOX activity. Regulatory factors include the protein's redox state, the redox poise of the mitochondrial ubiquinone pool, and the presence of α-keto acids such as pyruvate. These factors are not necessarily independent of each other. For example, AOX can exist as inactive covalently-bonded (oxidized) dimers or as active non-covalently bonded (reduced) pairs (Umbach & Siedow, 1993). Increased redox poise of the ubiquinone pool may therefore providing the reducing power needed to break the covalent bonds, thus providing an natural link between ROS risk and AOX activation (Hoefnagel & Wiskich, 1998, Millenaar *et al.*, 1998). In plants, for example, activation of AOX under high illumination appears to be regulated by the protein's redox state (Noguchi *et al.*, 2005). AOX has also been found to help decrease chloroplast membrane over-reduction by accepting reducing

equivalents through the mitochondrial external NADH dehydrogenases (Yoshida *et al.*, 2007, Yoshida *et al.*, 2011). There is also evidence of control by a cytosolic thioredoxin pathway that appears to be particularly targeted AOX and can chemically reduce AOX to its more active state (Gelhaye *et al.*, 2004). While redox regulation of AOX due to overreduction is easily understood, redox state appears to have other functions as well, such as during plant development (Lennon *et al.*, 1995)

Pyruvate is also a strong activator for AOX. For example, cell mitochondrial extracts show little AOX activity until pyruvate is added (Carre, Affourtit & Moore, 2011, Hoefnagel *et al.*, 1995, Juszczuk, Wagner & Rychter, 2001b). Pyruvate is a precursor to the citric acid cycle. Thus anything that may block downstream processes – adenylate restriction, for example – may result in an accumulation of pyruvate that would increase AOX activation. The role of pyruvate *in vivo* has been questioned recently, however, since the concentrations needed to activate AOX are considerably lower than typically found in intact plant cells (Millenaar & Lambers, 2003). Nevertheless, increased cellular carbohydrate status may serve directly to up-regulate the alternative pathway as a way to consume excess carbohydrates and maintain carbon balance when growth is limited by factors such as nutrient availability (Sieger *et al.*, 2005).

The relative activities of the two electron transport pathways may also be influenced by processes that block the other pathway. In laboratory settings it is well-established that inhibiting one pathway with selective respiratory toxins can increase activity of the other pathway even beyond the initial O_2 consumption rates (Day *et al.*, 1996, Meeuse, 1975, see also Appendix 1.5). In nature, the COX pathway may be inhibited by downstream restrictions. For example, phosphorus deficient cells may lack sufficient ADP to support ATP synthesis (Gonzalez-Meler *et al.*, 2001). This backlog would cause a proton buildup outside the mitochondrial membrane that would reduce the activity of the proton pumps including COX (Fig 1.1). Since AOX is not restricted by these proton pumps it can continue to operate unimpeded under such conditions. Conversely, AOX may be inhibited at low O_2 pressures due to its relatively low affinity for oxygen (Millar, Bergersen & Day, 1994), a condition that might apply in roots under anoxic conditions (Szal *et al.*, 2003).

Finally, it should be mentioned that AOX appears to be controlled by signaling molecules such as salicylic acid, ascorbic acid, and ethylene, as well (Lei *et al.*, 2010, Talla *et al.*, 2011, Zhu *et al.*, 2011).

1.1.3. Ecophysiological perspective

If a plant grows in an energy-rich (bright) environment that is deficient in some other way that restricts growth, it may not benefit from conserving energy at all costs. The overarching theme of the regulatory mechanisms just discussed is that AOX helps the plant in adapting to environmental stress by providing a safe outlet for excess energy charge. Laboratory studies confirm that AOX plays a role in plant stress responses including nutrient deficiency (Hachiya *et al.*, 2010, Juszczuk *et al.*, 2001b, Noguchi & Terashima, 2006), drought (Bartoli *et al.*, 2005, Costa *et al.*, 2007), flooding (Szal *et al.*, 2003), temperature extremes (Armstrong *et al.*, 2008, Atkin, Zhang & Wiskich, 2002), strong light (Florez-Sarasa *et al.*, 2011, Yoshida *et al.*, 2011), elevated CO_2 (Bruhn, Wiskich & Atkin, 2007, Gonzalez-Meler *et al.*, 2009) allelochemical attack (Kraus & Lambers, 2001, Penuelas, Ribas-Carbo & Giles, 1996) and herbicides (Gaston *et al.*, 2003). While such activity would benefit the plant, it may reduce a service humans have come to expect from plants. Sieger et al. (2005) demonstrated that increased AOX respiration reduces plant carbon use efficiency, and may therefore affect a plant's ability to sequester carbon from the atmosphere.

The above studies, however, have been limited to laboratory settings – largely due to constraints set by the measurement apparatus – leaving open the important question of how well such laboratory findings represent the response of plants growing under field conditions, which can be either more variable or longer-term than experienced under laboratory conditions. In the next two sections I therefore discuss how electron partitioning has been measured and, in particular, why it has necessitated the development of a new method for measuring respiration in field studies.

1.2. STABLE ISOTOPES IN ECOPHYSIOLOGY AND PLANT RESPIRATION

Here I provide a brief overview of isotopes in ecology, which provides the context for discussing the historical development of, and the issues related to measuring respiratory electron partitioning.

Stable isotopes have been a boon for ecophysiologists. Isotopes can be used as tracers by exposing a plant to inputs that differ in isotopic composition from background source. A much more versatile approach arises from the fact that differences in mass between isotopes of a single molecule can affect chemical kinetics of those isotopes.

Enzymatic reactions with heavier isotopes may be 1–3% slower than for the corresponding lighter isotopes (Dawson *et al.*, 2002). In biological systems, the actual rate of fractionation (aka discrimination) may vary with environmental conditions or due to competition between enzymes that fractionate at different rates, resulting in differences in the isotopic composition of plants relative to their source molecules. The plant itself, therefore becomes a record of the cumulative effects of otherwise transient ecological and physiological processes such as photosynthetic performance, water use efficiency, and growth temperature (Dawson *et al.*, 2002). Here, however, I measure the fractionation rates in real time, as fractionation is happening. AOX and COX differ in the rate at which they discriminate against heavier O_2 molecules. The product of respiratory O_2 consumption, water, is not easily tracked because it is rapidly diluted in the cytosol. Instead, the effects on the air surrounding the plant are measured. As the lighter isotope is removed preferentially by plant respiration, the surrounding air is enriched in the heavier isotope. The extent of enrichment is determined by the relative activities of the two oxidases. COX favors $^{16}O^{16}O$ (hereafter referred to as $^{32}O_2$) with a 20‰ (i.e. 2%) faster rate of reaction than for $^{18}O^{16}O$ ($^{34}O_2$), whereas AOX reduces $^{32}O_2$ 30‰ more rapidly.

If plant tissue respires in a closed container, then as O_2 is consumed the remaining air becomes increasingly enriched in $^{34}O_2$, in a process is similar to the kinetics of distillation first described by Lord Rayleigh (1902). The isotope ratio $^{34}R = {}^{34}O_2/{}^{32}O_2$ as a plant respires in a closed system increases as a power of the proportion of $^{32}O_2$ removed:

$$ {}^{34}R = {}^{34}R_0 \left(\frac{{}^{32}O_2}{{}^{32}O_{2,0}} \right)^{(\alpha-1)}, \qquad (1.1) $$

where the subscript 0 refers to the initial amount of the analyte and the term α is the ratio of the rates of reaction for $^{34}O_2$ *vs.* $^{32}O_2$. The rate of $^{34}O_2$ reduction is slightly slower than for $^{32}O_2$, making the exponent in Eqn (1.1) slightly negative. Biologist prefer to make the sign explicit by substituting $-D = \alpha - 1$ into Eqn (1.1), where D is referred to as the respiratory discrimination rate.

Eqn (1.1) can be used for linear regression by rearranging the terms into:

$$ \ln\left(\frac{{}^{34}R}{{}^{34}R_0} \right) = -D \ln\left(\frac{{}^{32}O_2}{{}^{32}O_{2,0}} \right), \qquad (1.2) $$

where *D*, the unknown respiratory discrimination value. Thus, if one collects a series of air samples representing increasing amounts of respiratory O_2 consumption, one can determine *D* by linear regression based upon the isotopic composition of those O_2 samples (Guy *et al.*, 1989, Robinson *et al.*, 1995).

Measured discrimination values can be converted into physiological terms by comparing them to measured "endpoints" representing the discrimination rate of each terminal oxidase. Thus, for example, if upon testing, AOX discriminated against $^{34}O_2$ at 30‰ and COX discriminated at 20‰, whereas a particular plant sample discriminated at 21.5‰, then, by linear interpolation, AOX O_2 consumption represented 15% of the total respiratory activity while COX consumed 85% of the O_2. In order to use this method successfully, one must be able to collect air samples from the closed container in which the plant tissue had been respiring, and to subsequently measure the O_2 isotope ratios accurately. In the next section I discuss previous approaches to these measurements and why I needed to develop a new method in order to take it into the field.

1.3. A BRIEF HISTORY OF RESPIRATORY ELECTRON PARTIONING MEASUREMENT

Historically, AP/CP partitioning was studied through the application of selective respiratory inhibitors. However, difficulties in accounting for the range of the inhibitor effects motivated the development of ^{18}O-discrimination methods (Guy *et al.*, 1989, Robinson *et al.*, 1995). Day *et al.* (1996) argued that the newly introduced stable isotope technique measured *in vivo* partitioning of respiratory electrons more reliably – a view that is now widely accepted (Ribas-Carbo, Robinson & Giles, 2005a). As described in the previous section, the method relies on the fact that AOX and COX discriminate against heavier oxygen isotopes (e.g., $^{34}O_2$) to different extents (Guy *et al.*, 1989). Published methods analyzed air samples that were sequentially withdrawn from a sealed incubation cuvette (Ribas-Carbo *et al.*, 2005a). Consequently, samples had to be small relative to the cuvette volume – typically 100 µL samples from cuvette volumes of 3–7 mL (Gaston *et al.*, 2003, Noguchi *et al.*, 2001, Robinson *et al.*, 1995). While the cuvette size allowed small quantities of plant material to be incubated relatively quickly – typically 0.2 to 2 g fresh mass measured over 1 to 4 h –great care was needed to avoid contamination, since even minute amounts of contamination would represent a large proportion of the sample. Cuvettes were therefore attached either directly to the mass spectrometer (Gaston *et al.*,

2003, Robinson *et al.*, 1995) or to a custom-built apparatus for storage of the gas in molecular sieves under vacuum (Noguchi *et al.*, 2001). Neither approach is sufficiently portable to allow quantification of AOX activity in the field, thus critically limiting one's ability to investigate this important aspect of plant response to changing environmental conditions along temporal and spatial environmental gradients or at remote locations.

A method suitable for experimental field trials and for broad-scale ecological surveys is therefore needed. Such an approach must be field portable, tolerate small amounts of contamination, enable relatively rapid processing of large numbers of samples, and allow the incubation air samples to be stored for some time before isotopic analysis. Contamination issues can be reduced by withdrawing larger air samples, but the consequent increase in incubation headspace necessitates longer incubation times, more plant material, and/or reduced numbers of samples per incubation (Angert & Luz, 2001, Nagel, Waldron & Jones, 2001). Thus, the challenge remains as to how best to minimize impacts of contamination while maximizing sample processing speed and efficiency.

In Chapter 3 I describe a new approach in which the incubation cuvette is kept small (a 12 mL vial) but only one sample, consisting of the entire headspace, is withdrawn thus maximizing sample volume relative to cuvette volume. Replicates consist of sets of incubations in which subsamples of the same plant material consume different amounts of O_2 (by varying either tissue amount or incubation time). Incubations can be conducted in parallel, thus allowing data points for several replicates to be collected in a relatively short period of time (2-6 h). Some contamination is inevitable with this approach, and I therefore also developed methods for estimating and correcting sample values for the extent of contamination.

1.4. THE DIFFICULTY IN MEASURING CONTAMINATION

While the mathematics for correcting contamination is relatively simple (Chapter 3), actually measuring the contamination can be technically daunting. Contamination is measured by preparing "blank" samples using O_2-free gas. The small amount of contaminating air in these vials can be as low as 1% of atmospheric air. In order to measure these samples accurately, the mass spectrometer must therefore have a 100-fold dynamic range. Isotope-ratio mass spectrometry (IRMS) instruments generally exhibit nonlinear responses over such ranges (Spotl & Vennemann, 2003, Werner, Rothe & Brand, 2001).

Formal mathematical linearity corrections have been developed for other types of mass spectrometry (Cappellin *et al.*, 2011) but I am not aware of similar methods applicable to continuous-flow IRMS. Instead, I developed an empirical method that, unlike the previous methods, does not assume that the correction is additive. The method treats the mass spectrometer as a black box, with all gas standards introduced to the instrument in the same way as unknown samples. The nonlinearity correction therefore avoids the need to characterize properties of each component of the measurement system. To further maximize dynamic range I also explored the effects of manipulating the sample open split, which in turn required additional mathematical attention. The corrected signal, with open split adjustments, provided the 100-fold dynamic range needed to support the contamination measurements, and thus completed the prerequisites needed for measuring plant respiratory discrimination in field samples.

1.5. MOTIVATION FOR THE PRESENT STUDY

Nutrient limitations reduce plant productivity globally both in agriculture and in the wild (Aerts & Chapin, 2000, Vance *et al.*, 2003). These limitations may be exacerbated by global climate change as changing temperature and precipitation patterns may release previously inaccessible nutrients or remove nutrients by increased leaching. In the Arctic tundra, for example, warming trends are expected to release nutrients as well as CO_2 currently locked in permafrost (Chapin *et al.*, 1995). Depending on how plants respond, the tundra may become a net source or sink for atmospheric CO_2 (Hobbie, Nadelhoffer & Hogberg, 2002). Warming or increased atmospheric CO_2 may have indirect effects as well, by creating relative nutrient deficiencies due to increased potential growth rate. What was a sufficient nutrient level for lower potential growth rate may be insufficient to support faster growth. Thus the plant is now nutrient-stressed. Even without impending global climate change plant-nutrient interactions are globally important, but with impending global change it behooves us even more to understand how these systems work and, if possible, incorporate the knowledge into predictive models and management practices. I do not expect the work in this project to shed light directly on global change, but I do believe it is an important step in understand plant respiration, which itself is an important factor in the global carbon cycle, as outlined above.

My PhD project has two distinct components: the development of novel methods for measuring plant respiratory electron partitioning in the field (Chapters 2 & 3), and the

application of these methods to three ecophysiological experiments (Chapters 4–6). I examined respiratory partitioning at two fields sites and in a greenhouse manipulation. Chapter 4 discusses an investigation of the Franz Josef chronosequence, a set of forested sites along the western coastal strip of the South Island of New Zealand. Retreat of the nearby Franz Josef glacier has created soils up to 120,000 years old. Soil nitrogen (N) and phosphorus (P) levels change in distinctive but differing patterns with the soil age (Richardson *et al.*, 2004), resulting in various combinations of nitrogen and/or phosphorus deficiency. In order to test hypotheses generated by the Franz Josef data, I subsequently conducted a factorial N- and P-deficiency experiment in a glasshouse on campus at the University (Chapter 5). Chapter 6 describes my investigations at a 20-year field-manipulation of Arctic tundra near Toolik, Alaska, USA, in which plots were fertilized, shaded, and/or warmed to simulate predicted effects of global change on plant growth and community composition (Chapin *et al.*, 1995).

Based on the previously cited laboratory studies, I formulated several hypotheses.

1. AP partitioning will be higher in plants growing in stressful conditions. Nitrogen and phosphate deficiency have been shown, in laboratory studies, to increase capacity or activity of the alternative pathway. Generally these studies look at only two states: stressed and nonstressed. Here I have examined plants that have grown under several levels of long-term nutrient stress and thus can establish a more realistic picture of AOX engagement due to stress.

2. AOX concentration will be higher in plants growing under long-term stresses such as nutrient deficient soils.

3. Furthermore combined stress, such as nitrogen and phosphate deficiency may result in stronger activation of the alternative pathway, especially if the enhancement effect on AOX is due to effects on different parts of the pathways.

2. Correcting for nonlinearity effects of CF-IRMS across a wide dynamic range

---

A version of this chapter has been published in Rapid Communications in Mass Spectrometry *(Kornfeld et al., 2012b) and is included as Appendix 7.*

2.1. INTRODUCTION

This chapter describes a novel solution to two problems I encountered while performing the measurements needed for determining respiratory electron pathway discrimination against $^{34}O_2$. The first difficulty, discussed briefly in the previous chapter (Section 1.4), was to be able to measure O_2 at concentrations varying by two orders of magnitude. The second problem relates to the way I measured oxygen consumption, which required the determination of O_2/N_2, as will be described in the following chapter. In addition to the differences in concentration, the O_2/N_2 ratio also varied over a very wide range of isotope ratio values. The solutions described here, however, can be applied in more contexts than just respiratory electron partitioning and I therefore start with a brief discussion of their general relevance.

Many applications of isotope ratio mass spectrometry require the measurement of samples at varying concentrations. For example, environmental studies of dissolved O_2 have examined waters of varying dissolved [O_2] (Barth, Tait & Bolshaw, 2004, Roberts, Russ & Ostrom, 2000). Likewise, studies of kinetic fractionation due to consumption of a sample gas such as O_2 require $\delta^{18}O$ values to be measured over a range of O_2 concentrations whether for biological processes such as plant respiration (Guy *et al.*, 1989) or abiotic oxidation (Oba & Poulson, 2009). In field studies, contamination in gas storage vials may need to be measured by filling "blank" vials with analyte-free gas (Cambaliza *et al.*, 2009). When measuring isotopes of disparate molecules, the range of isotope ratios may also be quite wide. For example, applications measuring $^{32}O_2/^{28}N_2$ as O_2 is consumed by biological processes may measure the ratio over ranges upward of 500‰ (Emerson *et al.*, 1999, Henry *et al.*, 1999). This wide range of concentrations and isotope ratios may exacerbate systematic measurement errors due to nonlinearities in the instrumentation. I therefore investigated ways to mathematically correct nonlinearities of the signal-response curve in continuous flow isotope ratio mass spectrometry (CF-IRMS).

Ideally, the mass spectrometer signal would be exactly proportional to the amount of analyte, in which case measured isotope ratios would be independent of absolute concentration. In practice, however, the signal response is not strictly proportional to the analyte concentration, and the ratio of two signals therefore depends on absolute concentration (Barth *et al.*, 2004, Merritt & Hayes, 1994). Conventional solutions to such nonlinearities include (1) careful sample processing to ensure a relatively constant signal

strength (Zeeman *et al.*, 2008) or (2) an empirical adjustment determined by measuring the isotope ratio of a working standard while varying its concentration. In the latter case, for example, it has been observed that the signal nonlinearity results in a linear change in measured ratio with respect to the major isotope signal (Thermo Electron Corporation, 2004). The first solution – maintaining constant signal strength – may not always be practical or desirable (Cappellin *et al.*, 2011), while the second solution is limited in range. Empirically-derived nonlinear functions have been proposed as the basis of additive corrections for nonlinearities at low signal strength (Spotl & Vennemann, 2003, Werner et al., 2001). Additive corrections, however, are not always appropriate since the curvature due to nonlinearity may depend on the actual isotope ratio.

Formal mathematical linearity corrections have been developed for other types of mass spectrometry, (Cappellin *et al.*, 2011) but I am not aware of similar methods applicable to CF-IRMS. Instead, I present here an empirical method that, unlike the previous reports cited, does not assume that the correction is additive. All gas standards are introduced to the mass spectrometer in the same way as unknown samples, thus enabling the nonlinearity correction to be valid without need to characterize the properties of each component of the measurement system. Although this empirical approach does not model actual processes it can nevertheless provide insights into the sources of nonlinearity, as I will discuss. Mathematical analysis also suggests that two sets of calibration standards with differing δ values and/or concentration of gas species may be necessary to properly deduce the empirical correction coefficients, and I therefore proceed along those lines. As a result, the linearity correction serves as a two-point calibration of the δ scale across a wide range of concentrations.

To further maximize dynamic range I also explored the effects of manipulating the sample open split, which in turn requires additional mathematical attention. Here I first develop the empirical formulas and then demonstrate the efficacy of my approach in correcting the data.

2.2. MATHEMATICAL DEVELOPMENT

Signals (e.g. voltages for specific isotopologues) produced by modern CF-IRMS instruments are very nearly linear with the material concentrations. Nevertheless, ratios of these signals have been observed to depend on signal strength, which implies a small

amount of nonlinearity. In order to correct the measured ratio, one should therefore consider the components of the ratio separately.

Stated formally, for the material quantities M_i, and corresponding signals, A_i, i=1 or 2, the actual isotope ratio is $R \equiv M_1/M_2$ and the measured signal ratio is $R_{meas} \equiv A_1/A_2$. If each signal, A_i, is strictly proportional to the corresponding M_i, the measured ratio will be independent of the signal strength. I will show later in this section, however, that curvature in the signal-response as well as non zero intercepts will make R_{meas} dependent upon signal strength.

The small amount of curvature in the signal response can be modeled, to a first approximation, by the quadratic equation

$$M_i = a_i^* A^2{}_i + b_i^* A_i + c_i^* \qquad (2.1)$$

with coefficientss a_i^*, b_i^*, and c_i^* to be determined. The true ratio, R, is then

$$R = \frac{M_1}{M_2} = \frac{a_1^* A_1^2 + b_1^* A_1 + c_1^*}{a_2^* A_2^2 + b_2^* A_2 + c_2^*}. \qquad (2.2)$$

One could determine the coefficients in Eqn (2.2) directly by preparing standards at several precisely determined concentrations and then performing a multiple linear regression for each species using Eqn (2.1). In my experience, however, coefficients derived using this approach did not correct R_{meas} adequately, especially at lower concentrations, possibly due to imprecision in my estimates of the actual concentrations (Appendix A2.1). A simpler approach would be to use dilutions of a single well-characterized standard. Since the isotope ratio of such a dilution series is constant one can regress on Eqn (2.2) directly without having to know the absolute concentrations, M_i, in each sample. Two issues must be addressed, however: first, Eqn (2.2) is overspecified for regression and second, as will be demonstrated, more than one actual R is needed in order to separate the c^* terms.

I therefore divide Eqn (2.2) by b_1^* to eliminate one coefficient, yielding:

$$R = \frac{M_1}{M_2} = \frac{a_1 A_1^2 + A_1 + c_1}{a_2 A_2^2 + b_2 A_2 + c_2}, \qquad (2.3)$$

where $a_i \equiv a_i^*/b_1^*$, $b_2 \equiv b_2^*/b_1^*$, and $c_i \equiv c_i^*/b_1^*$. Nonlinear regression may be used to find the remaining coefficients as long as dilution sets of two gas standards with distinct R values have been measured and "reasonable" starting values can be found for the

coefficients (but see also Appendices A2.6 and A2.7). A linearized version of Eqn (2.3) can be used to determine those starting values and may, in fact, be sufficient to correct the signal. In addition, the resulting equation provides insight into the sources of observed nonlinearity.

Dividing numerator and denominator by A_2 and rearranging produces the linearized form of Eqn (2.3):

$$R_{meas} = -a_1 A_1 R_{meas} + a_2 R A_2 + \left(c_2 R - c_1\right)\frac{1}{A_2} + b_2 R\,, \qquad (2.4)$$

where $R_{\text{meas}} \equiv A_1/A_2$ (keeping in mind that R_{meas} is known at the time of regression, so it can appear on both sides of the equation). Equation (2.4) demonstrates that two main effects contribute to the graph of the measured ratio *vs.* signal strength, A_2, (i.e. the graph commonly used to correct nonlinearity (Thermo Electron Corporation, 2004)): hyperbolic curvature at low signal strengths due to nonzero intercept terms c_i, and a linear change in the ratio at larger signal strengths due to curvature in the individual signal-response curves (see Fig 2.2, below). These effects can, in turn, provide information as to the physical sources of nonlinearity. For example, I have found that an increase in the hyperbolic curvature in the linearity graph was associated with a leak in the autosampling hardware, which had therefore increased the magnitude of the "blank" signal. Equation (2.4) also demonstrates that the actual isotope ratio, R, is a coefficient to both A_2 terms, thus implying that the magnitude of nonlinearity varies as the actual isotope ratio changes. I will return to this point below.

Recasting Eqn (2.4) as a regression equation yields:

$$R_{meas} = \beta_1 A_1 R_{meas} + \beta_2 R A_2 + \beta_3 \frac{1}{A_2} + \beta_4 R\,, \qquad (2.5)$$

where A_1 is the numerator of the isotope ratio (generally a minor isotope) and A_2 is the denominator of the isotope ratio (generally a major isotope). The regression coefficients correspond to the correction coefficients as follows:

$\beta_1 = -a_1$,

$\beta_2 = a_2$,

$\beta_3 = c_2 R - c_1$, and

$\beta_4 = b_2$.

The constant terms, c_i, cannot be determined by regression if only one value of R is available since the two are grouped together in β_3. (See Appendix A2.4 for further discussion of the need for two R standards.) If two calibration standards are available, each with a distinct R, say R_A and R_B, then c_i can be determined as:

$$c_2 = (\beta_{3A} - \beta_{3B})/(R_A - R_B) \tag{2.6}$$

$$c_1 = R_A c_2 - \beta_{3A} = R_B c_2 - \beta_{3B}.$$

It should be noted that for software such as ISODAT (Thermo Electron, Bremen, Germany), reported peak-area values for A_1 cannot be used directly in Eqn (2.5) when A_1 represents a minor isotope, because these values are neither corrected for drift nor reported with sufficient precision. An appropriate solution is discussed in Appendix A2.7. However, a better solution in such circumstances is to recast Eqn (2.4) in terms of δ values using the identity

$$1000\frac{R}{R_{\text{std}}} = \delta + 1000, \tag{2.7}$$

where R_{std} represents the isotope ratio of an arbitrary reference standard and δ is expressed in parts per thousand (permil). Multiplying Eqn (2.4) by $1000/R_{\text{std}}$ and rearranging yields:

$$\begin{aligned}\delta_{meas} = &-a_1(\delta_{meas} + 1000)A_1 + a_2(\delta + 1000)A_2 \\ &+ c_2(\delta - \delta_z)\frac{1}{A_2} + b_2\delta + 1000(b_2 - 1)\end{aligned} \tag{2.8}$$

where δ_{meas} represents the measured isotope ratio while δ_z, the "zero" delta corresponding to c_1/c_2, is a parameter to be determined.

In Appendix A2.5, I show how Eqn (2.8) corresponds with a change-of-standard conversion formula (Fry, 2006) and the conventional linearity correction mentioned above (Thermo Electron Corporation, 2004). In particular, the final term represents the δ value of the calibration standard relative to the measurement standard (i.e. reference tank gas). I therefore treat this term as an independent coefficient: $\beta_0 \equiv 1000(b_2 - 1)$. Also, for many isotope-ratio applications the ranges of δ and δ_{meas} are small relative to 1000, so that isotope-ratio dependencies in the first two terms of Eqn (2.8) can be safely ignored.

As a result, in these situations δ value linearity can be directly corrected by simplifying Eqn (2.8) to:

$$\delta_{meas} = -a_1 A_1 + a_2 A_2 + c_2(\delta - \delta_z)\frac{1}{A_2} + b_2\delta + \beta_0 \cdot \qquad (2.9)$$

The coefficient of the $1/A_2$ term remains dependent on the actual δ value of the calibration gas. An additive empirical correction based on a single isotopic reference material may therefore be incorrect for samples differing in isotopic composition from that standard. In practice, the extent of change in curvature at low signal strength depends on the magnitude of the actual isotope ratio, δ, in the sample. The practice cited in the Introduction of adding a correction based on the response of a single isotopic reference material may therefore not be valid if the value of δ is large relative to δ_z.

One can correct δ_{meas} regardless of the magnitude of δ_z, however, by rewriting Eqn (2.9) in regression format as:

$$\delta_{meas} = \beta_1 A_1 + \beta_2 A_2 + \beta_3 \frac{1}{A_2} + \beta_4\delta + \beta_0 , \qquad (2.10)$$

where A_1 is the numerator of the isotope ratio (generally a minor isotope) and A_2 is the denominator of the isotope ratio (generally a major isotope). The coefficient β_3 corresponds to $c_2(\delta - \delta_z)$. As with Eqn (2.5), if two distinct calibration standards are measured, one can solve for both c_2 and δ_z. Substituting $c_2(\delta - \delta_z) = \beta_3$ into Eqn (2.10) and solving for δ yields the correction equation:

$$\delta = \frac{\delta_{meas} - \beta_1 A_1 - \beta_2 A_2 + c_2\delta_z \frac{1}{A_2} - \beta_0}{c_2 \frac{1}{A_2} + \beta_4} \cdot \qquad (2.11)$$

A special case worth mentioning occurs when one calibration standard is the measurement standard, i.e. $\delta = 0$, in which case $-\beta_{3,\text{meas. std}} = c_2\delta_z$ could be substituted into Eqn (2.11).

In practice, A_1 and A_2 may be strongly correlated across a dilution series since dilution reduces the concentration of both isotopes equally. In such cases there may be little value added in keeping both terms in Eqn (2.11). I have had good success in correcting δ values without the A_1 term, for example but as mentioned above, if the A_1

term is necessary, the formulas described in Appendix A2.7 should be used for ISODAT-based systems.

In summary, I have shown that the shape of the graph of δ_{meas} *vs.* signal strength may depend on the composition of the calibration standard; i.e., in the most general case an additive linearity correction is not appropriate. I therefore presented two general solutions for simultaneously calibrating the isotope ratio scale and correcting nonlinearities, both of which ideally use two sets of standards, each prepared as dilutions of a well-characterized standard. For ratios reported as δ values that vary in a permil range that is small relative to 1000, Eqns (2.10) and (2.11) can correct δ_{meas} directly, thus utilizing the extra precision with which delta values are reported by software such as ISODAT. For ratios varying over a wider range, the fact that β_1 and β_2 depend on (1000 + δ) may introduce errors in Eqn (2.11). In such cases Eqns. (2.5) and (2.3) are more appropriate. Likewise, for ratios that are not reported directly by the IRMS software, such as $^{32}O_2/^{28}N_2$, there is no advantage to using Eqn (2.11), so Eqns. (2.5) and (2.3) are most appropriate. A more detailed guide to implementing these corrections, including Microsoft Excel data and R source code, can be accessed online from the University website: http://www.biol.canterbury.ac.nz/lab-protocols/.

Importantly, in all cases the calibration standards must be introduced to the mass spectrometer in the exact same way as the samples, so that the calibration and correction represents the sum of all effects of sampling, gas chromatography, open split dilution and mass spectrometery.

2.3. EXPERIMENTAL

2.3.1. Sample preparation

Two types of calibration standards were used: air sampled immediately outside a second-story window at the University of Canterbury, Christchurch, New Zealand (CCA – Christchurch Clean Air); or bottled mixtures of 5%, 10%, 15%, or 20% O_2 in N_2 that had been certified for O_2 and N_2 to ± 0.5%, but not for isotopic composition, by the manufacturer (BOC, Auckland, New Zealand). Atmospheric air composition has been reported to be consistent over time across the globe (Kroopnick & Craig, 1972), is often used as the reference standard for isotopic O_2 and N_2 studies (Barth *et al.*, 2004, Luz *et al.*, 1999), and is now recognized as an international measurement standard for $\delta^{18}O$

values(Wieser & Berglund, 2009). I therefore treated the CCA samples as the standard reference material for both O_2 and N_2.

Both of these calibration standards are distinct from the high-purity O_2 "reference" gas used by ISODAT to calculate drift-corrected δ_{meas} values. Unlike the reference gas, the calibration standards were flushed into sample vials of the same type as unknown samples and were introduced to the mass spectrometer in the same way as those samples.

Calibration air samples were flushed into open 3.7 mL chlorobutyl rubber septum-capped soda-glass vials (Labco, High Wycombe, UK, product # 778W) using a 20 mL needleless syringe. Bottled gas-mix samples were prepared by rinsing open vials with the mix, then capping and flushing for two minutes at 30 mL min^{-1} or greater through a 27G x ½ inch hypodermic needle (Terumo, Tokyo, Japan; product #NN-2713R) connected by plastic tubing to a needle valve attached directly to the gas tank. A second needle inserted through the septum acted as a vent. The vent needle was left in for 1 – 3 s after removing the inlet needle in order to equalize pressure with the atmosphere. Measurements against "blank" vials flushed with O_2-free N_2 or O_2-free He (BOC, Auckland, New Zealand; 99.99% pure) confirmed that the flush-time was adequate and that leaving the vent needle in did not introduce measurable contamination. (He-flushed vials were rinsed and flushed inverted to prevent loss of the lighter gas.)

Dilution series were made by injecting a calibration gas into a "blank" vial or *vice versa*, depending on dilution strength. Either way, a 1 mL or 5 mL hypodermic syringe (Terumo, Tokyo, Japan) was flushed several times with the gas via a three-way stopcock before injecting a measured amount into the vial. The plunger was held down for several seconds to allow full mixing before releasing the plunger and allowing it to rise on its own. Vials prepared this way are slightly overpressurized but since excess pressure is released during sampling in Gasbench II, the measured signal strength is not affected by the overpressure (see Appendix A2.2). Preliminary experiments confirmed that adding or withdrawing gases as described here does not fractionate the gases and does not contaminate the mixtures with lab air.

In order to support both the linear and inverse terms of Eqns (2.5) and (2.10), gas solutions were prepared to yield concentrations spaced at equal intervals in $1/A_2$ (i.e., A_2 = 0.01, 0.015, 0.02, 0.03, 0.05, 0.10 × initial concentrations) as well as roughly equal

spacing relative to A_2 at the higher concentrations. When injecting the analyte into an analyte-free vial, the final concentration, c (as a proportion of the concentration of the undiluted analyte), in the vial was computed as:

$$c = V_{inject}/(V_{inject} + V_{vial}),$$

where V_{vial} represents the volume of gas in the vial before injection and V_{inject} is the volume injected from the syringe. For a desired concentration I therefore injected:

$$V_{inject} = V_{vial} \times c/(1 - c).$$

When injecting analyte-free gas into a vial flushed with a known mixture, the variables V_{inject} and V_{vial} are swapped so that:

$$V_{inject} = V_{vial} \times (1 - c)/c.$$

The effects of sample-side open split dilution were measured using either BOC-prepared 5% O_2 in N_2 (for $\delta^{18}O$) or hand-prepared 5 – 20% CCA in He (for $\delta^{15}N$ and $\delta O_2/N_2$ analyses).

Analysis of the bottled gas samples suggested that $\delta^{18}O$ values were consistent across bottles but that $\delta^{15}N$ values were not. I therefore used the four bottled gas standards when calibrating $\delta^{18}O$ values, in addition to the He-dilutions of 10% O_2 and CCA, whereas $\delta^{15}N$ and $\delta O_2/N_2$ calibrations were based solely on He-dilutions of CCA and of bottled 10% O_2 in N_2.

All calibration samples were measured as described in the next section. Nonlinearities evidenced in the calibration samples therefore represent the sum of all effects of the automated sampling process, sample-side open split, Gaussian-shaped peak effects and mass spectrometer electronics. The calibration sets were measured at several intervals during two two-month sessions several months apart.

2.3.2. Isotopic analysis

All measurements were made on a DELTA V Plus CF-IRMS instrument with a universal triple collector (Thermo Electron, Bremen, Germany). Samples were introduced to the mass spectrometer through a Finnigan Gasbench II with autosampler (Thermo Electron, Bremen, Germany). Gas in septum-capped vials was flushed into a double-hulled needle that injected high-purity He at 1 mL min^{-1}. The sample/He mix passed through a Nafion tube for water-removal, then through a 10 μL sample loop attached to

an 8-port Valco valve. After flushing the sample loop for 60 s, the Valco valve was switched to "inject" mode for 30 s, during which time the sample was flushed into a 30 m, 0.32 mm ID, 5Å PLOT fused-silica molsieve gas chromatography (GC) column (Varian Inc., Santa Clara, CA, USA; product #CP7534) maintained at 35 °C. Eluent from the GC column passed through a second Nafion tube before entering the mass spectrometer via a two-position open split (the sample open split). Concurrent with these events, three reference peaks were introduced from an ultrahigh-purity O_2 tank through a separate open split. The third peak was used as the reference for $\delta^{18}O_{meas}$ values, which are reported directly by ISODAT. A fast peak jump to *m/z* 28 after the O_2 had fully eluted allowed the sample N_2 to be measured followed by a single N_2 reference peak (Fig 2.1). Default ISODAT peak-detection settings were used but with the minimum O_2 peak height reduced to 20 mV and with the O_2 peak start criterion raised to 10 mV/s in order to reduce interference from Ar, which arrives just before O_2 and produces a very small peak in *m/z* 34.

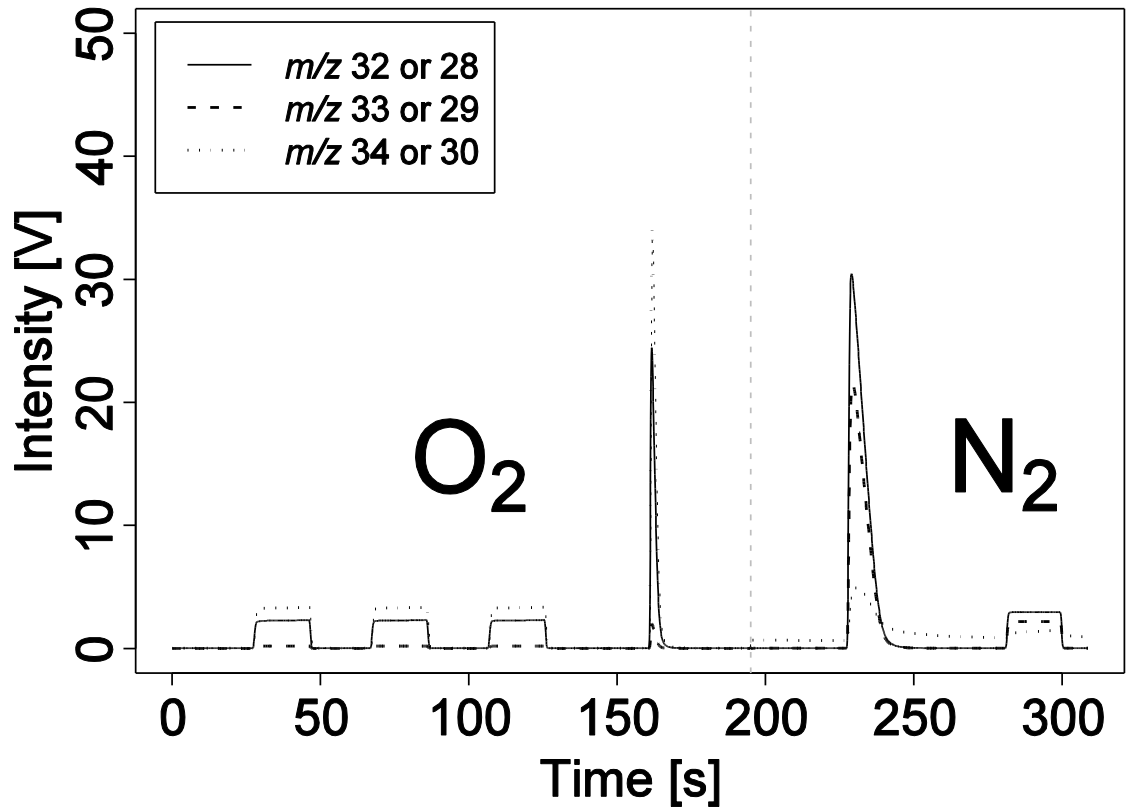

Fig 2.1. Sample mass spectrometer trace.

A fast peak jump to *m/z* 28 took place at 195 s (vertical dashed line).

The bracket holding the sample capillary in the open split was manually adjusted for maximum dilution when the bracket was raised. Software control allowed me to specify three different configurations that could be interspersed arbitrarily in a single run. In the standard configuration, the open split remained in high-dilution mode (*out*). For samples with high N_2 but low O_2 – i.e. standard gases diluted more than 75% in N_2 – the open split was set to concentrated mode (*in*) for O_2 but then *out* for N_2 measurements. Samples with low O_2 and low N_2 – i.e. standard gases diluted more than 75% in He – were measured with the open split *in* for the entire sequence. CCA- and 10% O_2-flushed vials were included for every 20 vials. Mean CCA peak areas were used to convert measured areas, A_i, to "proportion of ambient" values, F_i, adjusting for changes in open split settings as needed.

Because the square reference-peak shapes were very different from the Gaussian sample peaks (Fig 2.1), the reference peaks were used only for computing the drift-adjusted δ_{meas} values, which were then converted to calibrated δ values based on calibration coefficients derived from δ_{meas} and peak area values of the Gaussian-shaped peaks of the CCA and bottled gas standards.

Isotope ratios are expressed as δ_{refgas} [‰] for uncorrected data and δ_{air} [‰] for corrected values. In the case of O_2, for example,

$$\delta_{meas}{}^{18}O = [({}^{18}R_{sample}/{}^{18}R_{refgas}) - 1]\times 1000 \text{ and}$$

$$\delta^{18}O = \delta_{air}{}^{18}O = [({}^{18}R_{sample}/{}^{18}R_{CCA}) - 1]\times 1000,$$

where ${}^{18}R_{refgas}$ is the ratio of peak areas for the third O_2 reference peak and ${}^{18}R_{CCA}$ is the area under the Gaussian-shaped peak for the vials containing CCA, so that δ_{air} values are determined from the ratio of the area under peaks with similar shape. In practice, δ_{meas} values are reported by the ISODAT software and these values were converted to δ_{air} values using Eqn (2.11).

Both actual δ values and corrected δ values are reported relative to constituents of atmospheric air. When it is necessary to differentiate between these two values, "δ" without a subscript refers to the actual value while "δ_{corr}" refers to the corrected measurements.

For O_2/N_2 analysis I define

$$\delta O_2/N_2 = [(^{32}O_2/^{28}N_2)_{sample}/(^{32}O_2/^{28}N_2)_{CCA} - 1]\times 1000.$$

The corresponding formula for uncorrected values is:

$$\delta_{meas}O_2/N_2 = (F_{32}/F_{28} - 1) \times 1000.$$

Note that $F_{32}/F_{28} = (A_{32}/A_{32,CCA})/(A_{28}/A_{28,CCA}) = (A_{32}/A_{28})/(A_{32,CCA}/A_{28,CCA})$, so that $\delta O_2/N_2$ and $\delta_{meas}O_2/N_2$, are in fact of the same form.

Linearity corrections for $\delta_{meas}O_2/N_2$ values were calculated from peak areas using Eqn (2.5). The results were then converted to δ values for reporting purposes.

2.3.3. Statistical analysis

Statistical analysis was conducted using linear models and Student's *t*-test in R (R 2.13, R Development Core Team, Vienna, Austria).

Measurement error was determined as the standard deviation (SD) of the corrected calibration measurements across the dilution range. Because the calibration samples have been processed identically to unknown samples, the reported SD includes all sources of variability including sample preparation, Gasbench II processing, open split effects, ionization, detection, amplification, and mathematical correction. Note, however, that the mathematical corrections did not contribute substantially to the overall measurement error (see Appendix A2.3).

2.4. RESULTS AND DISCUSSION

The primary goal of this study was to determine how to measure samples over a wide dynamic range of concentrations. In order to maximize instrument sensitivity I used different sample-side open split settings depending on the concentration of analyte, as described above. The position of the open split, however, had a small but measurable effect on computed ratios; therefore, in the following discussion I first determine whether these effects were intrinsic to the open split – and therefore have to be corrected independently from signal-strength corrections – or simply due to changes in concentration at the inlet. I also investigate whether the appropriate independent variables, A_i, for the linearity correction equations should best be represented by the raw signal strength (i.e. peak area) or by gas concentration (i.e. peak area relative to that of the standard gas).

Table 2.1. Ratio of measurements with open split in "concentrating" mode (*in*) *vs* "diluting" mode (*out*) during two different sessions.

In vs. Out:	Session 1	Session 2	$P_{s1=s2}$
Area 32	2.40 ± 0.005 (*n* = 7)	2.515 ± 0.009 (*n* = 12)	$< 10^{-8}$
Area 28	2.336 ± 0.012 (*n* = 6)	2.432 ± 0.015 (*n*=3)	< 0.006
A_{32}/A_{28}	1.043 ± 0.003 (*n* = 6)	1.031 ± 0.002 (*n* = 3)	0.05
$\delta_{meas}{}^{18}O$	–0.21 ± 0.05‰ (*n* = 7)	–0.057 ± 0.02‰ (*n* = 12)	< 0.02
$\delta_{meas}{}^{15}N$	–0.21 ± 0.02‰ (*n* = 6)	+0.12 ± 0.05‰ (*n* = 3)	< 0.01

Values are reported as mean effect ± standard error for *n* paired observations, where peak-area effects are reported as ratios while δ value effects are reported as differences. $P_{s1=s2}$ indicates the probability that the effects were the same across sessions, based on Student's *t*-test. Session 1 and session 2 took place 6 months apart.

2.4.1. Correcting nonlinearities in $\delta^{18}O$ and $\delta^{15}N$ values

2.4.1.1. Effects of open split dilution

I measured identically-prepared samples with the sample open split either *in* (lower dilution), or *out* (higher dilution). Moving the open split *in* increased peak area for *m/z* 32 by a factor of 2.4–2.5, decreased $\delta_{meas}{}^{18}O$ values by 0.06–0.2‰, and had inconsistent effects on $\delta^{15}N$ across two sessions (Table 2.1).

The change in $\delta_{meas}{}^{18}O$ values cannot be explained by the change in signal strength, since $\delta_{meas}{}^{18}O$ values normally increase with signal strength (Fig 2.2 and Fig 2.3), whereas increasing the signal using the open split decreased $\delta_{meas}{}^{18}O$ values. Likewise, if background air was entering the split when it was *out*, then when the split is moved *in* the change in $\delta_{meas}{}^{18}O$ values should increase or remain the same (depending on the gas standard) rather than decrease, since the isotope ratio of the laboratory air was the same as for CCA. I therefore conclude that the change in $\delta^{18}O$ values is intrinsic to the open split. As a possible explanation, Elsig and Leuenberger (2010) suggest that increasing dilution in the open split may favor diffusion of molecules between the sample capillary and the inlet capillary, resulting in an enrichment in heavier isotopes when the split is more open. While my evidence with regard to $\delta^{18}O$ values corroborates their

findings, the inconsistent effect of open split settings on δ^{15}N values is intriguing. My experiments, however, were designed primarily for δ^{18}O values: a more thorough investigation is needed to reconcile my δ^{15}N data. Finally, I note that the open split effect depended on other factors such as system He pressure, and therefore cannot be generalized from one run to the next.

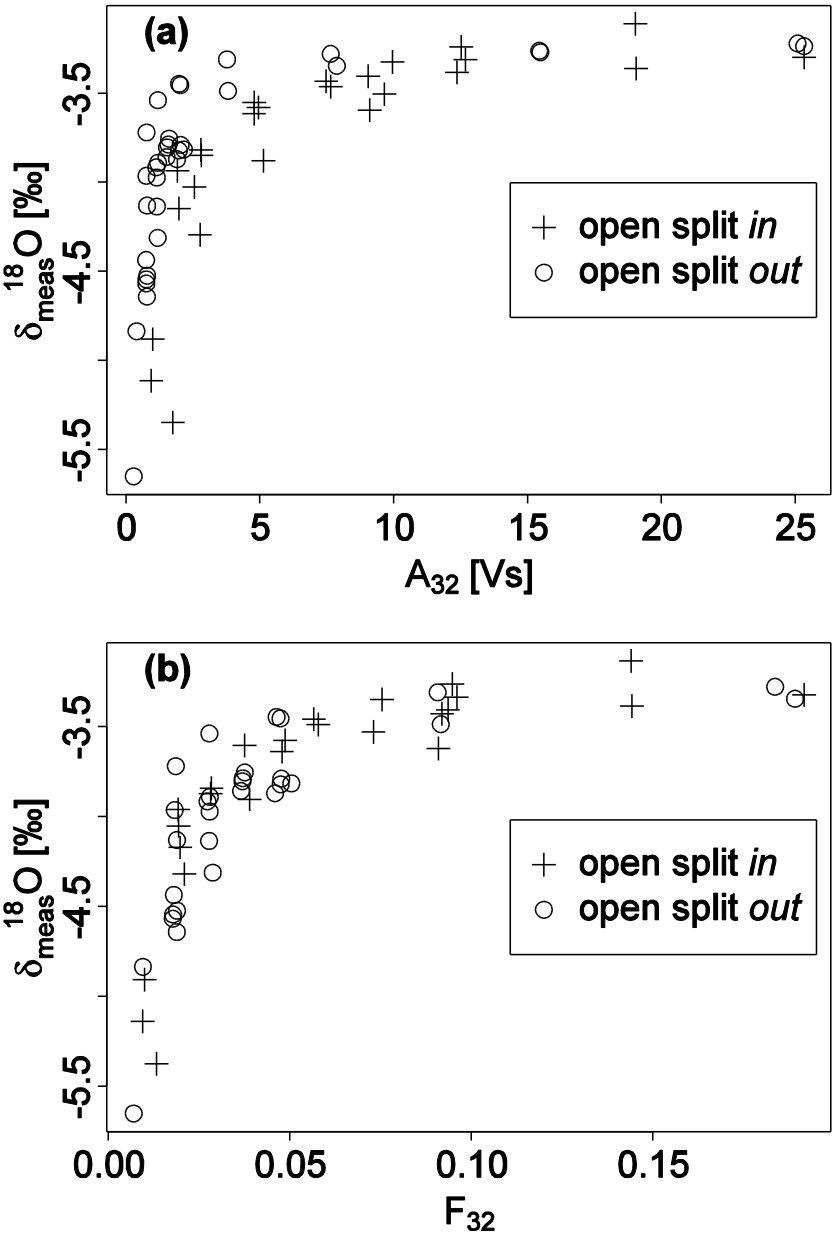

Fig 2.2. Nonlinearity in δ^{18}O values *vs* either (a) the measured peak area, A_{32}, or (b) the relative concentration of gas in the vial, F_{32}, which is adjusted for dilution effects of the open split. F_{32} is defined so that $F_{32,CCA} = 1$.

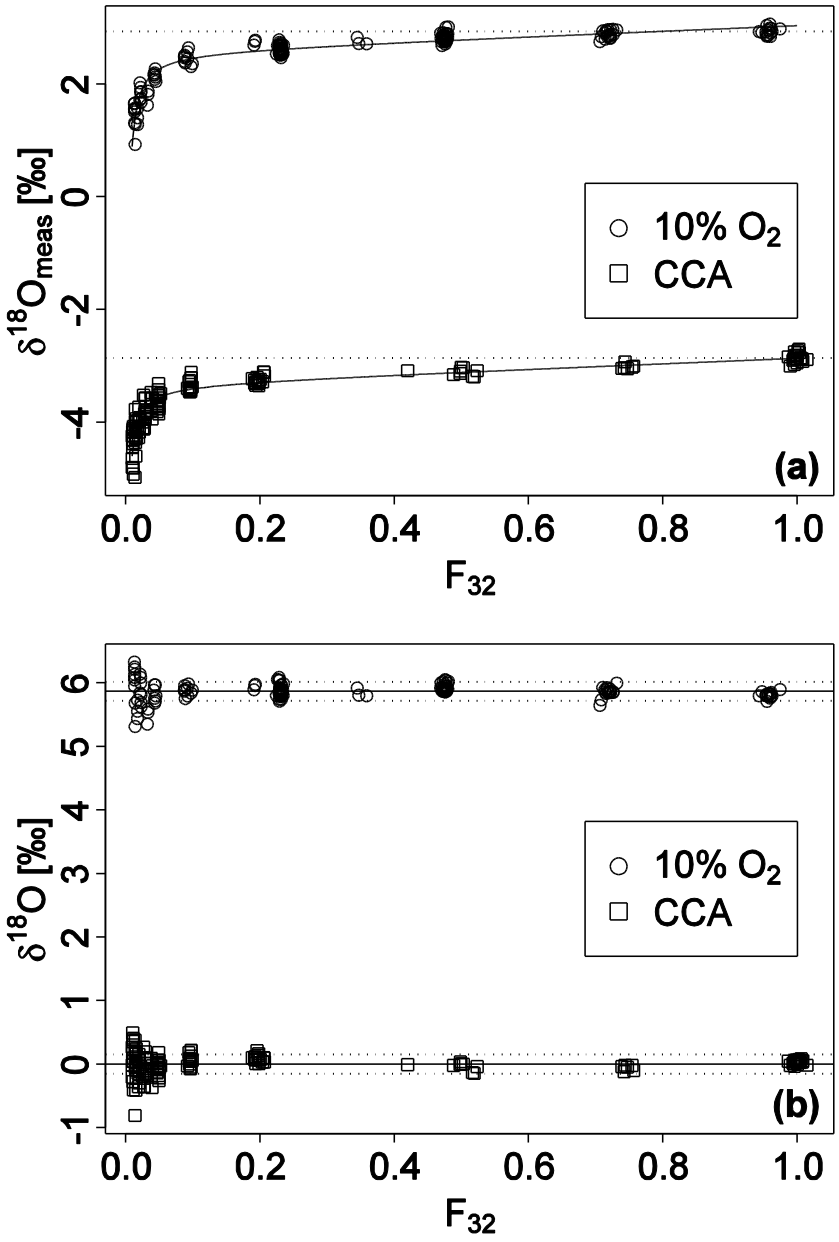

Fig 2.3. The regression curves for correcting nonlinearity in $\delta^{18}O_{meas}$ values (a), and the resulting correction (b).

Dotted lines in both graphs represent ± 0.15 ‰, representing approx. 2 standard deviations (SD).

2.4.1.2. Choice of quantity to represent signal strength

The trend in δ_{meas} values with signal strength may be due primarily (1) to nonlinearities in the mass spectrometer (i.e. ionization efficiency, detection, etc.) – in which case trends in δ_{meas} values will be most consistent with signal strength, i.e. peak area; or (2) to side-effects of the sample handling – in which case the nonlinearity would follow analyte concentration regardless of the open split position. I therefore plotted $\delta^{18}O_{meas}$ values for a range of sample concentrations measured at each open split setting *vs.* either the raw signal (A_{32}) or the split-adjusted signal, $F_{32} = A_{32}/A_{32,CCA}$, where $A_{32,\,CCA}$ represents the split-adjusted peak area for ambient air samples (Fig 2.2). In order to compare these two graphs, I first shifted the "open split *in*" data using either the previously-described shift for the F_{32} comparison, or a slightly larger shift for the A_{32} graph – determined manually by choosing an offset that produced similar δ values in the upper half of the signal range regardless of open split setting (Fig 2.2a). As seen in Fig 2.2, the $\delta^{18}O_{meas}$ values at the two open split settings align best when plotted against F_{32}. I therefore chose F_{32} as the measure of signal strength for purposes of calibration and linearity correction.

2.4.1.3. Calibration coefficients

Using Eqn (2.10) I found that the A_1 term, i.e. peak-area for *m/z* 34, made no substantial contribution to the $\delta^{18}O$ correction and it was therefore dropped. The model provided an excellent fit to the data, with $r^2 = 0.9976$ (Fig 2.3). For $F_{32} > 0.1$, the standard deviation of the corrected values was 0.08‰ for 10% O_2 and 0.07‰ for CCA (Fig 2.3). For concentrations between 1% and 10% atmospheric O_2, the standard deviation for samples was 0.24‰ and 0.21‰ for 10% O_2 and CCA respectively. Below 1% ambient O_2, i.e. $F_{32} < 0.01$, the noise level increased dramatically and I therefore considered 1% to be the lower usable limit of my calibration equation. This lower calibration limit is constrained by machine precision and operating parameters. I would expect the actual lower limit to vary based on operating parameters and machine construction. Since this low end of the signal range is often used to measure blanks when correcting for contamination, I also note that if the contamination is less than 1% of atmospheric samples, the increased uncertainty in δ values below 1% may be acceptable since the impact of such uncertainty is likely to be small. Alternatively, one can use an indirect method such as described by Fry et al. (1992) for determining delta values at very low concentrations.

The coefficients to the calibration equation used in Fig 2.3, based on Eqn (2.11),

$$\delta^{18}O = \frac{\delta^{18}O_{meas} + 0.0127 / F_{32} - 0.476 F_{32} + 3.333}{1.007 - 0.00070 / F_{32}}$$

provide insight into sources of nonlinearity. By definition, F_{32} varies from one to zero as O_2 concentration increases from zero to atmospheric O_2 levels. The inverse term, which could be attributed to nonzero signals in the absence of analyte, therefore shifts the signal by 1.3‰ at the lower calibration limit of $F_{32} = 0.01$, while at 10% ambient levels, the shift due to $1/F_{32}$ is only 0.13‰. The direct term – which could be attributed to nonlinearities in processes such as amplification or ionization efficiency – indicates that the effect of the "linear" part of the correction is 0.5‰ over the entire range of zero to one.

I corrected δ^{15}N values in the same way (data not shown) but in this case the curvature was too sharp for a global correction. Instead, a piecewise solution, as described next for $\delta O_2/N_2$ values, provided the best fit. The coefficient for F_{28} in the higher segment was 0.26, while the inverse coefficient for the low end was 0.002, implying less nonlinearity. Precision of the corrected data was 0.05‰ for $F_{28} > 0.1$ and 0.06‰ for $0.01 < F_{28} < 0.1$. The precision of the corrected values was within 0.02‰ of instrument precision for both δ^{18}O and δ^{15}N values (see Appendix A2.3 for an expanded discussion of precision and calibration uncertainty).

2.4.2. Correcting nonlinearities in $\delta O_2/N_2$ values

I diluted mixtures of O_2 and N_2 in two ways corresponding to different experimental protocols (Fig 2.4a). In one protocol N_2 displaces a mixture such as air, thus decreasing F_{32} (O_2 concentration) while increasing F_{28}. The second protocol dilutes the mixture with He, reducing the absolute concentrations of $^{32}O_2$ and $^{28}N_2$ proportionally and thus not changing $\delta O_2/N_2$ values. For the nitrogen dilutions, $\delta_{meas}O_2/N_2$ values correctly tracked changes in $\delta O_2/N_2$ values. In the helium dilutions, however, $\delta_{meas}O_2/N_2$ values were sensitive to absolute concentrations (Fig 2.4b, c). I therefore analyzed ratio *vs.* $^{28}N_2$ in the He dilutions (Fig 2.4c).

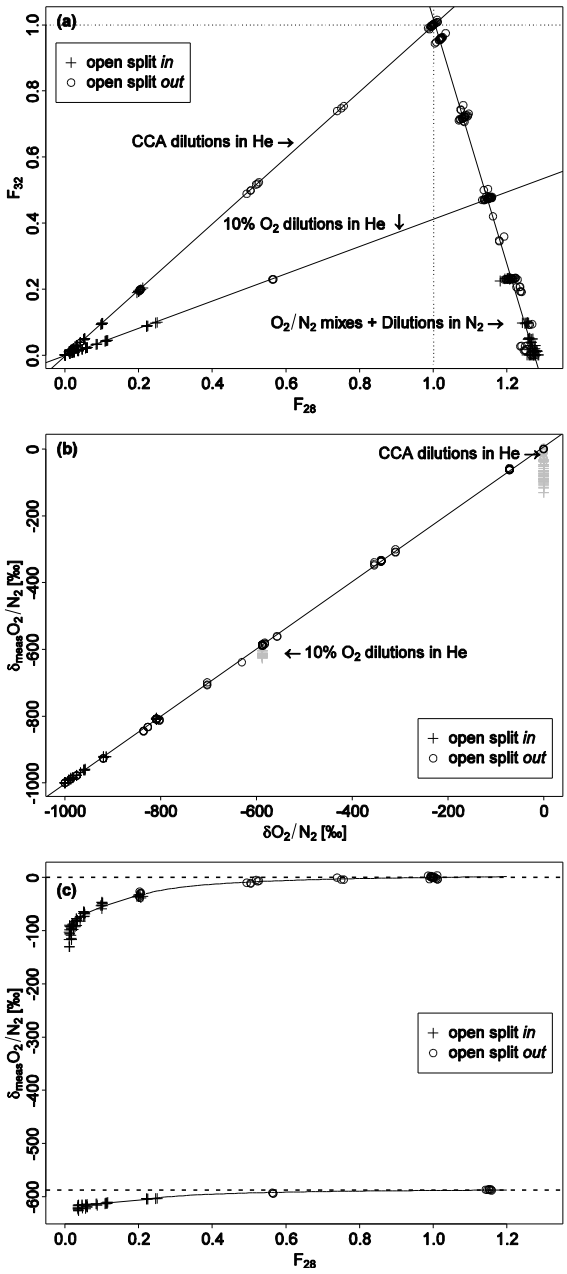

Fig 2.4. The effects of dilution on measured F_{32}, F_{28} and $\delta O_2/N_2$ values. Calibration samples were diluted in either N_2 or He.

(a) Both methods reduce O_2 concentration, but displacing the calibration gas with N_2 increases the N_2 concentration, and therefore F_{28}, while decreasing F_{32} (descending line to the right of F_{28} = 1.0), whereas diluting the standards in He decreases both F_{28} and F_{32} proportionally, as represented by the lines converging at (0,0) to the left of F_{28} = 1.0. (b) The uncorrected measurements, $\delta_{meas}O_2/N_2$ *vs*. actual $\delta O_2/N_2$ values compared with a 1:1 line (He dilutions shown in grey). (c) $\delta_{meas}O_2/N_2$ *vs* F_{28} for the He dilutions. Dashed lines represent the expected values.

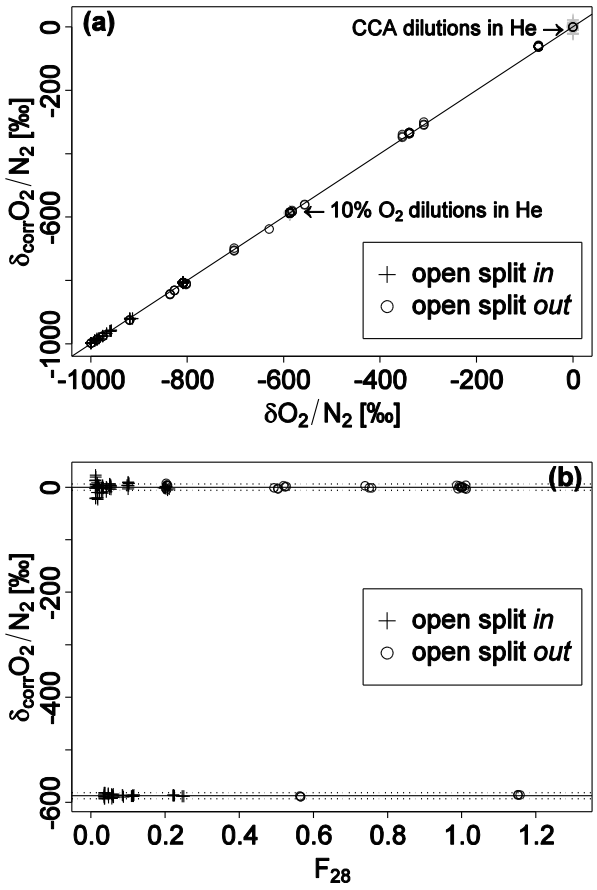

Fig 2.5. The corrected data, $\delta_{corr}O_2/N_2$, *vs*: (a) actual $\delta O_2/N_2$ values (He dilutions shown in grey), and (b) F_{28} (He dilutions only).

The solid line in (a) is the 1:1 line; the solid lines in (b) represent the expected values; the dashed lines indicate ± 6 ‰, approximately 2 SD.

2.4.2.1. Effects of open split dilution/Choice of quantity to represent signal strength

Setting the open split *in* (more concentrated) increased the *m/z* 32 slightly more than it increased *m/z* 28, resulting in a 3% increase in A_{32}/A_{28} (Table 2.1). The choice of A_{28} *vs.* F_{28} as independent variable could not be resolved regardless of whether A_{32}/A_{28} or F_{32}/F_{28} was used as the dependent variable. I chose to parameterize my corrections using F_{32}/F_{28} *vs* F_{28}, since the F_x values significantly reduce scatter due to drift over time.

2.4.2.2. Calibration coefficients

Regressing on the entire dataset using Eqn (2.5) captured the trend at low N_2, but was not acceptable for the mid ranges. I therefore divided the dataset into two segments overlapping at F_{28} = 0.2, the concentration at which I would generally switch the open split setting from *in* to *out*. The two segments therefore represent the two different states of the open split. The resulting correction (Fig 2.5) resolved the linearity issue across a

range of concentrations from 1% to 120% atmospheric concentrations as well as across a range of δ values from 0 to –590‰. Precision of CCA above the F_{28} = 0.2 cutoff was 3‰; below F_{28} = 0.2 precision was 9‰. Corresponding values for 10% O_2 samples are 1.3‰ and 3‰ respectively. These uncertainty values were almost entirely due to machine precision (Appendix A2.3).

The greater curvature in the $\delta O_2/N_2$ calibration graph (Fig 2.4c) as opposed to the $\delta^{18}O$ calibration graph (Fig 2.3a) suggests that $\delta O_2/N_2$ values are either more strongly affected by zero-offset issues or that curvature is not adequately represented by a second-order approximation. More importantly, curvature differed markedly between the CCA and 10% O_2 calibration sets (Fig 2.4c), consistent with my prediction, above, that an additive correction is not valid over very large ranges of δ values.

2.5. SUMMARY

Here I present a mathematical framework for increasing the usable operating range of CF-IRMS instruments both at low sample gas concentration and across a wide δ value range. The correction takes into account effects of the measurement process through the entire standard sampling pathway including the sample-side open split settings, and the mass spectrometer itself. These effects, and therefore the mathematical correction, depend on operating conditions specific to each session, including sampling-carrier flow rate, vial- or headspace size, sampling flush time, GC column temperature, source configuration, etc. It is therefore important measure standards periodically in order to track changes in instrument linearity.

I have also demonstrated here that my method can correct linearity issues even when an additive correction for nonlinearity is not appropriate. The method requires only two well-characterized calibration standards. The remaining calibration samples are made up as dilutions of these samples; the precise amount of dilution need not be known. As an added benefit, my method simultaneously corrects the nonlinearities and calibrates the reported δ_{meas} values to the δ value scale of the calibration standards.

3. A field-compatible method for measuring alternative respiratory pathway activities *in vivo* using stable O_2 isotopes

---

A version of this chapter has been published in Plant, Cell & Environment *(Kornfeld et al., 2012a) and is included as Appendix 8.*

3.1. INTRODUCTION

This chapter describes and validates my novel field-portable method for measuring respiratory electron partitioning *in vivo*. In one sense, the chapter therefore describes the methods used in the three subsequent chapters. However, the work is important in its own right, as it represents an important technological advance in my ability to investigate the ecophysiology of plant respiration. The methods described here may even apply to other processes such as N uptake and assimilation by whole roots (anonymous reviewer of Kornfeld *et al.*, 2012a).

The justification for developing these methods, as well as the background context is described in Chapter 1, particularly in Sections 1.3. Briefly, previous methods have been limited to laboratory settings due to the need for specialized equipment and the avoidance of very small amounts of contamination. In order for a method to be successful in the field it needs to be tolerant of "reasonable" amounts of contamination, allow many trials to be run in a relatively short period of time, and to allow for gas samples to be stored for some time before measurement.

Here, I describe a new approach in which a 12 mL vial is used as the incubation cuvette. A single sample, consisting of the entire headspace, is withdrawn at the end of incubation, thus maximizing sample volume relative to cuvette volume. Replicates consist of sets of incubations in which subsamples of the same plant material consume different amounts of O_2 (by varying either tissue amount or incubation time). Incubations can be conducted in parallel, thus allowing data points for several replicates to be collected in a relatively short period of time (2-6 h). Some contamination is inevitable with this approach, necessitating the development of methods for estimating and correcting for the extent of contamination.

Recently, my colleagues and I reported results of an investigation into respiratory acclimation to seasonal environment changes in alpine grasses using a preliminary version of this new field-deployable method (Searle *et al.*, 2011b). Here I present the refined method, describe my approach in detail, and present methods for measuring contamination and mathematically correcting for its effects. Detection, analysis, and handling of nonlinearities in the discrimination graph are a critical part of this method and, in fact, are relevant to any respiratory discrimination method. My goals in the following presentation are therefore twofold: first, to describe and validate the field-

portable method for determining AOX and COX activity *in vivo*, and second to introduce a new set of analytical tools that increase the flexibility of respiratory discrimination computations in the face of potentially nonlinear data.

3.2. MATERIALS AND METHODS

The experimental process is divided into five stages: *evacuation* of the storage vials, *incubation* of leaf tissue in sealed incubation vials, *gas transfer* from the incubation vials into the storage vials, and *storage* of the gases for subsequent *isotopic analysis* (Table 3.1). The following subsections describe each stage in general terms, followed by a discussion of my computational methods for correcting for vial contamination and for addressing possible nonlinearities in the data. I conclude this section with details of the biological experiments I conducted to validate the methods. The Appendices for this chapter (Appendix 3) include technical notes as well as derivations for all equations. A laboratory protocol is also available at: http://www.biol.canterbury.ac.nz/lab-protocols/.

Table 3.1. Illustrated key to symbols and their relationships.

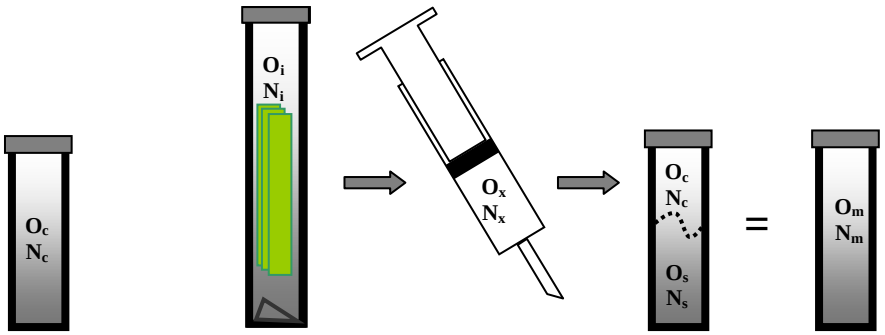

Quantity	*Storage vial: Contamination*	*Incubation vial*	*Transfer syringe*	*Storage vial: sample gas*	*Storage vial: mixture*
Total pressure (P)	$P_c = P_{atm} \times X_c$	$P_i = P_{atm} - O_r$	$P_x = P_{atm}$	$P_s = (1 - X_c)\, P_{atm}$	P_{atm}
Oxygen partial pressure (O)	O_c	$O_i = O_{atm} - O_r$	$O_x = O_i \times P_{atm}/P_i$	$O_s = (1 - X_c)\, O_x$	$O_m = O_s + O_c$
Nitrogen partial pressure (N)	N_c	$N_i = N_{atm}$	$N_x = N_i \times P_{atm}/P_i$	$N_s = (1 - X_c)\, N_x$	$N_m = N_s + N_c$
Isotope Ratio ($\delta^{18}O$)	$\delta^{18}O_c$	$\delta^{18}O_i$	$\delta^{18}O_x = \delta^{18}O_i$	$\delta^{18}O_s$ = (Eqn 5)	$\delta^{18}O_m$
${}^{32}O^* = {}^{32}O_2/N_2$	${}^{32}O_c{}^* = {}^{32}O_c/N_c$	${}^{32}O_i{}^* = {}^{32}O_i/N_i$	${}^{32}O_x{}^* = {}^{32}O_i{}^*$	${}^{32}O_s{}^*$ = (Eqn 6)	${}^{32}O_m{}^* = {}^{32}O_m/N_m$

The symbols O and N refer to the partial pressures of O_2 and N_2 or one of their isotopes. Subscripts refer to – *c*: contamination; *x*: transfer syringe; *s*: sample; *m*: mixture. (In the text subscripts "sample" and "mix" are spelled out for clarity.) The value X_c is the proportion of gases in the storage vial due to initial contamination, i.e., $X_c = (O_c + N_c + Ar_c)/P_{atm}$. Total pressure in the incubation vial, P_i, is reduced by the partial pressure of the oxygen consumed during respiration, O_r. Total pressure is restored to atmospheric levels upon transfer to the syringe, thus increasing O_x and N_x proportionally (Appendix A3.2 Fig S9). Partial pressure of the sample gas in the storage vial is reduced due to displacement by the initial contamination; total pressure remains one atm.

3.2.1. Evacuation

Septum-capped glass storage vials (Labco, High Wycombe, UK; product # 778W –3.7 mL) were evacuated for 60 s through a 27G × ½ inch hypodermic needle (Terumo, Tokyo, Japan; product #NN-2713R). Evacuated vials were stored at –17 °C but were returned to laboratory temperature (20 °C) before use.

3.2.2. Incubation

Incubations were conducted in 12 mL septum-capped glass vials (Labco product #738W). CO_2 traps consisting of an open plastic cone containing a half-pellet of KOH – approximately 35 mg – were inserted into the vials prior to the experiment in order to avoid side-effects of excessive CO_2 buildup.

Five to nine incubations were conducted in parallel for each biological replicate: either equal amounts of plant tissue were incubated for variable periods of time, or variable-sized portions were incubated for a fixed period of time, thus ensuring a range of O_2 consumptions. Tissue volume was kept under 2–3 mL per vial to avoid diffusion limitations. Expected respiration rates were determined in advance using standard lab and field equipment. Incubation times were determined such that the most extreme incubation would consume 30 – 50% of the O_2 in the vial (see Appendix A3.3.3 for further details). If actual O_2 consumption exceeded 50%, the samples were rejected from further analysis.

Plant tissue was cut to fit the vials using fresh razor blades. Incubation vials were flushed with lab air using a 20 mL needleless syringe; the tissue was inserted and the vial flushed again before being sealed and placed in a dark incubation chamber.

In addition to the plant samples, air- and N_2-filled incubation vials ("blanks") were prepared for every set of two replicates, i.e. 12 sample vials. Air blanks were prepared as above but without plant material. N_2 blanks were prepared by first rinsing incubation vials with O_2-free N_2 (BOC, Auckland, New Zealand; 99.99% pure) and then flushing the sealed vial for 7 min with a flow rate greater than 30 mL min^{-1} through a hypodermic needle attached by plastic tubing directly to the gas tank. A second, vent, needle through the septum was left in for 1-3 s after removing the flush needle in order to equalize pressure with the atmosphere without introducing O_2 contamination. In addition, several He-blanks were produced from evacuated storage vials stored alongside the samples and subsequently injected with O_2-free He (BOC; 99.99% pure) shortly before measurement in the mass spectrometer. For some experiments, air or N_2 were injected

directly into the storage vials after thoroughly flushing a syringe using a 3-way stopcock. No difference was found between the two ways of generating air blanks. The difference between directly injected N_2 and transferred N_2 was used to estimate contamination due to the gas transfer process. .

3.2.3. Gas transfer and storage

Air in the incubation vial was transferred to the storage vial under positive pressure using a pair of syringes. Displacement solution, 0.4 M Boric acid buffered at pH 6 to reduce the caustic effects of the CO_2 trap, was injected using a 20 mL syringe (Terumo, Tokyo, Japan; product #SS+20 ES) fitted with a 25G hypodermic needle. Since total pressure in the incubation vial had decreased due to O_2 consumption and CO_2 removal (Table 3.1), 1–2 mL of transfer solution was initially injected to re-pressurize the vial.

Without withdrawing the first syringe, an empty 10 mL gas transfer syringe (Terumo, Tokyo, Japan; product #SS+10 ES) with a 27G needle was inserted. The first mL of displaced air was discarded. The transfer syringe was then reinserted to receive the remaining incubation air as it was displaced by transfer solution. The air was immediately injected into a storage vial after noting the initial position of the plunger. In order to minimize effects of initial contamination in the 3.7 mL storage vial, a greater volume – typically 6 mL, but the same volume for all vials in the experiment – was injected into the vial and the plunger held down for several seconds to allow full mixing before allowing the plunger to rise back on its own. If net displacement of the plunger was less than 3.6 mL for freshly evacuated vials, the sample was excluded from analysis (see Appendix A3.2 Fig S1).

Vials were stored at –17 °C in order to reduce diffusional contamination. Shortly before measurement in a mass spectrometer, He-blanks were prepared from the stored evacuated vials by directly injecting 4 mL O_2-free He into the evacuated vial. Measured O_2 levels in the He-blank were multiplied by 4 mL/(volume injected into respiration storage vials) – typically 4/6 – to account for the higher dilution of initial contamination in the sample vials.

3.2.4. Isotopic analysis

Samples were measured as described by Kornfeld et al. (2012b), corresponding to Chapter 2, of this manuscript. Briefly, samples were introduced via a Finnigan Gasbench II (Thermo Electron, Bremen, Germany) with GC PAL autosampler (CTC Analytics,

Zwingen, Switzerland) to a DELTA V Plus continuous flow isotope ratio mass spectrometer (Thermo Electron). The autosampler tray was heated to 30 °C to ensure positive pressure in the sample vials. O_2 and N_2 were separated on a 30 m, 0.32 mm ID, 5Å PLOT fused-silica molsieve GC column (Varian Inc., Santa Clara, CA, USA; product #CP7534) at 30 °C. N_2 was measured in the mass spectrometer by executing a fast peak jump to *m/z* 28 after the O_2 had fully eluted from the GC column. Linearity correction, calibration of $\delta^{18}O$ and O_2/N_2 values, and the use of open split settings to maximize dynamic range of the mass spectrometer were performed as described by Kornfeld et al. (2012b; or Chapter 2).

3.2.5. Discrimination computations with contamination correction

Discrimination was computed from the measured isotope ratios, ${}^{34}R \equiv {}^{18}O^{16}O / {}^{16}O^{16}O \equiv {}^{34}O_2/{}^{32}O_2$ and ${}^{32}O^* \equiv {}^{32}O_2/{}^{28}N_2$ along the lines of Henry *et al.* (1999) with modifications to correct for contamination, as follows. Table 3.1 provides an overview of the symbols used in this discussion.

Isotope ratios are often reported using δ notation to highlight small deviations relative to a standard isotope ratio, ${}^{34}R_{std}$:

$$\delta^{18}O\ (‰) \approx \delta^{34}O_2\ (‰) \equiv \left(\frac{{}^{34}R}{{}^{34}R_{std}} - 1 \right) \times 1000 \quad . \tag{3.1}$$

$\delta^{18}O$ values are reported here relative to the O_2 isotope ratio of atmospheric air (Wieser & Berglund, 2009).

Discrimination is defined in a similar fashion as:

$$D\ (‰) \equiv -(\alpha - 1) \times 1000, \tag{3.2}$$

where the fractionation factor, α, represents a ratio of rate coefficients for the reduction reaction of ${}^{34}O_2$ *vs.* ${}^{32}O_2$ into water (Appendix A3.4).

The proportion of oxygen consumed in the incubation vial is represented by:

$$f^* \equiv \frac{{}^{32}O^*}{{}^{32}O_0^*} \equiv \frac{{}^{32}O_2/{}^{28}N_2}{({}^{32}O_2/{}^{28}N_2)_0}, \tag{3.3}$$

where the subscript, 0, indicates the initial state in the incubation vial, as determined by the air blanks. In Appendix 2 I explain why ${}^{32}O_2 / {}^{32}O_{2,0}$ by itself is inappropriate in this case.

Storage vials contain a mixture of contaminating air with air transferred from the incubation vial (Table 3.1). If one considers only the properties, ${}^{34}R_{\text{sample}}$ and f^{*}_{sample}, of the incubation air, then D is computed by the linear regression:

$$1000 \times \ln\left(\frac{{}^{34}R_{sample}}{{}^{34}R_{sample,0}}\right) = -D \ln f^{*}_{sample}, \tag{3.4}$$

where the subscript 0 denotes the initial state in the incubation vial and the regression is not forced through the origin (Guy *et al.*, 1989, Henry *et al.*, 1999). In practice, the ratio ${}^{34}R/{}^{34}R_0$ was replaced with the equivalent ratio, $(\delta^{18}O + 1000)/(\delta^{18}O_0 + 1000)$, since δ values were reported with greater precision by the mass spectrometer software (ISODAT; Thermo Electron).

In order to derive ${}^{34}R_{\text{sample}}$ or, equivalently, $\delta^{18}\text{O}_{\text{sample}}$, the measured properties of the air in the storage-vial, $\delta^{18}\text{O}_{\text{mix}}$ and ${}^{32}\text{O}^{*}_{\text{mix}}$, were converted to $\delta^{18}\text{O}_{\text{sample}}$ and ${}^{32}\text{O}^{*}_{\text{sample}}$ by mass balance, using N_2 transfer blanks to estimate the O_2 contamination, O_c, in the storage vials:

$$\delta^{18}O_{sample} = \frac{\delta^{18}O_{mix}\,{}^{32}O_{mix} - \delta^{18}O_c\,{}^{32}O_c}{{}^{32}O_{mix} - {}^{32}O_c}. \tag{3.5a}$$

Or, equivalently,

$${}^{34}R_{sample} = \frac{{}^{34}R_{mix}\,{}^{32}O_{mix} - {}^{34}R_c\,{}^{32}O_c}{{}^{32}O_{mix} - {}^{32}O_c}. \tag{3.5b}$$

Equations (3.5a) and (3.5b) are exact solutions in the sense that ${}^{32}O_2$ is not merely an approximation for total O_2 (Appendix A3.4.3).

In principle ${}^{32}O^{*}_{\text{sample}}$, can be computed as:

${}^{32}O^{*}_{\text{sample}} = ({}^{32}\text{O}_{\text{mix}} - {}^{32}\text{O}_{\text{c}})/ (\text{N}_{\text{mix}} - \text{N}_{\text{c}})$.

In practice, however, ${}^{32}O^{*}$ was treated as a fundamental quantitiy because I computed it as a nonlinear function of measured peak areas (Kornfeld *et al.*, 2012b; or Chapter 2). I therefore used the ratio ${}^{32}O_2/{}^{32}O^{*}$ to represent ${}^{28}N_2$, so that

$${}^{32}O^{*}_{sample} = \frac{{}^{32}O_{mix} - {}^{32}O_c}{\frac{{}^{32}O_{mix}}{{}^{32}O^{*}_{mix}} - \frac{{}^{32}O_c}{{}^{32}O^{*}_{c,He}}}, \tag{3.6}$$

where ${}^{32}O^{*}_{c,He}$ was estimated using the He blank vials. I discuss this equation further in Appendix A3.4.4.

3.2.6. Curvature analysis

Equation (3.4) can be used as a basis for linear regression only if respiratory *D* is constant. Uncorrected contamination is also a source of nonlinearity. The error in *D* computed using Eqn (3.4) under these conditions is sensitive to several factors including the actual discrimination value(s), the amount and isotopic composition of contamination and, most importantly, the extent of O_2 consumption (i.e. f^*). If left uncorrected, values of *D* computed for two processes with identical rates of actual discrimination could be erroneously declared to be statistically different if, for example, f^* or vial contamination differed between the two experiments.

Previous reports have suggested that r^2 values greater than 0.995 for a 6-point regression imply that *D* is constant (Lennon *et al.*, 1997, Millenaar *et al.*, 2001, Ribas-Carbo *et al.*, 1997). Using simulated and actual data, however, I show here that r^2 can remain above 0.995 even in the presence of substantial curvature. I therefore propose a lack-of-fit test to detect curvature by adding a second-order term to the regression (Fox & Weisberg, 2011):

$$1000 \times \ln\left(\frac{{}^{34}R}{{}^{34}R_0}\right) = \beta_2 \left(\ln\ f^*\right)^2 - \beta_1 \ln\ f^* . \qquad (3.7)$$

Statistical significance of the β_2 term, i.e. $P < 0.05$, indicates the presence of curvature and I therefore call the associated *P*-value P_{curv}. Additionally, since *D* is estimated as the slope of the graph of $\ln(R/R_0)$ *vs.* $-\ln(f^*)$, the derivative of Eqn (3.7) with respect to $-\ln f^*$ estimates instantaneous *D* in the presence of curvature, i.e.

$$D_q = -2\beta_2 \ln\ f^* + \beta_1 , \qquad (3.8)$$

where the subscript *q* indicates that *D* was derived using a quadratic equation. In particular, Eqn (3.8) indicates that β_1 estimates the value of *D* at the start of the incubation, when $\ln f^* = 0$. Since this initial value is generally of most interest, I report D_q as the value of the β_1 term in Eqn (3.7), unless otherwise noted.

Finally, to help visualize the effects of curvature on the linear regression, I constructed a *curvature graph* by using Eqn (3.4) to compute values of *D* on subsets of the respiration data created by successively deleting the point with the smallest f^* value

(Fig 3.1b, for example). The graph of D_x *vs.* x – where x is the lowest value of f^* in the subset (i.e. the greatest O_2 consumption), and D_x is the corresponding value of D computed using Eqn (3.4) – depicts the sensitivity of Eqn (3.4) to O_2 consumption. Error bars representing the standard error of the regression coefficient for D_x provide a visual indication of significance since uncertainty in the estimate may increase as points are eliminated from the regression (Fig 3.3b, for example).

3.2.7. Simulation

Simulated datasets were used for several purposes: to determine the statistical power of P_{curv}, to predict the precision of computed D, to determine the ideal number of replicates and O_2 consumption for an experiment, and to demonstrate the effects of nonlinearity on computed D. The simulation equation was derived from Eqn (3.4) – using the $(\delta^{18}O + 1000)/(\delta^{18}O_0 + 1000)$ form of R/R_0 – by removing the *sample* subscript, setting $\delta^{18}O_0 = 0$, and then solving for $\delta^{18}O$ to get:

$$\delta^{18}O = 1000\left[f^{*\left(\frac{-D}{1000}\right)} - 1 \right]. \qquad (3.9)$$

O_2 consumption was specified by decreasing f^* from 1.0 to a final value; D specified the "actual" (model) discrimination value(s). Contamination was simulated by computing $\delta^{18}O_{mix}$ and ${}^{32}O^*_{mix}$ respectively by rearranging Eqns (3.5) and (3.6). Random values were added to $\delta^{18}O$ and f^* to simulate measurement noise. Regression on the resulting values of $\delta^{18}O$ and f^* using Eqn (3.4) or (3.7) provided estimates of expected systematic error and uncertainty in computed D. Statistical power of P_{curv} was computed as the fraction of 500 simulations having P_{curv} less than 0.05.

3.2.8. Statistical analysis

Statistical analysis was conducted using linear models in the R statistical language (R Development Core Team, 2011). The laboratory protocol at the website: http://www.biol.canterbury.ac.nz/lab-protocols/ includes sample R code for the computations and graphs presented here.

3.2.8.1. Outlier analysis

To reduce the sensitivity of Eqns (3.4) and (3.7) to outliers, points were tested as described by Cook & Weisberg (1999): a dummy variable indicating the data point having the largest Cook's distance was added to the regression. The point was rejected as

an outlier if the P value for the dummy variable was less than $0.05/n$, the number of points in the regression. The process was repeated iteratively until no further points were rejected.

3.2.8.2. Mean, SE, and Inference on D

Since each data point comes from a different incubation, all points are statistically independent. In this study replicates, i.e. sets of six vials, generally did not represent biologically distinct groups. In such cases I evaluated all points together and used ANOVA to test for treatment differences, determined as statistical significance of the interaction term, Treatment × ln(f^*), in:

$$y = \beta_1 \text{ Treatment} + \beta_2 \ln(f^*) + \beta_3 \text{ Treatment} \times \ln(f^*) + \beta_0, \qquad (3.10)$$

where y is $1000 \times \ln(R/R_0)$ as in Eqn (3.4), and Treatment is an indicator variable for the treatments (Crawley, 2005). Eqn (3.10) can also be interpreted as a linear regression, in which case there are separate β_3 terms for all but one of the treatments. Significance of these terms was used to determine whether a particular treatment differed from the control. I also used Eqn (3.10) to confirm that incubations representing different biological replicates within a treatment could be combined. In such cases the Treatment variable referred to individual replicates within a single treatment. If the interaction term was significant, the mean and standard error of D were computed using a mixed-effects regression with Treatment (replicate) specified as a random effect (Pinheiro & Bates, 2000).

3.2.9. Experimental application of the methods

This section describes the experiments used to validate my methods. Species were chosen because of prior work with native New Zealand species – *Griselinia littoralis* Raoul and *Aristotelia serrata* Oliv. – and/or because established D values had been published for these species, i.e., *G. littoralis* and soybeans (*Glycine max* L.).

3.2.9.1. Variable D

Simulated replicates were specified as six values of f^* distributed at approximately equal intervals between 1.0 and the final value. D was either constant or was evenly distributed between 31‰ and the final value. $\delta^{18}O$ was computed using Eqn (3.9) with or without normally distributed "measurement" noise added to f^* and $\delta^{18}O$. In each of 500 simulation runs, "linear" and "quadratic" D were determined by regression, using Eqns (3.4) and (3.7) respectively on the combined 6–24 points (1–4 replicates).

3.2.9.2. Initial contamination

Branches of *G. littoralis* were harvested from trees at the University of Canterbury, Christchurch, New Zealand. The branches were recut under water before being brought to a laboratory and placed in the dark for at least 30 minutes. Each replicate consisted of six vials into which sets of 1 cm-wide leaf slices ranging from 0.25 to 2.0 g fresh mass were incubated in the dark for 4 h at 20 °C. Paired "clean" and "contaminated" samples were produced by first injecting 6 mL of the incubation air into He-flushed storage vials, waiting 5 s, then allowing the vial pressure to push the plunger back out. Of the resulting mixture 4 mL was immediately injected into a second storage vial that had been evacuated either 1.3 or 9 months prior to the experiment. Air and O_2-free blanks were prepared by direct injection. For the contamination correction, transfer contamination was estimated to be 1% atmospheric air with $\delta^{18}O = -2‰$, based on prior experiments (Appendix A3.3.6). Sensitivity analysis indicated that variations in the exact estimate of transfer contamination had little effect on the final result.

3.2.9.3. Storage contamination

Seven *G. littoralis* replicates were incubated as just described, but incubation air was transferred to freshly evacuated storage vials without He-flushed intermediates. Two replicates were measured immediately; the remainder were stored for 10 months either in a freezer at –17 °C ($n = 3$) or in a laboratory cabinet (20 °C; $n = 2$). Each replicate also included He-flushed storage vials and evacuated vials, which were brought back to atmospheric pressure shortly before measurement by injecting O_2-free helium. Because the initial contamination in these "evacuated blanks" had not been diluted before storage by overinjection, the contamination correction procedure was slightly modified, as described in Appendix A3.3.7.

3.2.9.4. Tissue volume effects

Two species were investigated to determine whether leaf structure interacted with tissue volume to restrict diffusion during incubation. Thick, stiff *G. littoralis* leaf-strips were incubated in groups of 2, 4, or 6 strips/vial (mean volume 0.98 ± 0.14, 1.9 ± 0.2, and 2.7 ± 0.2 mL) and incubated at 20 °C for variable durations up to 7.7, 3.8, and 2.9 h, respectively. Thinner and more pliable *A. serrata* strips were grouped in 4, 8, or 12 strips/vial (mean volume 0.63 ± 0.04, 1.57 ± 0.9, and 1.87 ± 0.18 mL) and incubated up to 6, 1.8, and 2.1 h, respectively (see Appendix A3.2 Fig S3 for photos of these treatments). Moistened strips of chromatography paper, flattened against the inside wall

of the vial, were added for the lowest-volume treatments to reduce drying effects during the longer incubation periods. A separate set of four *A. serrata* leaf strips were frayed by tearing the edges to test the effects of wounding on the measured discrimination values.

3.2.9.5. Respiratory inhibition tests

G. littoralis leaf slices were prepared as above. Soybeans plants were grown either in a glasshouse (the etiolation control), a dark cabinet (etiolated soybeans) or in growth chambers with 14 h/10 h cycles of 400 μmol m^{-2} s^{-1} PAR light/dark, measured at leaf level, and 27 °C/22 °C temperature. Soybean incubations consisted of 3–4 halved cotyledons per vial (etiolated cotyledons were not cut) or 3 whole root systems, rinsed thoroughly and gently dried with paper towels.

COX in both species was inhibited using gaseous cyanide (Millar *et al.*, 1998) by sealing plant tissue in 120 mL vials for 10 minutes together with a 1 x 8 cm strip of chromatography paper saturated with 1 M KCN (0.3 mL). Soybean root AOX was inhibited by sandwiching plant tissue between medical wipes saturated in 20 mM salicylhydroxamic acid (SHAM) in 2% dimethyl sulfoxide (DMSO) for 20 minutes. Soybean cotyledons and *G. littoralis* leaves did not show evidence of AOX inhibition using this method. Soybean cotyledons were successfully inhibited by stirring for 30 minutes in a slurry of $5\%_{vol}$ 400 grit silicon carbide grains in 20 mM SHAM. Cotyledons treated this way and subsequently inhibited with gaseous cyanide showed only 13.5% residual respiration – similar to the value reported by Ribas-Carbo *et al.* (1997).

Separately, *G. littoralis* COX and AOX were inhibited by vacuum infiltration with 10 mM KCN or 25 mM SHAM. Tissue was allowed to dry back to its initial fresh weight before incubation, as described by Nagel *et al.* (2001). Storage vials for the infiltration experiment were held for 80 days at laboratory temperature before measurement. All other vials were either measured immediately or stored at –17 °C for less than a month. Based on results in this paper, both of these storage conditions should have had negligible effects on computed *D*.

Inorganic oxidation: $FeSO_4$ oxidation was carried out at 54 °C using 0.5 M solutions of $FeSO_4$ buffered with 3-(N-Morpholino)propanesulfonic acid (MOPS) to pH 7, as described by Oba & Poulson (2009) except that I incubated 3 mL aliquots of the solution in 12 mL incubation vials and transferred gases as described above.

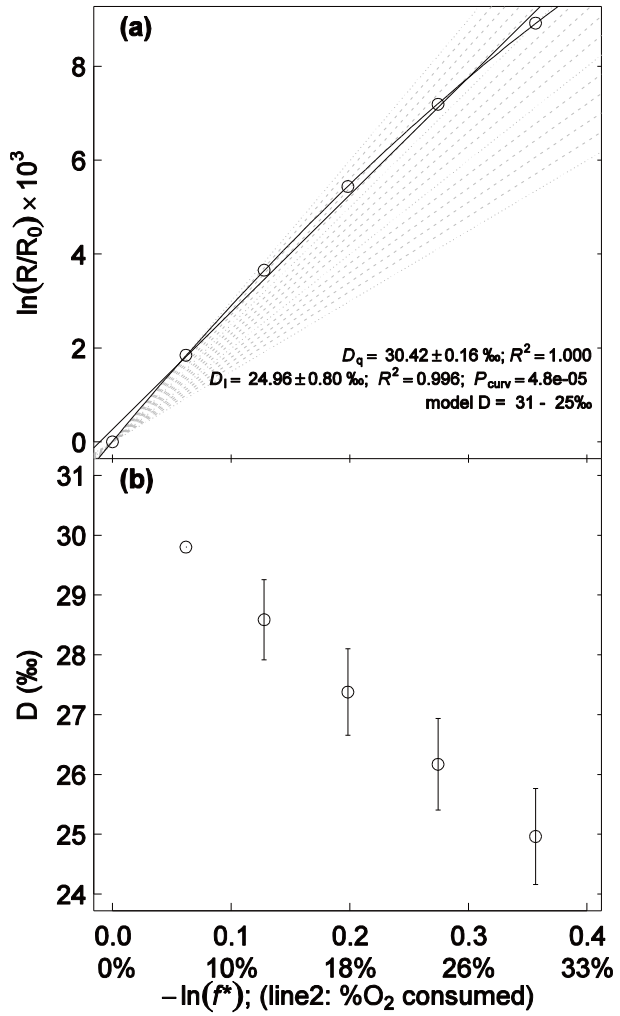

Fig 3.1. Simulated effects of *D* changing from 31 to 25‰.

In the discrimination graph (a), D_l was computed using the linear regression based on Eqn (3.4); D_q was computed using the quadratic formula, Eqn (3.7). P_{curv} represents the probability that the graph is linear. The grey dashed and dotted lines represent permil isoclines in *D* from 15–30‰. Values of *D* are reported as mean ± SE of the regression coefficient. In the curvature graph (b), each point represents the value of D_x computed using Eqn (3.4) on the subset of points for which $-\ln(f^*) \leq x$. Error bars represent the SE of the regression coefficient for D_x. (Compare (a) with Appendix A3.2 Fig S4a, which does not include guide lines.)

3.3. RESULTS AND DISCUSSION

This section starts with a discussion of variable *D* in order to introduce the analytical tools and concepts and to emphasize that nonlinearites arise even in the absence of contamination. I then discuss contamination, storage, and tissue-volume issues before concluding with a comparison of results obtained using my methods *vs.* published results.

3.3.1. Nonlinearity due to intrinsic variability in *D*

As noted in the Materials and Methods section, the conventional regression for estimating discrimination, Eqn (3.4), is valid only while *D* is constant. Discrimination may vary during the course of measurement for several reasons. Respiratory electron partitioning, or other oxygen-consuming processes, may change during the course of measurement for natural reasons or due to experimental conditions such as recovery from selective inhibition. Apparent discrimination may also change due to diffusional resistance (Angert & Luz, 2001) or changing O_2 gradients in dense or very active tissue (Miller *et al.*, 2011). Here I demonstrate an effective way to detect nonlinearity effects on the regression analysis and to estimate the "least perturbed," i.e. initial, discrimination value. Although well beyond the scope of this study, this approach also offers a potential means to examine rapid dynamics in discrimination, a topic that has not been addressed in the conventional "steady-state" approach but, as shown next, may deserve attention.

I evaluated the effects of nonlinearity by simulating experiments in which *D* varied. Fig 3.1 depicts an extreme example in which model *D* varied from 31 to 25‰ as f^* varied from 1.0 to 0.7 in the absence of noise. Since *D* is not constant, the model discrimination values represent the integrated effects of discrimination on “vial” air composition up to the moment it was “sampled.” Eqn (3.8), however, can be used to estimate instantaneous values of *D* based on the quadratic regression, Eqn (3.7). The final discrimination value was thus estimated as 19.5‰, indicating a change of instantaneous discrimination from 31 to 19.5‰.

Despite a change equivalent to shifting from 100% AOX respiration to 100% COX, the r^2 value of the linear fit was 0.996 (Fig 3.1a) and the curvature was not readily seen without the superimposed lines (Appendix A3.2 Fig S4a). Adding simulated measurement noise did not shift r^2 below the published 0.995 cutoff (Appendix A3.1 Table S3.1). The lack-of-fit test proposed here, on the other hand, correctly identified the curvature ($P_{curv} < 0.0001$, Fig 3.1a). Adding measurement noise typical of my instrumentation reduced statistical power, but P_{curv} correctly identified the nonlinearity 70% of the time for a single six-point replicate and 100% of the time if four replicates were combined (Appendix A3.1 Table S3.1). In general, the statistical power of P_{curv} depends on several factors including the extent of change in *D*, contamination level, total O_2 consumption, measurement noise, and the number of replicates (Appendix A3.2 Fig S5).

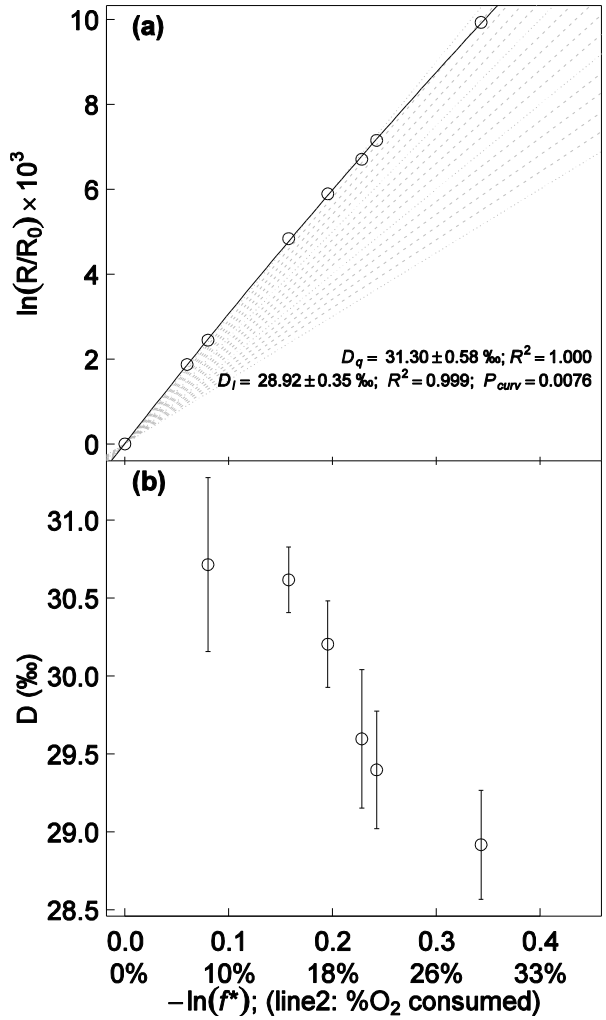

Fig 3.2. Example of curvature in real data: KCN-treated soybean cotyledons.

See Fig 3.1 for an explanation of the graph layout. Regression line represents the quadratic fit. (Compare (a) with Appendix A3.2 Fig S4b, which does not include guide lines.)

Returning to the simulated data, the traditional linear regression, Eqn (3.4), estimated D as 24.96‰ (D_l, Fig 3.1a). The associated curvature graph (Fig 3.1b) demonstrates that the linear method was strongly influenced by O_2 consumption: the computed value of D_x was generally close to the final value of model D for any particular value of $x = f^*$. The quadratic regression, Eqn (3.7), on the other hand, estimated initial D as 30.42‰ (D_q, Fig 3.1a), and more closely reflected the initial value of D regardless of O_2 consumption (Appendix A3.1Table S3.1 and A3.2 Fig S6).

Fig 3.2 shows an example of *D* varying during an actual incubation of COX-inhibited soybean cotyledons. The data were corrected for initial contamination; concurrent incubations of untreated tissue showed no curvature. I conclude that the curvature was due to physiological changes as the tissue recovered from the inhibitor. The initial, pre-recovery, value of *D* therefore best estimates the AOX discrimination endpoint. The linear calculation, D_l, is 28.9 ± 0.3‰, considerably lower than published values of 31.5 ± 0.3‰ (Ribas-Carbo *et al.*, 1997). As with the simulated data, the R^2 of 0.999 is well above the 0.995 cutoff, whereas $P_{curv} < 0.01$ suggests that the graph is not linear. The quadratic estimate, D_q, is 31.3 ± 0.6‰ (Fig 3.2a). Early points in the curvature graph are also above 30‰ (Fig 3.2b), confirming that the quadratic estimate reflects the initial value of *D*.

My simulations indicated that the quadratic estimate is closer to the initial value of *D* and is much less sensitive to O_2 consumption than is the linear estimate (see also Appendix A3.1 Table S3.1 and A3.2 Fig S6a). The increased accuracy, however, comes at the price of a 2- to 4-fold reduction in precision (Appendix A3.1 Table S3.1 and A3.2 Fig S7). I therefore recommend removing correctible sources of nonlinearity, discussed next, rather than relying solely on the quadratic estimate. Nevertheless, when nonlinearity cannot be remediated, such as in the examples above, the quadratic regression greatly improves accuracy. I propose the objective P_{curv} test associated with Eqn (3.7) to determine the choice of appropriate regression.

3.3.2. Contamination

Contamination may be introduced at several stages of the experimental process. I found three significant sources of contamination: First, incomplete pre-evacuation left a small amount of air in the storage vials; second, contaminating air was introduced during transfer from the incubation vial to the storage vial. Third, gases diffused into and out of the vial during storage. Here I discuss each source of contamination and how to address the effects.

3.3.2.1. Initial and transfer contamination

Freshly evacuated storage vials contained residual amounts of O_2 at 3 – 4% of atmospheric O_2 concentration with $\delta^{18}O$ not significantly different from 0 (the atmospheric isotope ratio) and O_2/N_2 of 0.276, very close to the atmospheric ratio of 0.269 (Table 3.2). The transfer process contributed an additional 1% of atmospheric O_2,

as determined by the difference between transferred and directly injected O_2-free gas (Appendix A3.3.6). The majority of the transfer contamination appears to be due to outgassing of the displacement fluid (Appendix A3.3.6), and should therefore be proportional to the gradient between pO_2 in the incubation sample and atmospheric pO_2. Nevertheless, in Appendix 2e I show that both initial and transfer contamination can be corrected based on O_2-free vials.

Table 3.2. Storage effects on "blank" vials stored for 10 months.

Type	Storage	$O_2/O_{2,atm}$	$\delta^{18}O$	O_2/N_2	*n*
He-flush					
	fresh	0.06 ± 0.02%	n/a	n/a	13
	–17 °C	0.34 ± 0.10%***	n/a	n/a	4
	20 °C	3.7 ± 0.2%***	–8.69± 0.02‰	0.756 ± 0.03	3
Vacuum					
	fresh	3.8 ± 0.5%	0.19 ± 0.13‰	0.276 ± 0.001	3
	–17 °C	4.0 ± 0.8%	-0.29 ± 0.10‰	0.282 ± 0.004	4
	20 °C	8.0 ± 1.7%**	–3.37 ± 1.0‰***	0.364 ± 0.038**	3

** $P < 0.01$ relative to fresh, *** $P < 0.001$ relative to fresh

Values are expressed as mean ± SD. Evacuated vials were injected with 4 mL He shortly before measurement; flushed vials were topped up before measurement to replace He that had diffused out over time. Fresh and frozen He-flushed vials did not contain enough O_2 to determine isotope ratios. Atmospheric air was defined as 100% $O_2/O_{2,atm}$ with $\delta^{18}O$ = 0‰, and O_2/N_2 = 0.2692.

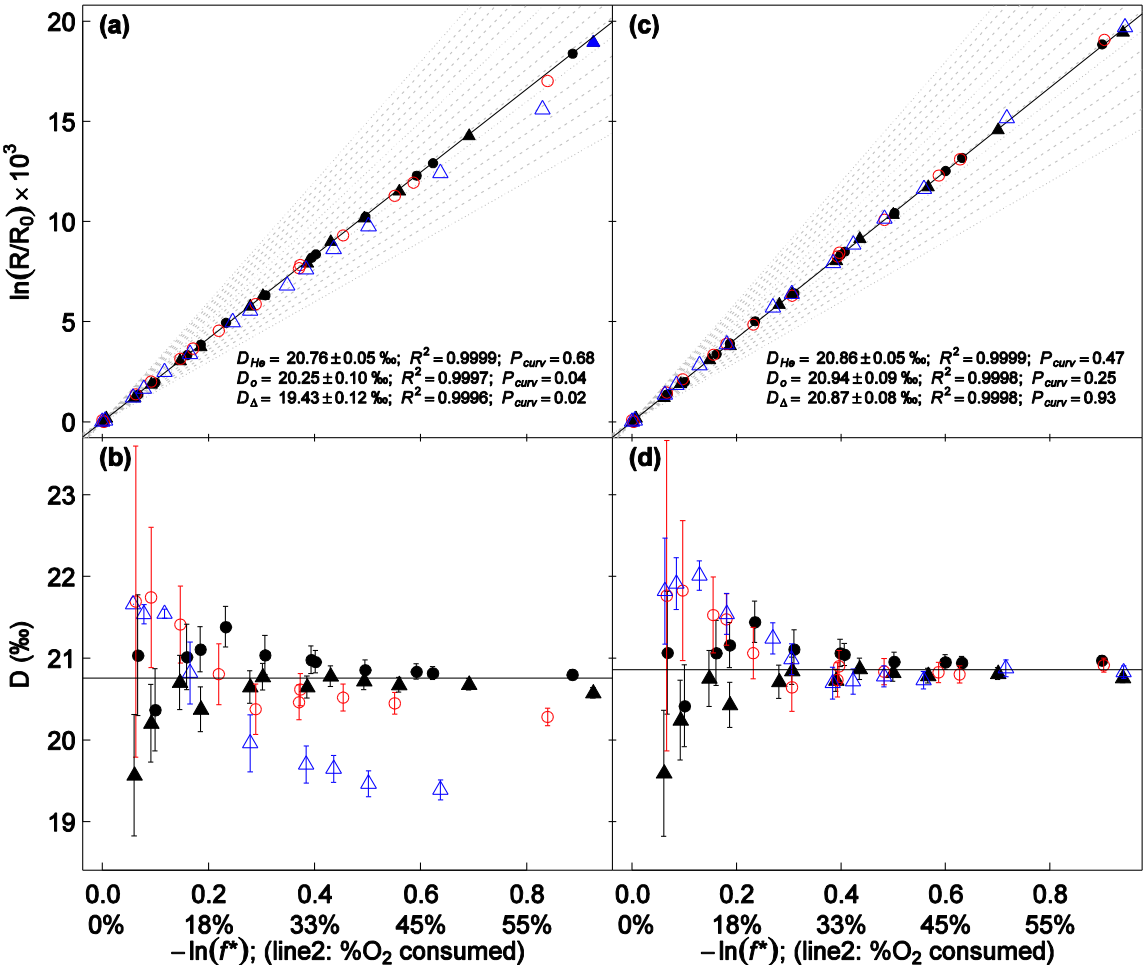

Fig 3.3. Effects of initial contamination: (a, b) uncorrected data; (c, d) after correction. Air from incubation vials was injected sequentially into He-flushed vials (filled symbols) and then into evacuated vials containing one of two levels of contamination. Open circles represent storage vials with 2.6% $O_2/O_{2,atm}$ contamination having $\delta^{18}O = 0‰$; open triangles represent evacuated vials with 5.4% $O_2/O_{2,atm}$ contamination with $\delta^{18}O = –6‰$. *D* was computed using Eqn (4). See Fig 3.1 for an explanation of the graph layout.

O_2-free "blanks" prepared alongside the respiratory samples were used to determine the levels of contamination, $\delta^{18}O_c$ and f_c^*. Eqns (3.5) and (3.6) were then used to compute $\delta^{18}O_{sample}$ and f^*_{sample} for use in Eqns (3.4) or (3.7). To validate the effectiveness of my contamination correction I sequentially injected incubation air samples into He-flushed vials (containing negligible contamination, Table 3.2) and evacuated vials, resulting in paired storage vials containing the same incubation gas but different levels of contamination. Two types of evacuated vials were used: freshly evacuated vials with "light" contamination (2.6 ± 0.7% $O_2/O_{2,atm}$ [mean ± SD] having

$\delta^{18}O = -0.09 \pm 0.19‰$) and older vials with "moderate" contamination ($5.4 \pm 0.2\%$ $O_2/O_{2,atm}$ with $\delta^{18}O = -6.2 \pm 0.5‰$). Fig 3.3a, b shows uncorrected measurements. Contamination shifted points to the left but decreased $\delta^{18}O_{mix}$ values even more strongly. Consequently, values of D derived using Eqn (3.4) were 0.5‰ and 1.3‰ lower than the contamination-free estimate of $20.76 \pm 0.05‰$ ($P < 10^{-5}$ for each difference) for the lightly and moderately contaminated vials respectively. Thus, the computed values of D would be considered statistically different from each other, even though the incubation air samples in these paired vials were identical. The r^2 values above 0.999 for the graphs were well above the published threshold of 0.995 for linearity, but curvature was detected by my proposed lack-of-fit test ($P_{curv} < 0.05$, Fig 3.3a). The effects of curvature can be seen in Fig 3.3b as a variation in D with total O_2 consumed. Simulation tests indicate that the magnitude of error due to contamination also depends upon the actual discrimination value (Appendix A3.1 Table S3.1 and A3.2 Fig S8).

Correcting for initial and transfer contamination using Eqns (3.4) – (3.6) brought the paired points into reasonable alignment, as indicated by the overlapping open and filled symbols (Fig 3.3c). The estimates of D are no longer significantly different for the three types of storage vial, $P > 0.66$ for the interaction term in Eqn (3.10). The data also appear to be linear ($P_{curv} > 0.25$, Fig 3.3c, d). Estimated D for the He-flushed vials increased 0.1‰ after correcting for transfer contamination.

The contamination correction, unlike the quadratic regression, was not biased nor did it substantially increase uncertainty: standard error of regression for the helium vials (±0.06‰ for each subset) was very similar to that of the evacuated vials (±0.08, ±0.09‰, Fig 3.3c). The increased uncertainty is likely due to variations in evacuation quality.

3.3.2.2. Storage contamination

Incubation air samples are enriched in N_2 and depleted in O_2 relative to the atmosphere (Table 3.1; see also Appendix A3.4.2). As a result, vial O_2 increases, $\delta^{18}O$ decreases, and vial N_2 decreases over time due to diffusion. Other processes such as oxidation of the septum may also alter vial air composition over time. I tested for storage effects in a set of simultaneously incubated *G. littoralis* leaves. Some vials were measured immediately; the remainder was stored for 10 months at either 20 °C ("bench") or –17 °C ("frozen"). Fig 3.4a and Table 3.2 show that frozen vials maintained

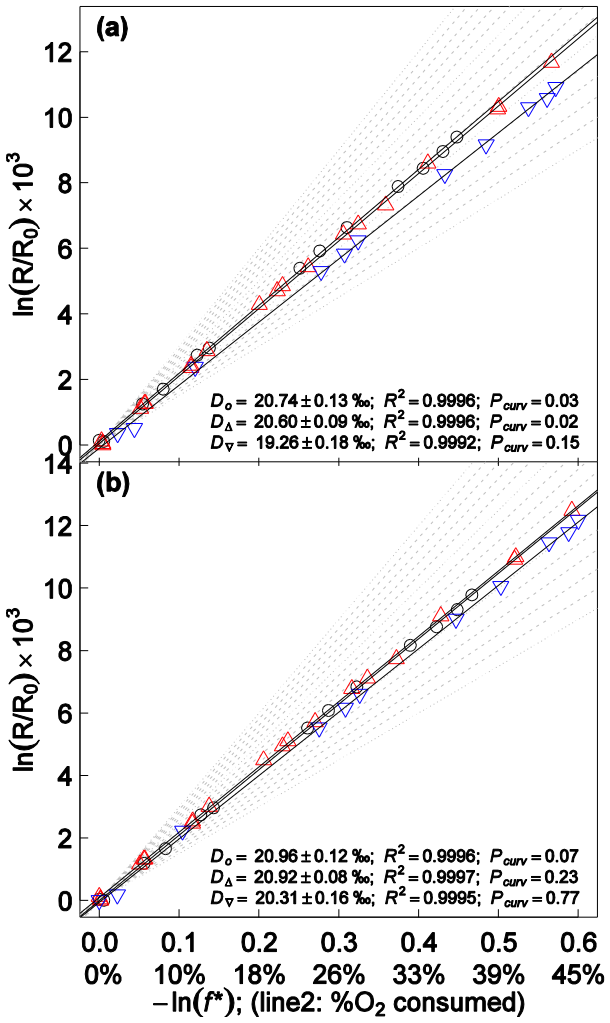

Fig 3.4. Long-term storage effects on respiration samples: (a) uncorrected data (b) corrected data.

Circles represent samples measured immediately after incubation; upward pointing triangles: vials stored at –17 °C for 10 months; downward triangles: vials stored at 20 °C for 10 months. See Fig 3.1 for an explanation of the graph layout.

their integrity for 10 months, whereas the contents of bench-stored vials changed significantly. D_l was reduced by 1.5‰ in the bench-stored vials before correction ($P < 10^{-8}$) whereas freezer-stored vials were not substantially affected (Fig 3.4a; $P > 0.4$). Correcting the data using blanks that had been stored alongside each set of vials fully corrected the data for the frozen vials, but left a statistically significant shortfall of 0.65‰ for the bench-stored vials ($P < 0.001$; Fig 3.4b). Thus, even though the remaining shortfall is relatively small, discrimination computed for the bench-stored vials would have been erroneously judged to be different than for the fresh vials even after correction.

My proposed curvature test does not detect curvature in the bench-stored vial data even without the contamination correction ($P_{curv} > 0.05$), possibly due to the increased variability (Table 3.2) or due to the relatively small shortfall in computed *D*.

A previous report (Nagel *et al.*, 2001) found no detectable O_2 leakage into 10 mL vials after six months storage at laboratory temperature, whereas I found 4% atmospheric O_2 leakage into my 3.7 mL vials after 10 months (Table 3.2). The absolute leak rates were probably similar in both experiments, since cap size is the same for both vial types. The smaller size of my vials, however, resulted in a greater effect as a percent of volume. Nevertheless, by storing vials at –17 °C, even the smaller vials remain viable much longer than six months.

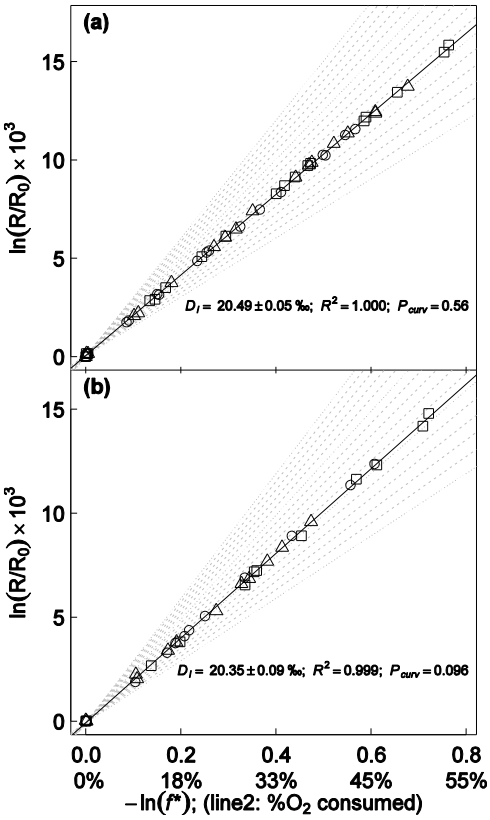

Fig 3.5. Tissue volume effects.

Incubations were conducted with one of three quantities of leaf tissue; respiration times were adjusted to achieve similar O_2 consumptions. Two species were examined. (a) *G. littoralis* with thick, stiff leaves. Circles: 2 strips; triangles: 4 strips; squares: 6 strips. (b) *A. serrata* with thin, pliable leaves. Circles: 4 strips; triangles: 8 strips; squares: 12 strips. Discrimination values are for the pooled data since differences between the groups were not statistically significant. See Fig 3.1 for an explanation of the graph layout.

3.3.3. Does tissue volume affect measured *D*?

As the amount of material in the vial increases, restrictions to gas mixing during incubation could result in a diffusion gradient that lowers measured *D* (Angert & Luz, 2001). I tested the effects of tissue volume on computed *D* in two types of leaves: *G. littoralis* leaves were thick (0.9 mm), stiff, and relatively smooth. *A. serrata* leaves were thin (0.25 mm) and pliable making the leaf strips more likely to fold and/or stick together to form air pockets in the incubation vial. No statistically significant effects were detected over a 3-fold change in leaf volume (Fig 3.5 and Table 3.3). I did not test leaf volumes greater than 3 mL because of difficulties inserting so much tissue into the vials. Wounding the tissue did not appear to change measured discrimination either (Table 3.3).

Table 3.3. Effects of tissue volume on computed *D*.

Species/Size	D_l	Linear R^2	P_{curv}	D_q	*n*	Max O_2 consumed
Griselinia						
2 strips	20.39 ± 0.08	0.9998	1.0	20.4 ± 0.3	17	43%
4 strips	20.43 ± 0.10	0.9996	0.03	21.1 ± 0.3*	18	49%
6 strips	20.56 ± 0.06	0.9999	0.7	20.6 ± 0.2	18	53%
Aristotelia						
4 strips	20.59 ± 0.15	0.9995	0.5	20.3 ± 0.5	12	45%
8 strips	20.17 ± 0.19	0.9991	0.2	19.3 ± 0.6	12	38%
12 strips	20.34 ± 0.17	0.9993	0.2	19.5 ± 0.6	12	51%
Aristotelia						
4 bruised	19.8 ± 0.3	0.998	0.2	18.3 ± 1.0	7	22%
4 ctl (25% dd)	20.1 ± 0.3	0.998	0.01	17.4 ± 0.7	8	22%

* $P = 0.06$ for the comparison of 4 strips to the other treatments.

Incubation vials were filled with the specified amount of leaf tissue and incubations times were adjusted to keep the ranges of O_2 consumption approximately equal. None of the differences in *D* within species were found to be statistically significant. *n* refers to the number of points in each regression. D_l was computed using Eqn (3.4); D_q, with Eqn (3.7).

Table 3.4. Comparison of computed discrimination values, *D*, based on my method *vs.* previously published data.

Species/Treatment	*D*	*reps*	Prior reports
G. littoralis leaves			
SHAM infiltrated	18.5 ± 0.5‰	4	15.7 ± 0.4‰ [d]
control infiltrated	20.0 ± 0.5‰	4	16.3 ± 0.5‰ [d]
control uninfiltrated	21.91 ± 0.07‰	4	17.0 ± 1.1‰ [d]
KCN infiltrated	25.3 ± 0.8‰ [a]	4	25.3 ± 0.5‰ [a, d]
KCN (gas) [b]	29.0 ± 0.1‰	4	(no prior report)
control 2 [b]	20.83 ± 0.05‰	5	17.2 – 20.2‰ [d]
Phaseolus vulgaris leaves			
SHAM	21.6 ± 0.4‰ [e]		19.0 ± 2.2‰ [f], 19.5 ± 0.5‰ [g]
control	20.5 ± 0.4‰ [e]		18.7 – 22.9‰ [f, g]
KCN	25.8 ± 0.5‰ [e]		26.7 ± 0.97‰ [f], 30.3 ± 0.4‰ [g]
Soybean roots			
SHAM	19.5 ± 0.7‰	3	16.2 – 20.8 [h]
control	20.3 ± 0.3‰	3	16.4 – 22.4 [h]
KCN	24.6 ± 0.7‰	4	24.3 – 27.1 [h]
Soybean cotyledons			
etiolated	18.3 ± 0.7‰	2	18.1 ± 1.4 [i], 18.6 ± 0.8 [j]
green	23.8 ± 0.3‰	2	(glasshouse grown)
control	24.4± 0.1‰	7	24.3 – 25.3 [i, j, k]
KCN [c]	30.0 ± 0.5‰	5	31.5 ± 0.3‰ [l]
SHAM abraded	21.5 ± 0.4‰	2	(20.0 ± 0.4‰ [l])
control abraded	23.4 ± 0.4‰	1	(no prior report)
KCN abraded [c]	29.6 ± 0.6‰	1	(no prior report)
KCN + SHAM abraded	28.7 ± 1.1‰	2	(21‰ [l])
$FeSO_4$ oxidation			
	9.6 ± 0.2‰	2	9.83 ± 0.11‰ [m]

reps refers to the number of replicate incubation sets, each consisting of approximately six vials.

[a] excluding one outlier. The outlier reduced computed *D* by 0.4‰ in my study and by 1‰ in the Nagel *et al.* study; [b] These were incubated at a different time of year than the first four treatments. [c] *D* computed using quadratic regression.

[d] (Nagel *et al.*, 2001); [e] (Searle *et al.*, 2011b); [f] (Noguchi *et al.*, 2001); [g] (Gonzalez-Meler *et al.*, 2001); [h] (Millar *et al.*, 1998, Ribas-Carbo *et al.*, 2005a); [i] (Robinson *et al.*, 1995); [j] (Ribas-Carbo *et al.*, 2000) precise values reported in (Ribas-Carbo *et al.*, 2005a); [k] (Penuelas *et al.*, 1996); [l] (Ribas-Carbo *et al.*, 1997), values reported for unabraded tissue; [m] (Oba & Poulson, 2009)

3.3.4. Metabolic endpoints and range of measurable discrimination

My method reliably reproduced published discrimination values with good precision across a range of 10 – 30‰ (Table 3.4). Values of *D* computed for untreated tissue matched reported values across a range of species and respiration rates. For vacuum-infiltrated *G. littoralis* tissue my estimate of 20.0 ± 0.5‰ (Table 3.4) was larger than the previously reported 16.3 ± 0.5‰ (Nagel *et al.*, 2001). More importantly, while that report did not find statistically significant effects of vacuum infiltration, I detected a 1.9‰ reduction in *D* ($P < 10^{-10}$). This infiltration effect may explain in part why I found discrimination in KCN infiltrated tissue (25.3 ± 0.8‰) to be lower than in leaves inhibited with gaseous cyanide (29.0 ± 0.1‰; Table 3.4). Vacuum infiltration also substantially increased the standard error, possibly due to irregular drying within the leaf. Excluding infiltrated tissues, I have observed a range of 9‰ for discrimination in *G. littoralis* (Table 3.4, Fig 3.5), which is similar to that reported by Nagel *et al*. (2001). The range compares favorably to the average range of 9.7‰ reported across a variety of green leaves (Ribas-Carbo *et al.*, 2005b). The observed range divided by the precision of ±0.1‰ in untreated leaves provides excellent resolution for detecting even relatively small differences in electron partitioning.

Results with soybean root tissue and *P.vulgaris* leaves compared favorably with the literature (Table 3.4). Soybean cotyledon discrimination in the presence of SHAM, however, appeared to be higher than previously published; whereas in the presence of KCN discrimination was slightly lower – even after using the quadratic regression to allow for recovery from the KCN treatment (Table 3.4). Residual respiration in the double-inhibition treatment was 13.5% of the untreated cotyledons, similar to previously reported values (Ribas-Carbo *et al.*, 1997), suggesting that the tissue had been adequately inhibited. The possibility that an external process (such as leakage) was drawing the values to a central value can also be ruled out since I have reproduced published discrimination values from 10‰ for $FeSO_4$ oxidation (Oba & Poulson, 2009) to 30‰ for soybean cotyledons treated with gaseous KCN (Table 3.4, Fig 3.2). Reported values for respiratory inhibition, however, have been somewhat inconsistent in the literature. Published discrimination values for the AOX endpoint, for example, can vary by 4‰ between laboratories: 26.7 – 30.3‰ for *Phaseolus vulgaris*, (Gonzalez-Meler *et al.*, 2001, Noguchi *et al.*, 2001), 27.2 – 31.4‰ for *Nicotiana tabacum* (Guy & Vanlerberghe, 2005, Lennon *et al.*, 1997) and, in the extreme, 23.7 – 31.2‰ for *Arabidopsis thaliana*

(Armstrong *et al.*, 2008, Florez-Sarasa *et al.*, 2007). Further work may therefore be necessary to standardize inhibition procedures across laboratories.

3.4. SUMMARY

Here I have presented two important improvements for studying respiratory electron partitioning *in vivo*: tools for analyzing nonlinear data, and a "contamination-tolerant" field-compatible incubation method. My mathematical tools greatly improve the method for detecting nonlinearities while providing a reliable way to estimate discrimination in the presence of nonlinearity. The second improvement, the new vial-based incubation technique, has the potential to greatly advance our understanding of respiratory electron partitioning. While previous methods were severely limited by equipment constraints, the method described here allow large numbers of samples to be processed rapidly in the field; contamination can be mathematically corrected using appropriate blanks collected alongside the incubations; samples can be sent to an external mass spectrometry facility if necessary; and the storage vials can be stored for at least 10 months while awaiting measurement. I have successfully used this technique, or its earlier variants, for several studies as will be described in subsequent chapters. My colleagues have also published studies using preliminary versions of this method (Searle *et al.*, 2011a, Searle *et al.*, 2011b, Searle & Turnbull, 2011). I therefore anticipate that the method will allow practitioners to greatly increase the breadth of investigations and will facilitate an improved understanding of respiratory metabolism.

4. Leaf total respiration and respiratory electron partitioning respond to different factors across nutrient gradients in the Franz Josef soil chronosequence

4.1. INTRODUCTION

Soil nutrient availability, especially soil nitrogen (N) and phosphorus (P), limits growth in terrestrial ecosystems across the world (Aerts & Chapin, 2000, Vitousek *et al.*, 2010). Mineral nitrogen is generally derived from the atmosphere by biological nitrogen fixation, by atmospheric deposition, or from the turnover of organic material; phosphorus, on the other hand, arises from the weathering of rocks and from organic turnover. As a result, the soil nutrient profiles – and consequent plant nutrient limitation – gradually change as soils age. Newly exposed soils tend to be phosphorus-rich but contain little nitrogen, and are therefore typically colonized by plants that host nitrogen-fixing symbionts. As the soil develops the nitrogen status therefore improves but ultimately P can become depleted due to weathering or immobilization resulting in a reversal from N-limitations to P-limitations (Vitousek *et al.*, 2010).

Since molecules needed for growth, such as amino acids and nucleotides, contain N and P but photosynthates (e.g. simple sugars) do not, plants growing under nutrient limitations may be faced with an excess of photosynthetic production relative to growth capacity. Excess photosynthate can be problematic if it leads to plant carbon imbalances (Smith & Stitt, 2007), but perhaps a greater concern is an increased likelihood of membrane damage due to increased reducing capacity. Photosynthesis converts solar energy into a series reduced chemical species, such as NADPH and plastiquinone, that can produce membrane-damaging reactive oxygen species (ROS). Excess photosynthetic production can also increase redox poise indirectly if carbohydrate surplus increases mitochondrial respiration beyond its capacity (due to N and P limitations) to safely consume reducing equivalents produced by the citric acid cycle. Plants have developed several energy-absorbing pathways to help avoid over-reduction in the chloroplast, including nonphotochemical quenching (Ruban & Horton, 1994), the water-water cycle (Asada, 1999), and plastid terminal oxidase (Josse *et al.*, 2000, see also the review in Wilhelm & Selmar, 2011). Recent evidence suggests that alternative oxidase (AOX) in the mitochondria also plays an important role in managing excess reducing equivalents produced by the chloroplast (Zhang *et al.*, 2011) as well as due to excess carbohydrates (Millenaar & Lambers, 2003).

Prior laboratory studies have found that relative AOX concentrations and AP activity or capacity increases in response to deficiencies of N (Noguchi & Terashima, 2006) or P (Gonzalez-Meler *et al.*, 2001, Juszczuk *et al.*, 2001b). Proposed mechanisms for the increase may depend on which nutrient is deficient. For example, N-deficiency may favor increased AOX protein synthesis since the molecular weight, and therefore N-content, of AP is one-tenth the size of the more energy efficient cytochrome *c* oxidase pathway (CP) (Noguchi & Terashima, 2006). P-deficiency, on the other hand may result in increased AOX activity because adenylate restrictions due to the scarcity of inorganic phosphate may suppress the CP, thus increasing the redox poise of the ubiquinone pool, which is the source of reducing power for both the AP and the CP (Juszczuk *et al.*, 2001b). Deficiencies of the micronutrients iron (Fe) and copper (Cu) may also affect respiration since both are essential metal cofactors in the electron transport chain. All five mitochondrial membrane electron transport complexes as well as AOX require iron for proper function but, while the cytochrome pathway also requires copper ion cofactors, AOX requires only iron (Vigani, Maffi & Zocchi, 2009). As a result, copper-deficient plants may increase AOX production or activity to make up for the decrease in Cu-dependent respiratory capacity. A recent study of *Chlamydomonas reinhardtii*, for example, found that the abundance of AOX doubled in Cu-deficient cells (Merchant *et al.*, 2006). A similar Cu-dependence of AOX expression has been reported in fungi (Borghouts *et al.*, 2001). Iron deficiency may also favor AOX, much like the argument for N deficiency, since AOX requires fewer Fe molecules than the corresponding CP complexes. Vigani *et al*. (2009), for example, found that iron-deficiency reduced COX concentration but not AOX concentration in cucumber root cells. Thus absolute declines in Fe and Cu or increase in Fe/Cu may all be expected to affect electron partitioning. While these laboratory finding are consistent with the hypothesis that AP activity is upregulated in response to nutrient deficiencies, only one of these studies measured *in vivo* electron partitioning (Gonzalez-Meler *et al.*, 2001). I am aware of no study of the interaction of nutrient deficiencies and, furthermore, the previously discussed laboratory results have yet to be tested in the field in plants growing under natural conditions. To address this knowledge-gap I used my newly-developed, field-portable, method for measuring *in vivo* activity of the two pathways (Chapter 3) to measure respiratory electron partitioning in plants growing along a natural soil nutrient gradient.

I examined canopy plants growing along the Franz Josef soil chronosequence, a series of forested sites located in a temperate rainforest along the west coast of the South Island, New Zealand (Almond, Moar & Lian, 2001, Richardson *et al.*, 2004, Stevens, 1968). New soils created by the retreat of the Franz Josef glacier contain little nitrogen and as a result support only a low, open, shrubland. Older soils support a succession of plant communities with increasing canopy heights from 7 m after 60 years to 30 m on soils aged 12,000 years. Leaching due to heavy precipitation, however, removes both N and P from the soils, resulting in a relatively stunted P-limited open canopy on soils older than 100,000 years (Richardson *et al.*, 2004). Previous studies found that, at the leaf-level, both photosynthetic capacity and respiration rates declined with increasing soil age (Turnbull *et al.*, 2005, Whitehead *et al.*, 2005). Here I investigate how respiratory electron partitioning might have influenced the differences in total respiration across sites. I hypothesized that macronutrient N and/or P deficiencies lead to increased AOX concentration and/or increased AP activity, as found in the above-mentioned studies (Gonzalez-Meler *et al.*, 2001, Juszczuk *et al.*, 2001b, Noguchi & Terashima, 2006). A secondary goal of this study was to investigate whether micronutrient Cu- and Fe-deficiency could also be associated with enhanced AP activity, as suggested by previous laboratory studies of cell cultures (Merchant *et al.*, 2006, Vigani *et al.*, 2009).

4.2. MATERIALS & METHODS

4.2.1. Field site description and harvest

Field samples were collected from the Franz Josef chronosequence (Table 4.1), a set of forested sites along the western coastal strip of the South Island, New Zealand (latitude 43.2ºS and longitude 170.3ºE). Retreat of the nearby Franz Josef glacier has created soils of varying age up to 120,000 years old along the chronosequence. A previous study found that new soils contained little nitrogen, but that soil N increased for the first 500 years (sites 1 – 4) after which they declined, soil phosphorus declined from a maximum at the newest site (Table 4.1), resulting in a steady increase in soil N/P with age. Soil Fe levels initially increase from moderate levels but after a peak at 300 years decline to very low levels at 120,000 years (Table 4.1). Soil Cu levels have not been measured along the sites (Richardson, S. personal communication). Nine sites have been described by Richardson *et al*. (2004), Almond *et al.* (2001), and Stevens (1968), however I made measurements at the six sites that had previously been assayed for photosynthesis and respiration (Turnbull *et al.*, 2005, Whitehead *et al.*, 2005). Sites one through six in this study correspond to

sites one – three, five, seven, and nine in Richardson *et al.* (2004), with soil ages < 10, 60, 130, 500, 12,000 and 120,000 years, respectively (Table 4.1).

Table 4.1. Franz Josef chronosequence site description and species sampled.

Site #	*Prev. #* [a]	*Est. Age*[a] *(y)*	*Soil N* [a,b] *g kg^{-1}*	*Soil P* [a,b] *g kg^{-1}*	*Soil Fe*[c] *g kg^{-1}*	*Elevation*[a] *(m)*	*Precip.*[a] *(mm)*	*Species Sampled*
1	1	10	0.05 ± 0.02	0.80 ± 0.03	1.6	240	6,520	*Hebe salicifolia* *Olearia avicenniaefolia* *Aristotelia serrata* *Coriaria arborea* *Griselinia littoralis*
2	2	60	2.2 ± 0.4	0.80 ±0.04	3.2	240	6,576	*Aristotelia serrata* *Coriaria arborea* *Griselinia littoralis* *Melicytus ramiflorus*
3	3	130	3.7 ± 0.4	0.55 ± 0.06	4.0	220	6,188	*Griselinia littoralis* *Pseudopanax colensoi* *Metrosideros umbellata* *Weinmannia racemosa*
4	5	530	8.0 ± 1.6	0.46 ± 0.03	2.3	200	6,278	*Griselinia littoralis* *Metrosideros umbellata* *Weinmannia racemosa*
5	7	12,000	6.9 ± 1.9	0.35 ± 0.07	1.4	265	3,706	*Metrosideros umbellata* *Weinmannia racemosa* *Dacrydium cupressinum*
6	9	120,000	3.6 ± 0.3	0.11 ± 0.01	0.2	145	3,652	*Metrosideros umbellata* *Weinmannia racemosa* *Dacrydium cupressinum*

Site numbers are based on Turnbull *et al.* (2005); previous numbering system is that of Richardson *et al.* (2004). Numers are shown as mean ± SE.

[a] Data from from Richardson *et al*. (2004), with particulars therein taken from Stevens (1968) and Almond et al. (2001).

[b] Based on soil mineral horizon samples. Only sites 4 – 6 had measurable organic horizons; total N and P in those layers was similar to that found in the mineral horizons.

[c] Data from (Turner *et al.*, 2007)

Ten species representing the canopy species at each site were sampled *Aristotelia serrata* (As), *Coriaria arborea* (Ca), *Dacrydium cupressinum* (Dc), *Griselinia littoralis* (Gl), *Hebe salicifolia* (Hs), *Melicytus ramiflorus* (Mr), *Metrosideros umbellata* (Mu), *Olearia avicenniaefolia* (Oa), *Pseudopanax colensoi* (Pc), and *Weinmannia racemosa* (Wr). Nomenclature follows Allan *et al*. (1961). Due to the successional nature of community development along the chronosequence, not every species was found at each site (Table 4.1). Plant material was collected as described by Turnbull et al. (2005). Branches were taken from the upper (sunlit) part of the canopy in five representative trees for each of the dominant canopy species. Shoots were placed in water before being returned to the laboratory where they were re-cut underwater. Previous studies have shown no differences in respiration between in situ leaves and leaves from detached branches in a range of species (Turnbull *et al.*, 2005, Turnbull *et al.*, 2003). Cut branches were placed in the dark for at least 30 minutes prior to incubation. Additional tissue samples from each replicate were collected for leaf tissue analysis as described in a subsequent section.

Respiratory inhibitions were conducted on several species harvested at the field site (As, Ca, Mr, Oa, and Wr). Inhibition tests for the remaining species, as well as all gaseous (HCN) inhibitions, were performed on samples taken from trees on campus at the University of Canterbury, Christchurch, New Zealand (UC).

4.2.2. Respiratory incubations

Respiratory incubations were conducted to determine total O_2 respiration as well as electron partitioning using the ^{18}O isotope discrimination methods described in Chapter 3. Leaf or root tissue was sliced into sections no larger than 1 cm × 7 cm and incubated in sealed septum-capped 12 mL vials (Labco, High Wycombe, UK; product #738W) in the dark. A half-pellet of KOH, in a protective holder, was also placed in the vial in order to remove respired CO_2. At the end of the incubation period, air was transferred under positive pressure from the incubation vial to a syringe by injecting water. The air in the syringe was immediately injected into a pre-evacuated 3.7 mL storage vial (Labco product #778W) for later analysis.

Five replicates were measured for each species per site. Tissue for each replicate was divided into four incubation vials in the approximate proportion 1:2:3:3 thus providing a three-fold range of O_2 consumption at the end of the 2.5–3 h incubation periods. Total sample size for each replicate, 3–9 g FM depending on species, was

determined based on previously measured respiration rates so that no more than 50% of the O_2 in any vial would be consumed. Vials in which actual consumption was greater than 60% were rejected from further analysis. Air "blank" vials for determining initial air compositiong were prepared alongside the incubations by injecting laboratory air directly into storage vials. O_2-free blanks were prepared by injecting O_2-free N_2 (BOC, Auckland, New Zealand; 99.99% pure) directly into storage vials as well as by flushing incubation vials with N_2 for at least five minutes and then transferring the nitrogen as if it were incubation air.

Discrimination of alternative oxidase (AOX) and cychrome *c* oxidase (COX) was measured by inhibiting the tissue with selective respiratory inhibitors. Initial inhibition experiments involved vacuum infiltration. Cut leaves were infiltrated with either buffer, 10 mM KCN or 25 mM salicylhydroxamic acid (SHAM) prepared without organic solvents according to Nagel et al. (2001). The effects of these inhibition methods were considered to be unsatisfactory (Appendix A4.2 Table S4.1), so additional methods were tried for selectively inhibiting COX and AOX. COX was inhibited using gaseous cyanide (HCN) by sealing tissue for 10–20 minutes in plastic jars containing a 1 × 8 cm strip of chromatography paper soaked 1 M KCN. I attempted to inhibit AOX in leaves by keeping cut branches or whole plants in a dark cabinet for 39, 72, or 88 h before incubation. Under such conditions (Ribas-Carbo *et al.*, 2000) reported that soybean cotyledon AOX activity diminished by 50 – 75%. For these latter inhibition trials (i.e. those without vacuum infiltration) each of six vials per replicate was filled with approximately the same amount of tissue (1–2 g each) but was incubated for variable amounts of time, in order to also test for the possibility of recovery from inhibition during incubation.

Storage vials from the second round of inhibition experiments were measured by mass spectrometry on the day of the incubations. Storage vials from the field trial and subsequent inhibition measurements were stored at laboratory temperature (20 ºC) for five and two months respectively prior to measurement.

4.2.3. Discrimination, electron partitioning and respiration computations

Isotopic composition of the respiratory air samples was measured in a Thermo Electron Delta V Plus isotope ratio mass spectrometer (Thermo Electron, Bremen, Germany) as described in Kornfeld *et al*. (2012b) and in Chapters 2 and 3. Measurements were corrected for contamination using the O_2-free blanks stored alongside the respiration samples as described in Chapter 3. For the field samples, significant curvature remained

in the data even after correction due to the long storage at 20 ºC. Discrimination values, *D*, for samples collected at the field trial were therefore computed using a quadratic regression described in Chapter 3, Eqn (3.7):

$$1000 \times \ln\left(\frac{^{34}R_s}{^{34}R_{s,0}}\right) = \beta_2\left(\ln\ f_s^*\right)^2 - D \ln\ f_s^* . \tag{4.1}$$

The second round of inhibition experiments, which did not suffer from storage contamination, were tested for curvature based on significance of the β_2 term in Eqn (4.1). If the coefficient was not statistically significant at the $P < 0.05$ level, then the quadratic term was dropped from the regression.

Discrimination values were converted to measures of electron partitioning through the AP, τ_a, by linear interpolation (Guy *et al.*, 1989):

$$\tau_a = \frac{D_s - D_c}{D_a - D_c}, \tag{4.2}$$

where D_s, D_a, and D_c represent the discrimination values for the sample, alternative pathway, and cytochrome pathway respectively. Discrimination values for the HCN incubation were used for D_a (Appendix A4.2 Table S4.1); the AOX inhibition experiments, however, did not yield credible values since neither inhibitory treatment lowered the measured discrimination values relative to controls. Published values for $D_{c,}$ however, are independent of measured D_a with mean ± SE of 19.8 ± 0.1‰ as long as diffusion issues, i.e. thick dense tissue, are not present (Ribas-Carbo *et al.*, 2005a). I therefore let D_c = 20‰ for all species except *Dacrydium* and *Olearia* both of which showed evidence of diffusional limitation by having abnormally low measured D_a (25.3 ± 0.4‰ and 26.6 ± 0.3‰ respectively). The physical structure in these species also suggests a high likelihood of diffusional constraint – *Dacrydium* samples were mostly stem tissue with scale-like leaves while *Olearia* leaves are tough and leathery with a fine tomentum on the underside that would likely interfere with diffusion. Values of D_c for these two species were assumed to be lower in proportion to the depression of D_a (Angert & Luz, 2001) and were therefore assigned values of 17.5‰ and 18.5‰ respectively. Because of the uncertainty in these values, however, and because respiration rates can artificially affect measured discrimination in diffusionally limited tissue (Miller *et al.*, 2011) the two species were excluded from statistical analyses of τ_a, v_{alt}, and v_{cyt}.

Respiration rates (R) were computed based on f^*, tissue mass ($mass$ g), vial volume (V_{vial}, mL), tissue volume (V_{plant}, mL), CO_2 trap volume (V_{other}, mL), incubation time (t, s) and incubation temperature (T, Kelvins) according to the equation:

$$R\,(nmol\ O_2\ g^{-1}\ s^{-1}) = \frac{0.21\, f_s^* \times (V_{vial} - V_{plant} - V_{other})}{mass \times t} \frac{10^6 P}{R_{gas} T}, \quad (4.3)$$

where P is the atmospheric pressure in atm and R_{gas} is the the ideal gas constant (0.082 mL atm K^{-1} $mmol^{-1}$). Tissue volume was estimated based on fresh mass divided by the density, measured by water displacement, of representative samples. Incubation temperatures during the field trial were 21 ± 1 ºC for sites 2–5; but were 17 ºC and 18 ºC for sites 1 and 6 respectively. Respiration rates for these two site were adjusted to 21 ºC based Q_{10} values measured during the same experimental period, according to the formula (Atkin, Bruhn & Tjoelker, 2005a):

$$R_{21} = RQ_{10}^{-(T-21°C)/10}. \quad (4.4)$$

Resipiration through each pathway was computed as

$$v_a = \tau_a R \quad (4.5a)$$

and

$$v_c = (1 - \tau_a) R, \quad (4.5b)$$

where, v_a and v_c correspond to the activities of AOX and COX respectively.

4.2.4. Leaf tissue analysis

Leaf tissue samples collected at the field site were analyzed for specific leaf area (SLA), dry matter content (DMC), N, P, Fe, Cu, starch, total sugars. Area fresh leaf tissue was determined by using ImageJ to measure the area of whole leaves in digital images. Tissue samples were dried in an oven at 60°C for a minimum of two days before determining dry mass. Dried leaf tissue was ground to a fine powder in a ball mill and sent to the Australian National University, Canberra, Australia for nitrogen, phosphorus and carbohydrate determination. Nitrogen and phosphorus were measured using a Technicon Auto-analyzer II (Bran + Luebbe Pty. Ltd, Norderstedt Germany) and Kjeldahl acid digests (Ayub *et al.*, 2011). Soluble sugars and starch were assayed as described by Loveys *et al.* (2003). Total nonstructural carbohydrate (TNC) content was computed as the sum of starch and total sugars. Additional samples were sent to New Zealand Laboratory Services Ltd (Hamilton, New Zealand) for Fe and Cu analysis using

inductively coupled plasma optical emission spectroscopy (ICP-OES) after digestion in HNO_3 and $HClO_4$.

A second set of samples, flash frozen to –80 ºC at the field site, were subsequently lyophilized for at least 24 h, ground to a fine powder in a ball mill and then stored at –80 ºC until assayed for AOX, COX, and Porin. AOX and COX concentrations were determined semiquantitatively using a Western blot protocol. Proteins were extracted as described by Laemli (1970) with modification. The powdered tissue was extracted in a solution containing 10% glycerol, 60 mM tris(hydroxymethyl)aminomethane (Tris) pH 8, 2% sodium dodecyl sulfate (SDS) 0.51 mM EDTA, and 0.05 mM tris(2-carboxyethyl)phosphine (Bond-Breaker TCEP solution, natural pH, Thermo Scientific, Rockford, IL, USA). The mixture was heated to 95 ºC for 10 minutes, centrifuged to remove coarse cellular debris and then separated by electrophoresis in a 4-12% gradient polyacrylamide gel (Life Technologies, Carlsbad, CA, USA) at 200 V for 45–60 minutes. Proteins were transferred to a nitrocellulose membrane using the iBLOT system (Life Technologies), and immunoblotting was performed using the Snap i.d. system (Millipore, Billerica, MA, USA) using an anti-AOX monoclonal antibody (Elthon, Nickels & McIntosh, 1989) at a dilution of 1:660 followed by anti-mouse horseradish peroxidase (HRP) conjugate. Results were visualized by chemiluminscence (ECL Advance, GE, UK) using a cryo-cooled digital camera (CHEMI GENIUS^2, Syngene, Cambridge, UK). COX and Porin were simultaneously probed with anti-COX antibodies (Agrisera, Vannas, Sweden) and anti-Porin antibodies isolated from a mouse hybridoma line (originally produced by Dr Tom Elthon, University of Nebraska, USA) each diluted 1:50,000, followed by anti-rabbit HRP conjugate for COX and anti-mouse HRP conjugate for Porin. Representative images of protein bands are shown in (Fig 4.7). Bands were quantified using the GeneTools software package (Syngene). Each blot contained at least one replicate from each field site (for a particular species) in order to avoid confounding due to differences between blots. Measured intensities were divided by the average intensity for each blot in order to remove interblot variation.

4.2.5. Statistical analysis

Statistical analyses were conducted using the R statistical language (R Development Core Team, 2011). All measurements were tested for Species and Site effects using two-way ANOVA. Uniformity of residual variance was tested using the Brown and Forsyth test (Brown & Forsythe, 1974). Where residual variances were not equal, residuals were

weighted by $1/var_s$, the residual variance within each species (Venables & Ripley, 2002). Residuals were tested for normality using the Shapiro-Wilk test (Royston, 1995). For several parameters a logarithmic transform was necessary to achieve normality. Post-hoc tests were computed using Tukey's HSD comparison of all pair-wise combinations, adjusted according to Westfall (Bretz, Hothorn & Westfall, 2011). These pairwise comparisons were used to generate the "letter groupings" indicating statistically significant groups in the graphs presented here.

Two further analyses: correlation and multimodel inference were used to investigate relationships between leaf trait measurements and respiration (R, τ_a, v_{cyt}, v_{alt}). Correlation analysis identified the best single covariate from among species identity and eleven leaf-level measurements: N, P, N/P, Fe, Cu, Fe/Cu, DMC, SLA, total sugars, starch, and TNC. For electron partitioning, respiration was also added as covariate. Multimodel analysis used the "finite-sample" approximation of Akaike's Information criteria, AIC_c, (Burnham & Anderson, 2002) to rank all possible (2^k) additive models involving the k explanatory variables (k = 12 for respiration, 13 for τ_a, v_{cyt}, v_{alt}). Models with lower AIC_c values are considered to fit the data better (Burnham, Anderson & Huyvaert, 2011). Due to the large number of models, however, considerable uncertainty remained as to which model was best. More importantly, P values for models selected this way were strongly biased low, i.e., statistical significance was overstated (Appendix A4.1 Fig S4.1a). Multimodel inference overcomes this shortcoming by computing weighted averages of the parameters and their standard errors (SE) based on AIC_c weights, which indicate the probability that each model most appropriately describes the data (Burnham *et al.*, 2011). The weighted-average values were then used to determine P values for each variable using the standard t-test. Only those variables with $P < 0.05$ were included in the final "best" model. The effectiveness of this method was confirmed using Monte Carlo simulations and I found that SE was slightly overestimated (Appendix A4.1 Fig S4.1b). Model-averaged standard error values were therefore multiplied by 0.92, which corrected the slight overestimates (Appendix A4.1 Fig S4.1c). The variables selected by this method were generally the same as the variables in the AIC_c best model. Only the coefficient and SE values differed. As a second measure of relevance, each parameter was assigned the sum of model weights for all models containing that variable (Burnham & Anderson, 2002). Adjusted r^2 (Montgomery & Morrison, 1973) is reported for the multimodel analysis.

4.3. RESULTS

4.3.1. Leaf traits

Leaf traits can potentially explain differences in respiration (R), electron partitioning (τ_a), and the CP and AP activities, v_{cyt} and v_{alt}. I therefore examined four groups of leaf traits: leaf structure, macronutrient status (N and P), micronutrient status (Fe and Cu) and nonstructural carbohydrates. Measures were strongly correlated within each group and, to a lesser extent across groups (Appendix A4.2Table S4.2). Nevertheless, distinct patterns emerged from each set of traits.

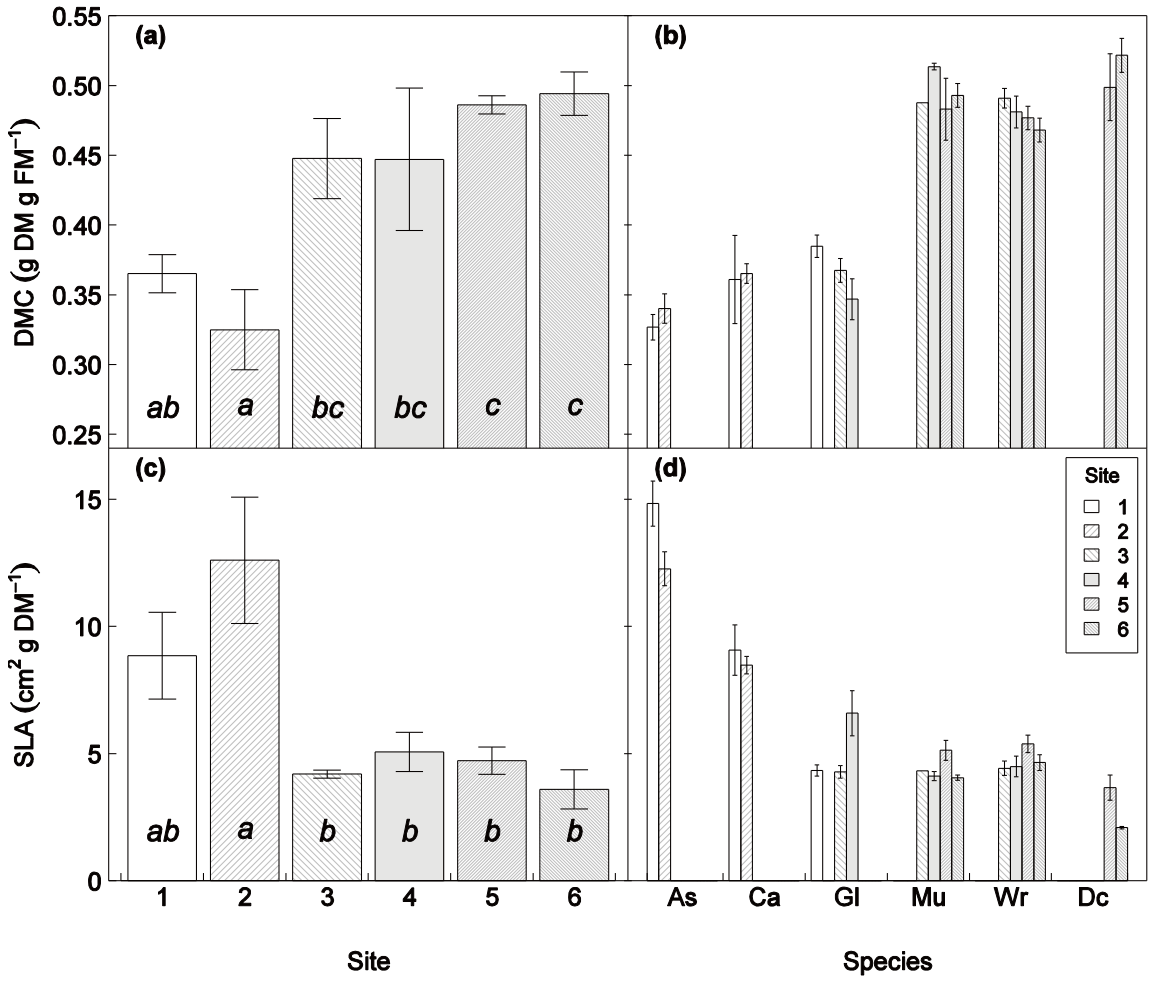

Fig 4.1. Structural leaf traits across the chronosequence sites.

(a, b) Dry matter content (DMC); (c, d) Specific leaf area (SLA). Letters in panels (a) and (c) indicate statistically distinct sites ($P < 0.05$). Soil age in sites 1 – 6 are 10, 60, 130, 530, 12,000, and 120,000 years, respectively; see Table 4.1 for a detailed description of the sites. Panels (b) and (d) only show species that were collected at more than one site, in order to highlight site differences within species.

Dry matter content (DMC) and specific leaf area (SLA) have been shown to correlate with soil nutrient status and growth rates (Witkowski & Lamont, 1991, Wright *et al.*, 2004) and are themselves inversely related, as was found here, with the correlation coefficient between these two measures, $r = -0.83$. Both were strongly correlated with *R* ($r^2 = 0.5$ and 0.6 respectively; Appendix A4.2 Table S4.2). Here, both measures showed similar trends at the site level with the lowest DMC (32 ± 3%) and highest SLA (12.6 ± 2.5 $m^2\ kg^{-1}$) in site two and with site 6 at the other extreme: DMC of 49 ± 1% and SLA of 3.6 ± 0.8 $m^2\ kg^{-1}$ in site 6 (Fig 4.1a, c). The differences between sites, however, were entirely due to differences in species composition (Fig 4.1b, d). Two-way ANOVA in which species effects were accounted for before site effects showed strong support for interspecific differences ($P < 0.001$ for SLA and DMC) but no statistically significant differences by site ($P > 0.15$ each).

Leaf N, P, and N/P varied significantly across sites (Fig 4.2). Site effects can be seen within species, although species composition appears to have had the largest influence on site differences for the leaf-N concentration, with the early-succession species having approximately 2 mg g^{-1} foliar N while later-successional species contained half that amount (Fig 4.2b). Foliar N/P, which is considered to be an indicator of the limiting nutrient (Tessier & Raynal, 2003), varied strongly across sites, even within species, ranging from 10 – 15 mg mg^{-1} in the younger sites to 20 – 30 mg mg^{-1} in the oldest site (Fig 4.2f). Leaf P concentrations were intermediate between these two measures, with a clear reductions within species across sites 4 – 6, but with the high P values in sites 1 and 2 not declining by soil age. Overall, foliar P declined from 1.3 to 0.3 mg g DM^{-1} as site age increased. Leaf N was negatively correlated with soil N due to the high leaf N values in sites 1 and 2 compare to the very low soil N. After excluding sites 1 and 2, leaf N was not correlated with soil N ($P > 0.18$). Leaf P on the other hand strongly correlated with soil P ($r^2 = 0.6$) and appeared to increase exponentially with soil P ($r^2 =$ 0.8 for log(leaf P) *vs.* soil P).

Leaf Fe and Cu both declined with site age whereas effects on Fe/Cu peaked in a manner similar to the soil Fe profile (Fig 4.3, Table 4.1). When averaged over all species within each site, only Cu levels differed by site, with a decline from 8 ppm in sites 1 and 2 to 4 ppm in the remaining sites (Fig 4.3c). Site effects were more pronounced within species. At the species level, Fe levels in *Corearia* clearly differed across sites (130 ppm and 70 ppm in sites 1 & 2 respectively; $P > 0.001$), while the declines from sites 4

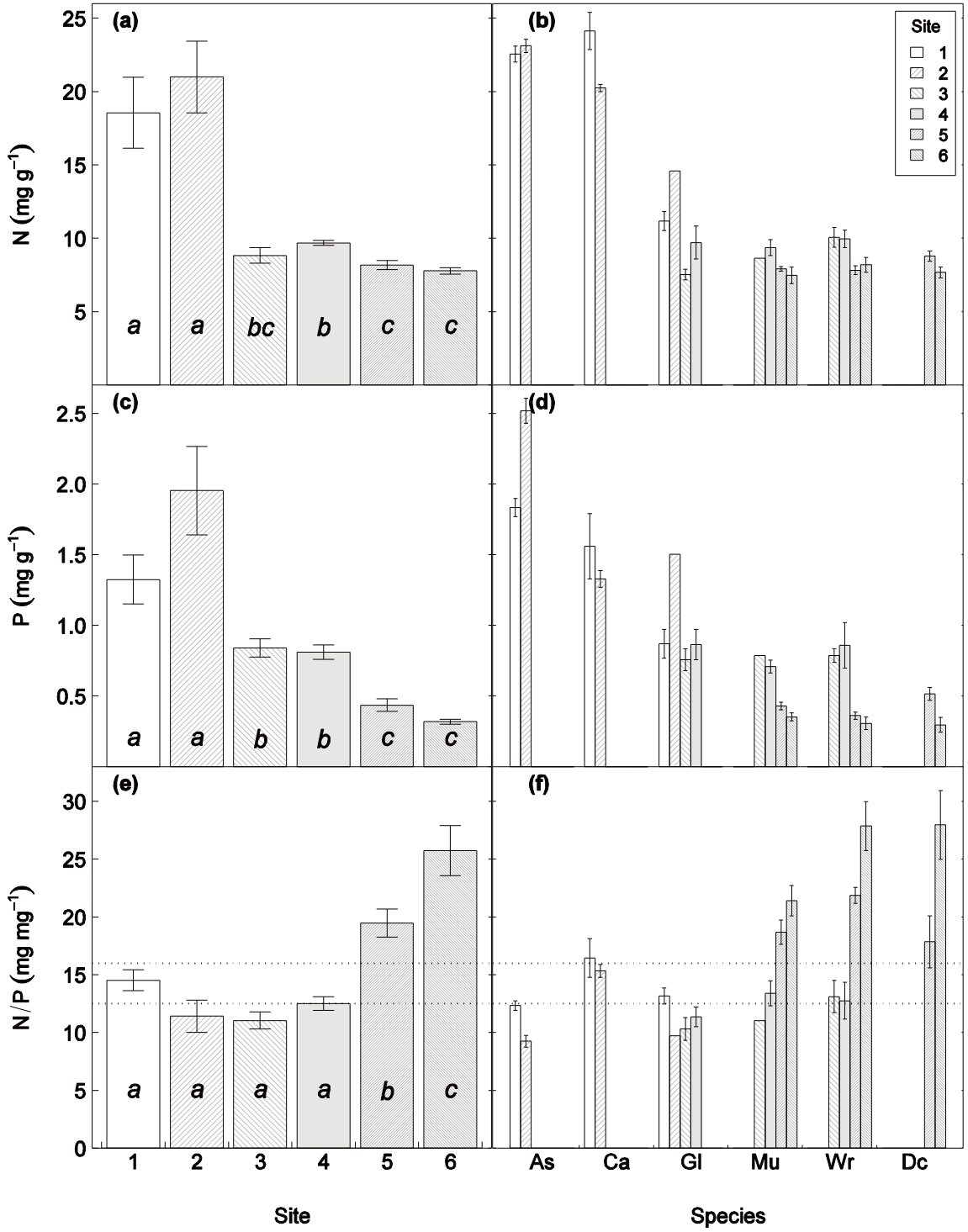

Fig 4.2. Leaf N (a, b), P (c, d) and N/P (e, f) across sites and by species within sites (for species collected at more than one site).

Dotted horizontal lines in (e) and (f) indicate the transition zone from N-limitation to P-limitation as described by Tessier & Raynal (2003). Letters in panels (a), (c), and (e) indicate statistically distinct groups at the $P < 0.05$ level.

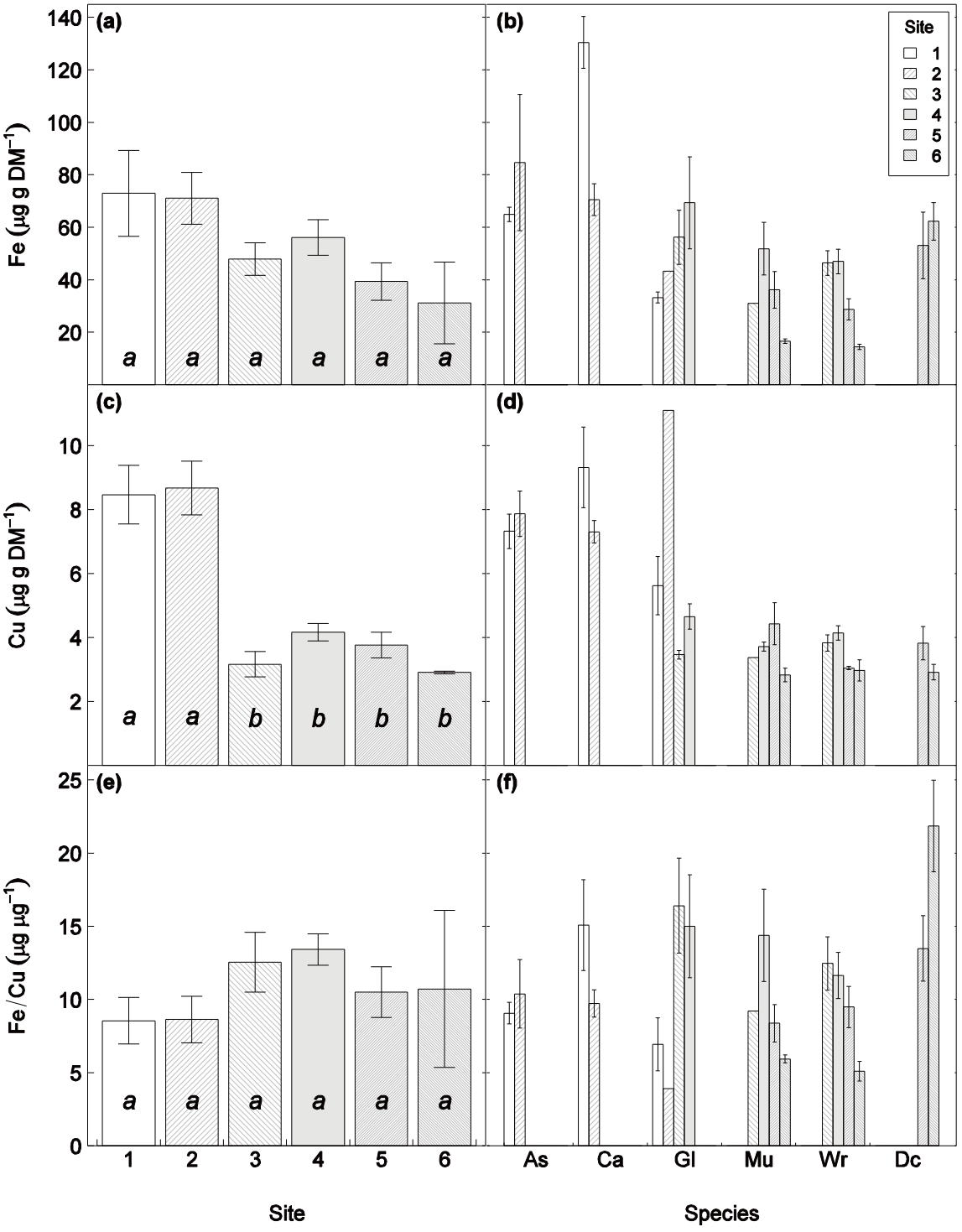

Fig 4.3. Leaf Fe (a, b), Cu (c, d) and Fe/Cu (e, f) across sites and by species within sites (for species collected at more than one site).

Letters in panels (a), (c), and (e) indicate statistically distinct groups for site effects at the $P < 0.05$ level, without accounting for within-species effects. After accounting for species effects, sites 5 and 6 differ from each other and from the other sites in Fe content; site 6 differs from the rest in Cu content; and site 5 and 6 differ in Fe/Cu for Mu and Wr but not for Dc.

through 6 in *Metrosiders* and *Weinmannia* leaves were also statistically significant ($P < 0.01$; Fig 4.3b). Leaf Cu in site 6 also differed modestly from the other sites after accounting for species differences ($P > 0.04$; Fig 4.3d). Site effects on Fe/Cu were mixed (Fig 4.3f): sites 1 & 2 were considered to differ from sites 3 &4, after accounting for species differences ($P < 0.001$), whereas site 5 was not statistically distinct from any of the earlier sites. Differences between sites 5 & 6 depended on species, however, with Fe/Cu cut in half for *Metrosideros* and *Weinmannia* ($P = 0.001$), whereas a statistically non-significant increase was seen in *Dacrydium* (Fig 4.3f).

Leaf starches, sugars, and total nonstructural carbohydrates (TNC) did not vary by site when all species were considered together (Fig 4.4; $P > 0.2$ for each measure). Clear differences by species were observed in two-way ANOVA with site ($P < 0.001$ for Species) but still no site effect was detected for starch or TNC. Total soluble sugar content differed by site in some species, however, with statistically significant changes in sugar concentration in two species: *Metrosideros* leaf sugar content in site 4 was 59 ± 3 mg g DM^{-1} in site 4, 44 ± 1 mg g DM^{-1} and 50 ± 2 mg g DM^{-1} in site 6. Sugar concentration in *Weinmannia* leaves increased monotonically with site age from 80 ± 4 to 103 ± 5 mg g DM^{-1} in sites 3 through 6.

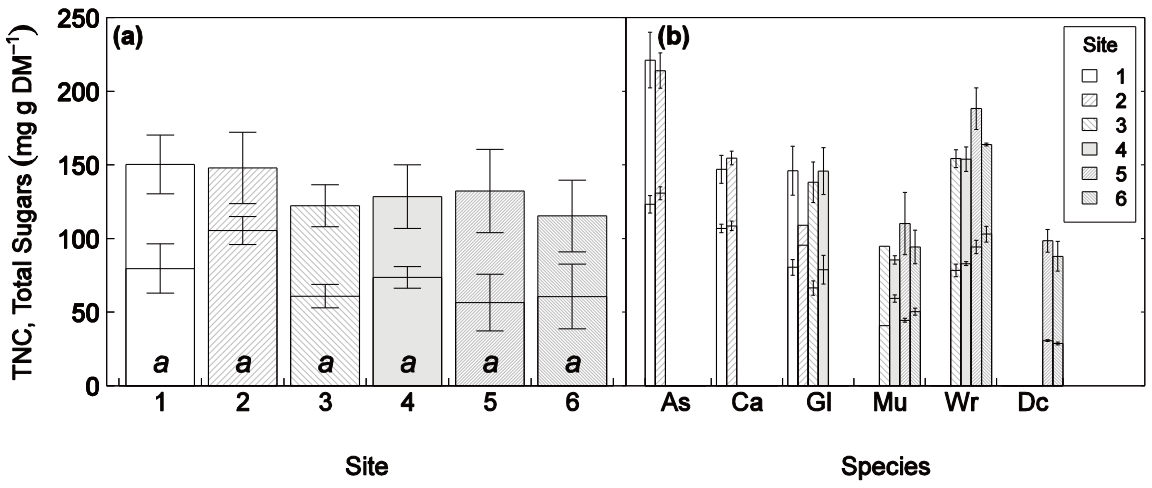

Fig 4.4. Total nonstructural carbohydrates (TNC) and total soluble sugars by site (a) and by species collected at more than one site (b).

The lower half of each bar represents total sugar concentrations; the upper half of the bar represents starch; the entire bar represents TNC. No statistically significant differences were found by site.

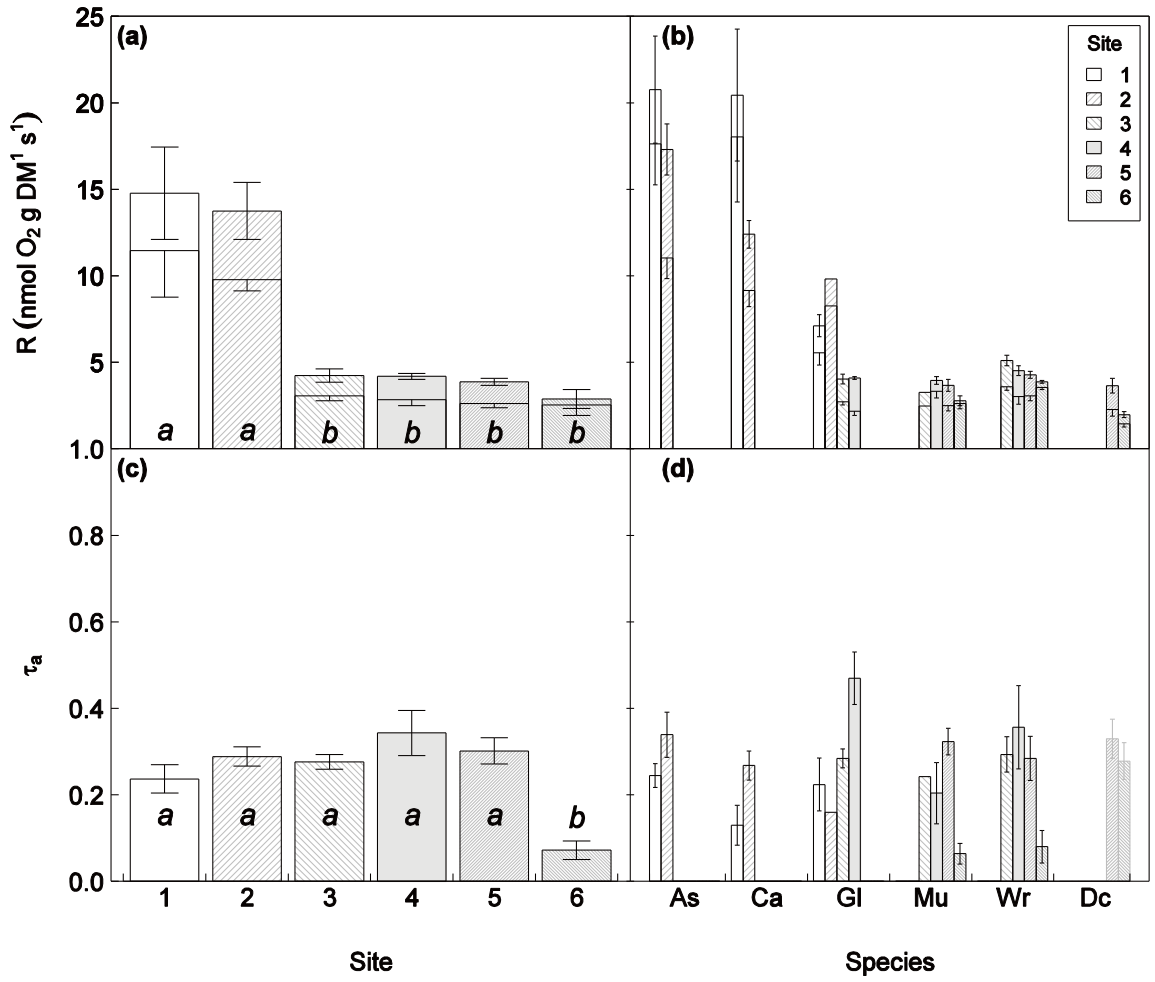

Fig 4.5. Respiration (a, b) and electron partitioning through the alternative pathway, τ_a (c, d), across sites.

Respiration is divided into v_{cyt} (lower portion of each bar) and v_{alt} (upper portion in each bar). Letters in panels (a) and (c) indicate statistically distinct groups at the $P < 0.05$ level. Differences in v_{cyt} across sites are statistically significant only for As and Ca. Difference in v_{alt} are for site 6, Mu and Wr, are statistically different from the other sites. For τ_a, site 6 is statistically distinct from sites 3 – 5; site 1 is statistically distinct from sites 2, 4, 5. (*Dacrydium* and *Olearia* were excluded from the analysis because of difficulty in establishing the discrimination endpoints. The values for *Dacrydium* shown in panel (d) are grayed out to emphasize that they were not part of the statistical analysis. *Olearia* was only collected at site 1 and therefore does not appear in panel (d), which only shows species that were at more than one site.)

4.3.2. Respiratory measurements

Respiratory O_2 consumption was highest in the youngest sites, at approximately 15 nmol O_2 g DM^{-1} s^{-1}, but the rate was a third of that value in the remaining sites (Fig 4.5a). A general decline in respiration with soil age was seen in all species found at more than one site (Fig 4.5b). Leaf N was the strongest single factor correlating with respiration

rates, explaining more than 80% of the variation within and across species (r^2 = 0.81; Fig 4.6a, Appendix A4.2 Table S4.2). Even with such strong correlation for a single factor, two other variables were found to contribute to the measured differences in respiration in this study. The best linear model according to the multimodel inference method was: R = N + Cu + TNC (r^2 = 0.83, $P = 10^{-8}$, 0.01, and 0.02 for the three terms, respectively; Table 4.2). Since the model is additive, each variable contributes independently to the dependent variable. The relative effect sizes of each variable can therefore be found by multiplying the regression coefficient for each explanatory variable by its range in this study. For example, the effect of varying N from the highest to lowest value measured in this study would cause a predicted shift in R of 19 ± 3 nmol O_2 g DM^{-1} s^{-1}, or 59 ± 9% of the 32.5 nmol O_2 g DM^{-1} s^{-1} range in measured R (Table 4.2). Corresponding effect sizes for Cu and TNC were 18 ± 6% and 16 ± 6% the R range (Table 4.2). It should be noted, that starch content was found to be nearly equal to TNC though it was rejected at the P < 0.05 significance level (Table 4.2).

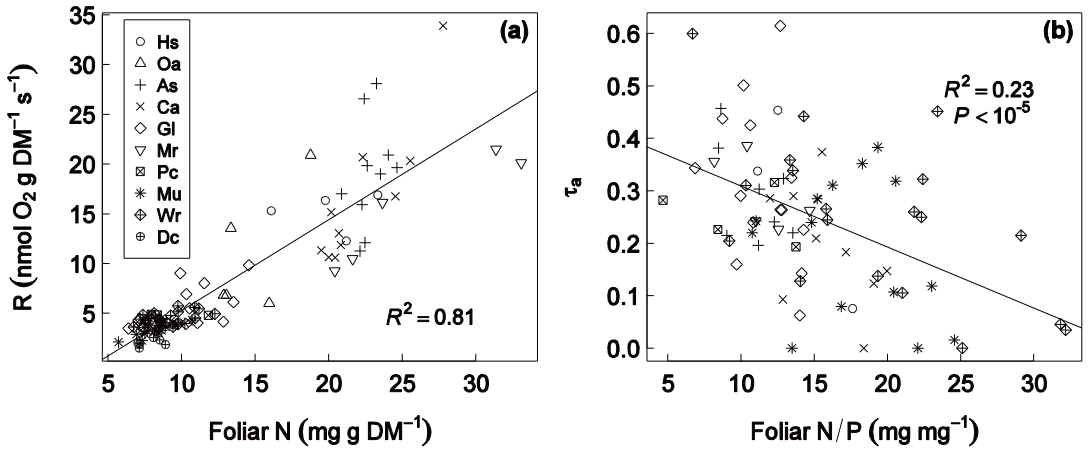

Fig 4.6. (a) Foliar N *vs.* R and (b) foliar N/P *vs.* τ_a.

τ_a is the proportion of electron transport chain electrons flowing through the AP. The variables N and N/P were chosen based on correlation analysis amongst the leaf traits measured in this study (Appendix A4.2 Table S4.2). n = 99 for the R analysis and 77 for the τ_a graph. (*Dacrydium* and *Olearia* were excluded from the τ_a analysis because of difficulty in establishing the discrimination endpoints.)

Electron partitioning, τ_a, was computed for all species, but because of uncertainty in determining the endpoints for *Dacridium* and *Olearia*, these two species were omitted from the statistical analysis, as described in the Methods section. ("Raw" discrimination values are reported in the AppendixA4.1, Fig S4.2.) Electron partitioning was strongly depressed in site 6, with τ_a decreasing from the range of 0.23 – 0.34 in the younger sites down to 0.07 ± 0.02 (P = 0.04). After accounting for species differences, the reduced τ_a in

site 6 was considered to be different than sites 3 – 5 ($P \leq 0.02$) while in sites 4 and 5 the proportion of electrons partitioned through the AP increased 0.20 ± 0.07 compared with site 1 ($P \leq 0.03$). The strongest single explanatory factor for τ_a was a negative correlation with leaf N/P ($r = –0.48$, $r^2 = 0.22$; Fig 4.6b, Appendix A4.2 Table S4.2). The best additive model was τ_a = N/P + R ($P = 0.003$ and 0.03 respectively; Table 4.2). The effect size of each explanatory variable was 53% (N/P), 51% (R) of the measured range of τ_a (Table 4.2). It should be noted that, on their own, τ_a and R were not correlated ($r = 0.02$, Appendix A4.2 Table S4.2).

Table 4.2. Explanatory variables for respiration, R, electron partitioning, τa, and the activities of AP and CP, valt and vcyt, respectively.

DV	r^2	*Support*	*EV*	*P*	*Coef.*	*Range*	*Effect on DV*	*% of DV range*
R	0.83					1.5 – 34	*32.5*	*100%*
		1.00	N	2×10^{-8}	0.70 ± 0.11	5.7 – 33	19.2	59 ± 9%
		0.87	Cu	0.01	0.47 ± 0.18	1.8 – 14	5.1	18 ± 6%
		0.57[b]	TNC[b]	0.02	0.022 ± 0.009	48 – 283	4.8	16 ± 6%
		0.52[b]	Starch[b]	0.06	0.023 ± 0.012	10 – 175	3.8	12 ± 6%
τ_a	0.24					0 – 0.61	*0.61*	*100%*
		0.88	N/P	0.003	–0.010 ± 0.003	4.7 – 37	–0.33	–53 ± 17%
		0.77	R	0.03	–0.010 ± 0.004	1.5 – 34	–0.32	–51 ± 23%
v_{alt}	0.71					0 – 8.3	*8.3*	*100%*
		1.00	P	5×10^{-6}	1.8 ± 0.4	0.2 – 4.0	7.0	84 ± 17%
		0.69	Cu	0.04	0.20 ± 0.10	1.8 – 13.3	3.3	28 ± 13%
		0.65	Starch	0.03	0.009 ± 0.004	9.8 – 175	1.6	20 ± 9%
v_{cyt}[a]	0.73					1.5 – 31	*29.2*	*100%*
		1.00	N	1×10^{-5}	0.74 ± 0.16	5.7 – 33	20.2	69 ± 15%
		0.67	P	0.045	–2.2 ± 1.1	0.2 – 4.0	–8.6	–30 ± 14%

The effect sizes are shown for each variable in the best regression model selected by AIC analysis. Columns are: *DV* – the dependent variable; r^2 – the adjusted correlation coefficient for the entire regression; *Support* – the sum of AIC_c weights for all models containing the explanatory variable. *EV* – the explanatory variable; *P* the *P*-value for each coefficient in the multiple linear regression; *Coef* – the regression coefficient; *Range* – the range of values taken on by the explanatory variable in the dataset; *Effect on DV* – the predicted change in the dependent variable for a change from the lowest to highest value the explanatory variable's range (i.e. *Coef* × range); *% of DV range* – the Effect on DV as a percent of the range of the DV.

[a] v_{cyt} computed with *R* excluded from the list of possible explanatory variables; with *R* included, the best model includes *R* together with the variables and coefficients for v_{alt} but with the sign reversed.

[b] Starch and TNC are interchangeable. Omitting Starch from the candidate variables increases support for TNC to 0.94; omitting TNC, support for Starch is 0.91 with P < 0.01 either way.

Table 4.3. Activities of the AP, v_{alt}, and CP, v_{cyt} (nmol O_2 g DM^{-1} s^{-1}), for each species within each site.

Site	*1*	*2*	*3*	*4*	*5*	*6*
v_{alt}						
Hebe	5.3 ± 1.1					
Olearia	4.2 ± 1.3					
Aristotelia	5.5 ± 0.5	5.8 ± 1.1				
Coriaria	2.4 ± 0.8	3.2 ± 0.3				
Griselinia	1.6 ± 0.4	1.57 ± na	1.08 ± 0.10	1.9 ± 0.2		
Melicytus		4.8 ± 1.2				
Pseudopanax			1.16 ± 0.10			
Metrosideros			0.79 ± na [a]	0.8 ± 0.3 [a]	1.17 ± 0.12 [a]	0.17 ± 0.07[b]
Weinmannia			1.5 ± 0.3 [a]	1.7 ± 0.5 [a]	1.2 ± 0.2 [a]	0.32 ± 0.15[b]
Dacrydium					1.08 ± 0.18	0.53 ± 0.05
v_{cyt}						
Hebe	9.5 ± 0.9					
Olearia	6.6 ± 1.7					
Aristotelia	18 ± 2	11.0 ± 1.2[*]				
Coriaria	18 ± 4 [a]	9.2 ± 0.9[b]				
Griselinia	5.5 ± 0.7[a]	8.25 ± na [a]	2.71 ± 0.17[b]	2.2 ± 0.3[b]		
Melicytus		10.7 ± 1.3				
Pseudopanax			3.5 ± 0.3			
Metrosideros			2.48 ± na	3.3 ± 0.4	2.5 ± 0.3	2.6 ± 0.3
Weinmannia			3.58 ± 0.20	3.0 ± 0.4	3.1 ± 0.3	3.55 ± 0.13
Dacrydium					2.3 ± 0.4	1.45 ± 0.19

Values are reported as mean ± SE; n = 4 or 5 replicates each, except for *Griselinia* in site 2 and *Metrosideros* in site 3, for which only one sample was available. *Olearia* and *Dacrydium* values are grayed out to indicate that they were not included in any statistical analyses (see the Materials and Methods section).

[a,b] Letters indicate statistically distinct sites within species at the P < 0.05 level.

The components of τ_a varied differently by site age. At site 6, the decreases in τ_a were attributed to a 20 – 40% decrease in AP activity relative to younger sites ($P < 0.005$; Table 4.3, Fig 4.5b). By contrast, in the youngest sites, changes were attributed solely to CP activity: a 42% reduction in CP activity in *Aristotelia* and in *Corearia* from sites 1 to 2, and a 50% reduction in CP activity in *Griselinia* from sites 1 and 2 to sites 3 and 4 ($P = 0.0003$; Table 4.3, Fig 4.5b). The model selection process further supported differences in the responses of the two pathways. The best model to describe the observed AP activities (upper bar segments in Fig 4.5a,b) was v_{alt} = P + Cu + Starch (Table 4.2), with effect sizes of 72%, 40% and 24% respectively. The model did not support any correlation of v_{alt} with total R, even though there was a clear correlation when R was considered by itself (Appendix A4.2 Table S4.2). Unlike the AP, CP activity strongly correlated with R: the best-selected model for v_{cyt} was essentially a mirror image of that for v_{alt}, with the

addition of *R*, i.e., $v_{cyt} = R - P - Cu - Starch$, with coefficients of the same magnitude as in the v_{alt} model (Table 4.2). When *R* was excluded from the analysis, the best-selected model was $v_{cyt} = N - P + TNC$ with effect sizes 80%, –30%, and 9% (Table 4.2). Thus, it would appear that the correlation between total R and Cu was mediated primarily through AP activity.

4.3.3. AOX/COX protein concentration

Western blot analysis was successful for only three species. No statistically significant differences were found (Fig 4.7).

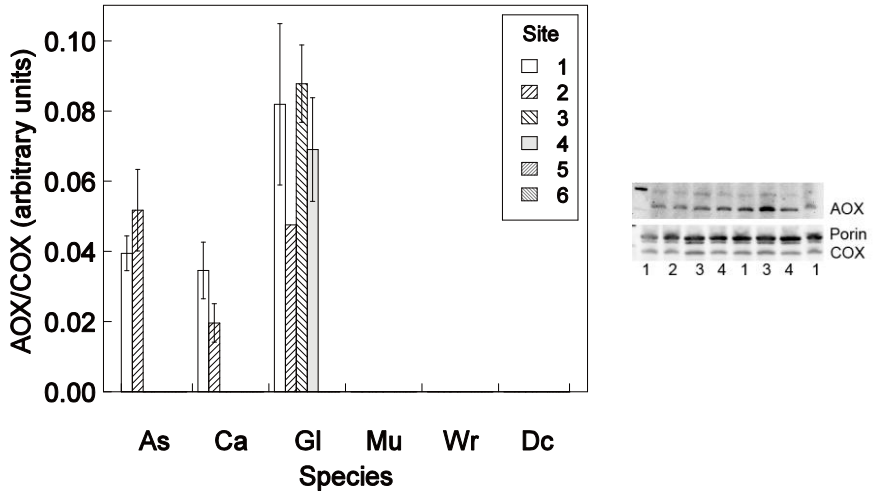

Fig 4.7. Western blot analysis.

(a) AOX/COX signal intensity (b) representative blot for *Griselinia*, numbers refer to the site. I was only able to get a signal from three species. No statistically significant effects were found.

4.4. DISCUSSION

The contrasting variations in soil mineral status along the Franz Josef chronosequence provide an excellent natural test-bed for examining how soil nutrients and their ratios affect plant growth and physiology. Previous studies have found that soil N initially increased from near absence in new soils to peak values after 500 years in site 4, falling thereafter to less than half the peak value; soil P, on the other hand decreased exponentially with soil age, leading soil N/P to increase with age; like N, soil Fe rose and then fell, but it peaked sooner than N at just 130 years in site 3 (Table 4.1). Previous studies found that respiration and photosynthesis declined with site age (Turnbull *et al.*, 2005, Whitehead *et al.*, 2005), and here I expand the analysis to include foliar micronutrients and DMC, and to consider multiple explanatory factors for the observed

changes in *R*. Most importantly the focus of this study has been on how the observed site differences affected the partitioning of respiration into AP and CP activities.

4.4.1. R scales with foliar N, τ_a scales with N/P

Of the traits measured here, leaf macronutrient status was most clearly associated with both *R* and τ_a but in different ways: *R* scaled with absolute N concentrations while electron partitioning was more strongly correlated with the N/P ratio (Fig 4.6, Table 4.2). The relationship between leaf respiration and absolute N concentration is well known and has been demonstrated previously on this site (Turnbull *et al.*, 2003) as well as in a database of measurements from nearly 300 species (Reich *et al.*, 2008). With such a clear relationship between N and respiration it may seem paradoxical that N/P ratios have been found to determine nutrient-limiting plant growth irrespective of absolute concentrations (Aerts & Chapin, 2000). The answer appears to be that while respiration and growth scale with absolute nutrient availability, concentrations of one or the other macronutrient may still provide a ceiling. Thus, in limiting-nutrient experiments, adding the limiting nutrient may still provide an increment in growth rates.

From the results of this investigation it appears that N/P ratio is also an important determinant of electron partitioning, such that relative nitrogen limitation (low N/P) leads to increased electron partitioning towards the AP whilst high N/P (P being relatively limiting) is associated with reduced AP activity (Fig 4.6b, Table 4.2). The relationship, however, while strongly significant statistically, has relatively low explanatory power (r^2 = 0.23) compared with the relationship between N and *R* (r^2 = 0.81), implying that the processes influencing electron partitioning may be more complex than those influencing total respiration. The data thus appear to partly confirm laboratory studies that found increased AP capacity due to N-deficiency (Noguchi & Terashima, 2006) but not studies that have found a similar increase in response to P-deficiency (Gonzalez-Meler *et al.*, 2001, Juszczuk *et al.*, 2001b). In contrast to either of those studies, however, it was not the absolute deficiency that mattered across the chronosequence, but rather the N/ P ratio. Nevertheless, the hypothesis proposed by Noguchi and Terashima (2006) may still apply: when N is scarce relative to growth capacity, the plant could still benefit from promoting the N-conserving but energy-inefficient AP over the energy-efficient but high-N CP. Some other, unknown, mechanism may also be responsible, since when AP activity itself was considered here, I found that increasing P concentrations, rather than changes in N, were responsible for the increased AOX activity (Table 4.2).

Statistical analysis of all possible explanatory factors measured in this study confirmed the importance of N relative to total respiration and to N/P relative to τ_a. The support probabilities for these variables in Table 4.2, for example, are very high. Support probabilities can be viewed as a measured of relevance since, by design, half of the models tested include each covariate and half don't. The sum of model weights for the models including a particular covariate, i.e. *Support* in Table 4.2, therefore indicates the likelihood that any combination of parameters could effectively replace the given parameter. In the case of N, for example, no combination of explanatory variables could make up for the absence of N (*support* = 0.999). Likewise, the support for N/P of 0.88 indicates that in sum, regression models including N/P as a term explained the data 7 times better (0.88/0.12) than models without N/P. By contrast, a support probability of 0.5 for a particular variable would indicate that models with and without that variable were equally "good" at explaining the outcome. It is interesting to note that in the analysis presented in Table 4.2, support of 0.5 coincided approximately with a *P* value of 0.05. None of the variables omitted from Table 4.2 had support greater than 0.5.

4.4.2. Cu and TNC (or Starch) also contribute to *R*

Despite the very strong correlation between N and *R*, two other foliar factors contributed independent explanatory power to the overall respiratory rate: Cu and TNC or Starch (Table 4.2). Although the support for TNC or Starch appears to be low, this is only because the model is over-specified since TNC = Starch + Sugar. If either TNC or Starch is removed from the consideration, support for the remaining variable increases above 0.9 and *P* decreases below 0.005 for the remaining variable (Table 4.2, note b). As with N, the relationship between *R* and carbohydrates has been well-explored. Intuitively one might expect such a relationship to exist, since carbohydrates provide the basic substrates for *R*, but the evidence to-date is inconclusive. Tjoelker *et al.* (2008), for example, found relatively strong correlations between R/N and soluble sugars across several sites and seasons. A weak correlation between R and TNC irrespective of N had been previously reported for this site (Turnbull *et al.*, 2003) and was confirmed in this study (Appendix A4.2 Table S4.2). The relationship between carbohydrates and *R* may be partially masked under nutrient limitations, however, since carbohydrate accumulation is also a known symptom of nutrient deficiency (Chapin, 1980, Noguchi & Terashima, 2006). In the current study, however, I found a positive, though weak correlation between TNC and either *R* or N (Appendix A4.2 Table S4.2).

4.4.3. The influence of Cu may be mediated by AP activity

Relative to the macronutrients and carbohydrates, very little appears to have been published on the effects of Cu deficiency on plant respiration, despite its important role as a cofactor to respiratory enzymes. In fact, a search of the literature suggests that Cu toxicity is considered to be more of an issue than its deficiency (He, Yang & Stoffella, 2005). The present study identified a direct relationship between Cu and total respiration but this appears to have been due to is influence on AP activity (Table 4.2). When R was included in the multimodel analysis, an inverse effect of Cu on CP activity was also detected (not shown), but this appears to be a side-effect of the definitions of v_{alt} and v_{cyt}. In fact, with R included in the set of explanatory variables, the same variables and coefficients were found to significantly affect v_{alt} and v_{cyt} except that v_{cyt} also included R as an explanatory variable (v_{alt} did not) and all other coefficients were the same as for v_{alt} and *v*alt but opposite in sign. When R was excluded from the analysis, Cu was not found to contribute to changes in CP activity (Table 4.2). Thus, it would appear that the dependence of total R on Cu may, in fact, be mediated by selective upregulation of AOX. The direction of the effect of Cu on AP activity, however, is the opposite of my hypothesis that under Cu-deficiency a plant would promote AOX as a Cu-independent respiratory pathway. Instead, it may be that plants are more optimized to cope with Cu toxicity than with Cu deficiency. In an investigation on Cu toxicity in sycamore cell suspensions, Padua *et al*. (1999) found greater cyanide-insensitive O_2 consumption in cells grown on an adequate amount of Cu (2 μM) than in Cu-deficient media (0.2 μM). Increasing Cu levels further (20, 50 μM), progressively suppressed total respiration and increased AOX capacity. Thus, it would appear that the initial increases in AOX capacity may have been related to a mechanism that has evolved to respond to Cu toxicity.

Some notes of caution should be raised in interpreting the multiple-factor analysis. First, although the additional factors were found to be statistically significant in the multiple regressions, and they were well-supported by the model-weighting evidence, adjusted r^2 values increased very little with the added variables (Table 4.2). I interpret this dichotomy to mean that while adding the variables may not have increased predictive power for management purposes, the additional factors may still be important in situations where the factors very more independently. The correlation between many of the variables in this study (Appendix A4.2 Table S4.2) raises a second issue: although the models evaluated for (Table 4.2) are strictly additive, i.e., effects of the variables a said to

be independent, the correlation among explanatory variables makes the variables interdependent with regard to the sites studied. It would be incorrect, for example, to suggest that the negative coefficient in Table 4.2 implies that P suppresses v_{cyt}. On its own, P correlated positively with v_{cyt} (r = 0.66), but only when considered together with N does P appear to be "counteracting" increases due to N. Finally, it should be noted that while the new correlations described here are intriguing and well-supported by the data, experimental manipulations are needed to confirm a causative effect. It is certainly possible, for example, that some other unmeasured factor that correlated with Cu was the real cause of the apparent relationship found here.

4.5. SUMMARY

This study demonstrates that the relatively simple picture of R responding to N and carbohydrates has much richer detail when leaf micronutrient status is considered and especially, when the respiratory O_2 consumption is broken down into its component alternative and cytochrome pathways. Along the Franz Josef chronosequence CP activity, which accounts for the majority of respiration (Fig 4.5a,b and Table 4.3), responded to both N and P levels (in opposite directions, when considered together), whereas AP activity was not influenced by N, but instead responded to P, Cu, and starch levels. As a result, while total respiration decreased with soil age in the Franz Josef chronosequence, the differences between the younger sites appear to have been solely due to changes in CP activity, presumably due to decreasing N, whereas the decreases in the oldest sites were primarily attributed to changes in AP due to decreases in P and in Cu. The effects on respiratory efficiency therefore appear to have been either neutral (no detected change in τ_a) or accompanied by a slight decrease in efficiency (based on the analysis of the AP and CP separately) at the younger sites, whereas at the oldest, most nutrient-deficient sites, reductions in R led to increased respiratory efficiency. To my knowledge, this is the first investigation of the effects of Cu on respiration and electron partitioning in leaf tissue and it is certainly the first field investigation of respiratory electron partitioning along a natural soil nutrient gradient. The insights from this study may well open up new avenues for investigating the response of respiration to micronutrient status – both with respect to total respiration and the relative activities of the alternative and cytochrome respiratory pathways.

5. Nutrient deficiency reduces cytochrome *c* oxidase but not alternative oxidase activity in greenhouse-grown *Griselinia littoralis*

5.1. INTRODUCTION

In the previous chapter I investigated how differences across the Franz Josef chronosequence, a natural soil nutrient gradient, affected plant respiration and respiratory electron partitioning. Differences in leaf nitrogen (N) were found to correlate with total respiration while differences in foliar nitrogen/phosphorus (N/P) appeared to affect respiratory electron partitioning.

Despite the widely appreciated importance of nitrogen – and phosphorus, to a lesser extent – in limiting plant growth, respiration, and photosynthesis in natural systems (Aerts & Chapin, 2000, Reich *et al.*, 2006, Wright *et al.*, 2004), relatively little has been published on the interactions between N availability and respiratory electron partitioning. Early studies using inhibitors demonstrated that N- or P-deficiency increased cyanide-resistant respiration and AOX concentrations in algae (Weger & Dasgupta, 1993) and plant cell suspensions (Hoefnagel, Vaniren & Libbenga, 1993). More recently similar results were found in N-deficient spinach leaves (Noguchi & Terashima, 2006), *Arabidopsis thaliana* shoots and roots (Watanabe *et al.*, 2010), and tobacco cell suspensions under N- or P-deficiency (Sieger *et al.*, 2005). Only one study I am aware of examined how *in vivo* respiratory electron partitioning responds to nutrient deficiency. Gonzalez- Meler *et al*. (2001) reported species-dependent responses to P-deficiency: electron partitioning and AP activity increased under P-deficiency in *Phaseolus vulgaris* (L.) and *Gliricidia sepium* (Jacq.) but not in *Nicotiana tabacum* (L.) leaves. I did not find any studies that measured the effects of N-deficiency on electron partitioning *in vivo*, nor am I aware of any studies that have examined possible interactions of N and P on electron partitioning, such as are described in the previous chapter.

In order to confirm the findings of the chronosequence survey, I therefore conducted a 2x2 factorial nutrient manipulation experiment in which either N, P, or both nutrients were withheld from the rooting medium. *Griselinia littoralis* Raoul was chosen from among the species measured along the chronosequence because it is a widespread shrub/tree species that is found in early-mid-late successional forests, with a broad distribution across New Zealand. Based on the results described in Chapter 4, I predicted that respiration rates would scale with tissue N concentrations, while electron partitioning would be increased by low N/P.

5.2. MATERIALS & METHODS

5.2.1. Plant material and growth conditions

I conducted a nutrient-manipulation experiment in a greenhouse at the University of Canterbury, Christchurch, New Zealand to test the effects of complete removal of nitrogen (–N), phosphorus (–P) or both N and P (–NP) for the growth medium. *Griselinia littoralis*, a native New Zealand tree species, was selected because of its prominence at several sites in the Franz Josef chronosequence and because of its ready availability and relatively rapid growth. Rooted cuttings of *Griselinia littoralis* were purchased from a local nursery. The roots were washed of their potting mix and replanted in 1:1 Perlite:vermiculite. Nutrients were supplied by watering with half-strength modified Hoaglands nutrient solution (Epstein & Bloom, 2005), which was prepared either with the full complement of nutrients ("ALL" or "control;" 2.5 mM $Ca(NO_3)_2$, 2.5 mM KNO_3, 1 mM $MgSO_4$, 0.5 mM KH_2PO_4, 14 μM NaFeEDTA, 4.5μM $MnCl_2$, 23 μM H_3BO_3, 0.4 μM $ZnSO_4$, 0.2 μM $CuSO_4$, 50 nM H_2MoO_4) or by replacing nitrate (–N), phosphate (–P) or both minerals (–NP) with chloride . Blocks of four plants each were randomly assigned to treatments and were watered with the appropriate solution as needed, typically once or twice a week. Pots were placed on saucers to help isolate roots from neighboring runoff and to provide a reservoir of nutrient solution. In addition, several plants were replanted in either unsupplemented media or media supplemented with Osmocote (The Scotts Co., Marysville, OH) according to the manufacturer's instructions, and were watered with tap-water only.

At the start of the experiment, the growing tips of each shoot were removed, in order to differentiate between existing leaves (on the main stem) that had grown outdoors and with sufficient nutrition *vs.* new leaves (on new branches) grown under the experimental regime in the greenhouse. Lighting in the greenhouse was supplemented to extend daylength to 12 h. Illumination in the greenhouse varied by location from 300 – 700 μmol m^{-2} s^{-1} photosynthetically active radiation (PAR) on a sunny day, to 150 – 250 μmol m^{-2} s^{-1} on cloudy days and under the artificial lights. Plants were maintained in the greenhouse for 12 weeks to allow sufficient new leaf formation for subsequent respiratory incubations.

5.2.2. Gas exchange measurements

During the 13^{th} week, respiratory and photosynthetic CO_2 gas exchange was measured using an LI-6400XT (LI-COR, Lincoln, Nebraska, USA). Photosynthesis was measured

at 20 ºC under saturating light levels, determined by measuring gas exchange at 200, 400, or 1,000 μmol m^{-2} s^{-1} PAR in 400 μmol CO_2 mol air $^{-1}$. Measurements were recorded after gas-exchange parameters had stabilized, generally 3–5 minutes.

5.2.3. Respiratory incubations

Respiratory incubations were conducted over the following two weeks (14^{th} and 15^{th}) on new leaf tissue, old leaf tissue and roots to determine both total O_2 respiration and electron partitioning based on the ^{18}O isotope discrimination methods described in Chapter 2. Whole plants were brought into a laboratory. Leaf tissue was kept in the dark for at least 30 minutes before harvesting. Replicates consisted of either leaves arbitrarily sampled from four plants or of entire roots systems combined from two plants. Plants that had either not been used or had not been substantially altered by leaf or root harvest were returned to the greenhouse and maintained on the nutrient regimen for an additional seven weeks. The remaining roots were used to determine discrimination endpoint values during weeks 21 – 23.

Leaf or root tissue was sliced into sections no larger than 1 cm × 7 cm and incubated in sealed septum-capped 12 mL vials (Labco, High Wycombe, UK; product #738W) in the dark. A half-pellet of KOH, in a protective holder, was also placed in the vial in order to remove respired CO_2. After 3-5 h, depending on tissue type and treatment, air was transferred under positive pressure from the incubation vial to a syringe by displacement with water. The air in the syringe was immediately injected into a pre-evacuated storage container (Labco product #778W – 3.7 mL) for later analysis.

Five replicates of each treatment were measured for new leaves, old leaves, and roots. For each replicate, tissue was distributed into six incubation vials in the proportions 1:2:3:4:5:6 by fresh mass, thus providing a six-fold range of O_2 consumption at the end of the incubation period. In some cases, particularly for new leaves deficient in N, replicates consisted of fewer than six vials due to lack of available tissue. (One replicate of –NP new leaves was omitted entirely due to lack of tissue.) Total sample size for each replicate was determined based on the previously measured CO_2 respiration rates so that no more than 50% of the O_2 in any vial would be consumed – 7 g fresh mass (FM) for new leaves and for roots, and 8 g FM for old leaves. Vials in which actual O_2 consumption was greater than 60% were rejected from further analysis. Air “blank” vials were prepared alongside the incubations by injecting laboratory air directly into storage vials. Additional O_2-free blanks were prepared by reserving pre-evacuated vials to be filled with O_2-free

He (99.99% pure; BOC, Auckland New Zealand) shortly before measurement in the mass spectrometer.

Discrimination "endpoints" for alternative oxidase (AOX) and cychrome *c* oxidase (COX) were measured by inhibiting the tissue with selective respiratory inhibitors. COX was inhibited using gaseous cyanide by sealing tissue for at least 20 minutes in plastic jars containing a 1 × 8 cm strip of chromatography paper soaked 1 M KCN. AOX in the control and –NP roots only was inhibited by soaking the tissue in 20 or 40 mM salicylhydroxamic acid (SHAM) in 2% dimethyl sulfoxide (DMSO) for 20 minutes. For the inhibition trials each of six vials per replicate were filled with approximately the same amount of tissue (1–2 g each) and were incubated for variable amounts of time, in order to test for the possibility of recovery from inhibition during incubation. The COX endpoint for leaves could not be determined and was therefore assumed to be 20‰, as described in the previous chapter.

Storage vials were stored at –17 ºC for less than two months before measurement, and thus did not suffer from contamination due to storage leaks (Chapter 3).

5.2.4. Discrimination, electron partitioning and respiration computations

Isotopic composition of the respiratory air samples was measured in a Thermo Electron Delta V Plus isotope ratio mass spectrometer (Thermo Electron, Bremen, Germany) as described in Kornfeld *et al*. (2012b) and Chapter 2. Measurements were corrected for contamination using the O_2-free blanks stored alongside the respiration samples as described in Chapter 3. Discrimination values, *D*, were computed by linear regression, Eqn (3.4), reproduced here, for convenience:

$$1000 \times \ln\left(\frac{{}^{34}R_s}{{}^{34}R_{s,0}}\right) = -D \ln f_s^* . \tag{5.1}$$

where ${}^{34}R$ is the isotope ratio, ${}^{18}O^{16}O$ /${}^{16}O^{16}O$, the subscript *s* refers to the contamination-corrected sample measurements, the subscript 0 indicates the measurement for the air blanks and

$$f^* \equiv \frac{{}^{32}O_2/{}^{28}N_2}{({}^{32}O_2/{}^{28}N_2)_0} . \tag{5.2}$$

The regression was not forced through zero (Henry *et al.*, 1999). All regressions were first tested for curvature based on the statistical significance of an added quadratic term in

Eqn (3.7), as described in Chapter 3. If the coefficient was statistically significant at the $P < 0.05$ level, then the quadratic term was kept in the regression.

Discrimination values were converted to measures of electron partitioning through the alternative pathway, τ_a, by linear interpolation (Guy *et al.*, 1989):

$$\tau_a = \frac{D_s - D_c}{D_a - D_c}, \tag{5.3}$$

where D_s, D_a, and D_c represent the discrimination values for the sample, alternative pathway, and cytochrome pathway respectively. Electron partitioning in leaves was determined using measured D_a of 29.24 ± 0.05‰ (n = 4) and assumed D_c of 20‰ (Ribas-Carbo *et al.*, 2005a). For roots, endpoints were measured only in –NP and control treatments due to tissue availability restrictions. For the purposes of display, based on the correspondence of measured D values (Appendix A5.1 Fig S5.3a), –P roots were assumed to have the same endpoints as control roots whereas –N roots were assumed to have the same endpoints as –NP. Statistical comparisons of τ_a, in roots were restricted to control and –NP treatments.

Respiration rates (R) were computed based on f^*, tissue mass (*mass* g), vial volume (V_{vial}, mL), tissue volume (V_{plant}, mL), CO_2 trap volume (V_{other}, mL), incubation time (t, s) and incubation temperature (T, Kelvins) according to the equation:

$$R\ (nmol\ g^{-1}\ s^{-1}) = \frac{0.21 f_s^* \times (V_{vial} - V_{plant} - V_{other})}{mass \times t} \frac{10^6 P}{R_{gas} T}, \tag{5.4}$$

where P is the atmospheric pressure in atm and R_{gas} is the the ideal gas constant (0.082 mL atm K^{-1} $mmol^{-1}$). Tissue volume was estimated based on fresh mass divided by the density, measured by water displacement, of representative samples. Incubation temperatures were 20.3 ± 0.3 ºC (mean ± SD).

Respiration by each pathway was computed as

$$v_a = \tau_a R \tag{5.5a}$$

and

$$v_c = (1 - \tau_a) R, \tag{5.5b}$$

where, v_a and v_c correspond to the activities of the alternative and cytochrome pathways respectively.

5.2.5. Leaf tissue analysis

Tissue samples for leaf trait analysis were collected from the replicates during the initial respiratory incubations (14^{th} – 15^{th} week). Specific leaf area (SLA) and dry matter content (DMC) was measured on representative samples by scanning images of fresh leaves on a flatbed scanner. Leaf area was determined from the images using Photoshop software (Adobe, California, USA). Tissue samples were dried in an oven at 60°C for a minimum of two days before determining dry mass.

A second set of samples, flash frozen to –80 ºC, were lyophilized for at least 24 h, ground to a fine powder in a ball mill and then stored at –80 ºC until assayed for respiratory proteins and carbohydrates, or sent to Landcare Research, (Palmerston North, New Zealand) for nitrogen and phosphorus determination by the Kjeldahl method. All of the leaf samples, but only three of the five replicate sets of root tissue were analyzed for N, P. Leaf and root carbohydrate contents were assayed colorimetrically using phenol:sulfuric acid according to the method of Tissue & Wright (1995). Soluble sugars were extracted directly from powdered leaf tissue into methanol:chloroform:water. Starch in the remaining pellet was dissolved by hydrolysis to glucose in 35% perchloric acid before conducting the assay. Total nonstructural carbohydrates (TNC) was computed as the sum of starch and sugar content. AOX, COX, and porin concentrations were determined by immunoblotting as described in Section 4.2.4.

5.2.6. Statistical analysis

Statistical analyses were computed using R 2.14 (R Development Core Team, 2011). Treatment effects were tested for significance using two-way ANOVA on tissue type and treatment. The data were unbalanced due to missing data, so that order of the variables affect computed *P* values. ANOVA tests were therefore conducted with variables in either order, but for reporting purposes, tissue type was specified as the first variable since tissue differences take precedence based on biological considerations (Hector, von Felten & Schmid, 2010). Post-hoc test were computed using Tukey's HSD comparison of all pair-wise combinations, adjusted according to Westfall (Bretz *et al.*, 2011). The pairwise comparisons were also used to generate the "letter groupings" indicating statistically significant groups in the graphs presented here.

Residuals variance was tested for uniformity by tissue type using the Brown and Forsyth test (Brown & Forsythe, 1974). If residual variance was not uniform, residuals in the statistical tests were weighted by $1/var_s$, the residuals variance within each tissue type

(Venables & Ripley, 2002). Normality was tested using the Shapiro-Wilk test (Royston, 1995) and, if necessary, variables were either transformed either logarithmically or with the Geary-Hinkley transformation (Hayya, Armstrong & Gressis, 1975), to restore normality. In these cases, transformed data were used to test for significance whereas untransformed data were used to determine effect sizes.

Uncertainty is reported here as mean ± standard error (SE) unless otherwise noted. Values of τ_a required special treatment to include uncertainty in all three component measurements in Eqn (5.3): the two endpoint discrimination values, D_a and D_c, and the sample discrimination value, D_s. The combined uncertainties in τ_a were therefore determined by propagating the uncertainty (ISO/IEC, 1995) and *t* tests were conducted using the corrected SE values. Assuming no correlation between the component variables, x_i, the combined standard error, *se*, for a function $f(x_1, x_2, \ldots, x_N)$ is estimated as:

$$se = \sqrt{\sum_i \left(\frac{\partial f}{\partial x_i} se_{x,i} \right)^2} , \tag{5.6}$$

where $\partial f/\partial x_i$ is the partial derivative of *f* with respect to the i^{th} component variable and $se_{x,i}$ is the standard error for x_i. Since D_a and D_c values were constant relative to the sample values, the assumption of independence holds. For τ_a, the resulting formula after simplification is:

$$se_\tau = \frac{\sqrt{(D_a - D_c)^2 se_s^2 + (D_s - D_a)^2 se_c^2 + (D_c - D_s)^2 se_a^2}}{(D_a - D_c)^2} . \tag{5.7}$$

Combined uncertainty for the alternative pathway activity, Eqn (5.5a), is:

$$se_{va} = v_a \sqrt{\left(se_\tau / \tau_a \right)^2 + \left(se_R / R \right)^2} , \tag{5.8}$$

and for the cytochrome pathway activity, Eqn (5.5b), the combined uncertainty is:

$$se_{vc} = v_c \sqrt{\left(se_\tau / (1 - \tau_a) \right)^2 + \left(se_R / R \right)^2} . \tag{5.9}$$

5.3. RESULTS

After 14 weeks of experimental treatment, plants differed visibly and displayed a strong phenotypic response to fertilizer treatment: the controls had grown substantially and the foliage was a glossy green; –P plants had also grown but the leaves looked duller and somewhat darker; the N-deficient plants had grown relatively little new tissue, and both new and old leave were chlorotic. Leaf and root physical and chemical traits also showed symptoms consistent with each treatment, as discussed next. These data provide the context for evaluating the measures of respiration, respiratory electron partitioning and AOX/COX ratios, which represent the central theme of this work.

5.3.1. Leaf traits

Nutrients deficiency strongly suppressed new leaf biomass (Fig 5.1a). After 14 weeks, the controls had produced 2.8 ± 0.2 g DM of leaves per plant. This was four times greater than the –N treatments (0.7 ± 0.1 g and 0.8 ± 0.1 g for –N and –NP) and 75% more than the –P treated plants (1.6 ± 0.3 g). The differences between each of these three groups were statistically significant, $P < 0.01$; the –N and –NP plants did not differ significantly. Total mass of pre-existing leaves and of roots did not differ by treatment after 14 weeks (Fig 5.1; $P = 0.98$ and 0.6 respectively).

Leaf dry matter content (DMC) changed similarly in both new and old leaves (Fig 5.1b). The fully fertilized controls had the lowest DMC: 28.3 ± 0.6% dry matter for new leaves, *vs.* 31.9 ± 0.6% for –N, and 32.4 ± 0.6% for –NP leaves ($P = 0.003$ for the difference from the controls). The –P leaves were intermediate between the two groups: 29.63 ± 0.6% ($P = 0.051$ for the difference from the N-deficient leaves). Root DMC did not differ by treatment ($P = 0.3$). Changes in specific leaf area (SLA) were considerably more pronounced in new leaves than in old leaves (Fig 5.1c). SLA declined from 8.9 ± 0.5 $m^2\ kg^{-1}$ in the control leaves to 6.4 ± 0.3 $m^2\ kg^{-1}$ in the –NP treatment. Withholding only a single nutrient resulted in intermediate SLA values of 7.5 ± 0.3 $m^2\ kg^{-1}$ in new leaves. Older leaves, responded similarly but with a smaller decline in SLA, due to the lower value of 7.9 ± 0.2 $m^2\ kg^{-1}$ in the controls.

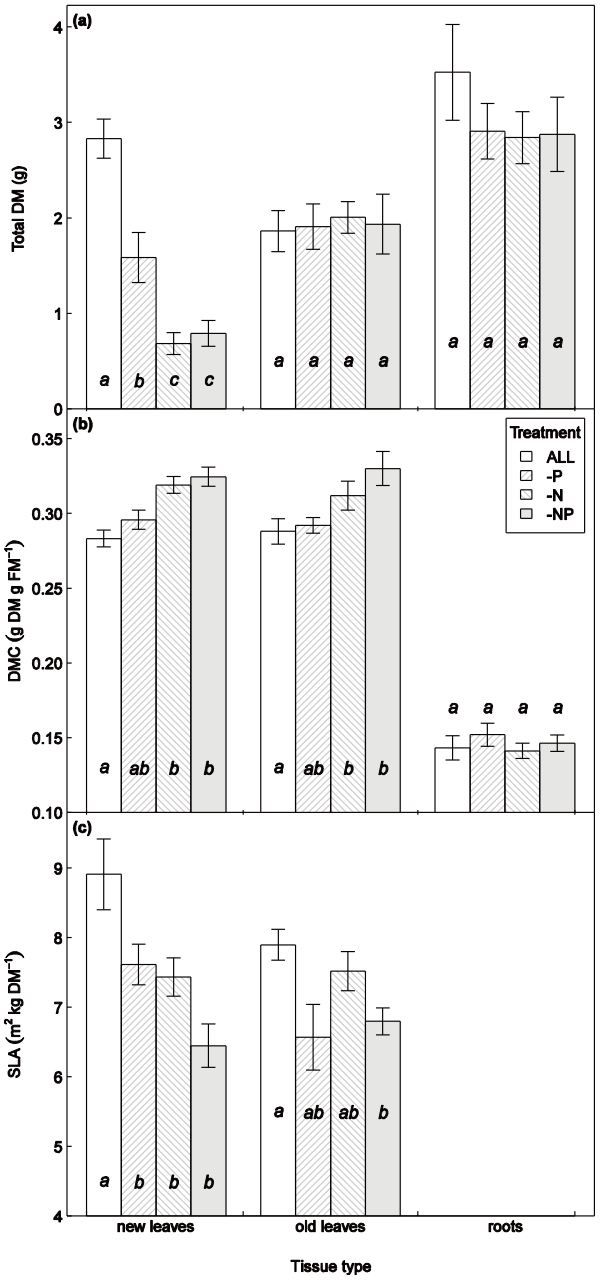

Fig 5.1. (a) Dry mass, (b) dry matter content (DMC), and (c) specific leaf area (SLA) for new leaves, old leaves.

Letters indicate statistically distinct treatments within each tissue type ($P < 0.05$). The vertical placement of letter groups indicates statistical groupings by tissue type.

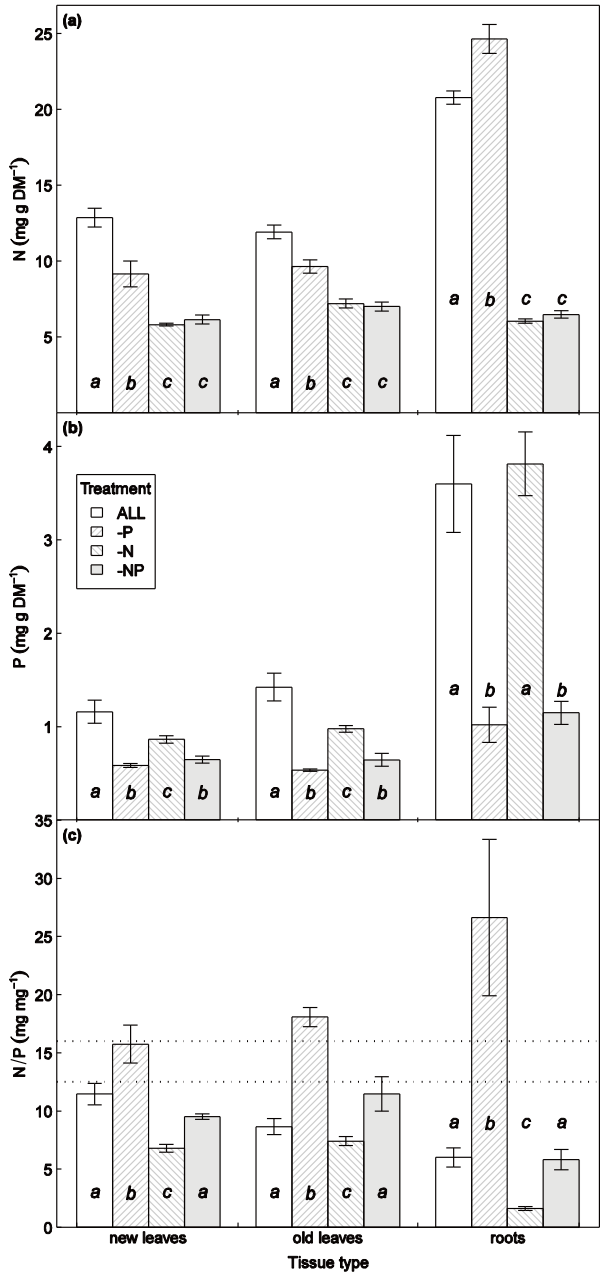

Fig 5.2. Leaf N (a), P (b) and N/P (c) for new leaves, old leaves, and roots.

Dotted horizontal lines in (e) and (f) indicate the transition zone from N-limitation to P-limitation according to Tessier & Raynal (2003). Letters indicate statistically distinct treatments within each tissue type ($P < 0.05$). The vertical placement of letter groups indicates statistical groupings by tissue type.

Leaf N, P, and N/P varied according to the composition of the nutrient solutions used in each treatment (Fig 5.2). Older and newer leaves responded similarly but differed from roots in the response to single-nutrient deficiency. In leaves, absence of one nutrient suppressed the concentration of the other nutrient. Thus, in –P leaves, the N-concentration of 9.1 ± 0.9 mg N g DM^{-1} was halfway between that of the controls (12.8 ± 0.6 mg N g

DM^{-1}) and –N leaves (5.8 ± 0.09 mg N g DM^{-1}; $P < 0.001$; Fig 5.2a). A similar pattern can be seen for P levels in N-deficient leaves (Fig 5.2b; $P < 0.001$). In roots, however, concentrations of the sufficient nutrient were not lower when the other nutrient was absent. In fact, the P-deficient roots accumulated a statistically significant 18 ± 4% more N than the control roots (Fig 5.2a; $P < 0.002$). Perhaps more importantly, concentrations of the supplied nutrients in roots were considerably higher than in leaves: 23 ± 1 mg N g DM^{-1} in N-fertilized roots *vs.* 10.9 ± 0.5 mg N g DM^{-1} in N-fertilized leaves; 3.7 ± 0.3 mg P g DM^{-1} in P-fertilized roots *vs.* 1.08 ± 0.10 mg P g DM^{-1}. This effect cannot be attributed to the lower DMC in roots (Fig 5.1a) since tissue N and P concentrations did not differ between leaves and roots in the nutrient deficient tissues (Fig 5.1a, b; $P > 0.1$ in each case). The N/P ratio was highest in the –P treatments and lowest in the –N treatments, as might be expected, but ratio did not differ significantly between the controls and the –NP treatments (Fig 5.1c).

Sugar, starch, and total nonstructural carbohydrates (TNC) concentrations did not vary among treatments in new leaves or roots (Fig 5.3; $P > 0.1$ each). Old leaves in the control plants, however, contained half the starch and 70% TNC relative to the nutrient-deficient plants ($P \leq 0.01$ each).

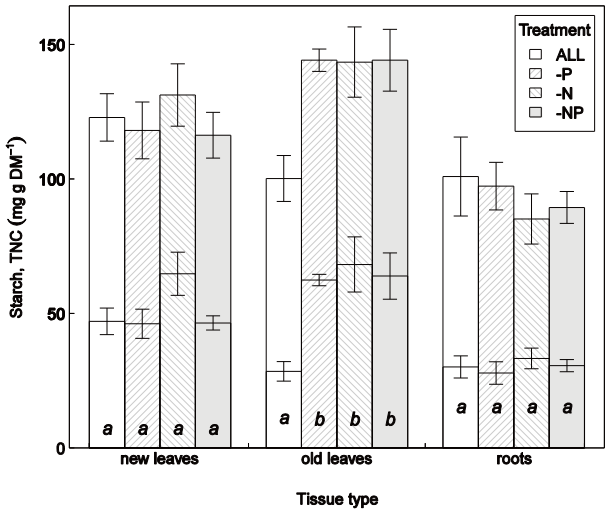

Fig 5.3. Total nonstructural carbohydrates and sugars for new leaves, old leaves, and roots.

Letters indicate statistically distinct treatments within each tissue type ($P < 0.05$) and apply to both Starch and TNC levels. No statistically significant differences were found between sugar levels. The vertical placement of letter groups indicates statistical groupings by tissue type.

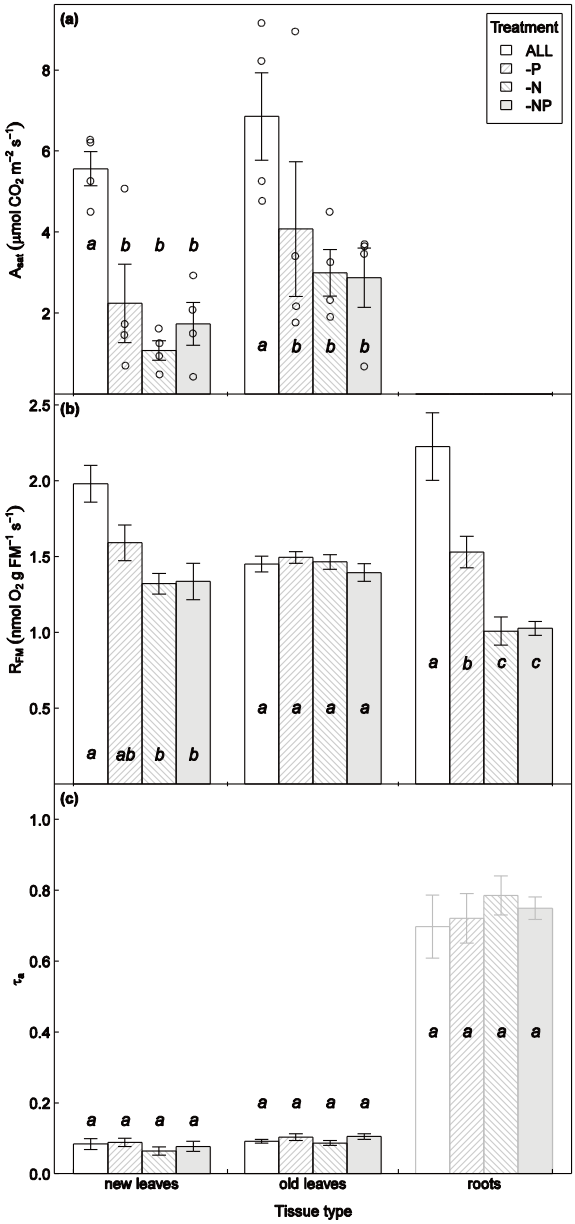

Fig 5.4. Photosynthetic capacity, A_{sat}, (a); respiration on a fresh mass basis, R_{FM}, (b); and electron partitioning through the alternative pathway, τ_a, (c), for new leaves, old leaves, and roots.

Respiration is shown on a fresh mass basis so that root and leaf value are in the same range (see Appendix A5.1 Fig S5.2). Letters indicate statistically distinct treatments within each tissue type ($P < 0.05$). The vertical placement of letter groups indicates statistical groupings by tissue type. $n = 4$ each for A_{sat} and 5 each for R and τ_a. Error bars in panel (c) reflect measurement error only; they do not include uncertainty in the endpoints. Root τ_a is grayed out to indicate uncertainty in the result. See text for details.

5.3.2. Photosynthesis and respiration

Photosynthetic capacity, measured 1-2 weeks prior to the respiratory incubations, was strongly inhibited by nutrient deficiency, declining from 5.5 ± 0.4 μmol CO_2 m^{-2} s^{-1} in new control leaves to 2.2 ± 1.0 (–P), 1.1 ± 0.2 (-N), and 1.7 ± 0.5 (–NP) μmol CO_2 m^{-2} s^{-1}, similar declines in the older leaves (Fig 5.4a). A closer look at photosynthesis in the –

P leaves indicates a dichotomous response: in both new and old leaves one P-deficient leaf responded similarly to the control plants whereas A_{sat} in the other three leaves were in the same range as the –N and –NP leaves (symbols in Fig 5.4a). The high-responding old and new leaves were not on the same plant, however. Stomatal conductance was strongly correlated with net photosynthesis across all treatments (Appendix A5.1, Fig S5.1), thus Fig 5.4a is representative of treatment effects on both photosynthetic capacity and stomatal conductance.

Nutrient deficiency depressed respiration rates in new leaves and in roots, but not in old leaves (Fig 5.4b). [Respiration is presented in Fig 5.4b on a fresh mass basis to put the root and leaf rates on a similar scale. The same patterns were found when *R* was analyzed on a dry mass basis (Appendix A5.1, Fig S5.2).] The responses of leaves and roots to the various treatments were similar, though more exaggerated in roots. *R* was highest in the controls (leaves: 2.0 ± 0.1 nmol O_2 g FM^{-1} s^{-1}; roots: 2.2 ± 0.2 nmol O_2 g FM^{-1} s^{-1}) and lowest in the N-deficient tissues (leaves: 1.3 ± 0.1; roots: 1.0± 0.5), with intermediate values in the P-deficient tissues (leaves: 1.6 ± 0.1; roots: 1.5± 0.1). The plants that had received only tap water, respired only 15% more slowly than corresponding controls despite complete cessation of new growth (Appendix A5.1, Fig S5.3a). Also, it should be noted that although treatment effects on *R* were not apparent in the older leaves, leaf *R* still scaled with foliar N in all three tissue types (Appendix A5.1, Fig S5.4).

Respiratory discrimination, *D*, and consequently electron partitioning through AP, τ_a, was measured with high precision in leaves (SE ≤ ± 0.15‰ for *D* in all treatments, or ± 0.016 for τ_a), yet no differences by treatment were detected in leaves (Fig 5.4c, see Appendix A5.1 Fig S5.3a for the corresponding discrimination values). Electron partitioning was also unaffected in plants that had been deprived of all nutrients for 22 weeks (Appendix A5.1 Fig S5.3c). In the two-way ANOVA, however, a small but statistically significant decrease of 0.018 ± 0.007, in τ_a, was detected between newer leaves and older leaves ($P = 0.02$; but see Discussion for consideration of biological significance). The response in roots was not as clear-cut. Discrimination values differed by 3.0 ± 0.8‰ between N-sufficient and N-deficient roots during the initial respiratory incubations, 14 weeks after the start of the treatments (Table 5.1, Appendix A5.1 Fig S5.3). However, the respiratory endpoints measured at 22 weeks indicated that D_a and D_c differed between control and –NP roots (Table 5.1). Assuming that the endpoints

measured at 22 weeks were representative of what would have been found at 14 weeks, then electron partitioning at 14 weeks did not differ between the controls and –NP treatments (P = 0.7; Fig 5.4c, Table 5.1). Two lines of evidence, however, suggest that the endpoints had changed between these two periods. First, the computed value of 70%, for τ_a at 14 weeks seems high relative to published values (Ribas-Carbo *et al.*, 2005a); second, the discrimination values in uninhibited roots measured at 22 weeks (10.7‰ and 15.8‰ for control and –NP respectively) were lower than the 14-week values (14.2‰ and 17.2‰; Table 5.1; P=0.01, 0.04). Restricting analysis to week 22, τ_a was 0.27 ± 0.03 for the fully-fertilized control roots, approximately half the value of 0.56 ± 0.10 for the –NP roots, P = 0.03 after accounting for the uncertainty in the endpoints using Eqn (5.7). When respiration was partitioned between AOX and COX, the difference is attributed entirely to a nearly 4-fold drop in v_{cyt} ($P = 10^{-4}$), with no change in v_{alt} (P = 0.6).

Table 5.1. D, R, τ_a, v_{cyt}, and v_{alt} after 14 and 22 weeks of nutrient-deficiency treatments.

	14 weeks[a]		*22 weeks*	
	control	*–NP*	*control*	*–NP*
D_{COX} (‰)			8.40 ± 0.20	11.79 ± 0.20
D_{AOX} (‰)			16.71 ± 0.58	18.97 ± 0.88
D (‰)	14.19 ± 0.74	17.17 ± 0.23	10.68 ± 0.17	15.79 ± 0.50
R (nmol g FM^{-1} s^{-1})	2.23 ± 0.22	1.03 ± 0.05	1.56 ± 0.05	0.67 ± 0.03
τ_a	0.70 ± 0.10	0.75 ± 0.10	0.27 ± 0.03	0.56 ± 0.10
v_{cyt} (nmol g FM^{-1} s^{-1})	0.7 ± 0.2	0.26 ± 0.10	1.13 ± 0.06	0.30 ± 0.07[b]
v_{alt} (nmol g FM^{-1} s^{-1})	1.6 ± 0.3	0.77 ± 0.11	0.43 ± 0.05	0.38 ± 0.07
n	5	5	3	6

Values are shown as mean ± SE, with the SE for τ_a, v_{cyt}, and v_{alt} adjusted for uncertainty in the endpoints using Eqn (5.7). Endpoints were only determined for the control (all nutrients) and –NP (lacking nitrogen and phosphorus) treatments. n = 2 – 3 for the inhibitions.

[a] Endpoint determinations made at 22 weeks were used for both time periods. All values measured at 14 weeks differed from the corresponding 22 week measurement, $P < 0.05$. Electron partitioning values are grayed out to indicate the uncertainty in the results; see text for details.

[b] Difference between control and –NP is statistically significant, P = 0.0001

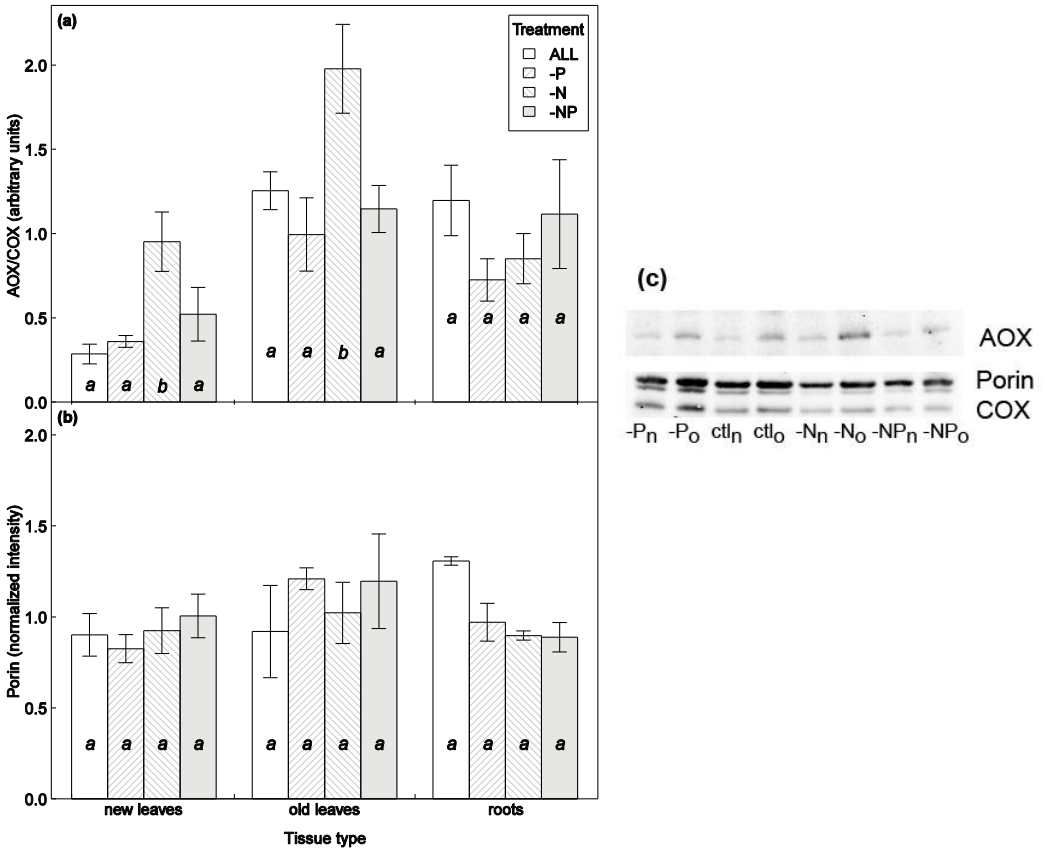

Fig 5.5. Western blot response: (a) AOX/COX, (b) Porin, (c) sample blot for leaf tissue.

Values for AOX, COX, and Porin were normalized to the mean intensity for each blot in order to minimize effects of interblot variation. Subscripts in panel (c) indicate old leaves (o) or new leaves (n). Tissue samples were collected 14 weeks after treatments started.

Although no differences in electron partitioning by treatment were found in the leaves, the Western blot assays indicated that the –N leaves had twice as much AOX relative to COX compared to the other treatments ($P = 0.0002$, Fig 5.5a). In addition, older leaves had nearly 3-fold higher AOX/COX signal ratios than new leaves ($P < 10^{-6}$, Fig 5.5a). No difference in AOX/COX was found in root tissue ($P > 0.4$). Porin levels, which are considered to be an indicator of mitochondrial protein levels (Noguchi *et al.*, 2005), did not differ by tissue ($P > 0.9$; Fig 5.5b).

5.4. DISCUSSION

In the previous chapter I found evidence that natural variations in soil mineral status correlated with plant respiration and respiratory partitioning. Respiration rates correlated most strongly with foliar N concentrations, whereas respiratory electron partitioning was more strongly related to the leaf N/P ratio. Here, by manipulating N and P levels in a greenhouse manipulation study, I tested whether a causative relationship could be established.

5.4.1. Plant phenotype corresponded with anticipated treatment effects

The plants in this experiment showed classical symptoms of selective nutrient deficiency in terms of color changes and total growth (Epstein & Bloom, 2005). Changes in DMC and SLA (Fig 5.1) also followed the generally understood patterns of increased DMC and reduced SLA in nutrient-deprived plants (Hodgson *et al.*, 2011). SLA, however, can also increase in response to poor illumination (Hodgson *et al.*, 2011). *Grisilenia* leaves, for example, that grow on exposed upper limbs have lower SLA than those growing in shaded lower limbs of the same tree (personal observation). In the fertilized controls, the difference in SLA between the pre-existing leaves and new growth (Fig 5.1c) therefore suggests that the newer leaves had developed in the greenhouse under lower illumination relative to the older leaves, which had developed in an outdoor lot. The relatively low illumination in the greenhouse may explain the lack of increased electron partitioning through AP, as will be discussed below.

Direct measures of leaf nutrient status further confirm the presence of nutrient deficiency and its absence in the control treatment: the reduced P and N concentrations in the pre-existing leaves of the –N and –P treated plants indicate that leaf N and P had been mobilized from old to new leaves when it hadn't been supplied in the nutrient media (Fig 5.2). Evidence for the absence of nutrient-deficiency in the control comes from the high root concentrations of supplied nutrients relative to the leaves, which suggests that nutrients had been supplied in excess of the plants' ability to consume them. The possibility that higher root concentrations were merely a side-effect of root DMC relative to leaves can also be ruled out since root nutrient concentrations of N or P were similar to leaf concentrations when the mineral was absent. Leaf levels of N in the fully-fertilized controls were only slightly higher than those measured at the Franz Josef chronosequence, while P and N/P ratios were similar to those found in the chronosequence (Chapter 4, Fig 4.2). Importantly, the difference in N/P ratio between the

–N and –NP treatments (Fig 5.2) provides the opportunity to test whether, as posited in the previous chapter, N/P rather than absolute N was more important with regard to respiratory electron partitioning.

5.4.2. Deficiency affected uptake and translocation of other minerals

Incidentally, I observed that plants appeared to reduce transport of available nutrients from roots to leaves when a different nutrient was absent. Thus, for example, while roots appeared to have taken up similar amounts of N regardless of whether P was present or absent in the nutrient medium, leaf N concentrations were reduced in the face of P-deficiency (Fig 5.2a). Unlike the response of *Griselinia*, Gonzalez-Meler *et al.* (2001) found that leaf N increased in P-deficient tobacco leaves, and did not differ from controls in *P. vulgaris* and *G sepium*. The response observed here in *Griselinia*, may also differ from Aerts and Chapin (2000), who reported that plants reduced the uptake rate of other minerals when stressed by a particular nutrient. Root status in the present study suggests that translocation, not uptake had been reduced, though it's possible that both processes had been limited. A second observation in the present study is the increase in root N status in P-deficient roots (Fig 5.2a). Gniazdowska *et al.* (1999) reported similar results in P-deficient *Phaseolus vulgaris* roots. Nitrate reductase activity had been severely suppressed in the P-deficient roots and they therefore suggested that the accumulation was due to a curtailed ability to reduce the nitrates.

Another contrast between root uptake and leaf concentrations can be seen by plotting respiration against tissue nitrogen concentration (Appendix A5.1 Fig S5.4): in leaves there was a relatively continuous distribution of leaf N concentrations and consequent respiration rates. In roots, however, N concentration was strongly bimodal, as was *R* (Appendix A5.1 Fig S5.4). Regardless, the strong relationship between *R* and leaf-N (irrespective of nutrient media N content) was confirmed here and is thus consistent with the chronosequence observations (Chapter 4) and published meta-analyses (Reich *et al.*, 2008). A closer look at the root data, however, suggests that leaf P played a role in respiration too, since R was lower in the –P roots even though N concentrations were actually higher than in the control roots (Fig 5.2a, Fig 5.4b, and put together Appendix A5.1 Fig S5.4c).

5.4.3. Nutrient deficiency suppressed photosynthesis more strongly than respiration

Deficiency of either N or P strongly suppressed photosynthetic capacity in leaves, reducing A_{sat} by 50% or more relative to the controls. In contrast, nutrient-deficiency

suppressed respiration by 0 – 25% (Fig 5.4 and Appendix A5.1 Fig S5.2). The preservation of respiratory machinery was also apparent in the fact that the abundance of the mitochondrial protein marker, porin did not differ by treatment (Fig 5.5b). By contrast, the leaf chlorosis observed in N-deficient leaves indicated a breakdown of the photosynthetic machinery. This result confirms published observations of decreased *A*/*R* at the Franz Josef chronosequence (Turnbull *et al.*, 2005, Whitehead *et al.*, 2005) and demonstrates one way that nutrient deficiency can alter a plant's ability to sequester carbon. The relative inflexibility of respiration relative to photosynthesis stands to reason since respiration is needed to maintain metabolic processes regardless of new input. The lack of response in the old leaves is difficult to explain, since it seems to imply that the new leaves in the control treatment acquired greater capacity to respire, rather than nutrient-deficient leaves having lost capacity.

5.4.4. Leaf AOX/COX but not electron partitioning responded to low N/P

Finally, despite the many symptoms of nutrient deficiency in the nutrient-deprived plants, including differences in *R*, no sign of change in electron partitioning was detected in leaves. This lack of detection was not due to biological variability or poor precision of the measurements. In fact, the analysis of the treatments was able to detect a 2% change in apparent electron partitioning between the new leaves and old leaves, yet not even such a small change was detected between treatments. Thus, while the 2% change detected between old and new leaves may not represent a biologically significant change, it does provide evidence for the lack of effect in leaves in the case of nutrient deficiency. In the only published study of *in vivo* electron partitioning due to nutrient deficiency, Gonzalez-Meler (2001) reported species-dependent responses: *Phaseolus vulgaris* and *Gliricidia sepium* increased partitioning through the AP in response to P-deficiency whereas *Nicotiana tabacum* did not. All three, however, had been grown from seed rather than from cuttings and had developed under higher illumination than in the current study.

Despite lack of detectable change of electron partitioning in response to nutrient deficiency, leaf AOX/COX protein ratios did increased markedly under the –N treatment in both new and old leaves, but not in the other treatments. This change is consistent in principle with my hypothesis that AOX was upregulated in response to low N/P rather than simply low N (see Fig 5.2). This finding is in agreement with other studies of N deficiency (Noguchi & Terashima, 2006, Sieger *et al.*, 2005, Watanabe *et al.*, 2010), however, the lack of increase in response to P-deficiency is in contrast with previous

reports in which AOX concentration increased in P-deficient tissue (Gonzalez-Meler *et al.*, 2001, Juszczuk *et al.*, 2001b, Sieger *et al.*, 2005). Not all species examined by Gonzalez-Meler *et al.* (2001), however, increased AOX concentrations in response to P-deficiency, thus it would appear that this study confirms the variability of response across species.

The lack of change in electron partitioning, despite an increase in AOX/COX, suggests that illumination may be an important component of AOX activation. As mentioned previously, physical attributes of the older leaves indicated that they had developed under a higher illumination regime than the greenhouse-developed leaves. This may also explain why the older leaves had higher AOX/COX than did the new leaves: the higher light environment under which the older leaves had developed may have "primed" them to produce more AOX. This hypothesis would be in agreement with Noguchi *et al*. (2005), who found higher AOX levels in plants grown under high light conditions and, further, that under low light conditions the AOX proteins were in the inactive dimerized form. Searle *et al*. (2011b) also found that discrimination increased with illumination under field conditions in a study of tussock grasses in New Zealand. Thus, in the present study, even though the protein is more abundant (Fig 5.5a), it did not participate in active respiration, perhaps being kept in reserve to allow flexibility when conditions (light) change. It may even be that the very small increase in respiratory electron partitioning detected in the older leaves reflects this increased, though largely inactivated, enzyme pool. It should be noted, however, that not all studies support the hypothesis that AOX is inactive in low light. For example Florez-Sarassa found that partitioning remained constant in cucumber (*Cucumis sativus*) and *Arabidopsis thaliana* leaves grown in high or low light even though respiration increased with light levels (Florez-Sarasa *et al.*, 2011, Florez-Sarasa *et al.*, 2009). Nevertheless, this finding is not universal. For example, in a comparison of sun and shade species Noguchi *et al*. (2001) that electron partitioning in the sun species *Spinacea oleracea* and *Phaseolus vulgaris* increased with illumination whereas AP activity was near zero and did not respond to illumination in the shade species *Alocasia odora*.

5.4.5. Root CP but not AP activity declined in response to nutrient deficiency

Root measurements were considerably more variable than leaf measurements (Fig 5.4c) and also more difficult to interpret due to uncertainty in the actual endpoints. The discrimination values for control and –P roots at 14 weeks were 3‰ lower than the N-

deficient roots (Appendix A5.1 Fig S5.3a) but when endpoints were measured 8 weeks later endpoints for control roots were 2-3‰ lower than for –N roots (Table 5.1). Diffusion limitation in roots provides the most likely explanation for the increased variability as well as the differences in endpoints. Unlike leaves that have internal airspaces, O_2 in roots must diffuse entirely through liquid to the sites of respiration. Since diffusion through liquids is relatively slow, O_2 is not replaced as quickly as it is removed by respiration. The resulting O_2 gradient, which increases with tissue thickness and/or respiration rate, artificially reduces measured discrimination values (Angert & Luz, 2001, Miller *et al.*, 2011). Thus, unlike in leaves, random variability in root thickness will increase the variability of measured *D*, and systematic changes in root thickness will cause systematic differences in *D*. Informal analysis of photographs from a single batch of –NP and control roots suggests that the –NP roots were thinner than the control roots (1.4 *vs* 1.7 mm) though the difference was not statistically significant. In addition to possible differences in diameter, the control roots also respired at twice the rate of –NP roots (Fig 5.4, Table 5.1) and this too may have contributed to lower measured discrimination values (Miller *et al.*, 2011). As outlined in the results section, and in light of the previous discussion, the data collected at 14 weeks, though showing clearly differences in respiratory O_2 discrimination (Appendix A5.1, Fig S5.3a), cannot be interpreted with confidence.

Nevertheless, partitioning computed for roots measured at the same time as both endpoints (22 weeks) indicates that CP activity was strongly suppressed in –NP roots while AP activity remained unchanged relative to the nutrient-sufficient controls (Table 5.1). Gonzalez-Meler *et al.* (2001), also found that reductions in CP activity were responsible for reductions in total respiration in leaves of two of the three species they examined. This reduction is consistent with the hypothesis that either N-deficiency or P-deficiency would limit the cytochrome pathway more than the alternative oxidase pathway.

5.4.6. How leaf response could be seen as similar to the root response

The results in roots may also explain why partitioning did not change in leaves. AP activity was already low, and in fact, due to uncertainty in the COX endpoint, it may have been nearer to zero than indicated in Fig 5.4c. If leaves responded similarly to roots – and similarly to *Nicotiana tabaccum* (Gonzalez-Meler *et al.*, 2001) – then the reduction in R was due entirely to reduced CP activity, with no increase in AP activity. But since AP activity was already near zero, respiratory electron partitioning was not affected.

Regardless, it would appear that a response in *Griselinia* to nutrient deficiency is to curtail ATP production and, consequently, growth. Recent studies of growth and development in *Arabidopsis thaliana* and *Nicotiana sylvestris* also found that CP activity scaled with growth rate while AP activity remained constant (Florez-Sarasa *et al.*, 2007, Priault *et al.*, 2007). One can also conclude that if there was an increase in oxidative stress due to the nutrient stress, it did not result in increase AP activity under my test conditions.

5.5. SUMMARY

The greenhouse study appears to have confirmed some of the hypotheses formed from the observational field study along the Franz Josef chronosequence. Respiration in the nutrient-manipulated plants clearly responded to foliar N levels and increased AOX enzyme concentrations were found in the treatment with the lowest N/P ratio. On the other hand, evidence from roots suggests that absolute concentration was the main driver of changes in electron partitioning, since N/P was the same in both –NP and the controls. Roots had not been tested in the field study because of the difficulty in extracting them from a mixed stand of trees. Nevertheless, as demonstrated here, they are an important component of plant stress responses. In *Griselinia*, it appears, the response to nutrient deficiency appears to be to slow down metabolic activity, producing less ATP and growing less. The fact that AOX did not "pick up the slack" suggests either tight regulation or a response to the low energy environment of the greenhouse.

6. Respiratory flexibility and efficiency are affected by simulated global change in Arctic plants

6.1. INTRODUCTION

The plant respiratory electron transport chain contains two pathways that differ in size and efficiency: the energy efficient cytochrome *c* oxidase pathway (CP), which is ten times larger, on a molecular weight basis, than the energy-wasteful alternative oxidase pathway (AP) (Noguchi & Terashima, 2006). If energy and nutrient availability are not equally abundant, a plant could potentially optimize growth by utilizing the pathway that conserves the less abundant resource. For example, under low-nitrogen (N) conditions it might be beneficial to increase production of the smaller AP proteins, in order to conserve scarce N at the expensive of the relatively abundant energy source. Noguchi & Terashima (2006) found evidence of such a response: spinach leaves grown in low-N rooting media had higher alternative oxidase (AOX) levels than plants grown in high-N. The AP can also help maintain carbon balance by consuming excess carbohydrates that would otherwise accumulate due to nutrient deficiencies (Sieger *et al.*, 2005). Increased AP activity might therefore be associated with the increased leaf carbohydrate status that is driving the AP activity under this hypothesis. A third hypothesis suggests a protective role for the alternative pathway: leaves receiving energy in excess of their metabolic energy requirements may engage the AP to safely remove energetic molecules that would otherwise contribute to the production of membrane-damaging reactive oxygen species (Millenaar & Lambers, 2003, Zhang *et al.*, 2011).

All three hypotheses suggest that an imbalance between received energy and metabolic needs is part of the AP/CP regulatory mechanism. Thus if energy is in excess, as in the previous examples, AP is up-regulated. If energy is limiting, AP should be down-regulated. For example, significantly less AP activity was detected in shade species or in species grown under low illumination (Noguchi *et al.*, 2001), whereas AOX was up-regulated when chloroplasts received too much energy (Yoshida *et al.*, 2007). In addition to the N-deficiency example mentioned above, increased AP activity or abundance has been reported in response to phosphorus (P) deficiency (Gonzalez-Meler *et al.*, 2001, Juszczuk *et al.*, 2001b) as well as to low temperatures, which could impede energy balance by lowering metabolic rates (Armstrong *et al.*, 2008, Fiorani, Umbach & Siedow, 2005). To place these results in a global context, laboratory studies have also found that engagement of the alternative pathway can reduce plant carbon use efficiency (Sieger *et*

al., 2005), thus implying a reduced ability to sequester atmospheric carbon. The hypothesized effects of environment on electron partitioning have not, however, been investigated in plants growing under field conditions in long-term environmental treatments and thus, considerable uncertainty remains as to what extent these studies, conducted under carefully-constrained laboratory conditions, can be generalized to species growing under natural conditions and exposed to long-term resource limitations.

In the Arctic tundra, interaction between plant mineral nutrition and plant metabolism may take on further significance, as global climate change may induce the release of stored carbon to the atmosphere. Arctic and boreal peatlands contain up to one third of terrestrial carbon stocks (Gorham, 1991, Turunen *et al.*, 2002), much of it locked in the permafrost. As permafrost melts, CO_2 is released from the organic soils and mineral nutrients are released into the soil solution. Whether the arctic tundra becomes a source or a sink of atmospheric CO_2, however, depends upon the extent to which plant growth increases in response to changing temperature, nutrient availability, and local pCO_2 (Hobbie *et al.*, 2002). Several field manipulations near the long-term ecological research field station at Toolik, Alaska (Arctic LTER) have been maintained for the past 20 years in order to help better predict the effects of nutrients, light and warming on Arctic tundra ecology (Bret-Harte *et al.*, 2001, Shaver & Chapin, 1980, Shaver & Chapin, 1995). These experiments have found that fertilization dramatically alters ecosystem productivity and community composition, but that the effects varied by light availability. In unshaded plots *Betula nana* abundance and canopy height increase to the extent that it ultimately overshadowed the other species in the plots (Bret-Harte *et al.*, 2001, Chapin *et al.*, 1995). Shading suppressed the growth of *Betula*, however, resulting in *Rubus chamaemorus* dominating those plots. Community-level responses as well as leaf trait- and leaf-level photosynthesis effects have been reported (Bret-Harte *et al.*, 2001, Chapin & Shaver, 1996, Chapin *et al.*, 1995) but I am unaware of any investigations of leaf-level respiration or respiratory electron partitioning in this Arctic system.

Here I describe results of the application of a field-portable methodology (Kornfeld *et al.*, 2012a, and Chapter 3) to investigate respiratory electron partitioning in three species that responded differently to experimental manipulations at the Arctic LTER site. I also measured leaf traits, nutrient and carbohydrate status, as well as alternative oxidase (AOX) and cytochrome *c* oxidase (COX) protein concentrations to determine to what extent measured changes in respiration and electron partitioning correlated with

these attributes. These data were used to investigate two primary hypotheses: (1) Relative AP activity in the long-term field nutrient and environmental manipulation would decrease in response to fertilization – which would relieve energy imbalance by increasing metabolic consumption – or by shade, which would relieve energy imbalance on the input side. (2) Relative protein abundance of AOX would decrease in response to fertilization, as had been seen in N- and P-deficient leaves in laboratory studies (Gonzalez-Meler *et al.*, 2001, Juszczuk *et al.*, 2001b, Noguchi & Terashima, 2006).

6.2. MATERIALS & METHODS

6.2.1. Site description

The field site is part of a continuing long-term field-manipulation of upland tussock tundra at the Arctic LTER (68º38' N, 149º34'W, elevation 760 m). Four replicate blocks, established in 1989, are each divided into several 5 × 20 m^2 randomly-assigned treatment plots separated by 2 m walkways (Boelman *et al.*, 2005, Bret-Harte *et al.*, 2001). Fertilized plots receive 10 g m^{-2} yr^{-1} nitrogen as slow-release granular NH_4NO_3 and 5 g m^{-2} yr^{-1} phosphorus as granular P_2O_5 each spring immediately following snow melt. The fertilizer input represents four times the annual N requirement for aboveground vascular production and 20 times the annual P requirement in this site (Shaver & Chapin III, 1991). Temperature has been raised an average of 4 ºC in greenhouse plots by covering 2.46 × 4.92 m areas with transparent 0.15 mm (6 mil) plastic sheeting (Cloud 9 commercial greenhouse plastic; Monsanto, Incorporated, St. Louis, Missouri) stretched over a wooden frame with a gable roof 65 cm above ground at the sides and 130 cm at the center. The heights of the greenhouses have been gradually increased over time to 1.5 – 2 m to accommodate increased plant canopy height (Boelman *et al.*, 2005). Similar structures were covered with shade cloth to reduce photosynthetically active radiation (PAR) by 50%. Two enclosures were constructed on each shade house or greenhouse plot. The soils under the downhill enclosures were fertilized with N and P, whereas unfertilized subplot was situated uphill to avoid runoff contamination. Coverings for both structures are removed during the winter and replaced at the beginning of each growing season. I sampled six treatments representing a factorial assignment of nutrient addition to open, shade, and temperature manipulations: control plots (ctl), nitrogen and phosphorus addition plots (NP), shade houses (SH), greenhouses (GH) and shade house/greenhouses with NP addition (SHNP, GHNP).

Effects of treatment on community composition in all treatments except SHNP were reported by Chapin & Shaver (1995) for a similar experiment at the Arctic LTER. I report here previously unpublished percent cover measurements made by Gough (2001, 2009). Percent cover was estimated using 1 m^2 quadrats, subdivided into 20 cm × 20 cm subquadrats, placed in 5 – 8 locations in each plot (Gough & Hobbie, 2003). Three species were selected for this study because they dominated the canopy in one or more of the treatment plots an: *Eriophorum vaginatum*, *Betula nana*, and *Rubus chamaemorus*. Nomenclature follows Hultén (1968).

6.2.2. Sampling procedure for respiratory incubations

All three species were sampled in each treatment in each block, yielding up to four replicates per treatment. *Eriophorum*, however, was not available in sufficient quantity for the respiratory incubations in SHNP, nor in all but one GHNP plot. Respiratory incubations were conducted to determine both total respiration and electron partitioning based on the ^{18}O isotope discrimination methods described in Kornfeld et al. (2012a, and Chapter 2). Shoots harvested from individual plots were placed on ice in a cooler and carried to a field laboratory a short distance away. Leaf tissue or, in the case of *Betula*, whole shoots were sliced into sections no larger than 1 cm × 7 cm and incubated in sealed septum-capped 12 mL vials ((Labco, High Wycombe, UK; product #738W) in the dark. A half-pellet of KOH in a protective holder was also placed in the vial in order to remove respired CO_2. After 2 h, air was transferred under positive pressure from the incubation vial to a syringe by injecting water. The air in the syringe was immediately injected into a pre-evacuated 3.7 mL storage container (Labco product #778W) for later analysis.

Tissue was divided among six incubation vials in the proportions of 1:2:3:4:5:6 by fresh mass (FM), thus providing a six-fold range of O_2 consumption at the end of the 2 h incubation period. Sample size was determined based on previously measured respiration rates, such that the tissue in the 6-portion vial would consume approximately 50% of the O_2 in the headspace in 2 h. Total sample size was approximately 2.5 g FM for *Betula* and *Rubus*, and 2.1 g FM for *Eriophorum*. In addition to the samples, additional "blank" incubation vials were prepared alongside the respiratory incubation vials. Air blanks were created by flushing air into open incubation vials using a needleless syringe; N_2 blanks were created by first rinsing an incubation vial with O_2-free N_2 and then flushing for at least five minutes through a hypodermic needled attached by plastic tubing to a needle valve on the gas tank. A second hypodermic needle, acting as a vent, was left in for 1-3

seconds after removing the flush needle in order to equalize pressure with the atmosphere without introducing contamination. The contents of the blank incubation vials were transferred to storage vials as above. Two additional types of blanks were prepared in order to measure contamination due to leakage during storage. A set of storage vials was directly flushed with O_2-free N_2; additional evacuated vials were set aside to be filled with O_2-free He just before measurement.

To measure "end-point" discrimination values for the alternative and cytochrome pathways, leaf sections were soaked in solutions of either KCN or salicylhydroxamic acid (SHAM) respectively, buffered with 2 mM $CaCl_2$ and 20 mM 4-(2-hydroxyethyl)-1-piperazineethanesulfonic acid (HEPES) pH 7.2. Appropriate inhibitor concentrations were determined by varying the concentration of one inhibitor in the presence of the other and measuring O_2 uptake using a liquid-phase Clark-type electrode (Digital Oxygen System Model 10, Rank Brothers, Cambridge, England). Based on these experiments *Betula* and *Rubus* were inhibited with 20 mM KCN and/or 30 mM SHAM while *Eriophorum* was inhibited with 100 mM KCN and/or 30 mM SHAM. Leaves taken from a fertilized plot were immersed for 1 h in buffer containing one, both, or neither inhibitor, after which they were allowed to dry for an hour before incubation. Measured discrimination values in the buffer-treated leaves did not differ from untreated leaves. Residual respiration in doubly-inhibited tissue, based on in-vial respiration values, was 11% for *Betula*, 13% for *Rubus*, and 26% for *Eriophorum*. Nevertheless, only *Betula* results were considered reliable and used for computing τ_a here. Discrimination values in *Rubus* decreased instead of increasing upon KCN treatment, whereas a narrow endpoint range for *Eriophorum* (3.5‰) combined with the large residual respiration cast doubt on those endpoints (Appendix A6.1 Table S6.1).

6.2.3. Discrimination, electron partitioning and respiration computations

Storage containers were shipped to Christchurch, New Zealand, and stored at laboratory temperature (20 ºC) for 10 months before measurement. Isotopic composition of the respiratory air samples was measured in a Thermo Electron Delta V Plus isotope ratio mass spectrometer (Thermo Electron, Bremen, Germany) as described in Kornfeld *et al*. (2012b).

Measurements were corrected for contamination using the O_2-free vials ("blanks") as described in Chapter 2, but because of the long storage time at 20 ºC, significant

curvature remained in the data even after correction. Discrimination values, *D*, were therefore computed using the quadratic regression (3.7):

$$1000 \times \ln\left(\frac{^{34}R_s}{^{34}R_{s,0}}\right) = \beta_2\left(\ln\ f_s^*\right)^2 - D\ln\ f_s^*,$$

Respiration, discrimination, electron partitioning, and activities of the AP and CP were determined as described previously (Section 4.2.3)

Incubation temperatures varied from 20 – 26 ºC across the three-week measurement period. Respiration rates adjusted to 20 ºC, R_{20}, were computed using Q_{10} values measured during the same experimental period or the following year, according to the formula (Atkin *et al.*, 2005a):

$$R_{20} = RQ_{10}^{-(T-20°C)/10}.$$

6.2.4. Leaf tissue analysis

Leaf area was measured on representative samples using a flatbed scanner and the WinRhizo program (Regent Instruments, Quebec, CA). After the area was measured, leaf samples were dried in an oven at 60°C for a minimum of two days before determining mass. The tissue was then sent to Columbia University (New York, New York, USA) for nitrogen and phosphorus determination. There, the samples were ground, weighed, and packaged for elemental analysis to determine [CHN] (2400 Series II, Perkin-Elmer, Boston, MA, USA). Remaining ground leaf samples were bulked by replicate block and sent to the North Carolina State University Environmental and Agricultural Testing Service (Raleigh, NC, USA) to determine total phosphorus concentration.

A second set of samples were frozen to –80 ºC and then lyophilized for at least 24 h. Samples were shipped to the University of Canterbury, Christchurch, New Zealand where they were ground to a fine powder in a ball mill and then stored at –80 ºC until assayed for alternative oxidase (AOX), cytochrome *c* oxidase (COX), and for carbohydrates.

Leaf carbohydrate content was assayed colorimetrically according to the method of Tissue & Wright (1995) as described in Section 5.2.5. AOX and COX concentrations were determined semi-quantitatively using a Western blot protocol as described in Section 4.2.4

6.2.5. Statistical analysis

Statistical analyses were computed using R 1.14 (R Development Core Team, 2011). Multiple samples from within each block were averaged prior to computations to avoid pseudoreplication and to avoid distortions due to oversampling in some plots. Each treatment set therefore consisted of up to four replicates. Treatment effects were tested for significance using ANOVA and the corresponding linear regression models. Explanatory variables included Species and either Treatment (ctl, NP, GH, GHNP, SH, SHNP), or the main-effects variables: Nutrient (ctl, NP) and Environment (shade, open, or greenhouse). Because of the missing SH data, ANOVA was sensitive the order of variables and, therefore, AIC, an order-independent measure of residual deviances, was used to select the best model out of the 19 valid combinations of Species (S), Nutrient (N), Environment (E) and their interactions. The AIC weight, w_i indicates the probability that any given model is the best of the set, given the data (Burnham & Anderson, 2002, Venables & Ripley, 2002). AIC was primarily used to determine whether-or-not effects were additive. ANOVA tests on the selected model were conducted with variables in the order S, N, E and S, E, N; the larger *P* value of these two analyses is reported here. Species was put in the first position since species differences are expected to take precedence based on biological considerations (Hector *et al.*, 2010). Post-hoc test were computed using Tukey's HSD comparison of all pair-wise combinations, adjusted according to Westfall (Bretz *et al.*, 2011). The pairwise comparisons were also used to generate the "letter groupings" indicating statistically significant groups in the graphs presented here.

Residuals variance was generally not homogenous across species, based on Hartley's test (Hartley, 1950) and the Brown and Forsyth test (Brown & Forsythe, 1974). Residuals in the statistical tests were therefore weighted by $1/var_s$, the within-species residuals variance (Venables & Ripley, 2002). The weighted residuals were tested for normality using the Shapiro-Wilk test (Royston, 1995). Residuals for SLA, R_{20}, and AOX/COX were transformed to normality using the Geary-Hinkley transformation (Hayya *et al.*, 1975). In these cases, transformed data were used to test for significance while untransformed data were used to determine effect sizes. Outlier analysis for the relative cover data was conducted by adding indicator variables representing candidate outliers and then testing for the significance of the indicator variables using linear regression (Weisberg, 2005).

Uncertainty is reported here as mean ± stanadard error (SE). If values did not differ by species, the data was pooled using the ANOVA. Uncertainty in τ_a and the associated AP and CP rates, v_a and v_c, were corrected as described in Section 5.2.6. A graph of discrimination *vs.* respiration confirmed that the variables were not correlated (Appendix A6.2 Fig S6.1).

6.3. RESULTS

The environmental manipulations described here had been maintained for 20 years prior to the start of the present investigation. During that time, community composition and production had responded dramatically to the nutrient, temperature, and illumination treatments. Here I examine to what extent the environmental changes affected total leaf-level respiration as well as respiratory efficiency as represented by the relative activities of the cytochrome and alternative electron transport pathways. To help interpret these findings in terms of leaf nutritional status, I also measured several leaf traits that are considered to be indicators of plant nutrient health or stress: dry matter content (DMC), specific leaf area (SLA), leaf N, P, and N/P, and leaf nonstructural carbohydrate status. Finally, to determine the extent to which changes in electron partitioning could be attributed to changes in enzyme expression, as opposed to enzyme regulation, I assayed leaf material for the respiratory terminal oxidase enzymes AOX and COX.

6.3.1. Community composition

Although 20 years of annual treatments had transpired, the most recent community composition measurements for all six treatments had been conducted 10 years prior (Gough, 2001); subsequent measurements excluded the shade house treatments (Gough, 2009).

Ten years of nutrient addition increased cover of *Betula* from the 14 ± 3% (mean ± SE) of the control plots to 55 ± 2% of the unshaded NP plots (Fig 6.1a). *Rubus* cover in the control plot was 8 ± 3%. Two extreme points in the *Rubus* data were eliminated as outliers ($P < 0.001$ each; Fig 6.1a, crossed circles). Without these outliers, *Rubus* cover of 30 ± 2% in the NP treatment, and 37 ± 6% in SHNP was significantly different from the controls (Fig 6.1a; $P < 0.005$). *Eriophorum*, which at 21 ± 3% cover was the largest component of the control plots, suffered in all treatments except greenhouse control, losing 50 – 90% of its cover relative to the control plot (Fig 6.1a). Only two other species covered more than 10% in any of the treatments: *Ledum palustre* and *Vaccinium vitis-*

idaea. Both species are short-statured woody plants that generally followed the fate of *Eriophorum*. Because of their small size, neither was available in sufficient quantities for the purposes of this study.

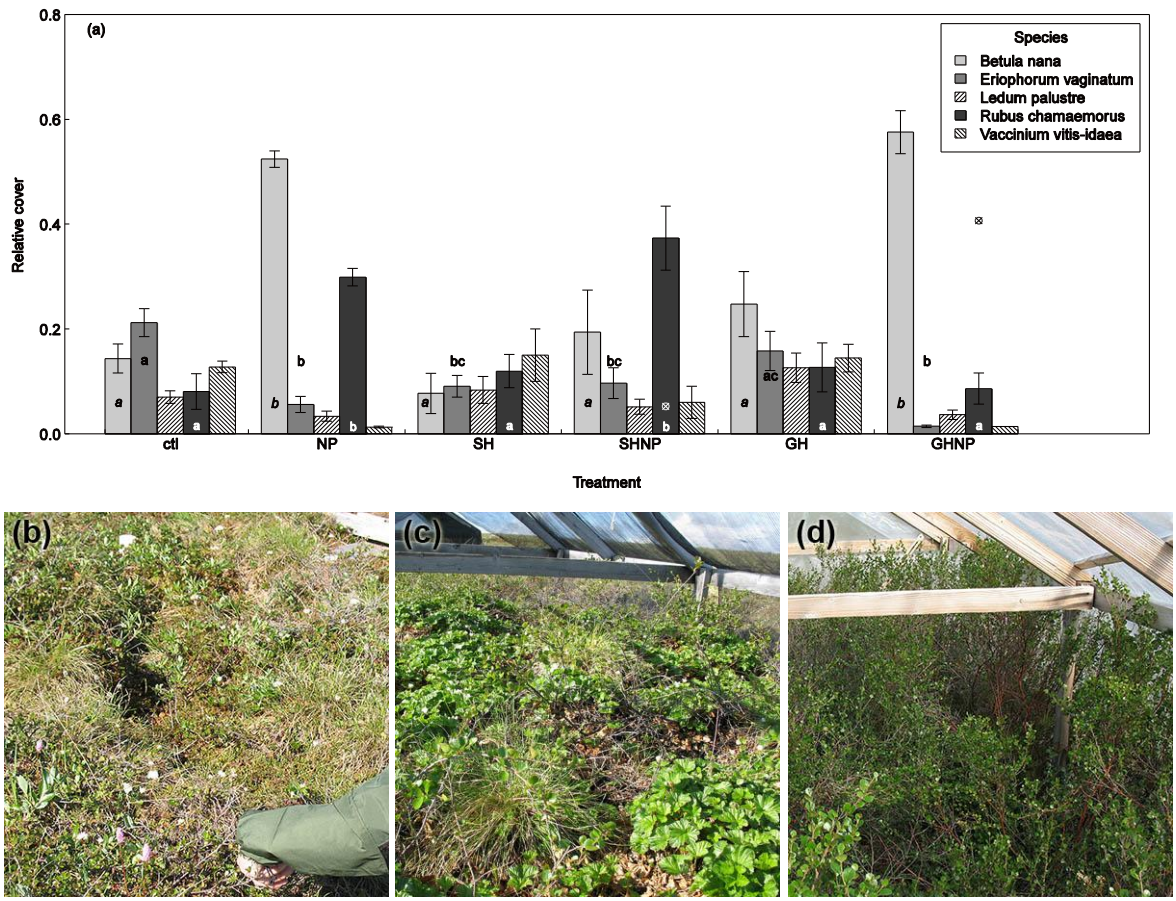

Fig 6.1. Effects of fertilization, light, and temperature modification on Alaskan tundra plant communities after 10 and 20 years.

(a) Relative cover after 10 years. All species with at least 10% cover in any treatment category are shown. Data from (Gough, 2001). (b-d) Representative images of plots after 20 years of treatment: (b) Control (with arm at bottom-right for scale), (c) SHNP, (d) GHNP. Symbols: ctl – control plot; NP – nitrogen and phosphorus fertilizer added annually; SH– shade house (50% reduction in light); SHNP – shade house with annual fertilization; GH– greenhouse (4 ºC warming); GHNP – greenhouse with annual fertilization. Error bars indicate standard error; $n = 4$ blocks each. Each block measurement is the mean of 5 – 8 quadrat assessments. Letters above or inside bars indicate statistically distinct treatment groups within each species at the $P < 0.05$ significance levels. Crossed circles indicate outlier points. Error bars indicate standard error.

The most recent data available at the time of writing was made two years before the present investigation by Gough (2009). Relative to the 10-year data, *Betula* coverage had increase to 73 ± 2% of NP and GHNP ($P < 0.001$; Appendix A6.2 Fig S6.2). Coverage was unchanged for any species in the corresponding control plots as well as for *Eriophorum* and *Rubus* in NP and GHNP ($P > 0.3$). Shade houses were not measured at that time, but *Rubus* cover in SHNP appears to have increased in the 10 years since the previous measurement while *Betula* further declined (Fig 6.1c; L. Gough, *personal communication*). Figures 6.1b–d illustrate the community composition at the time of the current investigation: representative examples of a control, SHNP, and GHNP treatment are shown, each visibly different from the other. Unfertilized GH and SH treatments, not shown, looked similar to the control plots (Fig 6.1b).

6.3.2. Leaf traits

Leaf traits were measured to determine to what extent they correlated with community level treatment effects. I examined the leaf dry matter content (DMC), specific leaf area (SLA), elemental nitrogen and phosphorus levels, and leaf carbohydrates.

The three species examined did not differ in the way DMC or SLA responded to the treatments (no support for species interaction, Table 6.1). There was, however, evidence for interaction between Nutrient and Environment in both treatments due to a lack of response to fertilization in the greenhouse treatments ($P > 0.001$ and $P = 0.048$ respectively; Fig 6.2a–c). Fertilization of uncovered plots lowered the DMC by 9 ± 2% ($P < 0.001$) relative to controls. Shade lowered DMC by 6 ± 2% relative to controls ($P = 0.02$) and these two effects added to a 17 ± 3% reduction in SHNP plots ($P < 0.01$). Leaf DMC in the GH and GHNP plots, on the other hand did not differ from the controls or from each other ($P > 0.4$). Although a similar pattern (though inverted, since DM is the denominator for SLA) can be seen in the response of SLA to treatment conditions (Fig 6.2d–f) only the increase of SLA in SHNP was significantly different from the unshaded treatments ($P < 0.03$) possibly due to the additive effect of shade and nutrients.

Table 6.1. AIC_c comparison of all valid combinations of species (S), nutrient addition (N) and Environment (E) effects.

model	*k*	Δ_i	w_i	*rank*	*model*	*k*	Δ_i	w_i	*rank*
Dry Matter					***TNC***				
N x (S + E)	11	4.95	0.07		S x N + E	9	4.56	0.05	
S + N x E	**9**	**-**	**0.88**	****	S + N x E	9	3.74	0.08	
SLA [a]					**S + N + E**	**7**	**-**	**0.52**	***
S + N x E	**9**	**3.43**	**0.10**		S + E	6	1.46	0.25	*
N x E	**7**	**-**	**0.55**	***	***R_{20}***				
N + E	5	1.68	0.24	*	N x (S + E)	11	2.38	0.10	
N					**S x N + E**	**9**	**0.37**	**0.26**	*
S x (N + E)	13	4.61	0.06		**S + N x E**	**9**	**-**	**0.31**	**
E x (S + N)	13	2.03	0.21	*	**S + N + E**	**7**	**0.47**	**0.25**	*
S x E + N	**11**	**-**	**0.57**	***	S + E	6	3.86	0.05	
S + N + E	7	4.19	0.07		**R_{20} "revised"** [b]				
N w/o Rubus NP					N x (S + E)	11	4.50	0.05	
N x (S + E)	11	1.82	0.19	*	S x N + E	9	2.48	0.14	*
S + N x E	**9**	**-**	**0.48**	**	S + N x E	9	2.11	0.17	*
S + N + E	7	1.83	0.19	*	S + N + E	7	2.58	0.13	*
P					**S_2 x N + E**[c]	**8**	**-**	**0.47**	**
S x N x E	**19**	**-**	**0.98**	*****	***D*** [d]				
Starch					S x E	10	3.69	0.06	
S x N + E	9	3.80	0.06		S + E	6	2.23	0.13	*
S + N + E	7	1.69	0.17	*	S x N	7	3.69	0.06	
S + E	**6**	**-**	**0.40**	**	S + N	5	2.23	0.13	*
S + N	5	3.61	0.07		**S**	**4**	**-**	**0.40**	**
S	4	1.44	0.19	*	null	2	4.11	0.05	
Sugar					***Western AOX/COX***				
S + N + E	**7**	**0.12**	**0.30**	*	S + N + E[e]	6	2.67	0.10	*
S + E	**6**	**-**	**0.31**	**	**S + E**[e]	**5**	**2.41**	**0.12**	*
S + N	5	2.15	0.11	*	N + E[e]	5	0.61	0.29	*
S	4	1.35	0.16	*	**E**[e]	**4**	**-**	**0.39**	**

Higher w_i scores are better; only models with w_i above 0.05 are shown; the best model in each set is highlighted. Columns are: *model* – the candidate linear models: "×" indicates interaction between two terms, "+" indicates additive effects; *k* – the number of parameter estimates in the model, plus one; Δ_i – the difference between AIC_c value for the current model and the lowest-scoring, i.e. best, model; w_i – the Akaike weight, or weight of evidence in support of this model being the best of the group (w_i values sum to 1); *rank* – a simple asterisk display: each asterisk represent approximately 20% of the total weight.

[a] species differences were removed by dividing Eriophorum SLA by 3, masking the actual Species effect.

[b] note that the AIC values are unchanged for the models shown in the first R_{20} analysis; only the weights are changed because of the new, better, model is now the reference point.

[c] S_2 = *Betula* and *Rubus* are collapsed into a single level, leaving two levels: "*B+R"* and *Eriophorum*.

[d] Using the *Betula* whole-shoot assays only.

[e] Species differences are ignored whenever the Species effects are additive, so S + E and E are equivalent models for my analysis, the total support for E by itself is therefore is 0.12 + 0.39 = 0.51. Likewise, the two other models are summed to indicate 0.39 for E + N

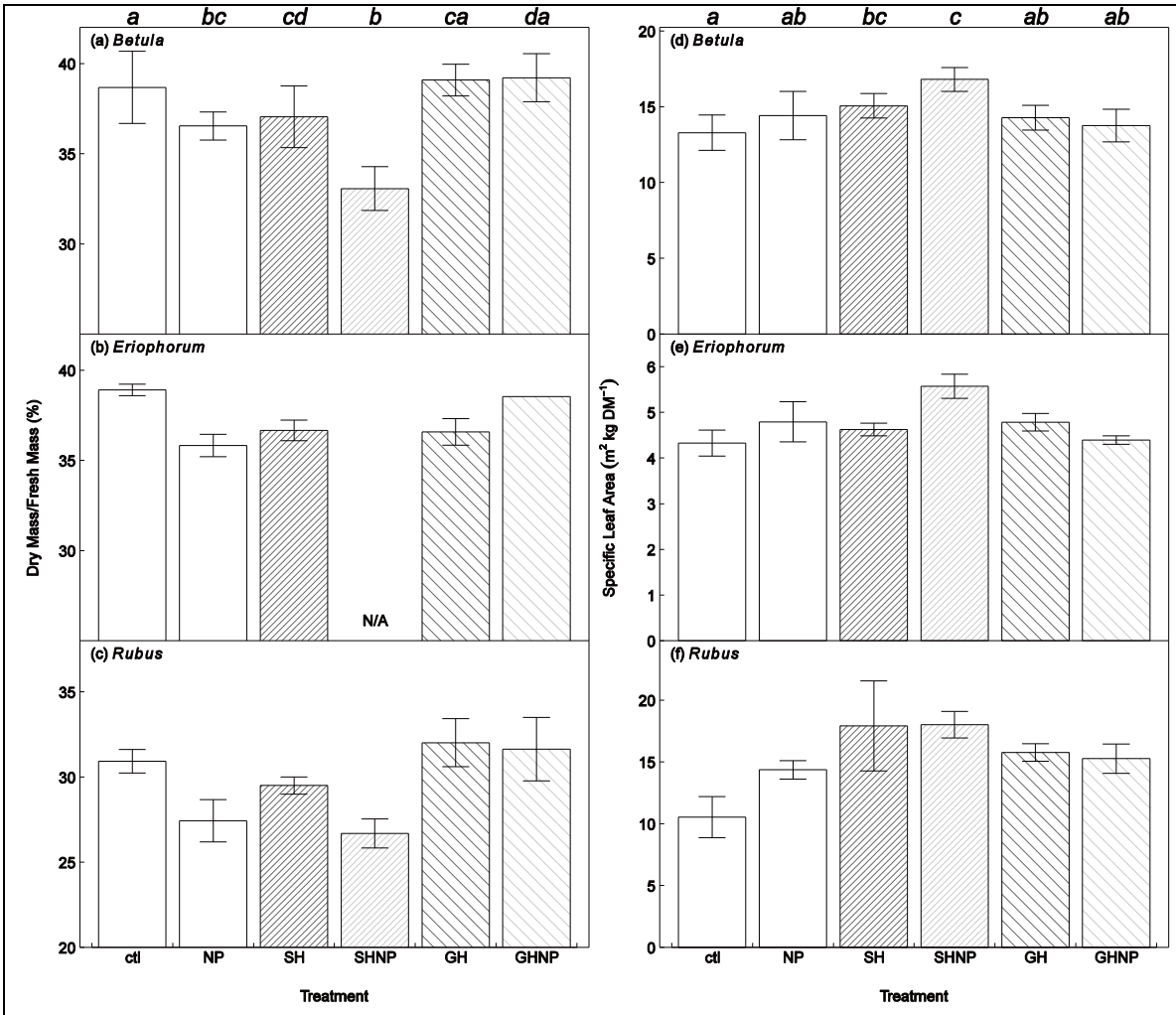

Fig 6.2. Leaf dry matter content (a–c) and specific leaf area (d–f) for the three species examined: (a, d) *Betula*, (b, e) *Eriophorum*, (c, f) *Rubus*.

Letters in the top margin of the graph indicate statistically distinct groups, pooled across all species, at the $P < 0.05$ significance level. No statistically significant interaction with species was detected for either measure. See Fig 6.1 for a key to the treatment codes. Note that the y axis scales differ by species. n =4 except for *Eriophorum* GHNP leaf dry matter, which consists of a single measurement. Error bars indicate standard error.

Table 6.2. Leaf nitrogen and phosphorus content (mg g DM^{-1}) and N/P ratio (g N g P^{-1}).

	ctl	*NP*	*SH*	*SHNP*	*GH*	*GHNP*
Betula						
N	27.8 ± 1.4 (4)	36.4 ± 1.1 (4)*	31 ± 3 (3)	35.6 ± 0.9 (3)†	26.2 ± 1.0 (4)	29.3 ± 1.3 (4)
P	3.0 ± 0.2 (4)	6.1 ± 0.3 (4)*	3.61 (1)	7.0 ± 0.4 (3)*	2.77 ± 0.20 (5)	4.3 ± 0.3 (4)*
N/P	9.4 ± 0.6 (4)	6.01 ± 0.19 (4)*	9.89 (1)	5.1 ± 0.3 (3)*	9.5 ± 0.9 (4)	6.9 ± 0.3 (4)*
Eriophorum						
N	24.6 ± 1.7 (4)	29.5 ± 1.2 (3)*		29.0 ± 0.7 (4)	22.8 ± 0.6 (4)	24.4 ± 1.6 (2)
P	2.69 ± 0.06 (4)	4.0 ± 0.3 (4)*	2.6 ± 0.2 (4)	4.7 ± 0.4 (3)*	2.85 ± 0.08 (4)	4.5 ± 0.4 (2)*
N/P	9.2 ± 0.7 (4)	7.7 ± 1.1 (3)†		6.4 ± 0.4 (3)	8.00 ± 0.13 (4)	5.39 (1)†
Rubus						
N	29.7 ± 1.6 (4)	29.0 ± 0.3 (4)	29 ± 2 (4)	37.6 ± 0.7 (4)*	31.1 ± 1.5 (4)	34 ± 2 (3)
P	3.3 ± 0.3 (4)	6.04 ± 0.05 (4)*	4.67 (1)	6.74 (1)*	3.1 ± 0.2 (4)	3.25 ± 0.18 (3)
N/P	9.3 ± 0.8 (4)	4.80 ± 0.04 (4)*	7.21 (1)	5.38 (1)	10.1 ± 0.4 (4)	10.0 ± 0.6 (2)

Numbers are expressed as mean ± SE (*n*) for *n* blocks. Multiple samples from within each block were averaged prior to these computations to avoid pseudoreplication; some P assays were combined from several plots due to insufficient material.

* significantly different from the corresponding unfertilized treatment in the same species ($P < 0.05$).

† significantly different from the unfertilized treatment in grouped analysis only ($P < 0.05$).

Leaf nitrogen effects were similar across species except for *Rubus* in the NP treatment (best model included species interaciton: S × N + E, when *Rubus* NP is included, but not when *Rubus* NP is excluded from analysis, Table 6.1). Leaf N increased by 27 ± 5% in *Betula* and *Eriophorum* in response to fertilization in the open and the shade (Table 6.2) but not in response to GH or GHNP ($P > 0.2$). Leaf phosphorus increased 43 – 133% across all species with the added soil P, with one exception, but with strong interaction by Species, Nutrient, and Environment (best model: S × N × E, Table 6.1). Only *Rubus* GHNP did not differ from the controls (Table 6.2; $P = 0.8$). Greenhouse warming alone did not affect leaf P levels in any species ($P > 0.5$ in each species). Only one sample was available for SH *Betula* and SH *Rubus* leaves, each bulked from two experimental blocks. Nevertheless, both measurements were higher than any of the corresponding leaf P values measured in the control plots, implying that shade house conditions may have increased P-availability for these two species. Leaf N/P is often used as an indicator of nutrient limitation: values below 12 generally indicate nitrogen limitation while values above 14 indicate P limitation (Aerts & Chapin, 2000, Tessier & Raynal, 2003). Leaf N/P was below 10 in all treatments examined in this study (Table 6.2). Adding fertilizer reduced the N/P ratio, due to the larger increase in leaf P.

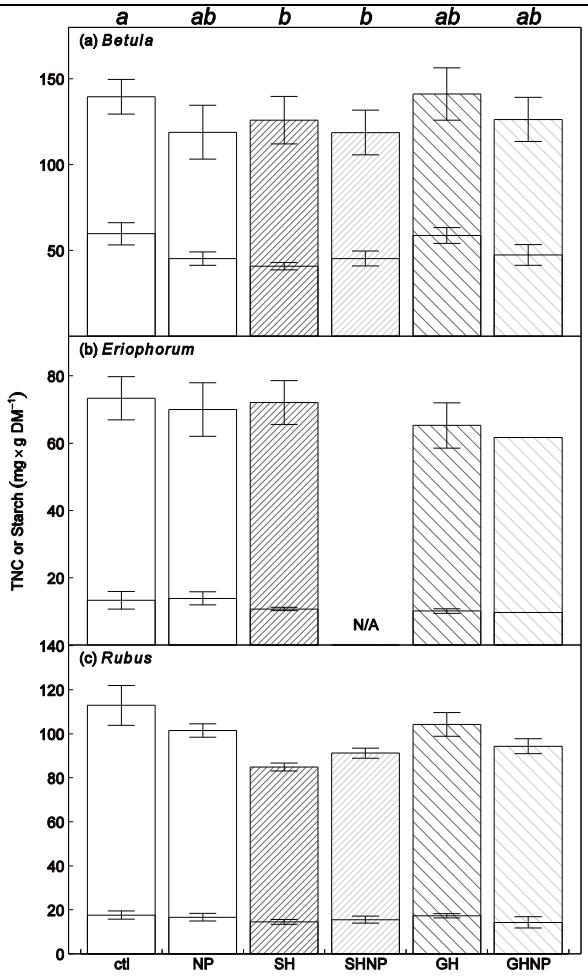

Fig 6.3. Starch, sugars, and total nonstructural carbohydrates (TNC = starch + sugars) for the three species examined: (a) *Betula* , (b) *Eriophorum*, (c) *Rubus*.

The entire bar indicates TNC, the lower segment represents starch content , while the upper segment depicts sugar content. Error bars indicate standard error for starch and TNC respectively. Letters in the top margin of the graph represent statistically distinct groups, pooled across all species, at the $P < 0.05$ significance level. No statistically significant interaction with species was detected for either measure. See Fig 6.1 for a key to the treatment codes. Note that the y axis scales differ by species. n =4 except for *Eriophorum* GHNP leaf, which consists of a single measurement. Error bars indicate standard error.

Leaf carbohydrate response to the treatments did not vary by species (no support for Species interaction, Table 6.1). Leaf starch content in shaded plants was 11 ± 5% lower than in the control plots across all species (Fig 6.3a–c; $P = 0.04$) but fertilization did not affect leaf starch levels ($P > 0.4$ for the Nutrient term). Total sugar concentrations similarly decreased 14 ± 6% in shaded *vs.* open plots ($P = 0.03$) while nutrient effects were not statistically significant ($P = 0.17$). TNC followed the same trends as its component measurements but with increased statistical significance: TNC decreased 13 ±

4% the shade house leaves *vs.* open plots (P = 0.001; Fig 6.3a–c). A 6 ± 3% decrease in TNC in response to nutrient addition was marginally significant (P = 0.06) but is weakly supported by the AIC analysis, which assigned a weight of 52% in support of the full additive model, S + N + E, with the next-best model, S + E excluding N, ranked at only 25% (Table 6.1).

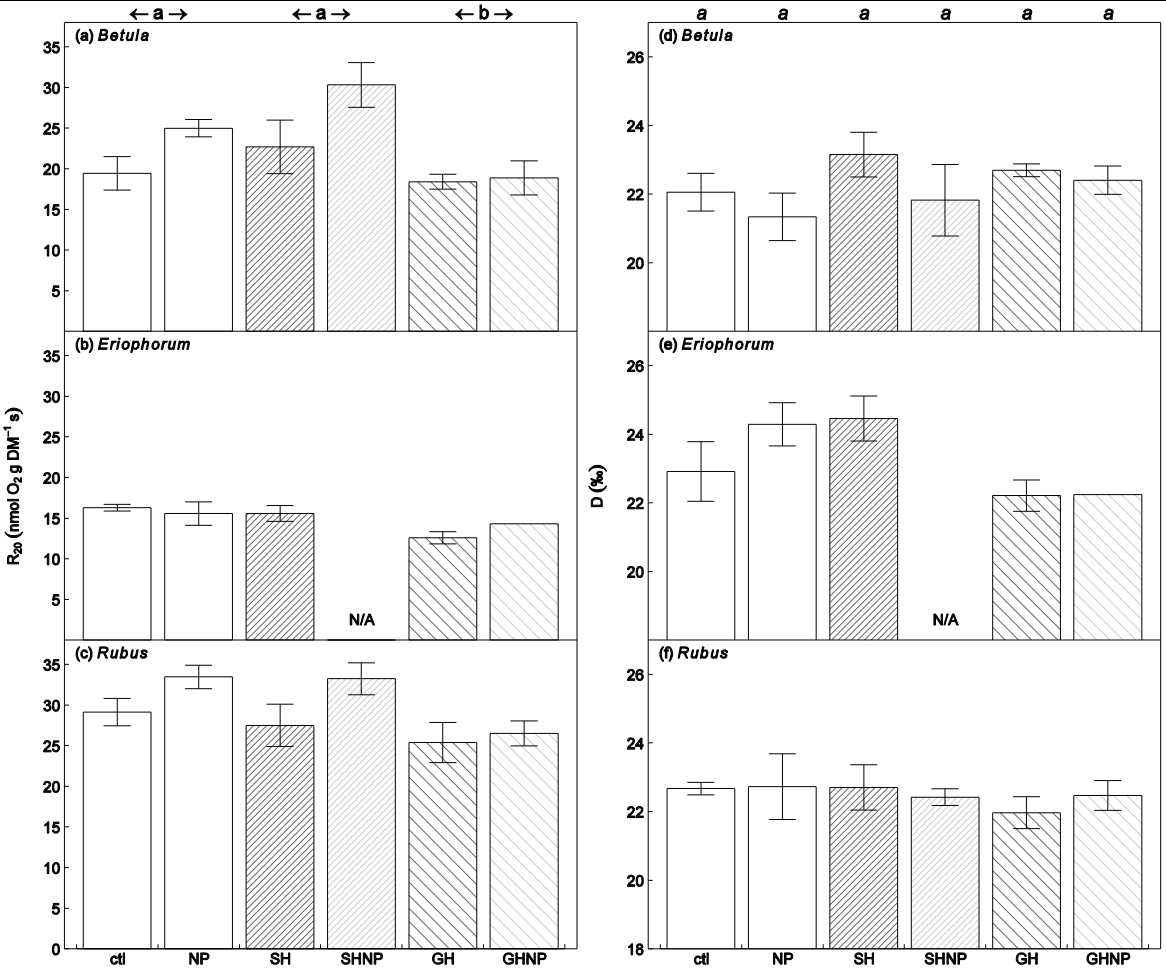

Fig 6.4. Respiration at 20 ºC on a leaf-mass basis, R_{20}, (a –c), and respiratory discrimination against ^{18}O in three species (d–f).

Betula values are for whole-shoot tissue. Letters in the top margin of the respiration graph represent statistically distinct 'Environment' groups at the $P < 0.05$ significance level. An additive increase in R_{20} in response to fertilization was also statistically significant in the pooled data. No statistically significant effects were found in the discrimination results. See Fig 6.1 for a key to the treatment codes. n =4 except for *Eriophorum* GHNP, which consists of a single measurement.

6.3.3. Respiration

Interpretation of the respiration results was confounded by missing data. Respiration rates increased in response to fertilization in two species (*Betula* and *Rubus*) but not in the greenhouses. *Eriophorum* was similar to the other two species in its greenhouse response, but because SHNP is missing, it is not clear if *Eriophorum* respiration had not responded to any treatment, and thus *Eriophorum* was different than the other species, or if *Eriophorum* was, in fact similar to the other species and the lack of observed difference in the open plots was simply due to random variation (Fig 6.4b). As a result, AIC analysis could not select between three candidate models (Table 6.1): S + N × E (w_i = 0.31), S × N + E (w_i = 0.26), and S + N + E (w_i = 0.25). The first model discounts the lack of response in *Eriophorum* NP, thus declaring the interaction with environment to be the same for all three species; the second model posits that *Eriophorum* is different from the other two in its reaction to nutrients but that greenhouses reduced R_{20} in across the board; the third model discounts all apparent interactions, implying, instead that nutrient addition raised R_{20} in all environments, and that greenhouses lowered R_{20} equally in all species. In order to resolve this dilemma I created a new variable, S_2, that grouped the apparently similar *Betula* and *Rubus* effects together, a method suggested by Crawley (2007). When compared with all previous models, the new model, S_2 × N + E, was judged to be 3-fold better than the other models (Table 6.1). ANOVA confirmed the significance of S_2 × N (P = 0.03) as well as the additive term ($P \leq 0.01$). Based on this model, leaf R_{20} in *Betula* and *Rubus* plants grown at ambient temperatures increased 20 – 30% in response to fertilization. R_{20}, was reduced by 14 ± 4% across species in plants grown in the greenhouse, with no effect of fertilizer on any of the species sampled in the greenhouse (Fig 6.4).

6.3.4. Electron partitioning

No treatment differences in respiratory discrimination were detected for *Betula* shoots or for *Eriophorum* or *Rubus* leaves (Fig 6.4d–f; best model includes only S, Table 6.1). Treatment effects for *Betula*, however, may have been masked by incubating stem and leaf tissue together: when leaves were incubated separately from stem tissue, discrimination in fertilized plants of 23.9 ± 0.3‰ was 1.6 ± 0.4‰ lower than in the control leaves (Fig 6.5b; P = 0.0006 in ANOVA with the corresponding *Eriophorum* and *Rubus* treatments). Discrimination in stems: 18.9 ± 0.8‰ and 19.8 ± 1.1‰ for NP and control respectively was lower and more variable than in leaves, resulting in

nonsignificant differences (P = 0.57). The reduced discrimination values in stems and increased variability is consistent with a known side-effect of dense tissue, in which discrimination values are reduced due to diffusion limitation so that D varies with tissue thickness (Angert & Luz, 2001, Guy *et al.*, 1989). As further evidence that variation in stem width increased uncertainty, note that the measures of total respiration, which are not as sensitive to diffusion limitations, do not show the increased variability of the discrimination measurements (Fig 6.5a).

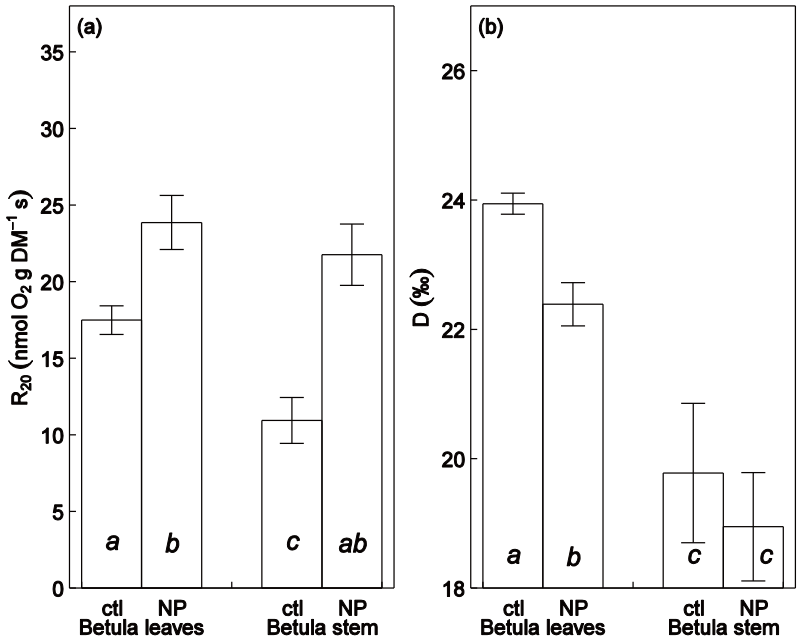

Fig 6.5. Respiration (a) and respiratory discrimination against ^{18}O (b) in *Betula* leaves and stems incubated separately.

Letters in the bars represent statistically distinct groups at the $P < 0.05$ significance level. ctl – control plots, NP – fertilized, open, plots. n =4 for each bar.

In order to translate measured discrimination values into enzyme activity, *Betula* leaves were inhibited with selective respiratory inhibitors. Leaf weight increased 20% as a result of immersion but the excess water did not affect measured discrimination, which was 21.9 ± 0.4‰ for the buffer-treated leaves *vs.* 22.4 ± 0.3‰ for untreated leaves (P = 0.4, Table 6.3; leaves for inhibition tests were taken from the NP plots). Measured

discrimination values for inhibited leaves were 26.4 ± 0.2‰, 21.0 ± 0.7‰, and 21.1 ± 1.3‰ for CP-inhibited, AP-inhibited, and double-inhibited leaves (Table 6.3). Residual respiration in the double-inhibited leaves was 11% of the buffer-treated leaves, indicating effectiveness of the inhibitors. The measured difference of 5.3‰ between the endpoints, however, was considerably smaller than the reported mean difference of 10‰ for green plant tissue (Ribas-Carbo *et al.*, 2005a). AOX and COX activity was therefore estimated using mean published values in addition to my measured endpoint values (Table 6.3). Regardless of the assumed endpoint range, the increase in leaf-level respiration in response to fertilization can be attributed to a near doubling of the COX pathway, from 9 to 17 nmol O_2 g DM^{-1} s^{-1}, whereas alternative respiration remained approximately 8 nmol O_2 g DM^{-1} s^{-1} (Table 6.3).

Table 6.3. Two scenarios for calculating electron partitioning in *Betula nana* leaves.

	D (‰)	τ_a	*R*	v_{cyt}	v_{alt}
Measured D_c and D_a					
COX	21 ± 0.7	0			
AOX	26.4 ± 0.2	1			
ctl	23.94 ± 0.16	0.54 ± 0.07	17.50 ± 0.9	7.97 ± 1.27	9.53 ± 1.30
NP	22.40 ± 0.3	0.26 ± 0.11	23.90 ± 1.8	17.70 ± 2.98	6.20 ± 2.70
Published D_c and D_a					
COX	19.9 ± 0.3	0			
AOX	29.2 ± 0.5	1			
ctl	23.94 ± 0.16	0.46 ± 0.03	17.50 ± 0.9	9.4 ± 0.8	8.1 ± 0.7
NP	22.40 ± 0.3	0.31 ± 0.04	23.90 ± 1.8	16.6 ± 1.6	7.3 ± 1.1

The first four rows are base on endpoints measured in this study; the second set of lines use the mean and SE of reported values for the endpoints (Ribas-Carbo *et al.*, 2005a). Quantities are: *D* – discrimination; τ_a –proportion of electrons partitioned through AOX; *R* – respiration (nmol O_2 g DM^{-1} s^{-1}); v_{cyt} and v_{alt} represent the activity of the cytochrome and alternative pathways in units of nmol O_2 g DM^{-1} s^{-1}.

6.3.5. Protein analysis

The best explanation for variations in AOX/COX included only the Environment term (Table 6.1). Additive effects of Species, however, are used only to allow pooling of results (i.e., by subtracting species mean values). Thus for explanatory purposes, models such as "S + E" and "E" are equivalent. The sums of Akaike weights for each of the two pairs of equivalent models in Table 6.1 are $w_i = 0.51$ for S + E and $w_i = 0.39$ for S + N + E, which indicates that one should not rule out an additive Nutrient effect. The uncertainty in the significance of a Nutrient effect shows up as an order-dependent significance for N in the ANOVA tests: the Nutrient term is significant if N appears before E ($P = 0.008$) but is not significant if E appears before N (P = 0.14). The Environment effect resulted from a 59 ± 12% reduction in the signal ratio for the greenhouse treatments and a 40 ± 13% reduction in the shade houses relative to open-air plots ($P \leq 0.001$ in both cases). The Nutrient effect increase in signal ratio 15 ± 12% (not statistically significant). The signal for *Rubus* was too low for analysis.

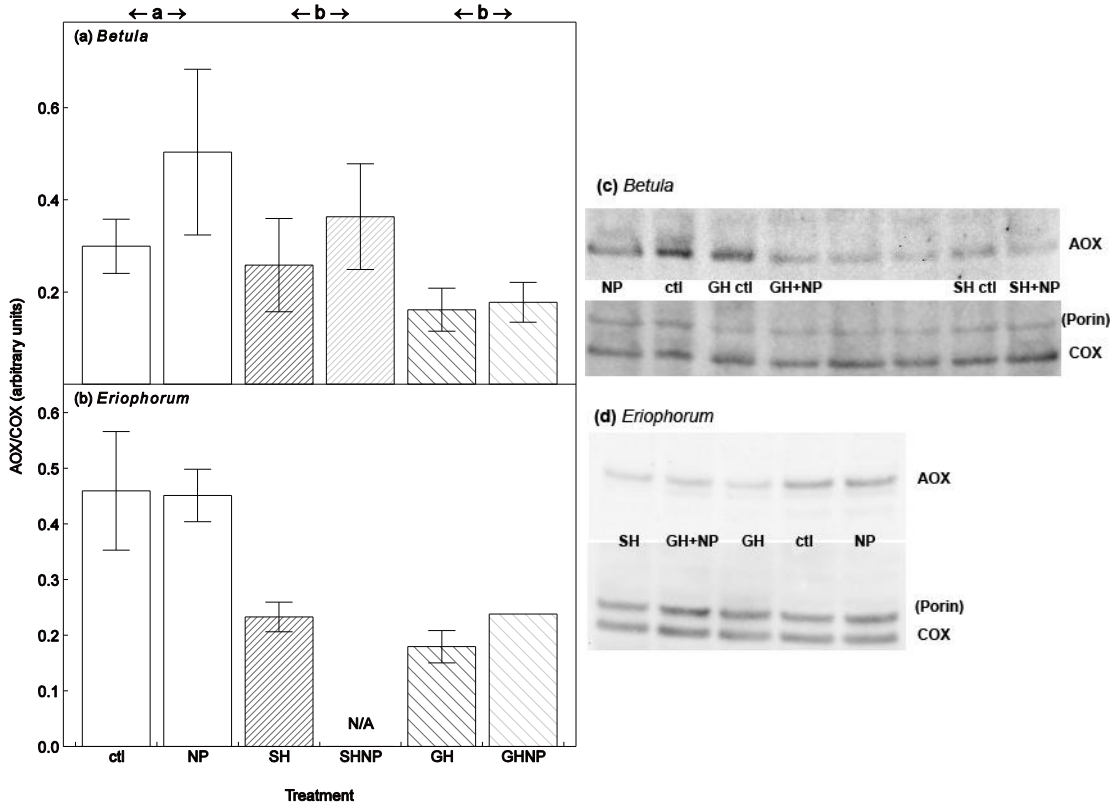

Fig 6.6. Western blot analysis of (a, c) *Betula* leaves and (b, d) *Eriophorum* leaves.

Letters in the upper marger represent statistically distinct Environment groups at the $P = 0.05$ significance level. No statistically significant effects were found for nutrient addition. See Fig 6.1 for a key to the treatment codes. n =4 except for *Eriophorum* GHNP which consists of a single measurement.

6.4. DISCUSSION

The primary goal of this study was to determine whether plants growing in the field modulated respiratory efficiency in response to environmental change. The answer may depend on species. Only the most successful species, *Betula*, decreased AP partitioning as hypothesized. Effects on community composition and leaf traits provide the context for interpreting these results, as nutrient supply interacted with changes in illumination and temperature to favor different species. These same environmental factors are also expected to affect plant energy balance, which I hypothesized is what drives AP/CP partitioning. I therefore begin with a discussion of how environment interacted with the other measured plant traits.

6.4.1. Community composition was strongly affected by nutrient addition

Twenty years of nutrient, light, and heat manipulation altered species dominance and production in this Alaskan moist tussock tundra. The untreated control plots contained a diverse, low-statured, assemblage of plants in which *Eriophorum* and *Betula* accounted for 35% of the relative cover (Fig 6.1). This assessment is similar to reported changes in biomass in an earlier experiment (Chapin *et al.*, 1995). As seen in Fig 6.1 and previous studies, shade or warming alone had little observable effect on community composition (Bret-Harte *et al.*, 2001, Chapin *et al.*, 1995). Fertilization with nitrogen and phosphorous fertilizer (NP), on the other hand, strongly influenced community composition and growth, depending on light and temperature. In open plots and in the greenhouses (Fig 6.1d), existing *Betula* ramets increased their growth rate, branch length, and branching until they overshadowed and crowded out the remaining vegetation (Bret-Harte *et al.*, 2001) covering three quarters of those plots after 20 years (Appendix A6.2 Fig S6.2). In the fertilized shade houses, however, *Betula* was not successful and, instead, *Rubus* formed dense mats that displaced much of the other vegetation (Fig 6.1c). *Eriophorum*, which was the tallest plant in the control plots, grew so poorly in GHNP and SHNP that I was not able to harvest sufficient plant material for the respiration incubations, excepting one GHNP treatment.

6.4.2. Leaf physical and chemical traits responded similarly in all species

Leaf DMC and SLA can provide a simple proxy for leaf nutrient stress (Hodgson *et al.*, 2011). Light availability also affects these characteristics, since shaded leaves are often

thinner and have less dry mass due to the reduced light availability (Hodgson *et al.*, 2011). Shading and nutrient addition are therefore both expected reduce leaf dry mass content and increase SLA, as was found in this study. Importantly, the three species examined did not differ in their response to the environmental manipulations (Fig 6.2), thus suggesting that, at the leaf level, the manipulations had affected them equally. The lack of difference in either measure between the GH and GHNP treatments is curious, especially since the species in the GHNP understory, *Eriophorum* and *Rubus* might have been expected to show a strong shade-response since incident illumination had been reduced by 90% (Bret-Harte *et al.*, 2001). Nevertheless, a theme throughout this study is that the warming treatment dampened leaf-level effects of fertilization.

Leaf N and P status is a more direct indicator of cellular nutrient availability than is leaf structure but some caution is still warranted when interpreting these data, since leaf nutrient levels may reflect vacuolar rather than cytoplasmic concentrations (Lee & Ratcliffe, 1993). Perhaps more importantly, increased growth will dilute leaf-level concentrations, as was seen in *Betula* grown in GHNP: no significant change in leaf N status was detected despite the large increase in biomass relative to controls (Fig 6.1b, c). Conversely, the very high P uptake seen in this study (Table 6.2) has been described as luxury uptake (Chapin & Shaver, 1996) since it appears to be in great excess of what the plant can utilize for growth. Nevertheless, the overall results indicate that adding soil nutrients generally improved leaf nutrient status. As with the leaf structural measures, however, improvements in leaf nutrient status were similar across species. The one exception, a lack of increased leaf N in *Rubus* NP leaves, is counterbalanced by the fact that growth of these plants had clearly been enhanced (Fig 6.1). The much smaller N increase in the fertilized greenhouses may be due to increased dieback in the fertilized plots due to increased shading of the lower leaves by the dense canopy (Chapin & Shaver, 1996).

Leaf carbohydrate status can be an indicator of nutrient deficiency, since plants that are nutrient-limited accumulate carbohydrates that would have been allocated to growth had sufficient nutrients been available (Hermans *et al.*, 2006). This relationship is not universal, however, or may depend on the extent of nutrient deficiency (Gonzalez-Meler *et al.*, 2001, Noguchi & Terashima, 2006). Reduced light would be expected to lower carbohydrate status due to lower production. Leaf carbohydrate status is also a possible regulator of AP/CP activity (Azcón-Bieto, Lambers & Day, 1983, Florez-Sarasa

et al., 2009). In the present study, as with the previous two measures, the responses of leaf carbohydrate responses to the experimental manipulations did not differ by species. TNC concentrations decreased by 13 ± 4% in response to shade as anticipated, and were independently reduced by 6 ± 3% in response to nutrient addition (Fig 6.3).

In summary, all leaf traits examined here were consistent with expected responses to nutrient- and light-response across all three species. Each measure suggested that the plants had responded equally well to the changes in light and nutrition, with no correlation to their relative success at the community or whole-plant level.

6.4.3. *Betula* increased electron partitioning to the cytochrome pathway in response to nutrient addition

Despite the lack of per-species differences in the leaf traits, I did find evidence for respiratory differences by species: whereas the two "winners" increased respiration rates in response to fertilization, leaf respiration in *Eriophorum* appears to have remained constant (Fig 6.5a). Of particular interest in this study, *Betula*, the most successful responder to NP addition in the unshaded plots, not only increased its respiration rate but it allocated the increase exclusively to the energy-efficient cytochrome pathway (Table 6.3) thus, in a sense, taking a double-benefit from the nutrient intake. At the whole-plant level, *Betula*'s success has been shown to be due to a change in growth patterns from producing mostly short shoots to producing many more long shoots, resulting in increased branching and increased leaf production (Bret-Harte *et al.*, 2001). My evidence suggests that as part of these changes, *Betula* also up-regulated its metabolic machinery to support the increased growth both by increasing output and increasing efficiency. The respiratory response in *Betula* is similar to that found a recent laboratory study of *Arabidopsis thaliana* leaves in which CP activity scaled with growth rate while AP activity remained nearly constant (Florez-Sarasa *et al.*, 2007, Priault *et al.*, 2007).

6.4.4. Energy balance may explain the lack of partitioning response in *Rubus*

I found no evidence of a similar change in respiratory electron partitioning in *Rubus* despite its corresponding growth success in the NP and SHNP plots (Fig 6.1). *Rubus*, however, functions as an understory species, which is in fact why it outcompeted the more light-dependent *Betula* in the shade houses. Under the energy-balance hypothesis I have proposed, low-light conditions, would lead to low AP activity, since energy-availability is now limiting growth. In a comparison of shade and sun species, for example, Noguchi & Terashima (2001) found little to no AP activity in the shade species,

Alocasia odora (Lodd.). Thus the lack of an electron partitioning response to fertilization in *Rubus* may simply reflect an already low AP activity. In support of this hypothesis I note that SHAM-inhibition of *Rubus* leaves did not lower the measured discrimination rate, even though residual respiration in doubly inhibited tissue was 13% of the controls (Appendix A6.1 Table S6.1).

6.4.5. Circumstantial evidence for respiratory acclimation

Warming resulted in a 15% reduction of R_{20} for all species grown in the greenhouse treatments (Fig 6.5a–c), suggesting that respiration in these species had partially acclimated to the higher growing temperature. Had there been no acclimation, R_{20} should have been unaffected by growth temperature. On the other hand, had the leaves fully acclimated, then respiration at growth temperature would have been the same in each treatment. In that case, based on the Q_{10} values and the 4 ºC difference in growth temperature, the R_{20} would have been reduced 25% in the GH treatments. Therefore, acclimation appears to have been 60% efficient. This evidence of acclimation may be of relevance to ecosystem model developers, since changes in *R* based on instantaneous measurements, i.e. Q_{10}, may not accurately reflect long-term changes in respiration rates (Gifford, 2003). Respiration did not respond to nutrient addition in the GHNP treatments (Fig 6.5a–c). This lack of response mirrors the lack of change in leaf N in these treatments (Table 6.2). In a recent meta-analysis, leaf *R* was shown to scale strongly with N (Reich *et al.*, 2008, see also Fig 4.6). The lack of respiratory response to fertilization in GHNP may therefore be explained by the trend in leaf N content, which may have remained constant due to dilution of the N through increased growth or due to increased dieback (Chapin & Shaver, 1996), as mentioned previously.

6.4.6. Plants grown in the light had higher AOX/COX concentrations

Changes in electron partitioning may be due to increased protein levels as well as metabolic regulation (Atkin *et al.*, 2005b). I had hypothesized, based on published laboratory studies, that nutrient stress would be associated with increases AOX abundance. In the two species I was able to assay, the Western blot analysis revealed an increase in AOX concentration at the highest light levels and a more ambiguous effect of nutrient addition, with only marginal statistical support for the effect. Furthermore, the effect in *Betula*, if present, is in the opposite direction of the discrimination response, i.e., an increase in AOX (Fig 6.6a) but a decrease in *D* (Fig 6.5b) in response to nutrient addition. The clearer result, an increase in AOX in the open plots, on the other hand, is

consistent with my energy-balance hypothesis as well as with published reports linking increased AP capacity with higher light conditions (Florez-Sarasa *et al.*, 2011, Noguchi *et al.*, 2001, Zhang *et al.*, 2011), as described in the introduction. Thus, even though I did not detect extra AP activity under the conditions of my respiratory incubations, it does appear that *Betula* and *Eriophorum* had increased AP capacity when grown in high light. Zhang *et al.* (2011) found that the AP may interact directly with photosynthetic intermediates in order to protect chlorplastic photosystems from photoinhibition. It is possible, therefore, that the increased AOX in the plants grown in the uncovered plots is active in the light, when it is needed, but deactivated in the dark.

6.5. SUMMARY

The evidence presented here partially supports the energy balance hypothesis for respiratory electron partitioning. Electron partitioning in *Betula nana* decreased as anticipated in response to fertilization, but the decrease was due to an increase in cytochrome pathway activity rather than a decrease in the alternative pathway. This ability to increase the more efficient respiratory pathway independently of the AP may have contributed to its developmental success in response to fertilization. *Rubus*, which thrived in the shade, appears not to have decreased AP activity, perhaps because activity was already low. *Eriophorum* which was the least successful in the fertilized plots had not increased leaf respiration (nor electron partitioning) in response to fertilization. Nevertheless, in agreement with the energy balance hypothesis, species growing in higher-light environments contained higher relative levels of AOX protein, implying an increased need for AP activity when energy is more abundant. Further investigations suggested by this study include measuring the response of the respiratory pathways in plots fertilized only with nitrogen – which would induce a relative phosphorus deficiency – and testing whether short-term light-intensity treatments would result in detectable changes in AOX activity.

7. Thesis… synthesis

(with apologies to Georg Wilhelm Friedrich Hegel)

7.1. OVERVIEW

The enigma of why plants maintain two respiratory pathways of drastically different efficiencies remains a question worthy of research. As mentioned in the Introductory chapter (Section 1.5) this project encompassed two distinct and significant components: the development and validation of novel methods for measuring respiratory electron partitioning in field studies, and the application of those methods to the study plant ecophysiology. Each of these components has borne fruit and, I believe, will help further our general understanding of plant interaction with the environment. In the first case, the new measurement methods will open up new avenues of research, allowing practitioners to examine plant respiration at greater levels of detail than was previously possible. In the second case, a picture emerging from my investigations is one of variability in how species respond to their environment. Also, I will advocate a possible shift of emphasis away from the concept of *partitioning* to what appears to be independent control of the two pathways. Each subsection, below, includes forward-looking statements. Section 7.3 provides my final synthesis and views for the future.

7.2. NOVEL METHODS, TIMES THREE

In Chapters 2 & 3, I presented three distinct technological advances that may be of more general utility than just the uses described in the previous chapters. First, I described a method for improving the dynamic range of continuous-flow isotope ratio mass spectrometry (CF-IRMS) measurements, second I presented and validated a vial-based incubation method for measuring respiratory discrimination in the field, and third I presented mathematical methods for dealing with contamination and nonlinearities in the collected data.

7.2.1. Improving the dynamic range of CF-IRMS

In one sense my mass spectrometry method is the most restricted of my innovations since it applies to a particular IRMS technology. On the other hand, CF-IRMS is used for numerous investigations and my method may therefore find application far afield from plant respiration.

The problem of nonlinearity across varying analyte concentrations is a well-known issue in mass spectrometry, and has thus generated numerous solutions including

specialized hardware to ensure constancy of the sample size (Zeeman *et al.*, 2008), formal mathematical analysis (Cappellin *et al.*, 2011), and additive empirical corrections (Spotl & Vennemann, 2003, Thermo Electron Corporation, 2004, Werner *et al.*, 2001). My approach is closest in spirit to the empirical solutions but adds a simple mathematical consideration: that the value being corrected is, in fact, the ratio of two physical signals. This simple point allowed me to demonstrate shortcomings of the purely empirical approach as well as to derive a formula for correcting the signal over a 100-fold range of analyte concentrations and across a δ-value range greater than 500‰. This sampling range was crucial for enabling me to correct the discrimination equations for routine levels of contamination in the respiratory sample storage vials.

The need for the linearity correction may not be universal – for example one may, instead, use hardware to keep analyte concentrations constant– but I believe it may still help to raise awareness of several issues including open split effects (again, a continuous flow issue), and the need for more than one calibration standard. This last point leads to a particular issue not previously discussed here: O_2 scale calibration. While it is common to use at least two standards when calibrating mass spectrometers for carbon analysis – using, for example, samples that have been certified against the Vienna Standard Mean Ocean Water (VSMOW) and Standard Light Antarctic Precipitation (SLAP), – my informal inquiries to several practitioners who measure O_2 isotopes indicated that atmospheric air is the only standard used or available for O_2 isotope measurements. This falls short of the recommendation that O_2 isotope ratios be scaled to the VSMOW-SLAP scale (Wieser & Berglund, 2009). Even on our own mass spectrometer I have noticed small changes in scale from run to run (data not shown) that were correctible only because we had used two air standards (Section 2.3.1). I believe that development of a second international gas-phase O_2 standard could be an important step in removing variations in discrimination values (and other isotopic measurements) across laboratories.

7.2.2. The field-compatible method for measuring respiratory electron partitioning

The value and novelty of my field-compatible methods is best summed up in the words of the referees to the published version of Chapter 3: "I welcome this technological advance…" (Graham Farquhar, Australian National University, handling editor, Plant Cell & Environment), "I certainly believe that this new application of the technique will be an important step forward in the field of plant respiration." (anonymous reviewer), and "I would not have initially believed that a vial technique, such as the one described here,

would have much field potential…but they have convincingly overcome these problems…the methods should allow more widespread use of ^{18}O isotope discrimination in studies of plant respiration in general…" I sincerely hope that these predictions come true.

Of course, this method did not sprout fully-formed from my brow (or the collective brows of my colleagues and supervisors) but, rather, it is the next step in a succession of methods for measuring respiratory discrimination *in vivo*. The original method introduced by Guy *et al*. (1989), involved a liquid-phase cuvette and conversion of O_2 to CO_2 by combustion before measurement in the mass spectrometer. This design was much improved and streamlined in the online gas-phase method introduced by Robinson *et al.* (1992). With relatively small variations and improvements, this method remains the standard tool for investigating *in vivo* respiratory electron partitioning (Florez-Sarasa *et al.*, 2011, Watling, Robinson & Seymour, 2006).

Previous attempts to develop portable off-line methods involved cumbersome and/or custom-built cuvettes that could not easily be used for multiple simultaneous incubations (Nagel *et al.*, 2001, Noguchi *et al.*, 2001), or required custom-built storage cuvettes (Angert & Luz, 2001). As well, the methods of Nagel *et al.* (2001) and of Angert & Luz (2001) required large incubation cuvettes that greatly increased incubation time, decreased the number of samples per replicate and/or increase the amount of leaf material used. Nevertheless, of these predecessors, Nagel *et al.* (2001) comes the closest to my method and, indeed, provided the inspiration for using commercial storage vial. From there it seemed to be a relatively small leap to try using commercial incubation vials as well. Because we used smaller storage vials, the development of appropriate storage techniques and contamination corrections became paramount, and I therefore developed mathematical corrections, developed a viable long-term storage method, a expended a large effort on validating the methods to ensure that results produced using this method were acceptable to the scientific community.

Now that the method, its accuracy, and its precision have been validated to my own satisfaction and the satisfaction of the scientific peer reviewers, the proof of the method will come in its use. To that extent, the three projects described in this thesis, as well as the published works of my fellow student, Stephanie Searle (Searle *et al.*, 2011a, Searle *et al.*, 2011b, Searle & Turnbull, 2011) and unpublished work by a peer in Chile

(Carolina Sanhueza Inalaf) are the best testaments to the viability of this method and for the possibility of its future acceptance as a tool for plant ecophysiology.

7.2.3. Correcting for contamination and for nonlinearity in discrimination

The linearity corrections, the methods of detecting nonlinearity, and the methods of coping with uncorrectable curvature are intrinsic parts of the field-portable methods. These mathematical tools, however, may be of much wider relevance than just as enablers for the field measurement of respiratory electron partitioning (as important as that is!). In the general sense, many measurement methods entail linear regression, with underlying assumptions of linearity that may not always hold. Examples from my own experience include spectrophotometric assays and the measurement of O_2 respiration rates using an oxygen electrode. Millenaar *et al* (2001) describe a similar situation in which respiration changed during the course of measurement. Accuracy and precision of such assays could be improved by considering second-order approximations, such as I have done here (Kirkup & Mulholland, 2004). The mathematical methods I've presented in Chapter 3 are certainly not ground-breaking from a mathematical perspective. Perhaps it would be more appropriate to consider my contribution as "consciousness raising," in bringing together the various methods needed for this particular application.

The test for nonlinearity and the solutions presented here (Chapter 3) are more than just a way to avoid "unintended consequences," however. There are several cases in which the methods can actually improve the granularity of analysis. For example, in section 3.3.1 (and Kornfeld *et al.*, 2012a) I use the quadratic-fit equations to compute the instantaneous discrimination values for a simulated experiment in which the tissue recovered from inhibition over the course of measurement. Thus, the technique could potentially be used to study rates of recovery from respiratory inhibition. The same method may be able to test for effects of diffusional limitation on measured discrimination. For example, Miller *et al*. (2011) proposed, based on indirect evidence, that measured discrimination values decrease as diffusionally restricted respiration progresses. The nonlinear methods described here could be used to test the hypothesis directly. Yet another application would be to test respiration under known or expected non-steady state conditions – such as the respiratory burst immediately after a photoperiod or, perhaps, a sudden change in temperature. In such cases one might be able to use or extend the current methods to study rapid dynamics in discrimination, a topic

that has generally been avoided due to the steady-state conditions required for many popular gas-exchange measurement methods (including respiratory discrimination).

Finally, the nonlinearity methods I have described are not limited to O_2 methods or to respiration. Thus, in addition to having the potential to greatly expand the scope of investigations in plant respiration, they may also be applied to other topics including, for example, N uptake and assimilation by whole roots, where discrimination is concentration dependent (anonymous reviewer of Kornfeld *et al.*, 2012a).

7.3. PHYSIOLOGICAL INSIGHTS

A theme that has emerged from my ecophysiological investigations, and one that is coincidentally reminiscent of the insight behind my CF-IRMS linearity correction (Sections 7.2.1 and 7.2.1), is that it might be instructive to consider that "partitioning" is actually the ratio of two independent processes. For example, several results presented here were best understood as changes in one pathway while the other was held constant. A second important theme is the idea of energy balance being a critical factor regulating alternative pathway (AP) activity. In particular, was the lack of observed changes in AP in some of the results largely due to low light levels? Here I discuss the miscellany of insights leading up to this final synthesis.

7.3.1. Benefits and drawbacks of ground-breaking field studies

My investigation at the Franz Josef chronosequence truly qualified as an examination of "plant response to changing environmental conditions along…spatial environmental gradients…at remote locations" (Section 1.3). While it inherits drawbacks as well as benefits of wide-ranging observational studies, the results demonstrate the potential for such studies to push science forward.

To start with the drawbacks, many of the explanatory factors were correlated among themselves. Furthermore, the apparent relationships found with the measures of respiration may have been influenced by other unmeasured variables that correlated with the measured ones (a problem with any observational study). Nevertheless, factors such as N and P, and to a lesser extent Fe, as well as the other measures examined are well-known to have major influences on plant growth and respiration (Aerts & Chapin, 2000, Reich *et al.*, 2008, Tjoelker *et al.*, 2008). Another drawback in this field study was that due to the large number of species involved, it was difficult to customize methods for any particular species. As a result, for example, Western blots were not successful for many

species, nor was I able to reliably determine the COX endpoint, instead relying on the relative constancy of 20‰ for D_c across studies (Ribas-Carbo *et al.*, 2005a).

Despite these potential drawbacks, the natural gradient allowed me to examine many species across a broad variety of conditions. Thus, I obtained a relatively continuous spectrum of values for N, R, N/P, τ_a, etc. (Fig 4.6) rather than a few clusters of values as one might expect, for example, from a 2×2 manipulation. In addition, and a common justification for conducting field studies (Section 1.3), these measurements represented the responses of plants growing in the wild under natural conditions. As a result, any conclusions drawn from this study might be said to have more direct relevance than controlled laboratory experiments on questions of global ecological change.

7.3.2. Did plant nutrient stress lead to higher AOX activity or concentrations?

In the Introduction (Section 1.5) I proposed three hypotheses. The first two suggested that nutrient deficiencies would lead to (1) higher AOX partitioning and (2) higher AOX concentrations, especially under long-term stress. The evidence towards the first hypothesis was contradictory: AOX partitioning was lowest at the most nutrient-deficient site along the Franz Josef chronosequence, was unchanged in nutrient-deficient *Griselinia* leaves, increased in nutrient-deficient *Griselinia* roots, and either was higher or unchanged in the low-nutrient (control) treatments at the Arctic LTER, depending on species. Relative AOX concentrations did not appear to be affected by soil nutrient status in any of my investigations; instead, I found correlations with light intensity.

This mix of evidence forced me to reconsider my general approach to several issues. One issue is how to address plant diversity, since it appears that different species responded differently to the same stimuli. Another issue is whether it is a mistake to consider effects of AP partitioning with respect to a single restriction (nutrient deficiency) without also considering the plants' overall environment, especially energy availability (i.e., illumination). Thirdly, a closer look at my data has made me wonder if "partitioning" is the right parameter to explore when formulating hypotheses. I will discuss each of these ideas separately and in combination in the subsequent sections.

7.3.3. Does N/P drive respiratory electron partitioning?

My third hypothesis for this study was that combined stresses, i.e. N and P, would lead to even stronger AOX activity or expression. I found no evidence to support this hypothesis in my greenhouse study (the only one that compared combined with individual

deficiencies). Rather, it appeared that N/P, which may vary in doubly-deficient plants may have been a more important determinant of respiratory electron partitioning. This novel finding arose primarily from the Franz Josef study (Chapter 4), in which a negative correlation was found between leaf N/P ratio and electron partitioning, rather than with absolute N concentrations. While the correlation coefficient was not strong ($r^2 = 0.23$) the trend is clearly visible in the graph (Fig 4.6b) and the relationship had strong support from the more inclusive multifactor analysis (Table 4.2). The the next-best single-variable correlations with τ_a were less than one-third the strength ($r^2 = 0.07$ for P and for DMC, though with opposite signs; Appendix A4.2 Table S4.2). The inverse relationship between N/P and τ_a has further, though weak, support from my subsequent nutrient manipulation experiment (Chapter 5). Although no changes in leaf electron partitioning were observed in that study, leaf AOX/COX concentrations were highest in the –N fertilized *Griselinia* leaves rather than in –NP leaves. The latter had an N/P ratio similar to the controls despite having low absolute foliar N levels much like the –N treatment (Fig 5.2). Results from electron partitioning in the roots contradicts this hypothesis, however, since τ_a increased in the –NP roots relative to controls despite having the same N/P as control roots (Table 5.1). Supporting evidence from the literature is essentially absent, since I am unaware of any studies of combined N and P effects on respiratory electron partitioning in plants. The one study of *in vivo* partitioning due to P-deficiency reported mixed results: τ_a and AP activity increased in two species and decreased in a third species (Gonzalez-Meler *et al.*, 2001). Studies of AOX capacity and/or relative concentration have found increases in AOX for –N (consistent with this report) but responses to –P have been found also, though not consistently (Gonzalez-Meler *et al.*, 2001, Juszczuk, Malusa & Rychter, 2001a, Noguchi & Terashima, 2006, Sieger *et al.*, 2005). Differences between my findings in *Griselinia* and those reports just cited may be related to species nutrient "set points" and/or relative growth rates (as will be discussed below). In general the levels of N and P measured in *Griselinia* were half to a third of the levels reported for species in the above-mentioned studies. Whether, or why, such differences might affect the respiratory response to nutrient deficiency would be overly speculative at this point, however.

There seems little doubt of the correlation between τ_a and N/P at the Franz Josef chronosequence, but was it due to a global regulation of partitioning or to independent control over the two respiratory pathways? The evidence at Franz Josef as well as the

subsequent greenhouse experiment supports the latter view. Increases in τ_a at the younger sites were driven solely by decreasing cytochrome pathway (CP) activity, whereas decreases across the older sites were due entirely to declines in AP activity (Table 4.3). Similarly in the multifactor analysis, AP activity was most strongly correlated with leaf P concentration, as opposed to N/P, whereas CP activity correlated with leaf N (Table 4.2). Thus the negative correlation between AP/*R* (i.e. τ_a) and N/P can be explained as independent positive correlations of AP activity with P and total *R* – which is dominated by CP – with N.

The greenhouse study also supports the idea that the two pathways were independently controlled, since CP activity in roots changed in response to nutrient deficiency, whereas AP activity in the roots was unaffected (Table 5.1). The lack of measured response in the leaves of the nutrient-starved *Griselinia* plants is also consistent with the independent-pathways interpretation, since AP activity was low enough that the independent changes in CP activity did not measurably affect the ratio of AP to total *R*.

7.3.4. Possible role for copper in respiration and AP activity.

The multifactor analysis of the Franz Josef data suggested that, in addition to the well-established correlations with N and nonstructural carbohydrates, foliar copper concentration also contributed explanatory power to the measured changes in leaf respiration. When respiration is partitioned into the AP and CP components, it is further evident that the effects of Cu on total *R* were due to is effect on AP activity.

This result is somewhat surprising partly because Fe, which is a metallic cofactor for AOX, did not show up in the analysis, and partly because the direction of the relationship –increasing AP activity for increasing Cu – is the opposite of the hypothesized effect (i.e., that Cu-deficiency would limit the Cu-dependent CP more than the AP). I was not able to conduct further tests of the imputed role of Cu as part of this project, so this finding should be considered tentative, at best. A possible explanation from the literature is that AP capacity was found to increase at sublethal concentrations of Cu (Padua *et al.*, 1999). Thus, it is possible that Cu levels were high enough in the youngest soils to increase AP activity due to incipient toxicity. Accepted "normal" concentrations of foliar Cu in agricultural crops is in the 2–7 mg kg DM^{-1} range, with toxicity starting as low as 5–20 mg Cu kg DM^{-1} (Jones, 2012). The values measured here fell between 2 – 14 mg Cu kg DM^{-1}. Thus, an experiment that attempts to confirm the

influence of Cu found at the Franz Josef chronosequence should consider both increased and deficient Cu conditions.

7.3.5. The role of leaf carbohydrate status in regulating *R* and AP activity

Leaf sugar and/or starch concentrations are believed to be important drivers of respiration, as has been found in numerous studies (Azcón-Bieto & Osmond, 1983, Tjoelker *et al.*, 2008, Turnbull *et al.*, 2003, Whitehead *et al.*, 2004). Such correlations stand to reason since carbohydrates provide the substrates for respiration. Less obvious, though also well established, is the importance of sugars for AP activation (Azcón-Bieto & Osmond, 1983, Florez-Sarasa *et al.*, 2009). Sugars may regulate AP activity through pyruvate, an end-product of glycolysis (Hoefnagel *et al.*, 1997, Juszczuk *et al.*, 2001b).

In the present study sugar concentration was correlated with *R* across the Franz Josef chronosequence (Appendix A4.2 Table 4.2), but this effect appears to have been mediated through its correlation with N. In the multifactor analysis, sugar was not found to contribute significantly but, instead, starch was found to play a role. Interestingly, on its own, starch was not correlated with *R* in this dataset (Appendix A4.2 Table 4.2). In the greenhouse manipulation, neither sugars nor starch correlated with leaf *R*. At the Arctic LTER, on the other hand, respiration appears to have varied strongly with sugars and not starch (data not shown). It is worth noting that respiration is a complex, highly regulated process, and therefore, need not be strictly substrate-limited (Millar *et al.*, 2011). Likewise for AP activity, although the above-cited reports found an important role for sugar, Millenaar *et al.* (2001) reported that root AP activity in grasses did not respond to sugar addition or sugar starvation. I therefore suggest that while carbohydrate status alone may be an important factor regulating respiration, its effect may often be masked by other regulatory processes, depending on growth conditions. It is also likely that regulation acts at the level of key carbohydrates (or the flux through key pathways) rather than at the level of gross sugar or starch concentrations.

7.3.6. The importance of energy balance in respiratory electron partitioning

In the Arctic LTER chapter (Chapter 6) I suggest that energy balance may be an important factor for predicting how respiratory electron partitioning responds to environmental changes. This hypothesis is compatible with proposed functions of the alternative pathway as a "reductant overflow" valve (Millenaar & Lambers, 2003) or as a way of maintaining plant carbon balance (Sieger *et al.*, 2005). The important point, though, is that one should consider both the input conditions (light, CO_2, water) as well as

the consumption needs of the plant, i.e. other factors limiting growth when predicting AP/CP activity. The clearest-cut evidence in favor of the energy balance hypothesis comes from studies of the interaction between light availability and alternative respiration. For example, Noguchi *et al.* (2001) found AP activity to be low or absent in the leaves of a shade species. In other species AP activities increased with increasing growth illumination levels, though in some case AP and CP increased proportionally (Florez-Sarasa *et al.*, 2011, Florez-Sarasa *et al.*, 2009, Noguchi *et al.*, 2001). Recent research has also linked alternative respiration directly to photosynthetic redox protection (Noguchi & Yoshida, 2008, Yoshida *et al.*, 2011), again suggesting that energy input is an important determinant of AP activity.

In both the greenhouse study (Section 5.4.6) and the Arctic LTER investigation (6.4.4) I have suggested that low illumination counterbalanced nutrient deficiency with respect to their effects on alternative pathway activity. In both studies, AOX/COX levels appeared to be higher in sun-grown leaves than in shade-grown leaves. Another line of evidence of the importance of growth-illumination comes from work not reported previously: I had initially tried growing soybeans in a greenhouse that was relatively shaded by surrounding trees, translucent roofing, and overhead light fixtures. Measured discrimination in cotyledons from these plants were generally 1–2‰ lower than for the soybeans that I subsequently grew in a growth chamber under longer photoperiods and presumably, higher illumination (as evidenced by a shortened period to reach the same growth stage). Studies of AP activity may therefore need to take into account the plants' energy environment in addition to other factors being tested.

7.3.7. Growth and maintenance respiration

Leaf respiration can be divided into growth and maintenance components, where growth respiration is the portion that contributes to increased biomass, while maintenance respiration represents the proportion of respiration needed to maintain cellular process, primarily through the production of ATP (Amthor, 2000). Recent studies have suggested that, even though the AP is a poor route to ATP production, AP activity appears to be behave like maintenance respiration. For example, while total respiration increased with relative growth rate in *Arabidopsis thaliana* (Florez-Sarasa *et al.*, 2007) and *Nicotiana sylvestris* (Priault *et al.*, 2007), the increase was attributed entirely to CP activity, whereas AP activity remained constant.

My observations here largely confirm this hypothesis. *Griselinia* roots in the greenhouse nutrient manipulation experiment maintained AP activity levels in the face of nutrient deficiency whereas CP rates decreased (Table 5.1). The response of leaves in the same experiment was compatible with this hypothesis as well (Section 5.4.6). At the Arctic LTER, fertilization increased *Betula* respiration through the CP, but again, AP activity was unchanged. At the Franz Josef chronosequence, the evidence was mixed: changes to respiration in the youngest sites were consistent with the maintenance hypothesis. At the older sites, however, v_{alt} decreased at site six while v_{cyt} remained stable (Fig 4.5, Table 4.3). In this case the results may be in agreement with a different study: Millenaar *et al.* (2001) found that roots of faster-growing growing grass species had higher AP activity, though it is difficult to understand why this occurs. Clearly, no single mechanism will be able to explain the complex process of regulating respiratory electron partitioning. Nevertheless, I believe my studies provide compelling support for the concept that alternative pathway respiration fulfils a maintenance function.

7.4. SYNTHESIS AND CONCLUSIONS

Here I summarize what I believe to be two overarching themes of this study and present my visions for the future in three brief, but slightly provocative, essays.

7.4.1. Is electron partitioning (τ_a) an appropriate physiological parameter?

My investigations into how plant respiratory electron partitioning responds to environmental changes, makes me wonder if *partitioning* is the right way to look at these phenomena. This concept may seem counterintuitive at first: the two pathways branch from the ubiquinone pool in the mitochondrial membrane, so in a sense they are clearly competing for the same substrate. In addition, the technology we use to measure these processes forces us to think in terms of partitioning since respiratory discrimination is a measure of τ_a. Nevertheless, as I have demonstrated in the preceding sections, often the AP and CP appear to respond independently to environmental stimuli. Across, the Franz Josef chronosequence, for example, even though there seemed to be a general trend across sites, only one pathway changed at a time: the CP declined in younger sites, whereas the AP declined at the oldest sites. Perhaps this dichotomy explains why the intriguing correlation between N/P and τ_a (each a ratio!) is supported in the multifactor analysis with the relatively low r^2 of 0.23, whereas the best regression for v_{alt} has r^2 = 0.71, and likewise for v_{cyt} (Table 4.2; see also Appendix A4.2 Table S4.2).

Evidence of independent control has been reported elsewhere as well (Florez-Sarasa *et al.*, 2007, Priault *et al.*, 2007), and could be justified in the same way that I justified the observation that total respiration is not purely substrate controlled (Section 7.3.5), i.e., the processes are highly regulated. I am not suggesting that the two pathways are always independently controlled – clearly they sometimes scale in proportion (Florez-Sarasa *et al.*, 2011, Florez-Sarasa *et al.*, 2009). Nevertheless, I believe the evidence supports the existence of independent control pathways as well. Further, broader, studies will be needed to determine which of these two regulatory strategies are most prevalent in nature.

7.4.2. Ecological advantages of respiratory flexibility?

An area of research that seems to me to be ripe for exploration is how respiratory flexibility – in terms of total respiration or electron partitioning – can give plants an ecological advantage over neighboring plants. A recent review of plant phenotypic plasticity, for example, acknowledge the importance of understanding how respiration is modulated under climate change but devotes only a single sentence to the subject (Nicotra *et al.*, 2010). Much research on respiration has focused on "universal" properties of respiration across species, such as the scaling of *R* with N (Reich *et al.*, 2006, Reich *et al.*, 2008), or formulas for temperature response (Kruse & Adams, 2008) or the "leaf economics spectrum" (Wright *et al.*, 2004). Despite these impressive commonalities across a diverse array of species, plants do differ in their abilities to respond to environmental factors. Even in the above, a substantial portion of the scaling is due to differences across species rather than within species. Thus it may well be worth investigating what advantage, if any, would be conferred to a plant that is better able to modulate *R* and electron partitioning in changing environments.

I believe that research of this nature is where my new field-compatible methods can really shine – where it can enable measurement of R, τ_a, v_{cyt}, and v_{alt} across several species under differing growth conditions, under field conditions, and/or across environmental gradients. As an initial example of this line of inquiry, my investigations at the Arctic LTER uncovered differences in the respiratory responses of three dominant species in the Arctic tundra. Two of the species, *Betula nana* and *Rubus chamaemorus*, increased growth and respiration in response to fertilization, whereas *Eriophorum vaginatum* did not. *Eriophorum* was also the species to have lost the most ground in the treated plots (Fig 6.1). Was the ability to modulate leaf-level respiration (and, by

implication, presumably general metabolism) a critical part of the *Betula* and *Rubus* success story? For example, *Betula* dominance in the fertilized, unshaded, plots was explained at one level of abstraction as changes in extension and branching (Bret-Harte *et al.*, 2001). What metabolic factors might be involved? Did the fact that *Betula* independently increased respiration through the more efficient CP, without changing the less efficient AP activity, play a part in this success?

7.4.3. My lasting contribution?

If forced to pick one aspect of my PhD project that I believe or hope will be my most important contribution to the future of plant ecophysiology, I would have to choose the field-compatible respiratory methods (which is a bit of a cheat, since it's really more than one thing). Insights gained from my ecophysiological studies (Chapters 4–6), interesting as they are, are but instances of particular investigations. The new methods, however, have the potential to open up whole new avenues of research that were not previously available. This is true both in the sense of allowing measurements to be taken to the field, as well as in the sense of expanding the types of investigations one might consider, such as exploring rapid dynamics of electron partitioning (whether using the vial method in its entirety or just using the mathematical tools developed to support the method) [Section 7.2.2].

It is my sincere hope that these methods find acceptance and use among the plant ecophysiological community and that they lead to interesting and significant improvements in our understanding of plants and our environment.

Thank you for having read this manuscript!

Literature cited

Aerts R. & Chapin F.S. (2000) The mineral nutrition of wild plants revisited: A re-evaluation of processes and patterns. In: *Advances in Ecological Research, Vol 30* (eds A.H. Fitter & D.G. Raffaelli), pp. 1-67. Elsevier Academic Press Inc, San Diego.

Allan H.H., Moore L.B., Edgar E. (1961) *Flora of New Zealand*. Government Printer, Wellington, N.Z.

Almond P.C., Moar N.T. & Lian O.B. (2001) Reinterpretation of the glacial chronology of South Westland, New Zealand. *New Zealand Journal of Geology and Geophysics*, **44**, 1-15.

Amthor J.S. (2000) The McCree-de Wit-Penning de Vries-Thornley respiration paradigms: 30 years later. *Annals of Botany*, **86**, 1-20.

Angert A. & Luz B. (2001) Fractionation of oxygen isotopes by root respiration: Implications for the isotopic composition of atmospheric O_2. *Geochimica Et Cosmochimica Acta*, **65**, 1695-1701.

Armstrong A.F., Badger M.R., Day D.A., Barthet M.M., Smith P.M.C., Millar A.H., Whelan J. & Atkin O.K. (2008) Dynamic changes in the mitochondrial electron transport chain underpinning cold acclimation of leaf respiration. *Plant Cell and Environment*, **31**, 1156-1169.

Asada K. (1999) The water-water cycle in chloroplasts: Scavenging of active oxygens and dissipation of excess photons. *Annual Review of Plant Physiology and Plant Molecular Biology*, **50**, 601-639.

Atkin O., Bruhn D. & Tjoelker M. (2005a) Response of plant respiration to changes in temperature: mechanisms and consequences of variations in Q_{10} values and acclimation. In: *Plant Respiration: From Cell to Ecosystem* (eds H. Lambers & M. Ribas-Carbo), pp. 95-135. Springer, Dordrecht, The Netherlands.

Atkin O.K., Bruhn D., Hurry V.M. & Tjoelker M.G. (2005b) The hot and the cold: unravelling the variable response of plant respiration to temperature. *Functional Plant Biology*, **32**, 87-105.

Atkin O.K., Scheurwater I. & Pons T.L. (2007) Respiration as a percentage of daily photosynthesis in whole plants is homeostatic at moderate, but not high, growth temperatures. *New Phytologist*, **174**, 367-380.

Atkin O.K., Zhang Q.S. & Wiskich J.T. (2002) Effect of temperature on rates of alternative and cytochrome pathway respiration and their relationship with the redox poise of the quinone pool. *Plant Physiology*, **128**, 212-222.

Ayub G., Smith R.A., Tissue D.T. & Atkin O.K. (2011) Impacts of drought on leaf respiration in darkness and light in Eucalyptus saligna exposed to industrial-age atmospheric CO(2) and growth temperature. *New Phytologist*, **190**, 1003-1018.

Azcón-Bieto J., Lambers H. & Day D.A. (1983) Effect of photosynthesis and carbohydrate status on respiratory rates and the involvement of the alternative pathway in leaf respiration. *Plant Physiology*, **72**, 598-603.

Azcón-Bieto J. & Osmond C.B. (1983) Relationship between photosynthesis and respiration - the effect of carbohydrate status on the rate of CO_2 production by respiration in darkened and illuminated wheat leaves. *Plant Physiology*, **71**, 574-581.

Barth J.A.C., Tait A. & Bolshaw M. (2004) Automated analyses of $^{18}O/^{16}O$ ratios in dissolved oxygen from 12-mL water samples. *Limnology and Oceanography-Methods*, **2**, 35-41.

Bartoli C.G., Gomez F., Gergoff G., Guiamet J.J. & Puntarulo S. (2005) Up-regulation of the mitochondrial alternative oxidase pathway enhances photosynthetic electron transport under drought conditions. *Journal of Experimental Botany*, **56**, 1269-1276.

Boelman N.T., Stieglitz M., Griffin K.L. & Shaver G.R. (2005) Inter-annual variability of NDVI in response to long-term warming and fertilization in wet sedge and tussock tundra. *Oecologia*, **143**, 588-597.

Borghouts C., Werner A., Elthon T. & Osiewacz H.D. (2001) Copper-modulated gene expression and senescence in the filamentous fungus Podospora anserina. *Molecular and Cellular Biology*, **21**, 390-399.

Bret-Harte M.S., Shaver G.R., Zoerner J.P., Johnstone J.F., Wagner J.L., Chavez A.S., Gunkelman R.F., Lippert S.C. & Laundre J.A. (2001) Developmental plasticity allows Betula nana to dominate tundra subjected to an altered environment. *Ecology*, **82**, 18-32.

Bretz F., Hothorn T. & Westfall P.H. (2011) *Multiple comparisons using R*. CRC Press, Boca Raton.

Brown M.B. & Forsythe A.B. (1974) Robust tests for equality of variances. *Journal of the American Statistical Association*, **69**, 364-367.

Bruhn D., Wiskich J.T. & Atkin O.K. (2007) Contrasting responses by respiration to elevated CO_2 in intact tissue and isolated mitochondria. *Functional Plant Biology*, **34**, 112-117.

Burnham K.P. & Anderson D.R. (2002) *Model selection and multimodel inference : a practical information-theoretic approach*. (2nd ed.). Springer, New York.

Burnham K.P., Anderson D.R. & Huyvaert K.P. (2011) AIC model selection and multimodel inference in behavioral ecology: some background, observations, and comparisons. *Behavioral Ecology and Sociobiology*, **65**, 23-35.

Cambaliza M.O.L., Harlow B.A., Ubierna N., Mount G.H., Marshall J.D. & Evans R.D. (2009) Analysis of low-concentration gas samples with continuous-flow isotope ratio mass spectrometry: eliminating sources of contamination to achieve high precision. *Rapid Communications in Mass Spectrometry*, **23**, 3868-3874.

Cappellin L., Biasioli F., Schuhfried E., Soukoulis C., Mark T.D. & Gasperi F. (2011) Extending the dynamic range of proton transfer reaction time-of-flight mass spectrometers by a novel dead time correction. *Rapid Communications in Mass Spectrometry*, **25**, 179-183.

Carre J.E., Affourtit C. & Moore A.L. (2011) Interaction of purified alternative oxidase from thermogenic Arum maculatum with pyruvate. *FEBS Letters*, **585**, 397-401.

Chapin F.S. (1980) The mineral nutrition of wild plants. *Annual Review of Ecology and Systematics*, **11**, 233-260.

Chapin F.S. & Shaver G.R. (1996) Physiological and growth responses of arctic plants to a field experiment simulating climatic change. *Ecology*, **77**, 822-840.

Chapin F.S., Shaver G.R., Giblin A.E., Nadelhoffer K.J. & Laundre J.A. (1995) Responses of Arctic tundra to experimental and observed changes in climate. *Ecology*, **76**, 694-711.

Cook R.D. & Weisberg S. (1999) *Applied regression including computing and graphics*. Wiley, New York.

Costa J.H., Jolivet Y., Hasenfratz-Sauder M.-P., Orellano E.G., da Guia Silva Lima M., Dizengremel P. & Fernandes de Melo D. (2007) Alternative oxidase regulation in roots of *Vigna unguiculata* cultivars differing in drought/salt tolerance. *Journal of Plant Physiology*, **164**, 718-727.

Crawley M.J. (2005) *Statistics : an introduction using R*. J. Wiley, Chichester, West Sussex, England.

Crawley M.J. (2007) *The R book*. Wiley, Chichester, England ; Hoboken, N.J.

Dawson T.E., Mambelli S., Plamboeck A.H., Templer P.H. & Tu K.P. (2002) Stable isotopes in plant ecology. *Annual Review of Ecology and Systematics*, **33**, 507-559.

Day D.A., Krab K., Lambers H., Moore A.L., Siedow J.N., Wagner A.M. & Wiskich J.T. (1996) The cyanide-resistant oxidase: To inhibit or not to inhibit, that is the question. *Plant Physiology*, **110**, 1-2.

Ederli L., Morettini R., Borgogni A., Wasternack C., Miersch O., Reale L., Ferranti F., Tosti N. & Pasqualini S. (2006) Interaction between nitric oxide and ethylene in the induction of alternative oxidase in ozone-treated tobacco plants. *Plant Physiology*, **142**, 595-608.

Elsig J. & Leuenberger M.C. (2010) C-13 and O-18 fractionation effects on open splits and on the ion source in continuous flow isotope ratio mass spectrometry. *Rapid Communications in Mass Spectrometry*, **24**, 1419-1430.

Elthon T.E., Nickels R.L. & McIntosh L. (1989) Monoclonal-Antibodies to the Alternative Oxidase of Higher-Plant Mitochondria. *Plant Physiology*, **89**, 1311-1317.

Emerson S., Stump C., Wilbur D. & Quay P. (1999) Accurate measurement of O_2, N_2, and Ar gases in water and the solubility of N_2. *Marine Chemistry*, **64**, 337-347.

Epstein E. & Bloom A.J. (2005) *Mineral nutrition of plants : principles and perspectives*. (2nd ed.). Sinauer Associates, Sunderland, Mass.

Feng H.Q., Sun K., Li M.Q., Li H.Y., Li X., Li Y. & Wang Y.F. (2010) The expression, function and regulation of mitochondrial alternative oxidase under biotic stresses. *Molecular Plant Pathology*, **11**, 429-440.

Fiorani F., Umbach A.L. & Siedow J.N. (2005) The alternative oxidase of plant mitochondria is involved in the acclimation of shoot growth at low temperature. A study of Arabidopsis AOX1a transgenic plants. *Plant Physiology*, **139**, 1795-1805.

Florez-Sarasa I., Flexas J., Rasmusson A.G., Umbach A.L., Siedow J.N. & Ribas-Carbo M. (2011) *In vivo* cytochrome and alternative pathway respiration in leaves of *Arabidopsis thaliana* plants with altered alternative oxidase under different light conditions. *Plant Cell and Environment*, **34**, 1373-1383.

Florez-Sarasa I., Ostaszewska M., Galle A., Flexas J., Rychter A.M. & Ribas-Carbo M. (2009) Changes of alternative oxidase activity, capacity and protein content in leaves of *Cucumis sativus* wild-type and MSC16 mutant grown under different light intensities. *Physiologia Plantarum*, **137**, 419-426.

Florez-Sarasa I.D., Bouma T.J., Medrano H., Azcon-Bieto J. & Ribas-Carbo M. (2007) Contribution of the cytochrome and alternative pathways to growth respiration and maintenance respiration in *Arabidopsis thaliana*. *Physiologia Plantarum*, **129**, 143-151.

Fox J. & Weisberg S. (2011) *An R Companion to Applied Regression, 2nd Edition*. (2 ed.). Sage Publications, Los Angeles.

Fry B. (2006) *Stable Isotope Ecology*. Springer, New York.

Fry B., Brand W., Mersch F.J., Tholke K. & Garritt R. (1992) Automated analysis system for coupled $\delta^{13}C$ and $\delta^{15}N$ measurements. *Analytical Chemistry*, **64**, 288-291.

Gaston S., Ribas-Carbo M., Busquets S., Berry J.A., Zabalza A. & Royuela M. (2003) Changes in mitochondrial electron partitioning in response to herbicides inhibiting branched-chain amino acid biosynthesis in soybean. *Plant Physiology*, **133**, 1351-1359.

Gelhaye E., Rouhier N., Gerard J. (2004) A specific form of thioredoxin h occurs in plant mitochondria and regulates the alternative oxidase. *Proceedings of the National Academy of Sciences of the United States of America*, **101**, 14545-14550.

Gifford R.M. (2003) Plant respiration in productivity models: conceptualisation, representation and issues for global terrestrial carbon-cycle research. *Functional Plant Biology*, **30**, 171-186.

Gniazdowska A., Krawczak A., Mikulska M. & Rychter A.M. (1999) Low phosphate nutrition alters bean plants' ability to assimilate and translocate nitrate. *Journal of Plant Nutrition*, **22**, 551-563.

Gonzalez-Meler M.A., Blanc-Betes E., Flower C.E., Ward J.K. & Gomez-Casanovas N. (2009) Plastic and adaptive responses of plant respiration to changes in atmospheric CO_2 concentration. *Physiologia Plantarum*, **137**, 473-484.

Gonzalez-Meler M.A., Giles L., Thomas R.B. & Siedow J.N. (2001) Metabolic regulation of leaf respiration and alternative pathway activity in response to phosphate supply. *Plant Cell and Environment*, **24**, 205-215.

Gorham E. (1991) Northern peatlands - role in the carbon-cycle and probable responses to climatic warming. *Ecological Applications*, **1**, 182-195.

Gough L. (2001) Relative percent cover was measured for plant species on Arctic LTER experimental plots in moist acidic and moist non-acidic tundra, Toolik Field Station, Alaska, Arctic LTER 1999.

Gough L. (2009) Arctic LTER 2007: Relative percent cover was measured for plant species on Arctic LTER experimental plots in moist acidic tussock and dry heath tundra.

Gough L. & Hobbie S.E. (2003) Responses of moist non-acidic arctic tundra to altered environment: productivity, biomass, and species richness. *Oikos*, **103**, 204-216.

Guy R.D., Berry J.A., Fogel M.L. & Hoering T.C. (1989) Differential fractionation of oxygen isotopes by cyanide-resistant and cyanide-sensitive respiration in plants. *Planta*, **177**, 483-491.

Guy R.D. & Vanlerberghe G.C. (2005) Partitioning of respiratory electrons in the dark in leaves of transgenic tobacco with modified levels of alternative oxidase. *Physiologia Plantarum*, **125**, 171-180.

Hachiya T. & Noguchi K. (2011) Integrative response of plant mitochondrial electron transport chain to nitrogen source. *Plant Cell Reports*, **30**, 195-204.

Hachiya T., Watanabe C.K., Boom C. (2010) Ammonium-dependent respiratory increase is dependent on the cytochrome pathway in *Arabidopsis thaliana* shoots. *Plant Cell and Environment*, **33**, 1888-1897.

Hartley H.O. (1950) The maximum F-ratio as a short-cut test for heterogeneity of variance. *Biometrika*, **37**, 308-312.

Hayya J., Armstrong D. & Gressis N. (1975) A note on the ratio of two normally distributed variables. *Management Science Series a-Theory*, **21**, 1338-1341.

He Z.L.L., Yang X.E. & Stoffella P.J. (2005) Trace elements in agroecosystems and impacts on the environment. *Journal of Trace Elements in Medicine and Biology*, **19**, 125-140.

Hector A., von Felten S. & Schmid B. (2010) Analysis of variance with unbalanced data: an update for ecology & evolution. *Journal of Animal Ecology*, **79**, 308-316.

Henry B.K., Atkin O.K., Day D.A., Millar A.H., Menz R.I. & Farquhar G.D. (1999) Calculation of the oxygen isotope discrimination factor for studying plant respiration. *Australian Journal of Plant Physiology*, **26**, 773-780.

Hermans C., Hammond J.P., White P.J. & Verbruggen N. (2006) How do plants respond to nutrient shortage by biomass allocation? *Trends in Plant Science*, **11**, 610-617.

Hobbie S.E., Nadelhoffer K.J. & Hogberg P. (2002) A synthesis: The role of nutrients as constraints on carbon balances in boreal and arctic regions. *Plant and Soil*, **242**, 163-170.

Hodgson J.G., Montserrat-Marti G., Charles M. (2011) Is leaf dry matter content a better predictor of soil fertility than specific leaf area? *Annals of Botany*, **108**, 1337-1345.

Hoefnagel M.H.N., Millar A.H., Wiskich J.T. & Day D.A. (1995) Cytochrome and alternative respiratory pathways compete for electrons in the presence of pyruvate in soybean mitochondria. *Archives of Biochemistry and Biophysics*, **318**, 394-400.

Hoefnagel M.H.N., Rich P.R., Zhang Q.S. & Wiskich J.T. (1997) Substrate kinetics of the plant mitochondrial alternative oxidase and the effects of pyruvate. *Plant Physiology*, **115**, 1145-1153.

Hoefnagel M.H.N., Vaniren F. & Libbenga K.R. (1993) In suspension cultures of *Catharanthus roseus* the cyanide-resistant pathway is engaged in respiration by excess sugar in combination with phosphate or nitrogen starvation. *Physiologia Plantarum*, **87**, 297-304.

Hoefnagel M.H.N. & Wiskich J.T. (1998) Activation of the plant alternative oxidase by high reduction levels of the Q-pool and pyruvate. *Archives of Biochemistry and Biophysics*, **355**, 262-270.

Hultén E. (1968) *Flora of Alaska and neighboring territories*. Stanford University Press, Stanford, California, USA.

Huppe H.C. & Turpin D.H. (1994) Integration of carbon and nitrogen metabolism in plant and algal cells. *Annual Review of Plant Physiology and Plant Molecular Biology*, **45**, 577-607.

ISO/IEC (1995) *Evaluation of measurement data — Guide to the Expression of Uncertainty in Measurement*. International Organization for Standardization, Geneva.

Jones J.B. (2012) *Plant Nutrition and Soil Fertility Manual*. (2nd ed.). CRC Press, Hoboken.

Josse E.M., Simkin A.J., Gaffe J., Laboure A.M., Kuntz M. & Carol P. (2000) A plastid terminal oxidase associated with carotenoid desaturation during chromoplast differentiation. *Plant Physiology*, **123**, 1427-1436.

Juszczuk I., Malusa E. & Rychter A.M. (2001a) Oxidative stress during phosphate deficiency in roots of bean plants (*Phaseolus vulgaris* L.). *Journal of Plant Physiology*, **158**, 1299-1305.

Juszczuk I.M., Wagner A.M. & Rychter A.M. (2001b) Regulation of alternative oxidase activity during phosphate deficiency in bean roots (*Phaseolus vulgaris*). *Physiologia Plantarum*, **113**, 185-192.

Kirkup L. & Mulholland M. (2004) Comparison of linear and non-linear equations for univariate calibration. *Journal of Chromatography A*, **1029**, 1-11.

Kornfeld A., Horton T.W., Yakir D., Searle S.Y., Griffin K.L., Atkin O.K., Subke J.-A. & Turnbull M.H. (2012a) A field-compatible method for measuring alternative respiratory pathway activities in vivo using stable O2 isotopes. *Plant, Cell & Environment*, DOI: 10.1111/j.1365-3040.2012.02507.x.

Kornfeld A., Horton T.W., Yakir D. & Turnbull M. (2012b) Correcting for nonlinearity effects of continuous flow isotope ratio mass spectrometry across a wide dynamic range. *Rapid Communications in Mass Spectrometry*, **26**, 460–468.

Kraus E. & Lambers H. (2001) Leaf and root respiration of *Lolium perenne* populations selected for contrasting leaf respiration rates are affected by intra- and interpopulation interactions. *Plant and Soil*, **231**, 267-274.

Kroopnick P. & Craig H. (1972) Atmospheric Oxygen: Isotopic Composition and Solubility Fractionation. *Science*, **175**, 54-55.

Kruse J. & Adams M.A. (2008) Three parameters comprehensively describe the temperature response of respiratory oxygen reduction. *Plant Cell and Environment*, **31**, 954-967.

Laemmli U.K. (1970) Cleavage of structural proteins during assembly of head of bacteriophage-T4. *Nature*, **227**, 680-&.

Lambers H., Robinson S. & Ribas-Carbo M. (2005) Regulation of respiration *in vivo*. In: *Plant Respiration: From Cell to Ecosystem* (eds H. Lambers & M. Ribas-Carbo), pp. 1-15. Spring, Dordrecht, The Netherlands.

Lee R.B. & Ratcliffe R.G. (1993) Subcellular distribution of inorganic-phosphate, and levels of nucleoside triphosphate, in mature maize roots at low external phosphate concentrations - measurements with P-31-NMR. *Journal of Experimental Botany*, **44**, 587-598.

Lei T., Feng H., Sun X., Dai Q.L., Zhang F., Liang H.G. & Lin H.H. (2010) The alternative pathway in cucumber seedlings under low temperature stress was enhanced by salicylic acid. *Plant Growth Regulation*, **60**, 35-42.

Lennon A.M., Neuenschwander U.H., Ribas-Carbo M., Giles L., Ryals J.A. & Siedow J.N. (1997) The effects of salicylic acid and tobacco mosaic virus infection on the alternative oxidase of tobacco. *Plant Physiology*, **115**, 783-791.

Lennon A.M., Pratt J., Leach G. & Moore A.L. (1995) Developmental regulation of respiratory activity in pea leaves. *Plant Physiology*, **107**, 925-932.

Loveys B.R., Atkinson L.J., Sherlock D.J., Roberts R.L., Fitter A.H. & Atkin O.K. (2003) Thermal acclimation of leaf and root respiration: an investigation comparing inherently fast- and slow-growing plant species. *Global Change Biology*, **9**, 895-910.

Luz B., Barkan E., Bender M.L., Thiemens M.H. & Boering K.A. (1999) Triple-isotope composition of atmospheric oxygen as a tracer of biosphere productivity. *Nature*, **400**, 547-550.

Meeuse B.J.D. (1975) Thermogenic respiration in aroids. *Annual Review of Plant Physiology and Plant Molecular Biology*, **26**, 117-126.

Merchant S.S., Allen M.D., Kropat J., Moseley J.L., Long J.C., Tottey S. & Terauchi A.M. (2006) Between a rock and a hard place: Trace element nutrition in Chlamydomonas. *Biochimica et Biophysica Acta (BBA) - Molecular Cell Research*, **1763**, 578-594.

Merritt D.A. & Hayes J.M. (1994) Factors controlling precision and accuracy in isotope-ratio-monitoring mass-spectrometry. *Analytical Chemistry*, **66**, 2336-2347.

Millar A.H., Atkin O.K., Menz R.I., Henry B., Farquhar G. & Day D.A. (1998) Analysis of respiratory chain regulation in roots of soybean seedlings. *Plant Physiology*, **117**, 1083-1093.

Millar A.H., Bergersen F.J. & Day D.A. (1994) Oxygen affinity of terminal oxidases in soybean mitochondria. *Plant Physiology and Biochemistry*, **32**, 847-852.

Millar A.H., Whelan J., Soole K.L. & Day D.A. (2011) Organization and regulation of mitochondrial respiration in plants. In: *Annual Review of Plant Biology, Vol 62* (eds S.S. Merchant, W.R. Briggs, & D. Ort), pp. 79-104. Annual Reviews, Palo Alto.

Millenaar F.F., Benschop J.J., Wagner A.M. & Lambers H. (1998) The role of the alternative oxidase in stabilizing the in vivo reduction state of the ubiquinone pool and the activation state of the alternative oxidase. *Plant Physiology*, **118**, 599-607.

Millenaar F.F., Gonzalez-Meler M.A., Fiorani F., Welschen R., Ribas-Carbo M., Siedow J.N., Wagner A.M. & Lambers H. (2001) Regulation of alternative oxidase activity in six wild monocotyledonous species. An *in vivo* study at the whole root level. *Plant Physiology*, **126**, 376-387.

Millenaar F.F. & Lambers H. (2003) The alternative oxidase: in vivo regulation and function. *Plant Biology*, **5**, 2-15.

Miller R.E., Grant N.M., Giles L., Ribas-Carbo M., Berry J.A., Watling J.R. & Robinson S.A. (2011) In the heat of the night - alternative pathway respiration drives thermogenesis in *Philodendron bipinnatifidum*. *New Phytologist*, **189**, 1013-1026.

Montgomery D.B. & Morrison D.G. (1973) A note on adjusting R^2. *Journal of Finance*, **28**, 1009-1013.

Nagel O.W., Waldron S. & Jones H.G. (2001) An off-line implementation of the stable isotope technique for measurements of alternative respiratory pathway activities. *Plant Physiology*, **127**, 1279-1286.

Nicotra A.B., Atkin O.K., Bonser S.P. (2010) Plant phenotypic plasticity in a changing climate. *Trends in Plant Science*, **15**, 684-692.

Noguchi K., Go C.S., Terashima I., Ueda S. & Yoshinari T. (2001) Activities of the cyanide-resistant respiratory pathway in leaves of sun and shade species. *Australian Journal of Plant Physiology*, **28**, 27-35.

Noguchi K., Taylor N.L., Millar A.H., Lambers H. & Day D.A. (2005) Response of mitochondria to light intensity in the leaves of sun and shade species. *Plant Cell and Environment*, **28**, 760-771.

Noguchi K. & Terashima I. (2006) Responses of spinach leaf mitochondria to low N availability. *Plant Cell and Environment*, **29**, 710-719.

Noguchi K. & Yoshida K. (2008) Interaction between photosynthesis and respiration in illuminated leaves. *Mitochondrion*, **8**, 87-99.

Oba Y. & Poulson S.R. (2009) Oxygen isotope fractionation of dissolved oxygen during reduction by ferrous iron. *Geochimica Et Cosmochimica Acta*, **73**, 13-24.

Padua M., Aubert S., Casimiro A., Bligny R., Millar A.H. & Day D.A. (1999) Induction of alternative oxidase by excess copper in sycamore cell suspensions. *Plant Physiology and Biochemistry*, **37**, 131-137.

Penuelas J., Ribas-Carbo M. & Giles L. (1996) Effects of allelochemicals on plant respiration and oxygen isotope fractionation by the alternative oxidase. *Journal of Chemical Ecology*, **22**, 801-805.

Pinheiro J.C. & Bates D.M. (2000) *Mixed-effects models in S and S-PLUS*. Springer-Verlag, New York.

Plaxton W.C. (1996) The organization and regulation of plant glycolysis. *Annual Review of Plant Physiology and Plant Molecular Biology*, **47**, 185-214.

Plaxton W.C. & Podesta F.E. (2006) The functional organization and control of plant respiration. *Critical Reviews in Plant Sciences*, **25**, 159-198.

Priault P., Vidal G., De Paepe R. & Ribas-Carbo M. (2007) Leaf age-related changes in respiratory pathways are dependent on complex I activity in *Nicotiana sylvestris*. *Physiologia Plantarum*, **129**, 152-162.

R Development Core Team (2011) R: A language and environment for statistical computing. R Foundation for Statistical Computing, Vienna, Austria.

Rayleigh L. (1902) On the distillation of binary mixtures. *Philosophical Magazine*, **4**, 521-537.

Reich P.B., Tjoelker M.G., Machado J.L. & Oleksyn J. (2006) Universal scaling of respiratory metabolism, size and nitrogen in plants. *Nature*, **439**, 457-461.

Reich P.B., Tjoelker M.G., Pregitzer K.S., Wright I.J., Oleksyn J. & Machado J.L. (2008) Scaling of respiration to nitrogen in leaves, stems and roots of higher land plants. *Ecology Letters*, **11**, 793-801.

Rhoads D.M. & Subbaiah C.C. (2007) Mitochondrial retrograde regulation in plants. *Mitochondrion*, **7**, 177-194.

Ribas-Carbo M., Lennon A.M., Robinson S.A., Giles L., Berry J.A. & Siedow J.N. (1997) The regulation of electron partitioning between the cytochrome and alternative pathways in soybean cotyledon and root mitochondria. *Plant Physiology*, **113**, 903-911.

Ribas-Carbo M., Robinson S. & Giles L. (2005a) The application of the oxygen-isotope technique to assess respiratory pathway partitioning. In: *Plant Respiration: From Cell to Ecosystem* (eds H. Lambers & M. Ribas-Carbo), pp. 31-42. Springer, Dordrecht, The Netherlands.

Ribas-Carbo M., Robinson S.A., Gonzalez-Meler M.A., Lennon A.M., Giles L., Siedow J.N. & Berry J.A. (2000) Effects of light on respiration and oxygen isotope fractionation in soybean cotyledons. *Plant Cell and Environment*, **23**, 983-989.

Ribas-Carbo M., Taylor N.L., Giles L. (2005b) Effects of water stress on respiration in soybean leaves. *Plant Physiology*, **139**, 466-473.

Richardson S.J., Peltzer D.A., Allen R.B., McGlone M.S. & Parfitt R.L. (2004) Rapid development of phosphorus limitation in temperate rainforest along the Franz Josef soil chronosequence. *Oecologia*, **139**, 267-276.

Roberts B.J., Russ M.E. & Ostrom N.E. (2000) Rapid and precise determination of the $\delta^{18}O$ of dissolved and gaseous dioxygen via gas chromatography-isotope ratio mass spectrometry. *Environmental Science & Technology*, **34**, 2337-2341.

Robinson S.A., Ribas-Carbo M., Yakir D., Giles L., Reuveni Y. & Berry J.A. (1995) Beyond sham and cyanide - opportunities for studying the alternative oxidase in plant respiration using oxygen-isotope discrimination. *Australian Journal of Plant Physiology*, **22**, 487-496.

Robinson S.A., Yakir D., Ribas-Carbo M., Giles L., Osmond C.B., Siedow J.N. & Berry J.A. (1992) Measurements of the engagement of cyanide-resistant respiration in the crassulacean acid metabolism plant *Kalanchoe daigremontiana* with the use of online oxygen isotope discrimination. *Plant Physiology*, **100**, 1087-1091.

Royston P. (1995) A remark on algorithm AS-181 - The W-test for normality. *Applied Statistics-Journal of the Royal Statistical Society Series C*, **44**, 547-551.

Ruban A.V. & Horton P. (1994) Spectroscopy of nonphotochemical and photochemical quenching of chlorophyll fluorescence in leaves - evidence for a role of the light-harvesting complex of photosystem-II in the regulation of energy-dissipation. *Photosynthesis Research*, **40**, 181-190.

Searle S.Y., Bitterman D.S., Thomas S., Griffin K.L., Atkin O.K. & Turnbull M.H. (2011a) Respiratory alternative oxidase responds to both low- and high-temperature stress in *Quercus rubra* leaves along an urban-rural gradient in New York. *Functional Ecology*, **25**, 1007-1017.

Searle S.Y., Thomas S., Griffin K.L., Horton T., Kornfeld A., Yakir D., Hurry V. & Turnbull M.H. (2011b) Leaf respiration and alternative oxidase in field-grown alpine grasses respond to natural changes in temperature and light. *New Phytologist*, **189**, 1027-1039.

Searle S.Y. & Turnbull M.H. (2011) Seasonal variation of leaf respiration and the alternative pathway in field-grown Populus x canadensis. *Physiologia Plantarum*, **141**, 332-342.

Shaver G.R. & Chapin F.S. (1980) Response to fertilization by various plant-growth forms in an Alaskan tundra - nutrient accumulation and growth. *Ecology*, **61**, 662-675.

Shaver G.R. & Chapin F.S. (1995) Long-term responses to factorial NPK fertilizer treatment by Alaskan wet and moist tundra sedge species. *Ecography*, **18**, 259-275.

Shaver G.R. & Chapin III F.S. (1991) Production: Biomass relationships and element cycling in contrasting arctic vegetation types. *Ecological Monographs*, **61**, 1-23.

Sieger S.M., Kristensen B.K., Robson C.A., Amirsadeghi S., Eng E.W.Y., Abdel-Mesih A., Moller I.M. & Vanlerberghe G.C. (2005) The role of alternative oxidase in modulating carbon use efficiency and growth during macronutrient stress in tobacco cells. *Journal of Experimental Botany*, **56**, 1499-1515.

Smith A.M. & Stitt M. (2007) Coordination of carbon supply and plant growth. *Plant, Cell & Environment*, **30**, 1126-1149.

Spotl C. & Vennemann T.W. (2003) Continuous-flow isotope ratio mass spectrometric analysis of carbonate minerals. *Rapid Communications in Mass Spectrometry*, **17**, 1004-1006.

Stevens P.R. (1968) *A chronosequence of soils near the Franz Josef Glacier*. Thesis (Ph D), Lincoln College, 1968.

Szal B., Jolivet Y., Hasenfratz-Sauder M.P., Dizengremel P. & Rychter A.M. (2003) Oxygen concentration regulates alternative oxidase expression in barley roots during hypoxia and post-hypoxia. *Physiologia Plantarum*, **119**, 494-502.

Talla S., Riazunnisa K., Padmavathi L., Sunil B., Rajsheel P. & Raghavendra A.S. (2011) Ascorbic acid is a key participant during the interactions between chloroplasts and mitochondria to optimize photosynthesis and protect against photoinhibition. *Journal of Biosciences*, **36**, 163-173.

Tessier J.T. & Raynal D.J. (2003) Use of nitrogen to phosphorus ratios in plant tissue as an indicator of nutrient limitation and nitrogen saturation. *Journal of Applied Ecology*, **40**, 523-534.

Thermo Electron Corporation (2004) *Finnigan GasBench II Operating Manual*. Thermo Electron Corporation, Bremen, Germany.

Tjoelker M.G., Oleksyn J., Reich P.B. & Zytkowiak R. (2008) Coupling of respiration, nitrogen, and sugars underlies convergent temperature acclimation in *Pinus banksiana* across wide-ranging sites and populations. *Global Change Biology*, **14**, 782-797.

Turnbull M.H., Tissue D.T., Griffin K.L., Richardson S.J., Peltzer D.A. & Whitehead D. (2005) Respiration characteristics in temperate rainforest tree species differ along a long-term soil-development chronosequence. *Oecologia*, **143**, 271-279.

Turnbull M.H., Whitehead D., Tissue D.T., Schuster W.S.F., Brown K.J. & Griffin K.L. (2003) Scaling foliar respiration in two contrasting forest canopies. *Functional Ecology*, **17**, 101-114.

Turner B.L., Condron L.M., Richardson S.J., Peltzer D.A. & Allison V.J. (2007) Soil organic phosphorus transformations during pedogenesis. *Ecosystems*, **10**, 1166-1181.

Turunen J., Tomppo E., Tolonen K. & Reinikainen A. (2002) Estimating carbon accumulation rates of undrained mires in Finland - application to boreal and subarctic regions. *Holocene*, **12**, 69-80.

Umbach A.L. & Siedow J.N. (1993) Covalent and noncovalent dimers of the cyanide-resistant alternative oxidase protein in higher-plant mitochondria and their relationship to enzyme activity. *Plant Physiology*, **103**, 845-854.

Valentini R., Matteucci G., Dolman A.J. (2000) Respiration as the main determinant of carbon balance in European forests. *Nature*, **404**, 861-865.

Vance C.P., Uhde-Stone C. & Allan D.L. (2003) Phosphorus acquisition and use: critical adaptations by plants for securing a nonrenewable resource. *New Phytologist*, **157**, 423-447.

Venables W.N. & Ripley B.D. (2002) *Modern applied statistics with S*. (4th ed.). Springer, New York.

Vigani G., Maffi D. & Zocchi G. (2009) Iron availability affects the function of mitochondria in cucumber roots. *New Phytologist*, **182**, 127-136.

Vitousek P.M., Porder S., Houlton B.Z. & Chadwick O.A. (2010) Terrestrial phosphorus limitation: Mechanisms, implications, and nitrogen-phosphorus interactions. *Ecological Applications*, **20**, 5-15.

Watanabe C.K., Hachiya T., Takahara K., Kawai-Yamada M., Uchimiya H., Uesono Y., Terashima I. & Noguchi K. (2010) Effects of AOX1a deficiency on plant growth, gene expression of respiratory components and metabolic profile under low-nitrogen stress in *Arabidopsis thaliana*. *Plant and Cell Physiology*, **51**, 810-822.

Watling J.R., Robinson S.A. & Seymour R.S. (2006) Contribution of the alternative pathway to respiration during thermogenesis in flowers of the sacred lotus. *Plant Physiology*, **140**, 1367-1373.

Weger H.G. & Dasgupta R. (1993) Regulation of alternative pathway respiration in *Chlamydomonas reinhardtii* (Chlorophyceae). *Journal of Phycology*, **29**, 300-308.

Weisberg S. (2005) *Applied Linear Regression, Third Edition*. John Wiley & Sons, Inc.

Werner R.A., Rothe M. & Brand W.A. (2001) Extraction of CO_2 from air samples for isotopic analysis and limits to ultra high precision $\delta^{18}O$ determination in CO_2 gas. *Rapid Communications in Mass Spectrometry*, **15**, 2152-2167.

Whitehead D., Boelman N.T., Turnbull M.H., Griffin K.L., Tissue D.T., Barbour M.M., Hunt J.E., Richardson S.J. & Peltzer D.A. (2005) Photosynthesis and reflectance indices for rainforest species in ecosystems undergoing progression and

retrogression along a soil fertility chronosequence in New Zealand. *Oecologia*, **144**, 233-244.

Whitehead D., Griffin K.L., Turnbull M.H., Tissue D.T., Engel V.C., Brown K.J., Schuster W.S.F. & Walcroft A.S. (2004) Response of total night-time respiration to differences in total daily photosynthesis for leaves in a Quercus rubra L. canopy: implications for modelling canopy CO2 exchange. *Global Change Biology*, **10**, 925-938.

Wieser M.E. & Berglund M. (2009) Atomic weights of the elements 2007 (IUPAC Technical Report). *Pure and Applied Chemistry*, **81**, 2131-2156.

Wilhelm C. & Selmar D. (2011) Energy dissipation is an essential mechanism to sustain the viability of plants: The physiological limits of improved photosynthesis. *Journal of Plant Physiology*, **168**, 79-87.

Witkowski E.T.F. & Lamont B.B. (1991) Leaf specific mass confounds leaf density and thickness. *Oecologia*, **88**, 486-493.

Wright I.J., Reich P.B., Westoby M. (2004) The worldwide leaf economics spectrum. *Nature*, **428**, 821-827.

Yoshida K., Terashima I. & Noguchi K. (2007) Up-regulation of mitochondrial alternative oxidase concomitant with chloroplast over-reduction by excess light. *Plant and Cell Physiology*, **48**, 606-614.

Yoshida K., Watanabe C.K., Hachiya T., Tholen D., Shibata M., Terashima I. & Noguchi K. (2011) Distinct responses of the mitochondrial respiratory chain to long- and short-term high-light environments in *Arabidopsis thaliana*. *Plant Cell and Environment*, **34**, 618-628.

Zeeman M.J., Werner R.A., Eugster W., Siegwolf R.T.W., Wehrle G., Mohn J. & Buchmann N. (2008) Optimization of automated gas sample collection and isotope ratio mass spectrometric analysis of $\delta^{13}C$ of CO_2 in air. *Rapid Communications in Mass Spectrometry*, **22**, 3883-3892.

Zhang L.T., Zhang Z.S., Gao H.Y., Xue Z.C., Yang C., Meng X.L. & Meng Q.W. (2011) Mitochondrial alternative oxidase pathway protects plants against photoinhibition by alleviating inhibition of the repair of photodamaged PSII through preventing formation of reactive oxygen species in Rumex K-1 leaves. *Physiologia Plantarum*, **143**, 396-407.

Zhu L., Li Y.M., Li L., Yang J.H. & Zhang M.F. (2011) Ethylene is involved in leafy mustard systemic resistance to Turnip mosaic virus infection through the mitochondrial alternative oxidase pathway. *Physiological and Molecular Plant Pathology*, **76**, 166-172.

Appendices

Appendix 1. The cutting room floor

The main purpose for this appendix is to allow the numbering on the remaining appendices to correspond with their associated chapter numbers in the main text. Here I briefly discuss some aspects of the project the either weren't successful (but deserve mention) or didn't fit elsewhere.

A1.1. The mobile mass spectrometer

At the outset of this project, we had intended to use a mobile mass spectrometer to conduct field measurements at the Franz Josef chronosequence. I went to the University of York, England to learn how to use it under the tutelage of Phil Ineson and and Jens Arne-Subke. We then shipped it over to New Zealand, drove it from Christchurch to the West Coast and did our best to make it work. Alas, we did not succeed, though not for lack of trying. Still, I put enough effort in trying not to at least mention it and to thank Phil and Jens for their generosity, time, and tolerance.

A1.2. Hawkesbury experimental forest

Another experiment that did not bear fruit was a brief foray to the University of Western Sydney, to investigate respiratory electron partitioning at an experiment run by David Tissue. Greenhouse rooms had been set up in a factorial trial of three CO_2 levels × two temperature regimes × 2 water treatments × 2 species (one drought tolerant, the other less-so). We made a valiant effort in performing all the necessary incubations, including inhibition treatments. The discrimination data came back completely uniform. This would have been perfectly acceptable if the endpoint discrimination values had shown some separation. Unfortunately, that was not the case and we therefore had no way of determining if the lack of variation in uninhibited tissue was due to lack of change in partitioning or because something intrinsically problematic in measuring discrimination in those Eucalyptus species. If I had to guess, it would be that the problem was in the inhibitions (we used vacuum infiltration) and, like my *Griselinia* experiment described here (Chapter 5), the greenhouse was just not light enough to keep the AP active.

A1.3. Gas leakage and/or oxidation of septa

Because we had stored many vials at room temperature before I had the epiphany to try storing them in the freezer, I spent some time seeing if we could correct the storage contamination in those vials. I could not figure out a way to do so, as stated in Chapter 3. Along the way, though, I did find evidence that something was consuming O_2 in the vials over the long term. Presumably this was due to microbial consumption of the septa. I can think of no other way that the O_2/N_2 ratio declined in these vials. I did confirm that the vials were not overpressurized. Based on the leak rates shown in Table 3.2, it would have taken a fairly substantial overpressure to produce the small decline (around 2%) that I detected.

A1.4. Proof of concept for my in-vial respiration measurements

Here is a graph comparing O_2 consumption rates I computed from the mass spectrometry data using Eqn 4.3 and CO_2 production rates measured by Owen Atkin during the same field season at the Arctic LTER, Toolik Alaska. Each "cross" represents a single species-treatment group. Error bars show the standard error for each set of replicates.

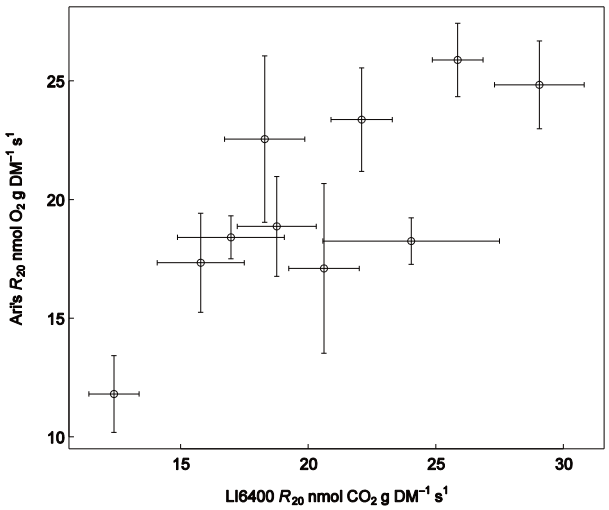

Fig S1.1. Comparison of in-vial respiration measurements (Eqn 4.3) against standard equipment.
The x axis represents respiration values measured using a LICOR LI-6400 at Toolik Alaska. The y axis corresponds to values I obtained from the mass spectrometry data.

A1.5. CN increases respiration rates despite being effective

With the gaseous HCN inhibitions, respiration rates generally increased over controls, based on in-vial measurements, even though discrimination increased considerably. [Meeuse (1975) had also observed this effect.] Exposing the tissue to HCN for longer periods (> 30 minutes) eventually caused respiration to decline, but so did measured discrimination. My conclusion: making total R go down is not necessarily a good indicator of inhibition.

A1.6. Temperature may affect measured *D*

I did a one-off experiment using KCN-inhibited Griselinia leaves to see if incubation temperature affected measured discrimination. These are based on a single replicate each (6 vials + 1 blank). Based on this very small sample, one may want to be cautious in interpreting results obtains at low temperatures.

T_{incub}	D_{KCN} (‰)	$D_{control}$ (‰)
30 ºC	29.0 ± 0.2	20.62 ± 0.16
20 ºC	29.0 ± 0.3	20.62 ± 0.06
11 ºC	27.8 ± 0.5	20.01 ± 0.11

Appendix 2. Supporting Information for Chapter 2

A2.1. Can isotope ratios be corrected using A_{28} and A_{32} directly?

Using Eqn 1 to correct A_{28} and A_{32} against "known" concentrations of N_2 and O_2, respectively, was adequate only for higher absolute concentrations, even if separate regressions were run for samples with higher (+) and lower (o) values of F_{28}.

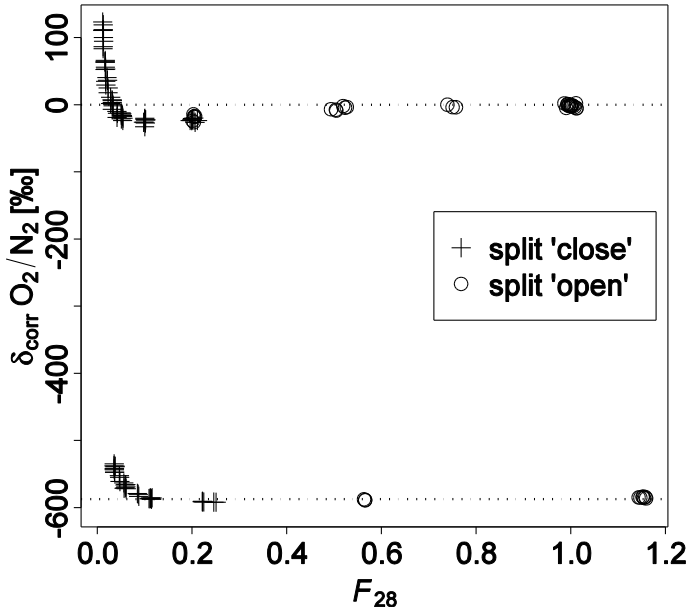

Fig S2.1a. Corrections based on a single regression per species over the entire range of values.

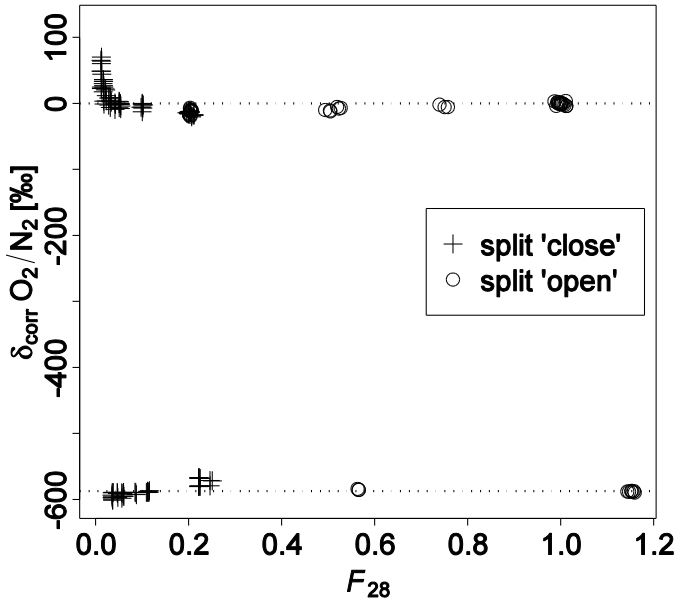

Fig S2.1b. Piecewise correction. Separate fits were computed above and below F_x = 0.2.

A2.2. How Gasbench II responds to vial over- and under-pressure

Vials were flushed with air or with O_2-free N_2. For some vials, gas was removed via a syringe, leaving a partial vacuum. The total pressure in some of these partially-evacuated vials was returned to 1 atm by injecting O_2-free He. Additional air-flushed vials were overpressurized by injecting either air or He after the cap had been sealed: injecting He increased the total pressure, reduced [O_2] and [N_2] but left $pO_2 + pN_2$ unchanged, whereas injecting air increased both total and partial pressures without changing concentration.

The sum of measured $O_2 + N_2$ was first plotted against vial $pO_2 + pN_2$ (a). Neither under- nor over-pressurized vials lie on the 1:1 line (dashed line). Furthermore, air vials overpressurized with He fall below the 1:1 line, suggesting that concentration and not absolute pressure determined the final signal. The signal for vials pressurized with additional air rises only 3.7 ± 0.6 % for a 100% increase in pressure (grey line).

When plotted against concentration (b), however, the data for fully- and over-pressurized vials lie on the 1:1 line. The signal for underpressurized vials, however, is still too high, indicating that additional $O_2 + N_2$ had entered the vial by suction through the Gasbench II open sampling path.

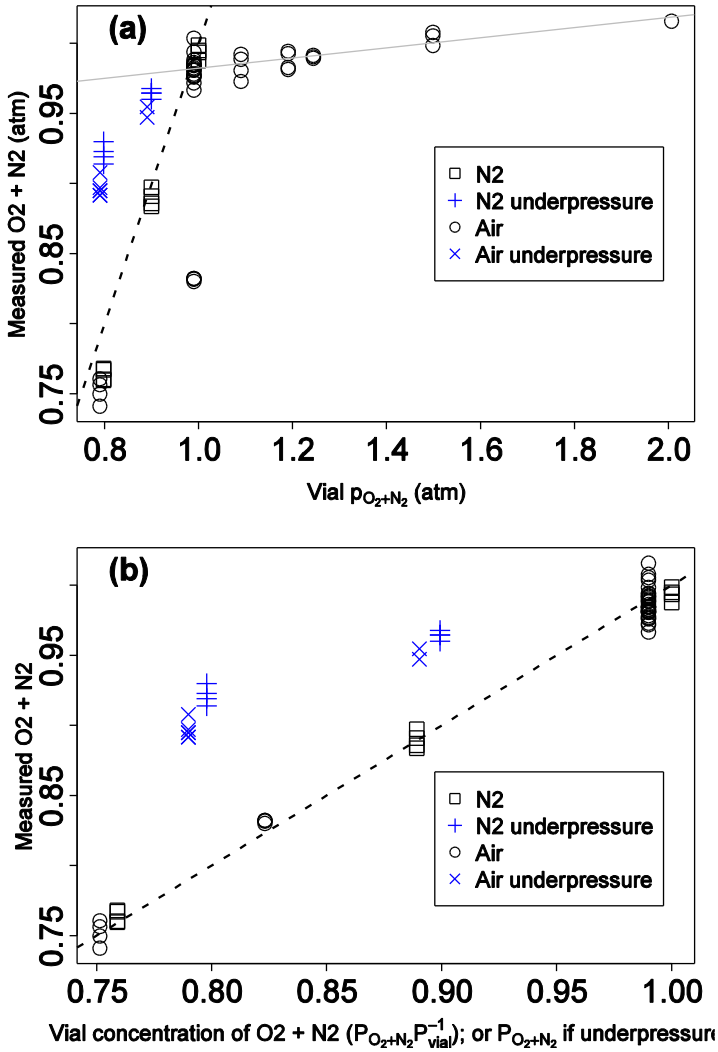

Figure S2.2. a, b. See description, above. (*atm* = atmospheres)

A2.3. Variability introduced by the correction equations

The data that I used for calibration is naturally clustered at various concentrations of the analyte, as can be seen in Figure S1, above, or Figures 3–5. Since the corrections are generally small, any variation within a cluster should reflect the instrument precision. One can compare the within cluster-variability with the overall variability to estimate the extent of error in the correction equations. (Note: although the standard deviation of the group means may seem like a good estimate of calibration error, it actually overestimates the error since variation in the group means is also influenced by the standard error of each group.) I compute the overall error, which includes both instrument error and correction error, as the standard deviation (SD) of all corrected measurements, while the instrument SD is calculated by first subtracting the cluster mean from each corrected measurement.

Standard deviation is defined as $SD = \sqrt{\frac{1}{n-1}\sum_{i=1}^{n}(x_i - \bar{x})^2}$, for n values, x_i, whose mean is $\bar{x}$.

Comparison of the first two columns of Table S2.3 shows that the correction equations generally added very little error to the overall measurement error.

Table S2.3. Overall variability in the corrected calibrations (*Overall SD) vs.* instrument variability (*Instrument SD)*. The final column represents an upper bound on the error introduced by the correction equations since *Between-cluster SD* includes a reduced amount of instrument error.

	Overall SD	*Instrument SD*	*Between-cluster SD*
$F_{32} > 0.15$			
$\delta^{18}O$	0.08‰	0.06‰	0.04‰
$\delta^{15}N$	0.05‰	0.04‰	0.02‰
$\delta O_2/N_2$	2.6‰	2.5‰	0.06‰
$F_{32} < 0.15$			
$\delta^{18}O$	0.22‰	0.21‰	0.06‰
$\delta^{15}N$	0.07‰	0.06‰	0.01‰
$\delta O_2/N_2$	7.6‰	7.4‰	2.0‰

Another consideration is uncertainty in the accuracy of the calibration. For measurements in which the value relative to an international measurement standard must be reported, uncertainty due to the calibration must be accounted for in addition to measurement uncertainty.

Here I show the correction equation that was reported in the Results section of the main text but also showing the uncertainties in each term, determined as standard errors of the regression coefficients, as reported by the *lm* function in R.

$$\delta^{18}\mathrm{O} = \frac{\delta^{18}\mathrm{O}_{\mathrm{meas}} + (0.0127 \pm 0.0005)/F_{32} - (0.476 \pm 0.034)F_{32} + (3.333 \pm 0.024)}{(1.0069 \pm 0.0040) - (0.00070 \pm 0.00013)/F_{32}}$$

One can simplify the uncertainty analysis by noting that, typically, only one of F_{32} or $1/F_{32}$ dominates the correction. At high values of F_{32}, i.e. values above 0.1, the F_{32} term dominates, so that using standard propagation of uncertainty methods,(ISO/IEC, 1995) the total uncertainty in the correction – i.e. all terms except $\delta^{18}\mathrm{O}_{\mathrm{meas}}$ – should be very nearly

$$\sqrt{(0.034F_{32})^2 + 0.024^2} \leq 0.04\text{‰}\ (F_{32}\text{ near 1}),$$

since the impact of the $1/F_{32}$ terms will be very small and the denominator is essentially 1.0. This "accuracy" uncertainty could be combined with the previously determined uncertainty in $\delta^{18}\mathrm{O}_{\mathrm{meas}}$ to provide an overall uncertainty in point estimates. For example, if the measurement uncertainty is found to be 0.06‰ for large F_{32} (O_2 in Table S2.3), the total uncertainty would be

$$\sqrt{0.06^2 + (0.034F_{32})^2 + 0.024^2} \leq 0.07\text{‰}\ (\text{combined uncertainty; } F_{32}\text{ near 1}).$$

The added uncertainty due to calibration is therefore no more than 1‰.

To complete the analysis, I examine the uncertainty at the lower end of the F_{32} range, where $1/F_{32}$ dominates (ignoring the term in the denominator whose uncertainty is much smaller):

$$\sqrt{(0.0005/F_{32})^2 + 0.024^2} \leq 0.055\text{‰}\ (F_{32}\text{ near 0.01}),$$

and, except for F_{32} <0.02, the uncertainty is less than 0.04‰. I can therefore conclude that for my data the added uncertainty due to the regression is modest across the entire calibration range.

Finally, I note that this analysis of uncertainty only applies to the measurement of a single point. In many environmental and biological applications we are more interested in the relative differences among several points. In these cases, the contribution of the constant term cancels out, so that the net added uncertainty due to the correction is even smaller than indicated by the "point" estimate just described.

A2.4. The need for two calibration standards

When trying to determine coefficients using the regression:

$$R = \frac{a_1 A_1^2 + A_1 + c_1}{a_2 A_2^2 + b_2 A_2 + c_2} \qquad \text{(S2.1)}$$

the constant terms, c_i, can only be determined if more than one value of R is available in the dataset (i.e. more than one calibration standard is needed). A nonlinear regression, for example, will not converge. To understand why a second dilution series is needed, one can consider two general functions, $f(x)$ and $g(y)$ for which the sets of points $\{(x_1, y_1), (x_2, y_2), \ldots, (x_i, y_i), \ldots\}$ have been selected such that

$$R = \frac{f(x_i)}{g(y_i)} = k, \qquad \text{(S2.2)}$$

is constant for all (x_i, y_i) in the set, i.e., the measured signal values for the dilution series of a single substance. The graph of $g(Y)$ vs. $f(X)$ is a straight line through the origin (line R):

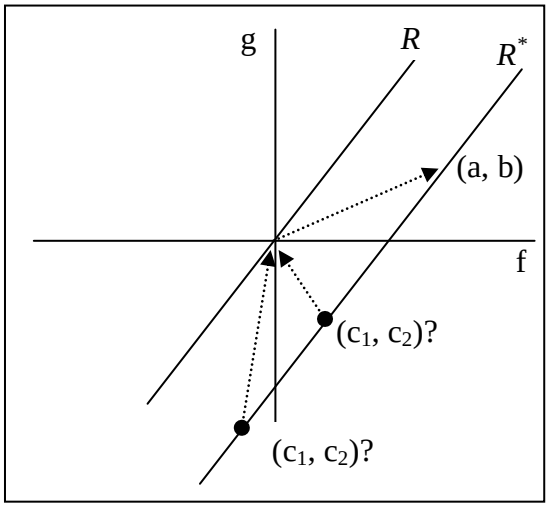

Now consider f^* and g^*, which differ from f and g only by a constant, a and b, respectively, i.e.

$$R^* = \frac{f^*(X)}{g^*(Y)} = \frac{f(X) + a}{g(Y) + b}, \qquad \text{(S2.3)}$$

The line is translated from (0, 0) to (a, b) and proportionality is lost. When trying to recover the original function, however, i.e. to find the constants such that:

$$\frac{f^*(X) - c_1}{g^*(Y) - c_2} = k, \qquad \text{(S2.4)}$$

any point on the translated line can be used (see diagram, above). Specifically, for any point c_1 on the f axis, one can choose the corresponding point $c_2 = b + (c_1 - a)k$ that will suffice.

Only the true offset, (a, b), however, will correct f^* and g^* for any value of R. To illustrate the problem, consider a second set of points, $\{(x_i', y_i')\}$, i.e. a second dilution series, such that

$$R' = \frac{f(x_i')}{g(y_i')} = k', \qquad \text{(S2.5)}$$

where $k' \neq k$. The two lines intersect at the origin as in the figure, below. The translated lines now intersect at (a, b), and the only solution that will translate *both* lines back to the origin (i.e. recover the proportionality for both standards) is $c_1 = a$, $c_2 = b$.

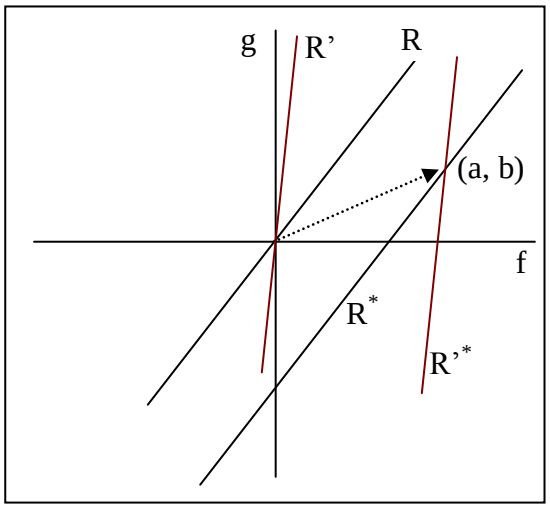

A2.5. Comparing Equation 8 with known equations

Equation 8 in the main text reduces to two other established formulae under appropriate conditions: a change-of-standard equation(Fry, 2006) (Equation S2.7, below) and the conventional linearity correction(Thermo Electron Corporation, 2004) (Equation, below).

Starting with Eqn 2.8, renumbered here as Equation S2.6:

$$\delta_{meas} = -a_1(\delta_{meas} + 1000)A_1 + a_2(\delta + 1000)A_2 + c_2(\delta - \delta_z)\frac{1}{A_2} + b_2\delta + 1000(b_2 - 1) \quad \text{(S2.6)}$$

The change-of-standard equation converts δ values expressed relative to one standard gas in terms of a new standard:

$$\delta^a_{std2} = \frac{\delta^a_{std1} - \delta^{std2}_{std1}}{\frac{\delta^{std2}_{std1}}{1000} + 1}, \quad \text{(S2.7)}$$

where $\delta^x_{std\,i} = (R_x/R_{std\,i} - 1)\times 1000$.

The change-of-standard equation, which is intended for actual (as opposed to measured) δ values, can be derived from Equation S2.6 by requiring that the signals are proportional to the physical quantities (i.e., $a_i = c_i = 0$). The remaining terms in Equation S2.6 are:

$$\delta_{meas} = b_2\delta + 1000(b_2 - 1). \quad \text{(S2.8)}$$

Let $\beta_0 = 1000(b_2 - 1)$, then $b_2 = \beta_0/1000 + 1$, so

$$\delta_{meas} = \left(\frac{\beta_0}{1000} + 1\right)\delta + \beta_0.$$

Solving for δ yields:

$$\delta = \frac{\delta_{meas} - \beta_0}{\frac{\beta_0}{1000} + 1},$$

which has the same form as Equation S2.7. Thus, the "intercept" term, $\beta_0 \equiv 1000(b_2 - 1)$, in Equation S2.6 represents (at least in the reduced case) the δ value of the measured standard relative to the instrument's reference tank gas (*std1*). Importantly, if one does not want to change the reference ratio, then $\beta_0 = 0$ and $b_2 = 1$. This fact will be used next, to relate Equation S2.6 to the conventional linearity correction.

In the conventional linearity correction mentioned in the introductory section of the main text, a correction coefficient, β_1 is determined by linear regression on a dilution series using:

$$\delta_{meas} = \beta_1 A_2 + \delta, \quad \text{(S2.9)}$$

where A_2 is the signal corresponding to the major isotope, and the intercept term, δ, is regarded as the "true" isotope ratio. The measured ratio for a sample of unknown δ value can then be corrected by subtracting $\beta_1 A_2$.

This additive correction corresponds to Equation S2.6 when $1/A_2$ is sufficiently small, *and* the curvature due to a_1 is small, *and* the reference ratio does not need to be changed. Under those conditions, terms 1, 3 and 5 become insignificant so that Equation S2.6 is reduced to:

$$\delta_{meas} = a_2(\delta + 1000)A_2 + \delta . \qquad \text{(S2.10)}$$

Comparing the coefficients of A_2 in Equations S2.9 and S2.10, the slope of the conventional linearity correction, β_1, corresponds to $a_2(\delta + 1000)$, thus indicating that the linear change in δ_{meas} with respect to A_2 is due to curvature in the response to M_2 (since a_2 is the coefficient of the quadratic term). Furthermore, the correction coefficient, β_1, in Equation S2.9 is, strictly speaking, only valid for substances with an isotope ratio identical to that of the calibration standard, since the coefficient in Equation S2.10 includes $\delta + 1000$. In practice, however, the range of δ values being measured, together with the magnitude of the β_1 term itself, may be small enough that error introduced by ignoring changes in δ values is well below the instrument precision.

Equation S2.9, however, does break down as $1/A_2$ increases, i.e., for small values of A_2. In addition, for values such as $\delta O_2/N_2$, which can vary by more than 500‰, it may not be safe to ignore the effect of δ values on the A_2 coefficient in Equation S2.10.

A2.6. A nonlinear regression/correction in δ values

Starting with Equation S2.1 in section A 2.4, divide top and bottom by A_2. In the numerator, substitute R_{meas}/A_1 for $1/A_2$, then factor out R_{meas}. Finally, multiply both sides by $1000/R_{std}$ and convert to δ notation:

$$(\delta + 1000) = \frac{(\delta_{meas} + 1000)(a_1 A_1 + 1 + c_1 / A_1)}{a_2 A_2 + b_2 + c_2 / A_2} . \qquad \text{(S2.11)}$$

The result can be used to correct δ_{meas} directly, but has the disadvantage of requiring A_1 values, which may not be reported with as high precision as the A_2 values. In addition, while the δ_{meas} values are corrected for drift over time, the corresponding A_1 values are not drift-corrected by ISODAT. In either case, $A_1 = {}^{34}R_{ref}\, A_{32}\, (1 + \delta_{meas}/1000)$ is more suitable, where ${}^{34}R_{ref}$ is the reference ratio specified in the *Evaluation@xx* tab of the ISODAT method. (See the following section for more details.)

A2.7. Area values for the minor isotope in ISODAT NT

Two problems arise when using peak area values to correct reported ratios. (1) Whereas isotope ratios (R $^{34}O_2/^{32}O_2$, for example) and delta values ($d^{18}O/^{16}O$, for example) are corrected for drift in the electronics over time, the reported areas, whether raw (*rArea 34*, e.g.) or "cooked" (*Area 34*), are not corrected in this way. (2) By default, ISODAT reports area values to only three decimal places. Since *Area 34*, for example, is generally less than one, it is never reported with more than 3 digits of precision, which is not adequate for computing ratios with sub-permil precision. Three decimal places in δ values, on the other hand corresponds to seven significant digits due to the mathematical properties of δ when reported in permil units.

To get the best precision and accuracy, I therefore recommend using ISODAT values:

d 18O/16O *as is*.
Area 32 = *as is* (or *rArea 32* / 1000)
Area 34 = ${}^{34}R_{ref}$ × *Area 32* × (1+ *d 18O/16O*/1000)
$F_{34} = F_{32} \times (1000 + d\ 18O/16O) / (1000 + d\ 18O/16O_{atm})$
R 34O2/32O2 = 0.0040105 × *rR 34O2/32O2* / ref *rR 34O2/32O2*,

where the value ${}^{34}R_{ref}$ is the reference ratio derived from the *Evaluation@O2* specification in the ISODAT method. The value is reported as *R 34O2/32O2* for the reference peak, eg. 0.0040105 for O_2 by default. The value ref *rR 34O2/32O2* is the raw ratio for the reference peak..

Note: This discussion of precision is based on the default precision values in ISODAT. It is possible to change these defaults globally for all area values in the *Configurator* program but that will not solve the lack of a drift correction in Area values.

Appendix 3. Supporting information for Chapter 3

A3.1. Table S3.1 Results of simulated respiration experiments.

Table S3.1. Results of simulated respiration experiments.

D_0	D_{final}	*min f**	*noise*	*reps*	*'linear' D* ‰	*'linear'* R^2	$1–\beta_{curv}$	*'quadratic' D* ‰
Noise only								
31		***0.7***	***yes***	***4***	31.00 ± 0.18	0.9993 ± 0.0002	0.07*	31.0 ± 0.6
31		***0.5***	***yes***	***4***	± 0.12	0.9998 ± 0.0001	0.08*	± 0.4
Variable D, no contamination								
31	***25***	***0.7***	***no***	***1***	25.0 ± 0.8	0.996	1	30.4 ± 0.2
31	***25***	***0.7***	***yes***	***1***	± 0.4	0.995 ± 0.002	0.72	± 1.5
31	***25***	***0.7***	***yes***	***4***	± 0.2	0.994 ± 0.001	1.00	± 0.8
31	***28***	***0.7***	***no***	***1***	28.0 ± 0.4	0.9992	1	30.71 ± 0.08
31	***28***	***0.7***	***yes***	***1***	± 0.4	0.9987 ± 0.0008	0.42	± 1.0
31	***28***	***0.7***	***yes***	***4***	± 0.17	0.9985 ± 0.0004	0.99	± 0.6
Constant D, 5% contamination, δ_{contam} *= 0‰*								
31		***0.7***	***no***	***1***	30.67 ± 0.05	0.99999	1	31.04 ± 0.01
31		***0.7***	***yes***	***1***	± 0.4	0.9995 ± 0.0004	0.10	± 1.3
31		***0.7***	***yes***	***4***	± 0.19	0.9993 ± 0.00024	0.09	± 0.6
31		***0.5***	***no***	***1***	30.22 ± 0.14	0.9999	1	31.18 ± 0.06
31		***0.5***	***yes***	***1***	± 0.2	0.9997 ± 0.0001	0.21	± 0.7
31		***0.5***	***yes***	***4***	± 0.13	0.9996 ± 0.0002	0.78	± 0.4
Constant D, 5% contamination, δ_{contam} *= –9‰*								
31		***0.7***	***no***	***1***	30.15 ± 0.07	0.99998	1	30.60 ± 0.01
31		***0.7***	***yes***	***4***	± 0.18	0.9992 ± 0.0003	0.14	± 0.7
31		***0.5***	***no***	***1***	29.61 ± 0.17	0.9999	1	30.76 ± 0.06
31		***0.5***	***yes***	***4***	± 0.13	0.9996 ± 0.0001	0.89	± 0.3

* Since H_o is true in this case, 1–β should equal 0.05, i.e. α, in theory.

The first five columns indicate the model conditions: initial *D* (D_0), final *D* (D_{final}), extent of respiration (*min* f^*), added noise, and number of replicates (*reps*). Each replicate consisted of 6 points. The output variables are reported as mean ± SD of 500 simulation runs if noise was added; otherwise the uncertainty corresponds to standard error of the regression coefficient. Result values are: *D* computed using Eqn 4 (*'linear' D*), R^2 of that regression (*'linear'* R^2), statistical power for the lack-of-fit test ($1–\beta_{curv}$), and *D* computed using Eqn 7 (*'quadratic' D*). Noise, when added was normally distributed with SD similar to our instrumental precision: 0.06‰ for $\delta^{18}O$ and 0.0006 for f^*.

A3.2. Supporting figures

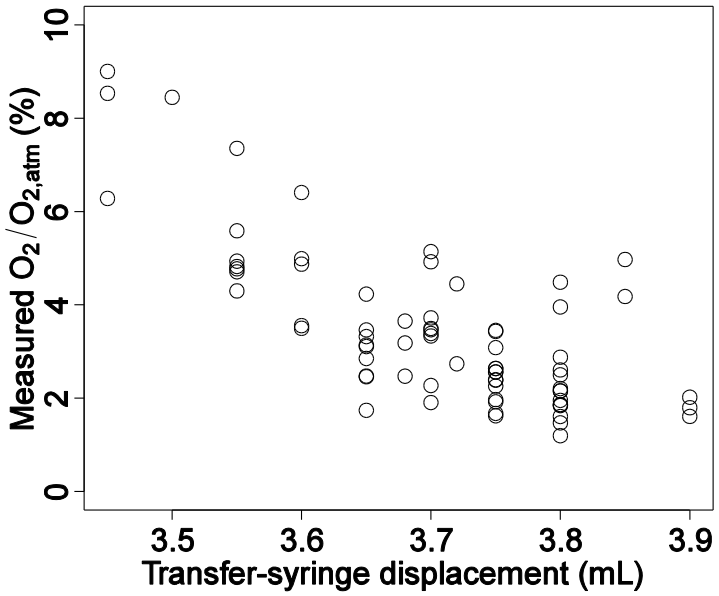

Figure S3.1. Estimating vacuum quality based on transfer-syringe displacement. Net displacement of the transfer-syringe plunger was plotted against the subsequently measured percent of atmospheric O_2 in blank vials. Displacement greater than 3.6 mL did not correlate with actual contamination. Below 3.6 mL, however, the contamination in the vial increases.

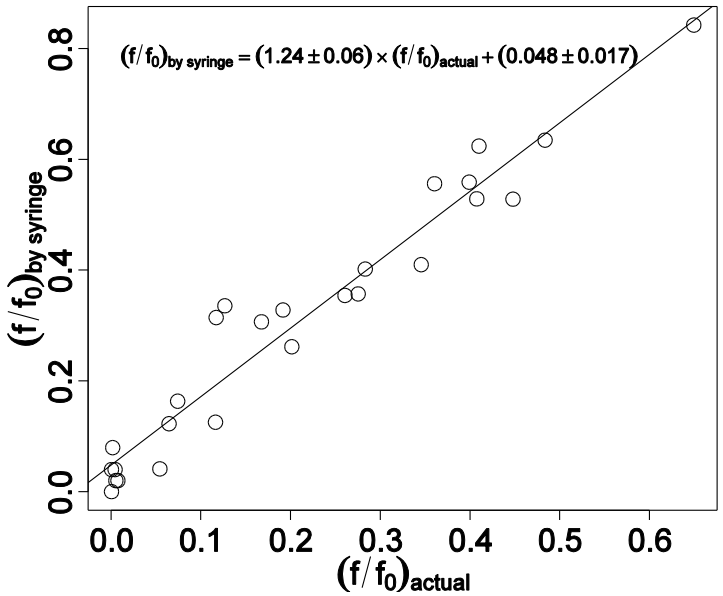

Figure S3.2. Estimating O_2 consumption by syringe displacement. $(f/f_0)_{actual}$ was computed from the mass spectrometer values; $(f/f_0)_{by\ syringe}$ was computed as described in Supporting Information Appendix S1c. Syringe displacement correlated well with the actual O_2 consumption, with $R^2 = 0.94$

Figure S3.3: Images of tissue volume effects treatments. *G. littoralis* (top row L–R: 2 and 6 strips) and *A. serrata* leaves (bottom row L–R: 4, 12) in incubation vials.

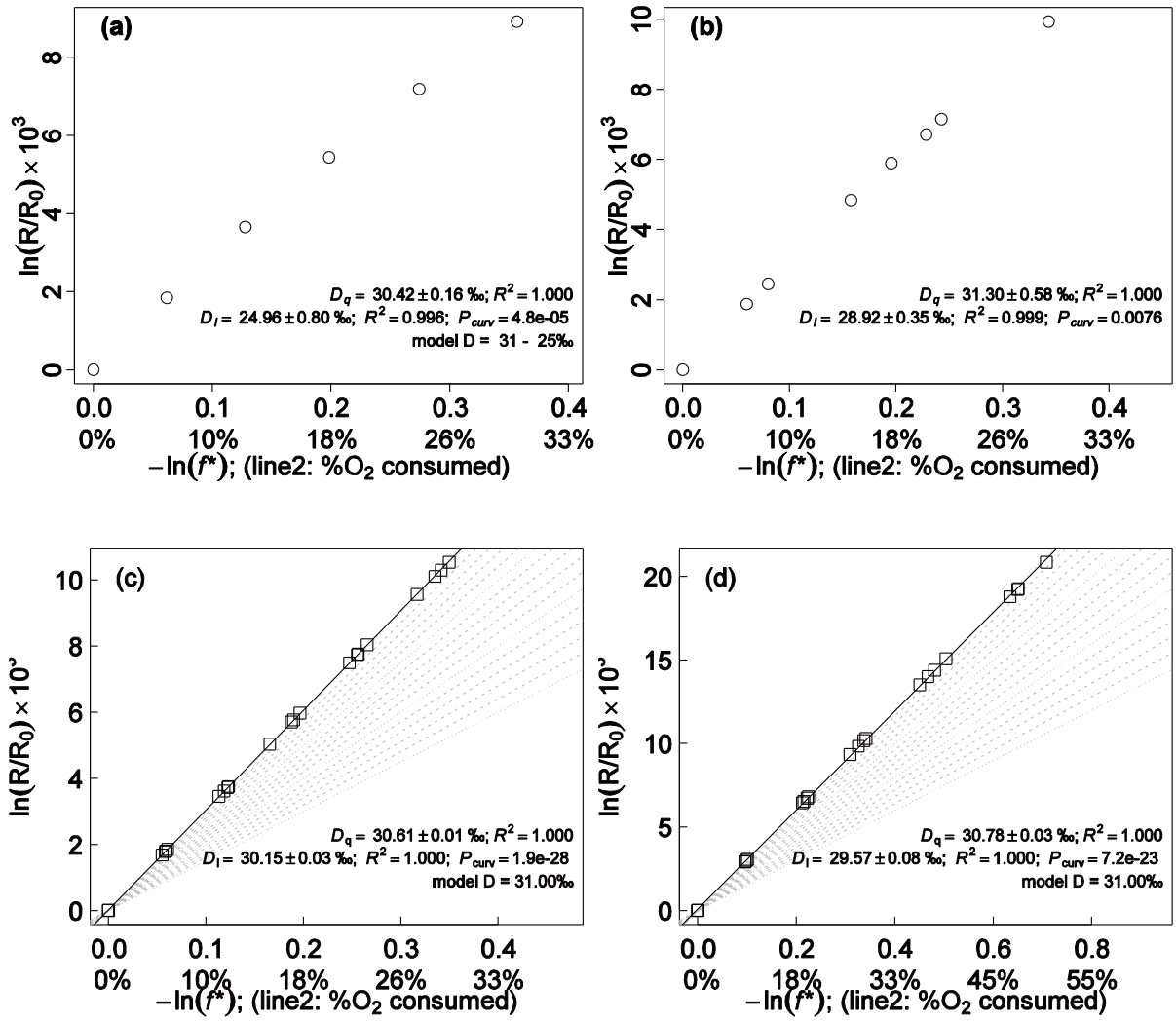

Figure S3.4: Curvature may be difficult to see. (a) Figure 2a without guide lines. D_{model} changes from 31 to 25‰ (b) Figure 3a without the guide lines – actual soybean KCN inhibition. (c) Simulated data with 5% contamination having $\delta^{18}O$ = –9‰ without added noise produces curvature that is not visibly apparent at 30% drawdown, but P_{curv} is highly significant. (d) Curvature is just barely visible at 50% drawdown. Note that in both cases linearly computed D is more than 2 SE less than the model value of 31‰. The solid line in (c) and (d) represents the linear regression line.

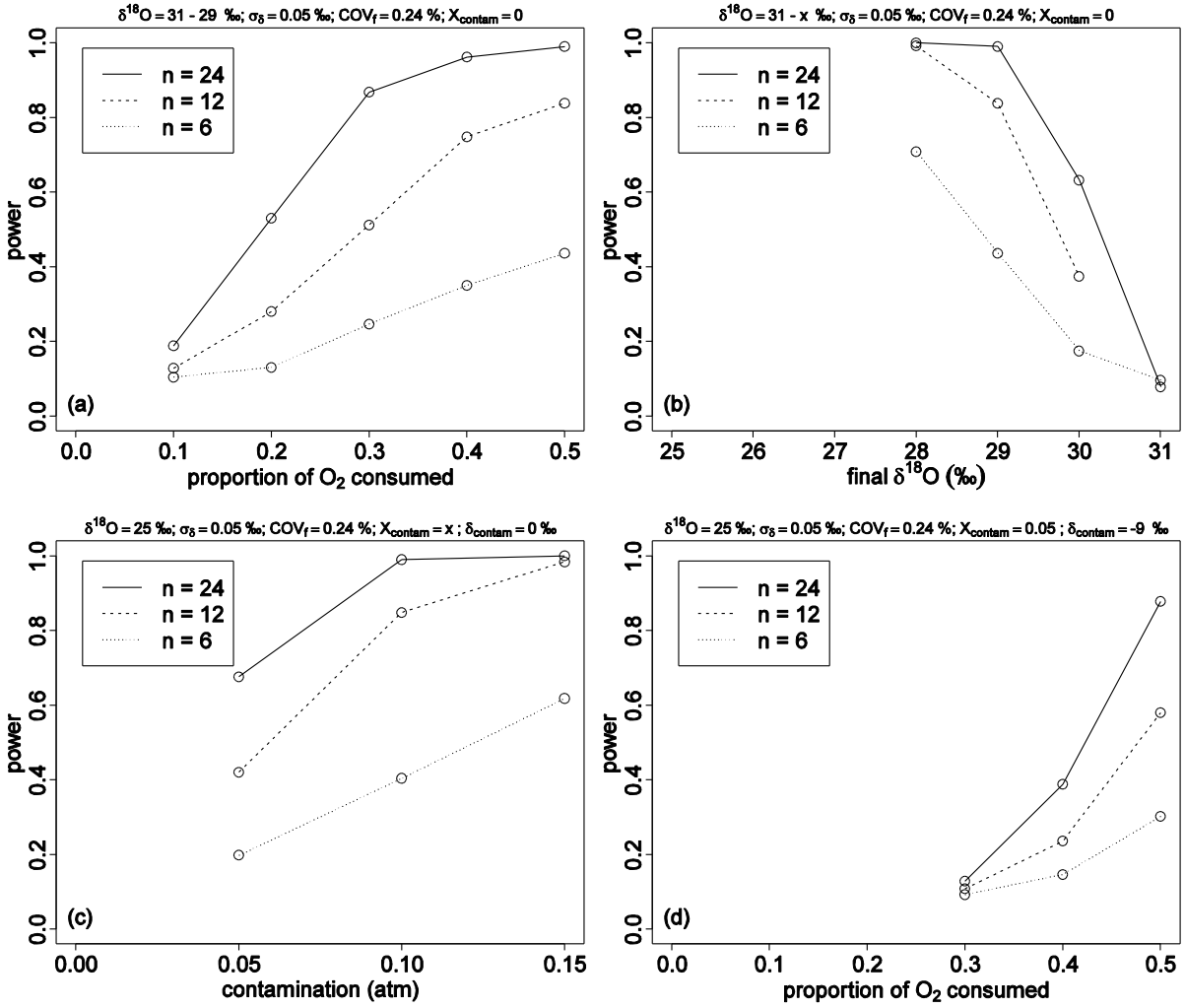

Figure S3.5. Statistical power to detect curvature (a) versus the maximum proportion of O_2 consumed by respiration as D_{model} changes from 31‰ to 29‰, (b) versus extent of decline in D_{model} from 31‰ to the indicated *x* value, (c) versus degree of initial contamination in the storage vial and (d) versus maximum proportion of O_2 consumed by respiration (initial contamination of 5% with $\delta^{18}O = –9‰$). Increasing measurement noise also reduces statistical power (data not shown).

Points connected by the solid lines correspond to 24 samples (four replicates), dashed lines: 12 samples (two replicates), dotted lines: 6 samples (one replicates). Power was computed based on 500 simulated experiments with measurement error of 0.05‰ in $\delta^{18}O$ and 0.0006 in O_2/N_2. (Machine precision similar to our equipment.) Based on (a), 24 points would be needed to reliably detect curvature due a 2‰ change in *D* with 30% O_2 consumption but only 12 points would be needed if O_2 consumption went to 50%.

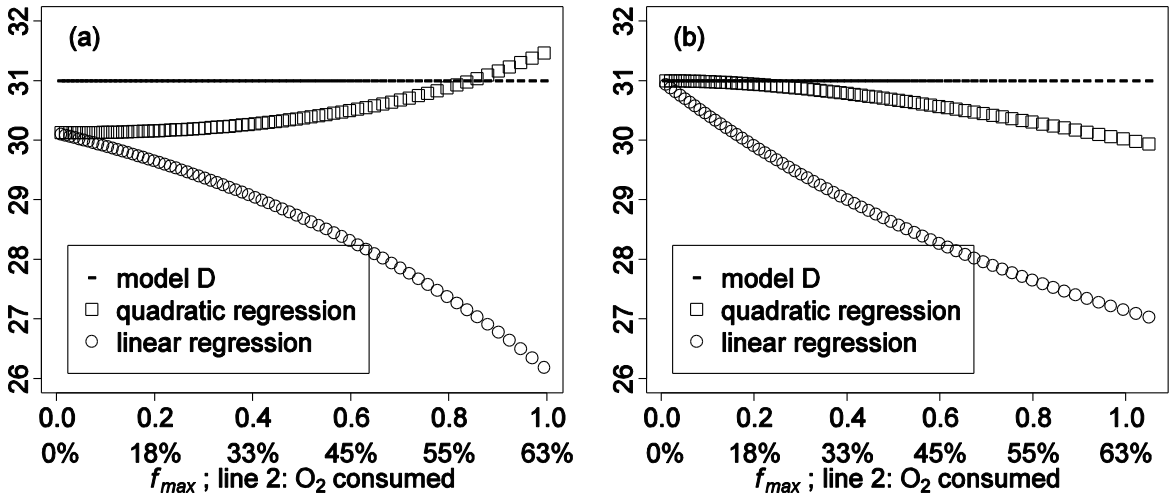

Figure S3.6. Computed *D* as a function of maximum O_2 consumption in the face of (a) uncorrected 'severe' contamination of 0.1 atm having $\delta^{18}O = -9‰$ and (b) declining *D* from initial value of 31‰ at a rate of 0.06‰ per percent O_2 consumed (so that $D_{model} = 28‰$ when 50% of the oxygen has been consumed). Each point represents a regression on six points distributed evenly from zero to the indicated x value with D_{model} distributed evenly from the starting value to the final value.

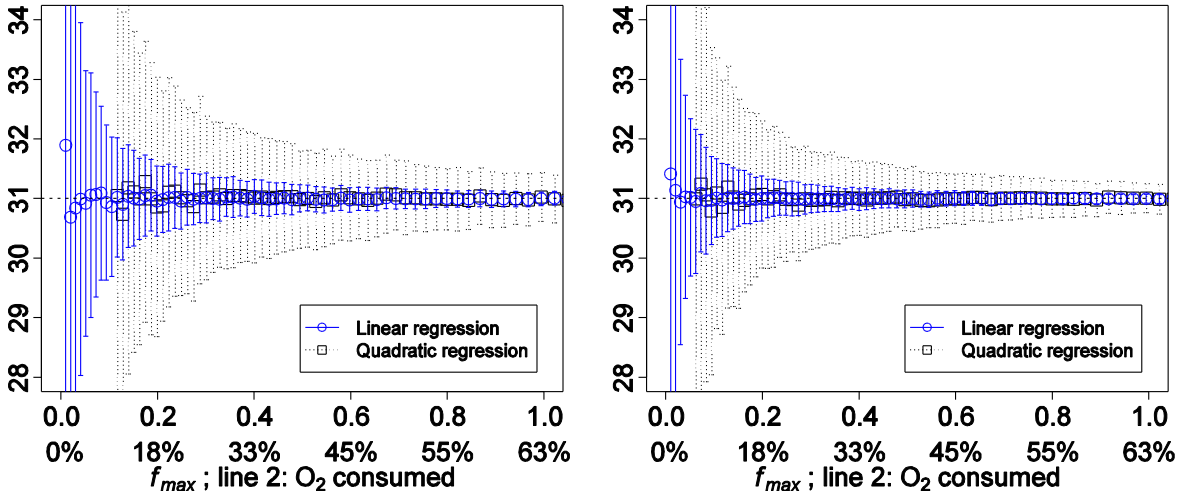

Figure S3.7. Standard error of the regression versus total O_2 consumption with (a) moderate and (b) low measurement noise ($\sigma_\delta = 0.1$ versus 0.06‰ and $\sigma_{O2/N2} = 0.00065$ versus 0.0005). Each point represents the mean of 400 repetitions of a six-point regression whose maximum O_2 consumption corresponds with the *x* coordinate. Error bars indicate the standard error of the regression coefficient determined as the standard deviation of the 400 repetitions. Model *D* was 31‰ in all cases.

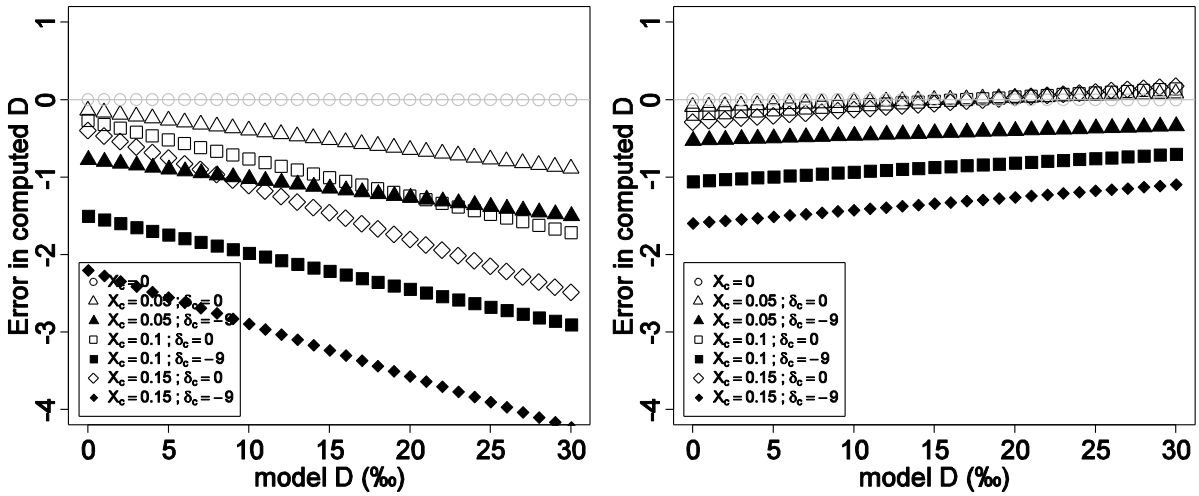

Figure S3.8. Error in computed *D* versus actual *D* due to various degrees of uncorrected contamination (a) when computed using the linear regression (b) when computed using the quadratic regression. Each data point represents a six-point regression with points evenly distributed between 0 and 50% O_2 consumption.

(Note: Error due to curvature does not appear to be sensitive to actual *D*. For example, a 3‰ decrease in *D* over the course of the incubation will lower linearly computed *D* by 3‰ and quadratic *D* by 0.5‰ regardless of the starting value of actual *D*.)

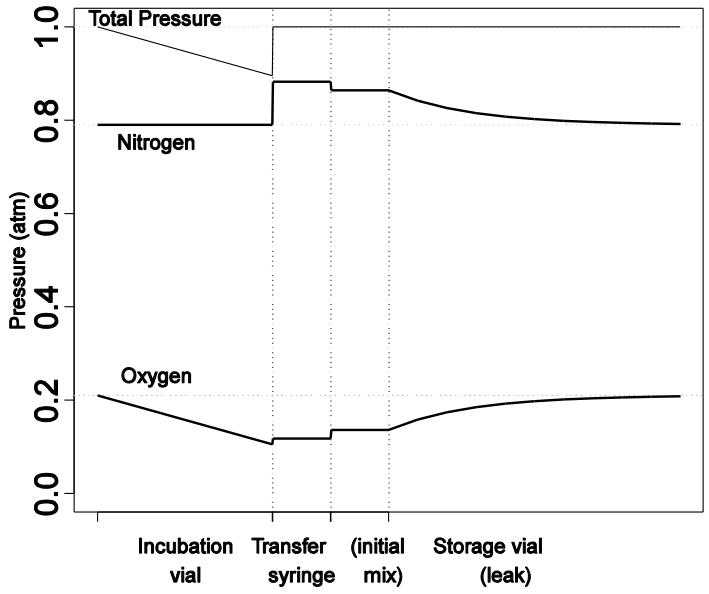

Figure S3.9. Changes in total pressure and partial pressures of N_2 and O_2 during a respiration experiment and subsequent storage. Total pressure declines in the incubation vial due to the combined action of respiration and the CO_2 trap. The transfer process equalizes pressure with the atmosphere, resulting in an increase in both pO_2 and pN_2. Contamination in the storage vials brings both values closer to atmospheric levels, as do diffusional effects over time.

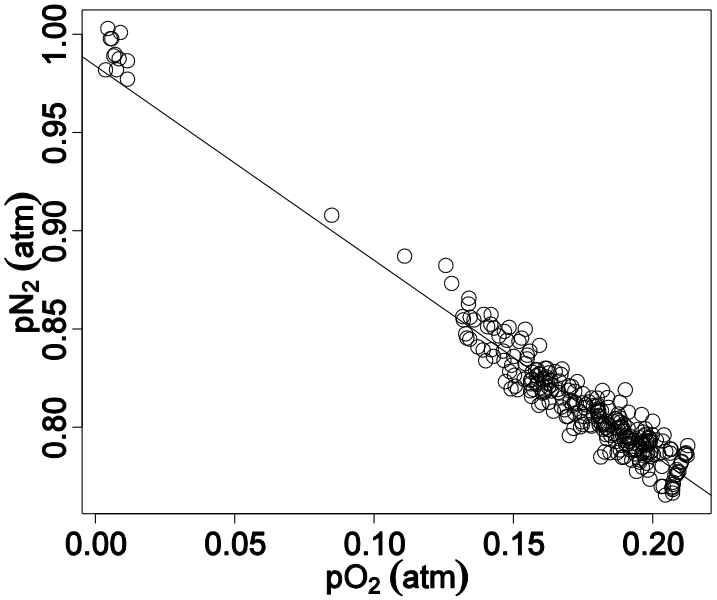

Figure S3.10. Measured changes in partial pressures of N_2 and O_2 during respiratory incubations (uncorrected for contamination). Values measured in the mass spectrometer confirm that N_2 in the storage vial rises as O_2 is consumed (see Supporting Information Appendix S2b). The points at the top left are N_2 blanks. The regression line, computed without the N_2 blanks, has an intercept of 0.983 ± 0.004 atm, consistent with the expected value of 0.99 atm. N_2 blanks are above this line because they are also Ar-free.

A3.3. Miscellaneous technical notes

The following are brief technical notes, mostly on the methods described in the main paper. More details on the methods along with a description suitable for designing a lab procedure can be found in the accompanying Lab Protocol document.

A3.3.1. Variable time *vs.* variable mass.

Variable time incubation is essential if one suspects that *D* changes over the course of the incubation – such as for inhibition treatments – whereas constant time/variable mass incubations are much simpler to coordinate, use less plant tissue, and can also be used to confirm a lack of tissue-volume effects.

A3.3.2. Alternative CO_2 trap.

I have recently experimented with using soda lime (Sofnolime #1025 GB, Molecular Products Limited , Essex, UK) instead of KOH as a CO_2 trap. Sofnolime has the advantage of not being hygroscopic, of being less soluble during the gas-transfer step, and potentially presenting greater surface area than a KOH pellet. The disadvantages are that the holder must be capped and perforated to prevent the grains from spilling out. The volume of the holder is therefore larger than for the KOH pellets. Preliminary tests indicate that there was no effect of the larger holder on computed discrimination and that Sofnolime was slightly better at scrubbing CO_2.

A3.3.3. Sample size, incubation time, and estimating O_2 consumption.

Unlike previous methods, I do not measure respiration during the tissue incubations. Instead, respiration rates are estimated in advance in order to estimate the ideal amount of tissue and incubation time needed. I have used standard lab and field equipment such as the LI-COR LI-6400 (Licor Environmental, Nebraska, USA) or Hansatech LD2 gas-phase oxygen electrode (Hansatech Instruments, Norfolk, England). Alternatively one may prepare incubation vials as described in the Materials and Methods section and then perform the initial gas-transfer step. The difference in volume between liquid injected and gas ejected using well-lubricated syringes can be used to estimate the O_2 consumption using the following formula (Fig S2):

$$(f / f_0)_{bysyringe} = \frac{V_{liquidinjected} - V_{gasejected}}{0.21 \times (V_{vial} - V_{plant} - V_{other})}.$$

This method assumes that a working CO_2 trap is in the incubation vial. One should be cautious in interpreting displacements less than 0.5 mL, however.

A3.3.4. Transfer solution.

Buffered “displacement solution,” pH 6, was prepared by adding a single pellet of KOH or NaOH to 0.4 M Boric acid. This solution serves two purposes (1) it buffers the plant tissue against the strong alkalinity of the CO_2 trap as it dissolves in the transfer liquid during gas transfer, and (2) it simplifies cleanup by maintaining pH of 8 – 9 after complete dissolution of the KOH pellet.

A3.3.5. Determining in-vial respiration.

I computed in-vial rates of respiration using the mass spectrometry data together with measured tissue volume, mass, and duration. Tissue volume was estimated as the fresh mass (FM) of each tissue sample multiplied by the specific volume of representative samples – determined by water-displacement in a 10 mL graduated cylinder. Dry mass (DM) was either

measured directly after drying the samples at 60°C for at least 48h, or based on FM multiplied by the DM/FM of representative samples.

The in-vial dark respiration rate, R_d, was then computed as

$$R_d\ (nmol\ g^{-1}\ s^{-1}) = \frac{0.21 f^* \times (V_{vial} - V_{plant} - V_{other})}{mass \times t} \frac{10^6 P}{R_{gas} T},$$

where the volumes in mL are: V_{vial}, the incubation vial volume (12.15 mL, determine by mass after filling with water); V_{plant}, the tissue volume; V_{other}, the volume of the CO_2 trap and moistened paper strip, if present. The remaining variables are: *mass* – either FM or DM – in grams; *t*, the incubation time in seconds; *P*, the atmospheric pressure in atm; R_{gas}, the ideal gas constant (0.082 mL atm K^{-1} $mmol^{-1}$); and *T*, the incubation temperature in Kelvins.

A3.3.6. Transfer contamination.

Because of its small magnitude, I had difficulty characterizing the exact amount and composition of transfer contamination. Initial experiments were conducted by subtracting the O_2 content of evacuated vials directly injected N_2 from that found in vial into which N_2 had been transferred from pre-flushed incubation vials. $\delta^{18}O_{transfer}$ was computed by mass balance using Eqn 5 in the main text. These tests, repeated over two sessions estimated $O_{2,transfer}$ as 1.3 ± 0.2% $_{O2atm}$ with $\delta^{18}O_{transfer}$ of –2.9 ± 0.4‰ (mean ± SE; n=41) in one session and 1.0 ± 0.6% $_{O2atm}$ with $\delta^{18}O_{transfer}$ = –0.5 ± 0.6‰ in the second session (n=44). Since the variability in evacuation quality (±1% $_{O2atm}$) is large relative to the magnitude of the transfer contamination, I then tried transferring O_2-free gas to He-flushed storage vials instead of evacuated vials. Also, to quantify the effects of syringe dead-space *vs.* outgassing of the transfer fluid, I either preflushed the transfer syringe with helium or with air before performing the transfer. The difference in O_2 between these two transfer methods represents air in the syringe deadspace. I prepared special low concentration air standards to calibrate the isotope ratios for these experiments, but the measured samples values turned out to be even lower. The experiment determined $O_{2,deadspace}$ = 0.23 ± 0.02%O_{O2atm}, $O_{2,outgassing}$ = 0.40 ± 0.01% $_{O2atm}$ (n = 5 each). Total $O_{2,transfer}$ in this experiment was 0.63 ± 0.02%$_{O2atm}$, somewhat smaller than found in the previous two sessions; $\delta^{18}O_{transfer}$ was between 0 and –2‰ based on worst- and best-case assumptions for the calibration curve.

A3.3.7. Correcting both initial and leakage contamination in the long-term storage experiment.

Initial contamination in the samples was diluted relative to the transfer blanks due to overinjection (i.e. 6 mL sample is initially injected into a 4 mL vial). The last step of the transfer process, however, returns vial pressure to atmospheric levels so leakage contamination is not similarly diluted. The evacuated vials used as blanks, however, had not been treated in this way: they were left undisturbed until filling with 4 mL He just before measurement. As a result, any leakage would have been diluted in a greater amount of initial contamination.

Two types of blanks were therefore used to correct for storage contamination: the above-mentioned evacuated vials, filled with He just before measurement, and He-flushed vials that were topped up with He just before measurement (since He leakage out of the vials was measured to be more than 0.1 mL mon^{-1}).

The final contents in the stored flushed vials, O_{flush}, represented net diffusion of oxygen into the vials, so ($O_{\text{evac}} - O_{\text{flush}}$) represented the initial contamination, where O_{evac} represents the

oxygen measured in the evacuated blanks. So the initial contamination, O_{init}, in the sample vials was:

$$^{32}O_{init} = (^{32}O_{evac} - ^{32}O_{flush}) \times 4/6 ,$$

where the factor 4/6 is the ratio of material injected into the blanks over the material injected into the sample vials. The total $^{32}O_2$ contamination was therefore:

$$^{32}O_c = ^{32}O_{init} + ^{32}O_{flush}.$$

The isotope ratio for initial contamination was determined by mass balance similar to Eqn 5:

$$\delta^{18}O_{init} = \frac{\delta^{18}O_{evac}\,{}^{32}O_{evac} - \delta^{18}O_{flush}\,{}^{32}O_{fush}}{{}^{32}O_{evac} - {}^{32}O_{flush}} .$$

and:

$$\delta^{18}O_{c} = \frac{\delta^{18}O_{init}\,{}^{32}O_{init} + \delta^{18}O_{flush}\,{}^{32}O_{fush}}{{}^{32}O_{init} + {}^{32}O_{flush}} .$$

The previous equations can be combined into:

$$\delta^{18}O_{c} = \frac{\frac{4}{6}(\delta^{18}O_{evac}\,{}^{32}O_{evac} - \delta^{18}O_{flush}\,{}^{32}O_{fush}) + \delta^{18}O_{flush}\,{}^{32}O_{fush}}{{}^{32}O_{c}} .$$

A similar equation is used for O_2/N_2. This extra computation improved the correction for both types of stored vials, although the effect on the freezer-stored vials was only 0.04‰. Without this added correction, the corrected values of *D* would have been 20.90 ± 0.08‰ and 20.03 ± 0.16‰ for frozen and bench vials, respectively.

(Leakage into the freezer-stored He-flushed blanks was below the isotope ratio calibration threshold of $1\%_{O2,atm}$, so the frozen-vial correction was computed by assuming that temperature did not affect leak fractionation.)

A3.3.8. Errors in variables

Previous reports have questioned whether standard linear regression is valid for computing *D* since the independent variable is also uncertain (Henry *et al.*, 1999, Nagel, Waldron & Jones, 2001). Fuller 1987 demonstrated that if the uncertainty in *x* is ignored, a linear regression estimate will be off by a factor called the *reliability ratio*, $\kappa = \sigma^2_x/(\sigma^2_x + \sigma^2_u)$, where the observed value $X = x + u$, in which *x* is the true value and *u* is a normally distributed random variable with mean 0 and variance σ^2_u. Thus the error in ignoring measurement uncertainty depends on total O_2 consumption, which determines σ^2_x.

The X variable in my regression is $-\log(f^*/f_0^*)$. I estimated measurement uncertainty, *u*, from the standard deviation of 0.0006 (O_2/N_2) for my calibration air samples ($O_2/N_2 = 0.2692$). Thus $\sigma_u = 0.002$ for $X = -\log(f^*/f_0^*)$, and $\sigma^2_u = 4 \times 10^{-6}$. For a six-point incubation with at least 20% O_2 consumption, $\kappa > 0.999$, so no bias is expected due to errors in variables.

Alternatively given the measurement uncertainty, σ^2_u, one can determine the minimum acceptable drawdown such that, $\kappa = \sigma^2_x/(\sigma^2_x + \sigma^2_u) \geq b$, where b is the acceptable level of bias. Solving for σ^2_x:

$$\sigma_x^2 \geq \sigma_u^2 \frac{b}{1-b}.$$

If we were to allow 1% bias, for example, the variance in the drawdown must be at least 99 times the measurement error variance, so a drawdown variance greater than 4×10^{-4} should be acceptable. The minimum variance for a set of points occurs when the values are spaced evenly. Assuming six evenly-spaced values of $-\log(f^*/f_0^*)$ from 0 to the minimum acceptable drawdown, the 6% drawdown is sufficient to avoid a 1% bias.

A3.4. Details and derivations of the discrimination calculations

Note on notation: As illustrated in Table 3.1 in the main text, subscripts are used in 2b – 2e to describe different stages of the experiment: i = incubation vial; r = respiration; x = transfer syringe; s = sample, in storage vial; c = contamination in storage vial; "m,t" = the mixture of s and c in the storage vial at time t. All terms refer to pressure, so that O_i, for example, refers to pO_2 in the incubation vial.

A3.4.1. Derivation of the Rayleigh distillation equation

I offer a short derivation of the discrimination equation (a.k.a. the Rayleigh distillation equation; Eqn A3.1, below and Eqn 4 in the main text) to highlight that $^{32}O_2$, not total O_2, is the precise value used on the right hand side (RHS) of the equation and to justify my claim that D represents a notation similar to δ notation.

During respiration the different isotopes of O_2 react at slightly different rates according to the partial chemical equation:

$$^{i}O_2 + 4H^+ + 4e^- \xrightarrow{k_i} H_2{}^{(i-16)}O + H_2{}^{16}O,$$

(i=32, 34), where the rate coefficient, k_i, is slightly different for $^{16}O^{16}O$ *vs.* $^{18}O^{16}O$ (abbreviated hereafter as $^{32}O_2$ and $^{34}O_2$).

In a closed system such as the incubation vials, reactants are stoichiometrically replaced by products so that by the law of mass action the rates of reaction are:

$$\frac{d[H_2{}^{18}O]}{dt} = -\frac{d[^{34}O_2]}{dt} = k_{34}[^{34}O_2][H^+]^4, \quad \text{and}$$

$$\frac{1}{2}\frac{d[H_2{}^{16}O]}{dt} = -\frac{d[^{32}O_2]}{dt} = k_{32}[^{32}O_2][H^+]^4$$

Dividing the two equations (and dropping the brackets for clarity) yields

$$\frac{d^{34}O_2/dt}{d^{32}O_2/dt} = \frac{k_{34}{}^{34}O_2}{k_{32}{}^{32}O_2},$$

which can be rearranged to

$$\frac{d\,{}^{34}O_2 / dt}{{}^{34}O_2} = \frac{k_{34}}{k_{32}} \frac{d\,{}^{32}O_2 / dt}{{}^{32}O_2}.$$

The ratios are now recognizable as derivatives of logarithms and can be rewritten as

$$\frac{d \ln {}^{34}O_2}{dt} = \alpha \frac{d \ln {}^{32}O_2}{dt},$$

where $\alpha \equiv k_{34}/k_{32}$ represents the relative rate of reactions for the heavier *vs.* the lighter molecule. Since the reaction prefers the lighter molecule, α is slightly less than 1. Integrating both sides from $t = 0$ to $t = t$ and combining terms using laws of logarithms yields

$$\ln \frac{{}^{34}O_{2,t}}{{}^{34}O_{2,0}} = \alpha \ln \frac{{}^{32}O_{2,t}}{{}^{32}O_{2,0}},$$

where ${}^{34}O_{2,t}$ is the concentration at time t, etc. Subtracting $\ln({}^{32}O_{2,t}/{}^{32}O_{2,0})$ from both sides:

$$\ln \frac{{}^{34}O_{2,t}}{{}^{34}O_{2,0}} - \ln \frac{{}^{32}O_{2,t}}{{}^{32}O_{2,0}} = \alpha \ln \frac{{}^{32}O_{2,t}}{{}^{32}O_{2,0}} - \ln \frac{{}^{32}O_{2,t}}{{}^{32}O_{2,0}}$$

$$\Rightarrow \ln \frac{{}^{34}O_{2,t}/{}^{32}O_{2,t}}{{}^{34}O_{2,0}/{}^{32}O_{2,0}} = (\alpha - 1) \ln \frac{{}^{32}O_{2,t}}{{}^{32}O_{2,0}}.$$

Substituting $D \equiv 1000 \times (1 - \alpha)$ and recognizing ${}^{34}O_2/{}^{32}O_2$ as R leads directly to the desired equation:

$$1000 \times \ln\left(\frac{{}^{34}R_t}{{}^{34}R_0}\right) = -D \ln\left(\frac{{}^{32}O_{2,t}}{{}^{32}O_2}\right). \qquad \text{Eqn A3.1}$$

Early studies used total oxygen as an approximation for ${}^{32}O_2$ (Guy *et al.*, 1989, Robinson *et al.*, 1992) but since I determine oxygen levels directly in the mass spectrometer it is useful to realize that the precise form of Eqn A3.1 involves only the major isotope, ${}^{32}O_2$ in the RHS. To simplify the notation in the remaining discussion I will generally write ${}^{16}O$ to represent ${}^{32}O_2$ and ${}^{18}O$ to represent ${}^{34}O_2$.

In practice, mass spectrometry software such as ISODAT reports δ values with more precision than isotope ratios. It is therefore useful to recast the left hand side of Eqn A3.1 in δ value terms. Starting with the definition:

$$\delta^{34}O_2(‰) \equiv \left(\frac{{}^{34}R}{{}^{34}R_{std}} - 1\right) \times 1000, \qquad \text{Eqn A3.2}$$

the equation can be rearranged to:

$$\delta^{34}O_2 + 1000 \equiv \frac{{}^{34}R}{{}^{34}R_{std}} \times 1000. \qquad \text{Eqn A3.3}$$

So that

$$\frac{(\delta^{34}O_2 + 1000)_t}{(\delta^{34}O_2 + 1000)_0} \equiv \frac{^{34}R_t}{^{34}R_0}.$$

Either $\delta^{18}O$ or $\delta^{34}O_2$ can be used, as the two values are essentially the same so that the final form of the Rayleigh distillation regression equation is:

$$1000 \times \ln\left(\frac{\delta^{18}O_t + 1000}{\delta^{18}O_0 + 1000}\right) = -D \ln\left(\frac{^{32}O_{2,t}}{^{32}O_2}\right).$$

A3.4.2. Why we need O_2/N_2 rather than O_2 in calculating *f*

As illustrated in Figs. S9 and S10, respiration consumes oxygen in the sealed vial thus reducing pO_2 in the vial without affecting pN_2. At the same time, however, KOH in the vial removes the CO_2 introduced by respiration, thus reducing the total pressure so $P_i < P_{atm}$.

Since the partial pressure of N_2 in the incubation vial is constant, $N_i = N_{i,0}$ where N_i is the pN_2 right before the transfer process and $N_{i,0}$ is the initial pN_2 (as measured in the air blank), so

$$\frac{^{16}O_i}{^{16}O_{i,0}} = \frac{^{16}O_i / N_i}{^{16}O_{i,0} / N_{i,0}}.$$

Eqn A3.1 can be rewritten as

$$1000 \times \ln\left(\frac{R_i}{R_{i,0}}\right) = -D \ln\left(\frac{^{16}O_i / N_i}{^{16}O_{i,0} / N_{i,0}}\right) \equiv -D \ln(f^*). \qquad \text{Eqn A3.4}$$

This equation is essentially Eqn 4 in the main text. Upon transfer to the storage vial, however, total pressure is restored to atmospheric pressure so that all partial pressures rise in proportion to the ratio P_{atm}/P_i (Fig S9, Table A1). But since P_i decreases with respiration, the O_2 ratio of the transfer gases, $^{16}O_x/^{16}O_{x,0}$, does not represent the fraction of O_2 in the incubation vial. Specifically, $P_{i,0} = P_{atm}$ so $P_{atm}/P_{i,0} = 1$, but as respiration continues, $P_i < P_{atm}$ so pO_2 in the transfer syringe is

$$\frac{^{16}O_x}{^{16}O_{x,0}} = \frac{^{16}O_i \times P_{atm}/P_i}{^{16}O_{i0} \times P_{atm}/P_{i,0}} = \frac{^{16}O_i}{^{16}O_{i0}} \frac{P_{atm}}{P_i} > \frac{^{16}O_i}{^{16}O_{i0}}.$$

Thus as respiration progresses, the $^{16}O_x/^{16}O_{x,0}$ in the transfer syringe (and therefore storage vial) is greater than it was in the incubation vial, making it seem as if less O_2 had been consumed. A graph based on Eqn A3.1 will be compressed along the *x* axis, resulting in an overestimate of discrimination (i.e. ln *R* rises faster per apparent change in ln *f*). For example, at 50% drawdown, $P_{atm}/P_i = 1/0.9$, so $-\ln(^{16}O_x/^{16}O_{x,0}) = -\ln(0.5/0.9) = 0.588$, which is 20% less than the correct value of $-\ln(0.5) = 0.693$. As a result, calculated discrimination values would be 3–6‰ too high (for true D = 15–30‰) at 50% actual O_2 consumption. The error also depends on actual drawdown, so that there is a 1‰ difference in the apparent discrimination for the same process measured at 25% *vs.* 50% drawdown.

Eqn A3.4, however is still valid since O_i and N_i rose proportionally, i.e.

$$\frac{^{16}O_x}{N_x} = \frac{^{16}O_i \times P_{atm}/P_i}{N_i \times P_{atm}/P_i} = \frac{^{16}O_i}{N_i}.$$

Thus O_2/N_2 ratios must be used for computing discrimination values for my method.

A3.4.3. Correcting $\delta^{18}O$ for initial contamination

Initial contamination adds fixed amount of gases, O_c and N_c, to each vial so that $O_s = O_m - O_c$ and $N_s = N_m - N_c$. The ^{18}O isotope ratio of the sample is therefore:

$$^{18}R_s = \frac{^{18}O_s}{^{16}O_s} = \frac{^{18}O_m - ^{18}O_c}{^{16}O_m - ^{16}O_c} = \frac{^{18}R_m\,^{16}O_m - ^{18}R_c\,^{16}O_c}{^{16}O_m - ^{16}O_c}. \qquad \text{Eqn A3.5}$$

To convert to δ notation, multiply both sides of Eqn A3.5 by $1000/^{18}R_{std}$, substitute Eqn A3.3 and simplify to:

$$\delta^{18}O_s = \frac{\delta^{18}O_m\,^{16}O_m - \delta^{18}O_c\,^{16}O_c}{^{16}O_m - ^{16}O_c}. \qquad \text{Eqn A3.6}$$

Note that no approximations were made in deriving Eqn A3.6: the use of ^{16}O makes it exact.

A3.4.4. Correcting O^* for initial contamination

For $O^* \equiv {}^{32}O_2/N_2$,

$$O^*_s = \frac{^{16}O_m - ^{16}O_c}{N_m - N_c} = \frac{^{16}O_m - ^{16}O_c}{^{16}O_m / O^*_m - ^{16}O_c / O^*_c}. \qquad \text{Eqn A3.7}$$

Note that the naïve approach of mixing O^* by direct imitation of Eqn A3.5, i.e.

$$O^*_s = \frac{O^*_m\,^{16}O_m - O^*_c\,^{16}O_c}{^{16}O_{mix} - ^{16}O_c}.$$

expands to:

$$O^*_s = \frac{\left(\frac{^{16}O}{N}\right)_m\,^{16}O_m - \left(\frac{^{16}O}{N}\right)_c\,^{16}O_c}{^{16}O_{mix} - ^{16}O_c},$$

which clearly does not equal $(^{16}O_{mix} - {}^{16}O_c)/ (N_{mix} - N_c)$.

Likewise,

$$\frac{^{16}O_m - ^{16}O_c}{N_m - N_c} \neq \frac{^{16}O_m}{N_m} - \frac{^{16}O_c}{N_c}.$$

For $^{32}O^*_s$, the N_2 transfer blanks, which include all sources of contamination, cannot be used to determine the contaminating N_2 in the sample vials, N_c. Instead N_c is approximated using evacuated vials filled with He right before measurement in the IRMS instrument. (While He could be used as the gas for the transfer blank, it is more prone to contamination both during the gas transfer process and, even more so, during storage, even at low temperature. Also, the gradient between gas in the displacement liquid and gas in the vial is very different between N_2 and He. In incubation transfers $pN_{2,i} = pN_{2,atm}$, so one might expect little effect on N_2 due to transfer, whereas in He the large N_2 gradient would have a larger effect.)

A3.4.5. Correcting $\delta^{18}O$ and O_2/N_2 when contamination is proportional to a gradient

Sections 2c and 2d considered the case of contamination whose quantity was independent of the composition of the sample. Sometimes, however, O_c is proportional to the gradient between the contents of the vial and O_{atm}. For example, net O_2 exchanged between vial air and O_2 dissolved in the displacement buffer, or O_2 diffusing during storage should be proportional to the gradient with atmospheric air. (The latter case assuming Fickian diffusion.) In such cases the contamination in a sample vial, O_c, cab be specified as a function of contamination that entered a corresponding O_2-free blank, O_{blank}, the oxygen content of the sample gas, O_s and atmospheric oxygen, O_{atm}, where the gradient is $O_{atm} - O_s$:

$$\begin{aligned} O_c &= O_{blank}\frac{(O_{atm}-O_s)}{O_{atm}} \\ &= O_{blank}(1-O_s/O_{atm}) \end{aligned}$$

Then, as in Section 2c, $O_s = O_m - O_c$, so:

$$O_s = O_m - O_{blank}(1-O_s/O_{atm})$$

$$\Rightarrow O_s - O_{blank}O_s/O_{atm} = O_m - O_{blank}$$

$$\Rightarrow O_s = \frac{O_m - O_{blank}}{1-O_{blank}/O_{atm}}.$$

Each isotope acts independently, so the isotope ratio correction is:

$$R_s = \frac{{}^{18}O_s}{{}^{16}O_s} = \frac{{}^{18}O_m - {}^{18}O_{blank}}{{}^{16}O_m - {}^{16}O_{blank}}\frac{1-{}^{16}O_{blank}/{}^{16}O_{atm}}{1-{}^{18}O_{blank}/{}^{18}O_{atm}}.$$

Thus, although Eqn A3.5 does not properly compute R_s, it is proportional to the correct value, since the extra coefficient is independent of O_s and O_m. When computing R_s/R_0 the error therefore cancels out.

Finally, for completeness, the value of R_s with both kinds of contamination is:

$$R_s = \frac{{}^{18}O_s}{{}^{16}O_s} = \frac{{}^{18}O_m - {}^{18}O_{c,1} - {}^{18}O_{blank}}{{}^{16}O_m - {}^{16}O_{c,1} - {}^{16}O_{blank}}\frac{1-{}^{18}O_{blank}/{}^{18}O_{atm}}{1-{}^{16}O_{blank}/{}^{16}O_{atm}},$$

where $O_{c,1}$ represents initial contamination, i.e. the portion that is independent of O_s. Thus, since measured O_c is, in fact, $O_{c,1} + O_{blank}$ Eqn A3.5 allows us to correctly compute D.

The same argument applies to O_2/N_2 corrections by direct substitution of ^{16}O for ^{18}O and N for ^{16}O.

Appendix 4. Supporting information for Chapter 4

A4.1. Supporting figures

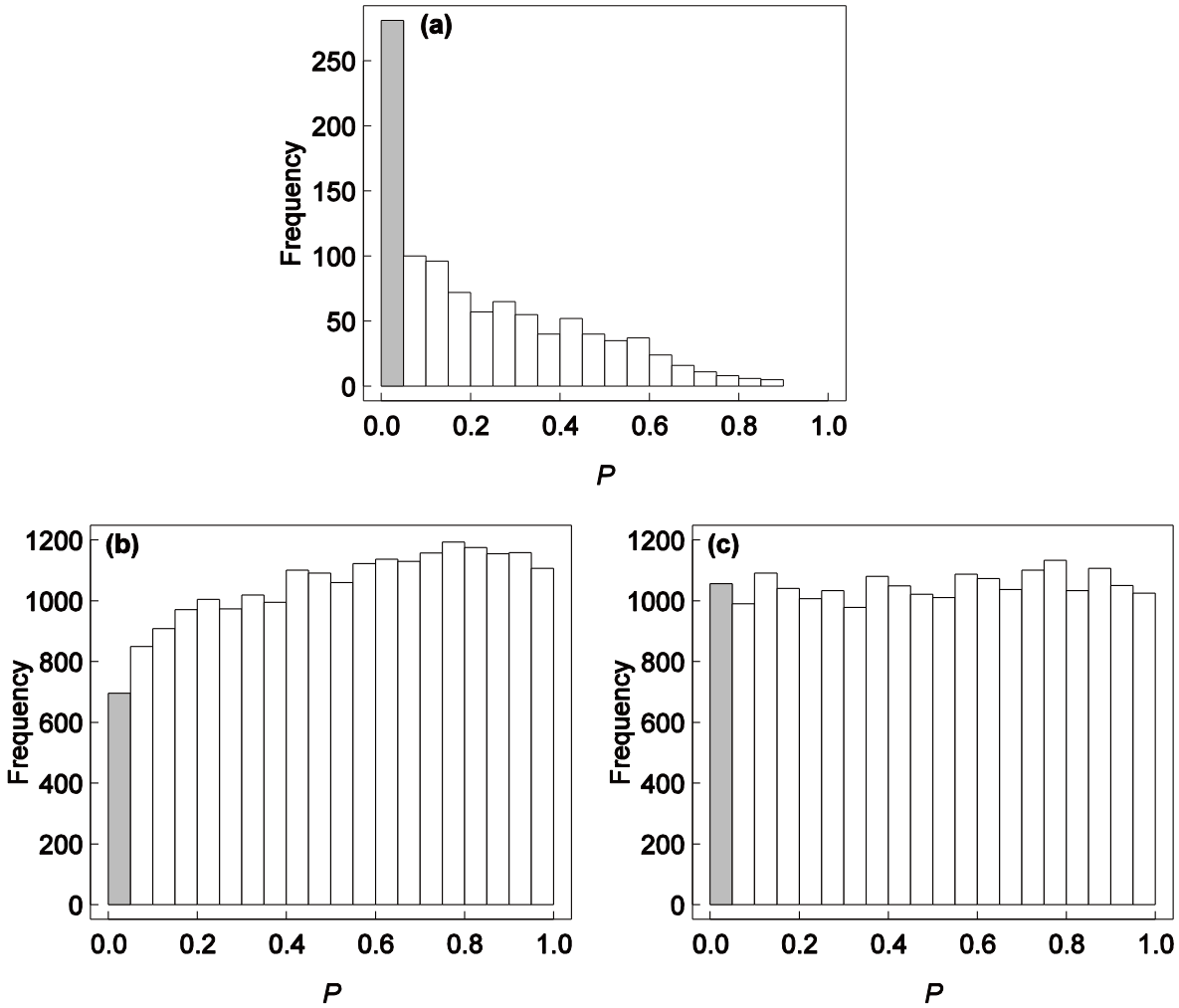

Fig S4.1. Histograms of (a) the AIC_c best-model *P* values, (b) uncorrected model-averaged *P* values and (c) model-averaged corrected *P* values from 1,000 simulation runs in which the dependent variable was completely random.

Explanation: AIC_c ranks models based on the data. Since this process chooses a model based on the data, *P* values of the model and of the model coefficients are strongly biased low. To illustrate the problem, I used AIC_c to select the best model from each of 1,000 simulated runs in which the variables were as described in the Materials and Methods but the dependent variable was purely random (normally distributed values with the same mean and SD as τ_a). By definition, under such conditions, *P* values should be uniformly distributed between 0 and 1, so that *P* will be less than 0.05, 5% of the time (i.e., satisfying the condition that Type I error occurs 5% of the time). Instead, in the simulation using random τ_a values, the *P* value of the best model was below 0.05 30% of the time (shaded bar, panel a). Thus statistical significance is greatly overstated. Model-averaging fixed most of the problem but the *P* values of the pooled coefficients were now biased slightly high (panel b). Multiplying the model-weighted standard errors by 0.92 restores the uniform distribution (panel c). The shaded bar corresponds to $P < 0.05$.

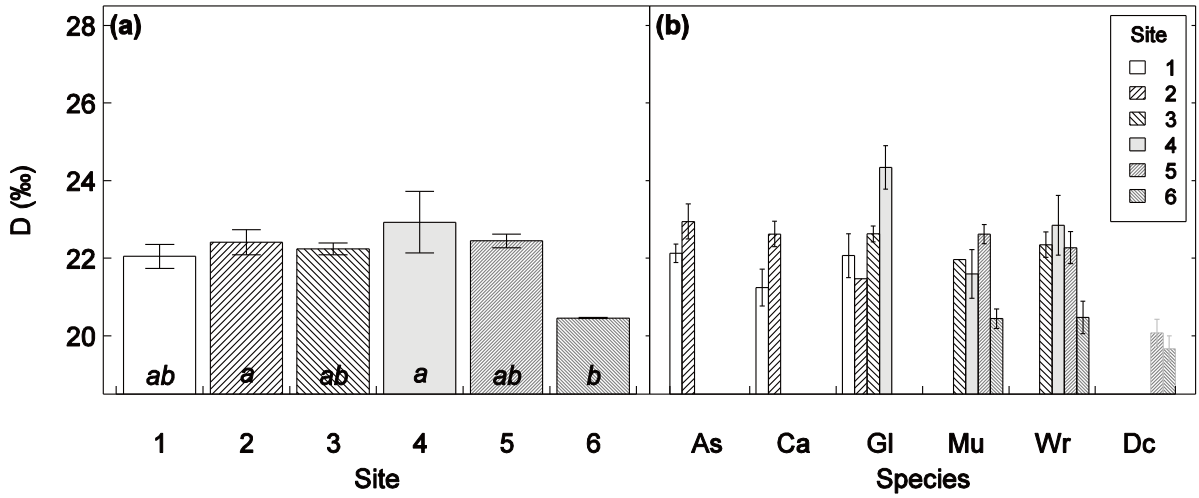

Fig S4.2. Changes in measured O_2 discrimination, *D*, across sites (a) and within species across sites (b).

A4.2. Supporting tables

Table S4.1. Measured discrimination values (*D*, ‰) in respiratory inhibition experiments. Species that I had sampled along the Franz Josef Chronosequence were subsequently incubated with respiratory inhibitors – either by vacuum infiltration or by exposure to gaseous cyanide. The initial control and infiltration experiments were conducted in Dec 2008 and Feb 2009; the HCN, dark and control2 measurement were conducted Sep 2010. Inhibition with HCN generally resulted in *D* = 28 – 30‰, whereas KCN infiltration varied from 23 – 31‰ with lower precision. Only one infiltration measurement appears to have been higher than the gas inhibition (*Melicytus*). Neither SHAM (relative to buffer) nor keeping branches in the dark for 3 days lowered *D*. *n* is number of 4- or 6-vial replicates. Low AOX endpoints appear to be associated with dense tissue (*Dacrydium*) or tomentose leaves (*Olearia*) both of which interfere with diffusion, thus artificially lowering *D* (Angert & Luz, 2001).

Species	***control***	***buffer infilt***	***SHAM infilt***	***KCN infilt***	***HCN (gas)***	***dark***	***control2***
Aristotelia serrata	22.3 ± 0.5	20.0 ± 1.3	21.2 ±0.8	29.1 ± 1.6	28.69 ± 0.11 (n=4)		21.18 ± 0.16 (n=2)
Coriaria arborea	22.2 ± 0.5	23.6 ± 0.4	22.9 ± 0.3	23.2 ± 0.7	29.8 ± 0.3 (n=2)		21.4 ± 0.4 (n=1)
Dacrydium cupressinum	19.2 ± 2	17.9 ± 1.5	18.1 ± 0.8	23.3 ± 2.0	25.3 ± 0.4 (n=2)	18.8 ± 0.2 (n=2)	19.1 ± 0.3 (n=1)
Griselinia littoralis	21.9 ± 0.2	20.5 ± 1.2	20.1 ± 1.1	27.6 ± 1.6	29.24 ± 0.05 (n=4)	21.0 ± 0.3 (n=2)	20.80 ± 0.09 (n=2)
Hebe salicifolia					27.84 ± 0.14 (n=2)	23.2 ± 0.3 (n=2)	21.72 ± 0.08 (n=1)
Melicytus ramiflorus	22.8 ± 0.4	22.4 ± 0.5	21.9 ± 0.4	30.6 ± 0.4	28.8 ± 0.2 (n=2)	21.36 ± 0.11 (n=2)	21.8 ± 0.3 (n=1)
Metrosideros umbellata	22.2 ± 0.5	20.0 ± 2.1	20.9 ± 1.1	29.4 ± 1.1	28.11 ± 0.12 (n=3)		20.39 ± 0.14 (n=2)
Olearia avicenniifolia	21.3 ± 0.3	15.4 ± 0.7	15.4 ± 0.6	22.9 ± 1.1	26.6 ± 0.3 (n=2)	21.5 ± 0.3 (n=1)	21.3 ± 0.7 (n=1)
Pseudopanax sp.	22.5 ± 0.3	21.9 ± 0.4	22.3 ± 0.3	27.4 ± 0.5	28.0 ± 0.2 (n=2)		21.1 ± 0.1 (n=1)
Weinmannia racemosa	22.11 ± 0.3	19.5 ± 0.5	20.8 ±0.4	24.5 ± 1.2	28.0 ± 0.2 (n=2)		20.47 ± 0.14 (n=1)

(note: For the infiltration experiments, *Aristotelia* from site 2, *Coriaria* from site 1, *Melicytus* from site 2, *Olearia* from site 1, *Weinmannia* from site 3. These controls were incubated a week prior to inhibitions; *Dacrydium*, *Griselinia*, *Metrosdideros* and *Pseudopanax* controls were from UC campus and were incubated at same time as the infiltrated tissue. All controls for the HCN and dark experiment were harvested at the same time as, and incubated alongside, their respective HCN treatments.)

Table S4.2. Correlations between the variables measured in this study using Pearson's product-moment correlation coefficient, *r*. Boxes indicate groups of closely correlated measures: macronutrients, micronutrients, leaf structure, and carbohydrates. The strongest correlations with τ_a and R are highlighted in boldface. (The correlation matrix is symmetric around the diagonal, but all numbers are left in to make it easier to assess correlations for any single variable.)

	τ_a	v_{alt}	R	N_{leaf}	P_{leaf}	N/P	Fe_{leaf}	Cu_{leaf}	Fe/Cu	DMC	SLA	sugars	starch	TNC
τ_a	1	0.52	0.02	0.07	0.26	-0.48	0.19	0.15	0.14	-0.26	0.19	-0.01	0.12	0.08
v_{alt}	0.52	1	0.75	0.77	0.80	-0.46	0.48	0.72	-0.07	-0.71	0.76	0.41	0.10	0.30
R	0.02	0.75	1	0.90	0.76	-0.29	0.59	0.79	-0.08	-0.71	0.77	0.53	0.02	0.32
N_{leaf}	0.07	0.77	**0.90**	1	0.87	-0.32	0.63	0.81	-0.05	-0.78	0.86	0.53	-0.09	0.24
P_{leaf}	0.26	**0.80**	0.76	0.87	1	-0.60	0.50	0.68	0.01	-0.77	0.83	0.45	-0.05	0.23
N/P	**-0.48**	-0.46	-0.29	-0.32	-0.60	1	-0.38	-0.35	-0.28	0.44	-0.31	-0.04	0.02	-0.01
Fe_{leaf}	0.19	0.48	0.59	0.63	0.50	-0.38	1	0.60	0.50	-0.65	0.57	0.33	-0.17	0.07
Cu_{leaf}	0.15	0.72	**0.79**	0.81	0.68	-0.35	0.60	1	-0.22	-0.72	0.68	0.36	-0.17	0.09
Fe/Cu	0.14	-0.07	-0.08	-0.05	0.01	-0.28	0.50	-0.22	1	-0.08	-0.04	-0.10	-0.12	-0.15
DMC	-0.26	-0.71	-0.71	-0.78	-0.77	0.44	-0.65	-0.72	-0.08	1	-0.83	-0.42	-0.03	-0.26
SLA	0.19	0.76	0.77	0.86	0.83	-0.31	0.57	0.68	-0.04	-0.83	1	0.50	0.07	0.33
sugars	-0.01	0.41	0.53	0.53	0.45	-0.04	0.33	0.36	-0.10	-0.42	0.50	1	0.18	0.71
starch	0.12	0.10	0.02	-0.09	-0.05	0.02	-0.17	-0.17	-0.12	-0.03	0.07	0.18	1	0.82
TNC	0.08	0.30	0.32	0.24	0.23	-0.01	0.07	0.09	-0.15	-0.26	0.33	0.71	0.82	1

Appendix 5. Supporting information for Chapter 5

A5.1. Supporting figures

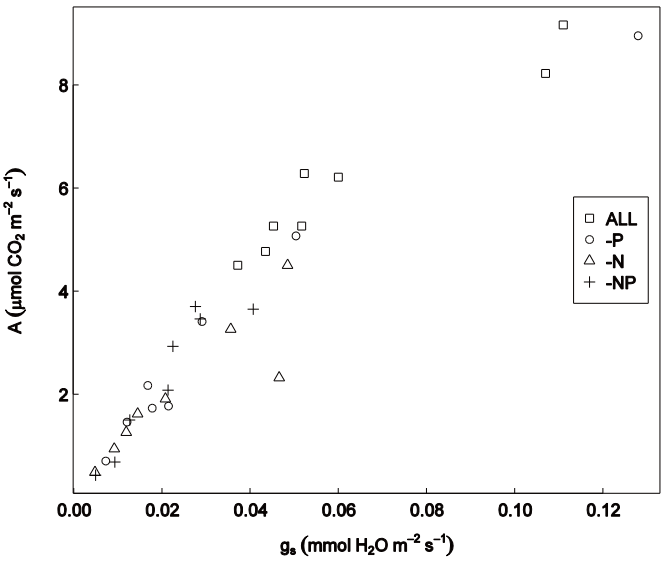

Fig S5.1. Stomatal conductance (g_s) was strongly correlated with net photosynthesis (A).

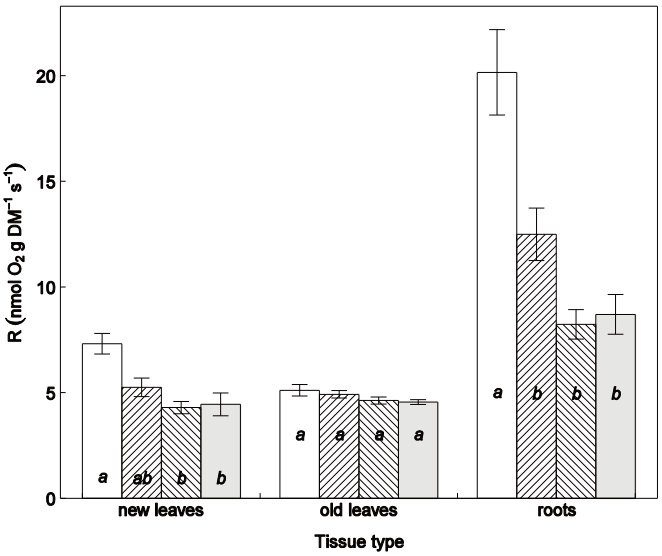

Fig S5.2. Respiration on a dry mass basis (compare with Fig 5.4 in the main text).

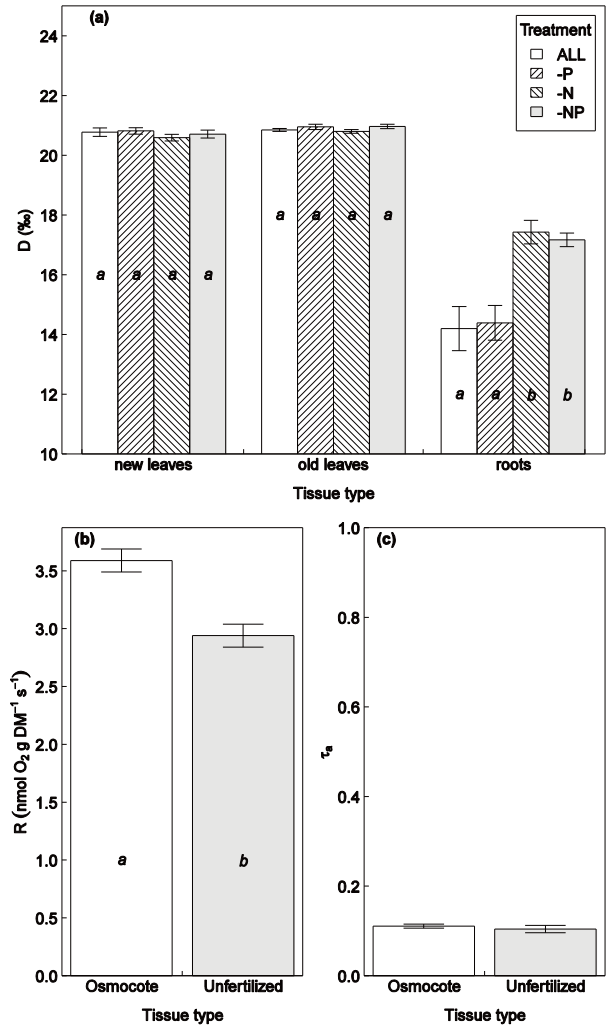

Fig S5.3. (a) "raw" discrimination, *D*, in *Griselinia* leaves and roots. (b) Respiration and (c) electron partitioning in conventionally fertilized and completely unfertilized *Griselinia* leaves. Osmocote-treated plants were fertilized with slow-release fertilizer as per the manufacturer's instructions; unfertilized plants were grown in sand, perlite or perlite-vermiculite media and were watered with tap-water only. The latter did not grow at all during the 22-week treatment period, though they did not show external signs of nutrient deficiency.

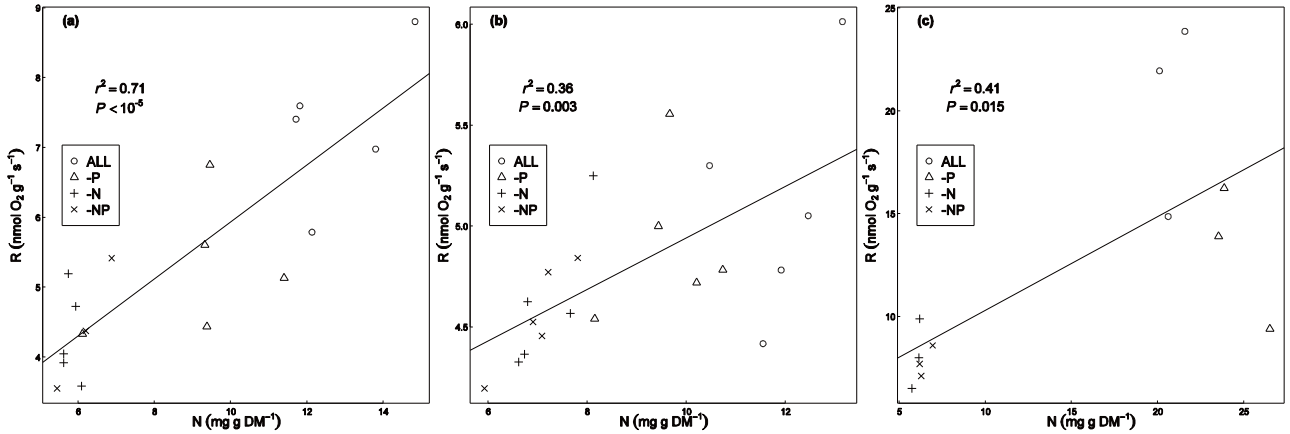

Fig S5.4. Respiration *vs.* leaf N concentration in (a) new leaves, (b) old leaves, and (c) roots. Note the large differences in axis scales between the three graphs.

Appendix 6. Supporting Information for Chapter 6

A6.1. Supporting table

Table S6.1. Respiratory endpoint measurements in *Betula*, *Eriophorum*, and *Rubus*.

Species	*SHAM*	*KCN*	*KCN+SHAM*[a]	*buffer*	*untreated*
Betula leaves	21.0 ± 0.7	25.5 ± 0.9	20.8 ± 1.6	21.9 ± 0.4	22.1 ± 0.6
Betula stem	17.3	25.4 ± 0.9		19.1 ± 1.3	19.9 ± 1.1
Eriophorum	21.9 ± 0.3	25.4 ± 0.2	23.4 ± 0.7	23.4 ± 1.2	22.9 ± 0.9
Rubus	23.7 ± 0.5	22.1 ± 1.9	18.4 ± 1.4	22.8 ± 0.3	22.7 ± 0.2

n = 4 each except n = 2 for KCN+SHAM and for *Betula* stem (n = 1 for *Betula* stem SHAM treatment)

[a] Residual respiration for doubly-inhibited tissue was 11% for *Betula*, 13% for *Rubus*, and 26% for *Eriophorum*.

A6.2. Supporting figures

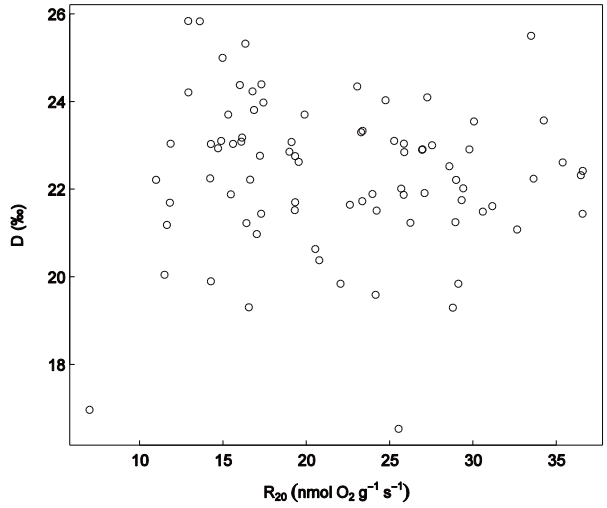

Fig S6.1. Discrimination (D) *vs.* respiration (R_{20}), showing lack of correlation between the two variables.

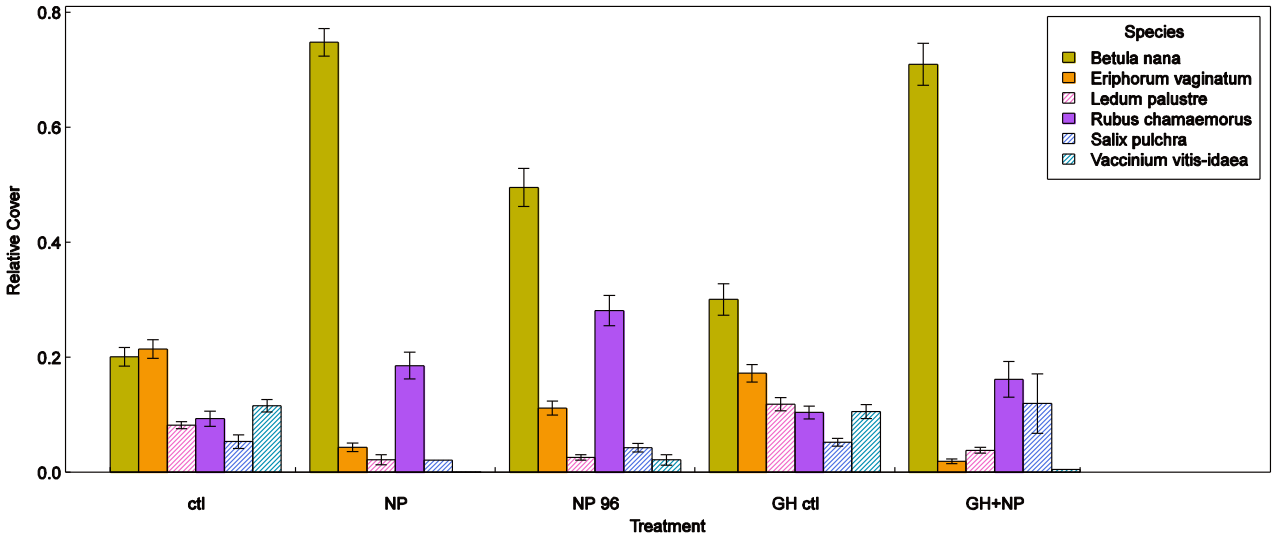

Fig S6.2. Relative cover of treatment plots in 2007. The treatment labeled "NP 96" received the same treatments as NP but treatments started in 1996 instead of 1989. (Compare the NP 96 treatment with the equivalent NP treatment in Fig 1, in the main paper.)

Appendix 7. & 8. Published versions of Chapters 2 and 3

Research Article

Received: 4 October 2011 Revised: 1 December 2011 Accepted: 1 December 2011 Published online in Wiley Online Library

Rapid Commun. Mass Spectrom. 2012, 26, 460–468
(wileyonlinelibrary.com) DOI: 10.1002/rcm.6120

Correcting for nonlinearity effects of continuous flow isotope ratio mass spectrometry across a wide dynamic range

Ari Kornfeld[1], Travis W. Horton[2], Dan Yakir[3] and Matthew H. Turnbull[1]*

[1]School of Biological Sciences, University of Canterbury, Private Bag 4800, Christchurch 8140, New Zealand
[2]Department of Geological Sciences, University of Canterbury, Private Bag 4800, Christchurch 8140, New Zealand
[3]Dept of Environmental Sciences & Energy Research, Weizmann Institute of Science, Rehovot, 76100, Israel

RATIONALE: Environmental and biological investigations may require samples that vary over a wide range of concentrations
and isotope ratios, making measurements using continuous flow isotope ratio mass spectrometry (CF-IRMS) problematic due to nonlinear signal response. We therefore developed a mathematical approach for correcting nonlinearities
over a wide range of sample concentrations and actual d values.

METHODS: Dilution series for two standards were prepared in septum-capped vials and introduced into the mass spectrometer
via the standard sampling pathway. Parameters for a nonlinear signal correction were determined by regression on measured isotope ratio vs. both signal strength and actual isotope ratio. We further extended the dynamic range by adjusting the position of an open split based on analyte concentration. Effects of the open split setting required additional
mathematical correction.

RESULTS: The nonlinearities were corrected over a 100-fold range of sample concentrations and across a 600%change in
isotope ratios (for dO_2/N_2 values). The precision, measured as standard deviation, across the upper 90% of the concentration
range was _0.08%, _0.05%, and _2.6%for $d^{18}O$, $d^{15}N$, and dO_2/N_2 values, respectively; the precision across the lower 10% of the range was _0.22%, _0.07%, and _7.6%, respectively. In all cases the linearity correction represented
only a small fraction of these precision values.

CONCLUSIONS: The empirical correction described here provides a relatively simple yet effective way to increase the
usable signal range for CF-IRMS applications. This improvement in dynamic range should be especially helpful for environmental and biological field studies, where sampling methods may be constrained by external factors.

Plant, Cell & Environment

Plant, Cell and Environment (2012) doi: 10.1111/j.1365-3040.2012.02507.x

A field-compatible method for measuring alternative respiratory pathway activities *in vivo* using stable O_2 isotopes

ARI KORNFELD[1], TRAVISW. HORTON[2], DAN YAKIR[3], STEPHANIE Y. SEARLE[1], KEVIN L. GRIFFIN[4,5], OWEN K. ATKIN[6], JENS-ARNE SUBKE[7] & MATTHEW H. TURNBULL[1]

[1]School of Biological Sciences, [2]Deparment of Geological Sciences, University of Canterbury, Private Bag 4800, Christchurch 8140, New Zealand, [3]Department of Environmental Sciences & Energy Research,Weizmann Institute of Science, Rehovot 76100, Israel, [4]Department of Earth and Environmental Sciences, Columbia University, New York, NY 10027, USA, [5]Lamont-Doherty Earth Observatory, Columbia University, 61 Rt 9W, Palisades, NY 10964, USA, [6]Division of Plant Sciences, Research School of Biology, The Australian National University, Canberra,ACT 0200,Australia and [7]University of Stirling, School of Natural Sciences, Biological and Environmental Sciences, Stirling FK9 4LA, UK

ABSTRACT

Plants can alter rates of electron transport through the alternative oxidase (AOX) pathway in response to environmental cues, thus modulating respiratory efficiency, but the ^{18}O discrimination method necessary for measuring electron partitioning *in vivo* has been restricted to laboratory settings. To overcome this limitation, we developed a field-compatible analytical method. Series of plant tissue subsamples were incubated in 12 mL septumcapped vials for 0.5–4 h before aliquots of incubation air were injected into 3.7 mL evacuated storage vials. Vials were stored for up to 10 months before analysis by mass spectrometry. Measurements were corrected for unavoidable contamination. Additional mathematical tools were developed for detecting and addressing non-linearity (whether intrinsic or due to contamination) in the data used to estimate discrimination values. Initial contamination in the storage vials was 0.03 _ 0.01 atm; storing the gas samples at -17 °C eliminated further contamination effects over 10 months. Discrimination values obtained using our offline incubation and computation method replicated previously reported results over a range of 10–31‰, with precision generally better than _0.5‰. Our method enables large-scale investigations of plant alternative respiration along natural environmental gradients under field conditions.

Key-words: alternative oxidase; cytochrome *c* oxidase; oxygen isotope discrimination; respiration; stable isotope ratio mass spectrometry (IRMS).